

LANDSCAPE-SCALE MODELING OF DROUGHT- AND INSECT-RELATED TREE MORTALITY
IN NORTHERN NEW MEXICO

BY

Gjertrud E. Aney, B.S.

A thesis submitted to the Graduate School
in partial fulfillment of the requirements
for the degree
Master of Applied Geography

Major: Geography

NEW MEXICO STATE UNIVERSITY

LAS CRUCES, NEW MEXICO

December 2020

Gjertrud E. Aney

Candidate

Geography

Major

This Thesis is approved on behalf of the faculty of New Mexico State University, and it is acceptable in quality and form for publication:

Approved by the Thesis Committee:

Dr. Michaela Buenemann

Chairperson

Dr. Christopher Brown

Committee Member

Dr. April Ulery

Committee Member

ACKNOWLEDGEMENTS

I owe a debt of gratitude to the following people – Will Brewer, for sharing with me his extensive library of pinyon and juniper endmembers collected from just outside the collective area of this study; Nathan Lopez-Brody for allowing me to use his R scripts for the statistical processing of the variables, thereby saving me many hours of time and effort; and Wayne Robbie at the USFS Region 3 office, who supplied me with a wealth of detailed soils data in the form of scanned copies of the raw field log sheets for soil mapping done within the four study Areas. I would also like to thank Dr. Caiti Steele for connecting me to the right people and for helping me collect the spectral data via field spectrometer from soil samples collected in the field, and my supervisor, Dr. Emile Elias, for her understanding and flexibility with me on the job as I completed my research. A big thank you goes to my advisor, Dr. Buenemann, for her help and guidance, patience with me, and her undying enthusiasm all the way along this road. I would also like to thank the members of my committee, Dr. Brown and Dr. Ulery, for their time and willingness to be part of this journey. Finally, from the bottom of my heart I thank all the many YouTubers and Stack Exchange contributors out there who share their time and talents to the benefit of folks like me doing a 2:00 am web search for why the code isn't working and how to make it dance – you saved my sanity more than once.

VITA

Educational Information

- 2009 Bachelor of Science in Agriculture, Soil Science, New Mexico State University, Las Cruces, NM
- 2001 Associate in Arts, General Studies, Palomar College, San Marcos, CA

Employment Information

- 2019-Present Program Manager, USDA Southwest Climate Hub, Jornada Experimental Range, Las Cruces, NM
- 2017-2019 Graduate Research Assistant, USDA Southwest Climate Hub, Jornada Experimental Range, Las Cruces, NM
- 2016-2018 Teaching Assistant, New Mexico State University, Las Cruces, NM
- 2015-2017 Soil Scientist and GIS Specialist, Self Employed, Las Cruces, NM
- 2014-2015 GIS Manager, Stetson Engineers Inc., Covina, CA
- 2010-2014 Assistant Soil Scientist, Stetson Engineers Inc., Albuquerque, NM

Field of Study

- Major Field Geography

ABSTRACT

LANDSCAPE-SCALE MODELING OF DROUGHT- AND INSECT-RELATED TREE MORTALITY IN NORTHERN NEW MEXICO

By

Gjertrud E. Aney

Master of Applied Geography

NEW MEXICO STATE UNIVERSITY

LAS CRUCES, NEW MEXICO

December 2020

Dr. Michaela Buenemann, Chair

Pinyon-juniper woodlands represent the third-largest vegetation type in the United States and an important ecotype for wildlife and humans. Large-scale woodland die-off events have implications for a range of ecosystem services and can contribute to increased wildfire hazard. Understanding the relationships between environmental factors and episodic drought- and insect-related mortality in pinyon-juniper woodlands can provide important information for land managers, particularly in the face of climatic changes, which may bring intense droughts with increasing frequency. I used random forest, logistic regression, and conditional inference trees with diverse bioclimatic, edaphic, topographic, and anthropogenic variables to predict and explain drought- and insect-related pinyon mortality in northern New Mexico. Mortality presence locations were identified using multiple endmember spectral mixture analysis.

Bioclimatic variables were the most explanatory of mortality, followed by edaphic and then topographic variables. The anthropogenic factor, presence of grazing, had no influence on mortality. The final random forest model predicted mortality occurrence with 80 to 83 percent balanced overall accuracy, and contained four bioclimatic variables – isothermality, minimum temperature of the coldest month, precipitation of the warmest quarter, and Normalized Difference Moisture Index (NDMI). These data are all available either pre-packaged or easily calculated by land managers for locations in the conterminous U.S., and may represent a rapid and cost-effective means of evaluating risk for drought related mortality at the landscape scale. Correlation tables referenced in section 3.6.3 are included as a supplemental file, and are identical to the information presented in Appendix C.

Keywords: pinyon, drought, die-off, random forest, logistic regression, conditional inference trees

TABLE OF CONTENTS

LIST OF TABLES.....	x
LIST OF FIGURES.....	xi
LIST OF ABBREVIATIONS	xiii
1. Introduction	1
2. Background	2
2.1 The physiology of drought-related pinyon mortality	7
2.2 Genetics	8
2.3 Stand density and tree size	9
2.4 Microsites.....	10
2.5 Historic range	10
2.6 Climatic variables	11
2.7 Topographic variables.....	12
2.8 Edaphic variables	14
2.9 Grazing and management.....	18
2.10 Scale and extent of previous studies	18
3. Methods.....	20
3.1 Study area description	20
3.2 Overview of methods.....	25
3.3 Mapping pinyon mortality	26
3.3.1 Image acquisition	27
3.3.2 Preprocessing.....	28
3.3.3 Multiple Endmember Spectral Mixture Analysis (MESMA).....	31
3.4 Image differencing	40
3.5 Selection of tree mortality presence and absence locations	41
3.5.1 Determination of tree mortality presence and absence	42
3.5.2 Determination of pre-drought woody plant cover classes.....	43
3.5.3 Sampling of tree mortality presence and absence sites.....	43
3.6 Potential explanatory variables	44

3.6.1 Acquisition of potential explanatory data layers.....	45
3.6.2 Preprocessing of potential explanatory data layers.....	46
3.6.3 Statistical preprocessing of variables.....	54
3.7 Modeling.....	56
3.7.1 Variables groupings for modeling.....	57
3.7.2 Logistic regression.....	58
3.7.3 Random forest.....	59
3.7.4 Conditional inference trees.....	60
3.7.5 Model comparison.....	61
3.7.6 Final model selection.....	62
3.7.7 Mortality prediction maps.....	63
4. Results.....	64
4.1 MESMA.....	64
4.2 Tree cover changes.....	67
4.3 Spatial models.....	73
4.3.1 Overall model performance.....	73
4.3.2 Comparison of model types.....	76
4.3.3 Factors explaining pinyon mortality.....	80
4.3.4 Factors selected for the final model.....	100
5. Discussion.....	105
5.1 MESMA performance.....	105
5.2 Tree cover changes.....	106
5.3 Model comparisons.....	108
5.3.1 Comparison of model types.....	109
5.3.2 Comparison of variable types.....	110
5.4 Factors explaining pinyon mortality.....	114
5.4.1 Variables used in the final model.....	114
5.4.2 Other top variables.....	117
5.5 Final model performance and implications.....	119

6. Conclusion.....	120
7. Literature Cited	122
Appendix A: Potential explanatory variables.....	135
Appendix B: Python code for calculating soil properties.....	150
Appendix C: Correlation matrices and variance inflation factors of potential explanatory variables.....	155
Appendix D: R scripts for spatial models	180
Appendix E: Model performance.....	188
Appendix F: Univariate conditional inference stumps	197

LIST OF TABLES

Table 1. Imagery used in the analysis.....	27
Table 2. Final endmembers used for the 2-, 3-, and 4-endmember run in each Area.....	36
Table 3. Mortality presence and absence sample points in each pre-drought GV cover category and overall for each of the four Areas.....	44
Table 4. Variables retained after statistical preprocessing.....	55
Table 5. Variables groupings used in models.....	57
Table 6. Accuracy of MESMA GV estimates.....	66
Table 7. Within-plot heterogeneity: training vs. testing points.....	66
Table 8. Top 10 variables by mean decrease in accuracy (random forest).....	81
Table 9. Accuracy of mortality prediction maps (validation dataset).....	101
Table 10. Accuracy of BCfin (analysis dataset).....	101

LIST OF FIGURES

Figure 1. Distribution of pinyon-juniper woodlands in the Southwestern U.S., as mapped by the Southwest Regional Gap Analysis Project (SWReGAP) (Lowry et al. 2005)	3
Figure 2. Influence of topography on microsite conditions.	13
Figure 3. Left: general location of the study area within the state. Right: names and locations of the individual study areas. World Topo Basemap Sources: Esri, DeLorme, HERE, TomTom, Intermap, increment P Corp., GEBCO, USGS, FAO, NPS, NRCAN, GeoBase, IGN, Kadaster NL, Ordnance Survey, Esri Japan, METI, Esri China (Hong Kong), swisstopo, MapmyIndia, and the GIS User Community.....	22
Figure 4. Flowchart of methods.....	26
Figure 5. From left to right, examples of (A) low, (B) medium, and (C) high cover plots.	38
Figure 6. Accuracy assessment plot transects.....	39
Figure 7. Observed vs. predicted green vegetation values.	67
Figure 8. Abundance of green vegetation in 2000, as modeled by MESMA.....	69
Figure 9. Abundance of green vegetation in 2005, as modeled by MESMA.....	70
Figure 10. Absolute change in vegetation cover from 2000 to 2005, based on MESMA results. 71	
Figure 11. Percent change in vegetation cover from 2000 to 2005, based on MESMA results. . 72	
Figure 12. Area 1, all models ranked by balanced overall accuracy. RF = random forest, LR = logistic regression, ctree = conditional inference tree.	77
Figure 13. Area 2, all models ranked by balanced overall accuracy. RF = random forest, LR = logistic regression, ctree = conditional inference tree.	78
Figure 14. Area 3, all models ranked by balanced overall accuracy. RF = random forest, LR = logistic regression, ctree = conditional inference tree.	79
Figure 15. Area 4, all models ranked by balanced overall accuracy. RF = random forest, LR = logistic regression, ctree = conditional inference tree.	80
Figure 16. Area 1, variable importance in random forest models.	83
Figure 17. Area 2, variable importance in random forest models.	84
Figure 18. Area 3 variable importance in random forest models	85
Figure 19. Area 4, variable importance in random forest models.	86
Figure 20. All areas combined, variable importance in random forest models.	87

Figure 21. Direction of the relationship between the variables identified in Table 9 and tree mortality, as indicated by the sign of the coefficient across all or the majority (where results were inconsistent) of logistic regression models run in each Area.....	88
Figure 22. Significance of the relationship between variables and tree mortality in logistic regression models for Area 1. Results presented are for the ten variables identified from random forest in Table 9.....	89
Figure 23. Significance of the relationship between variables and tree mortality in logistic regression models for Area 2. Results presented are for the ten variables identified from random forest in Table 9.....	90
Figure 24. Significance of the relationship between variables and tree mortality in logistic regression models for Area 3. Results presented are for the ten variables identified from random forest in Table 9.....	90
Figure 25. Significance of the relationship between variables and tree mortality in logistic regression models for Area 4. Results presented are for the ten variables identified from random forest in Table 9.....	91
Figure 26. Significance of the relationship between variables and tree mortality in logistic regression models, aggregated across all four Areas. Results presented are for the ten variables identified from random forest in Table 9.....	91
Figure 27. Area 1, univariate conditional inference tree. Cross-validated overall accuracy = 77.8 percent. Backtransformed value: 0.705 represents an isothermality value of 346.....	98
Figure 28. Area 2, univariate conditional inference tree. Cross-validated overall accuracy = 74.8 percent. Backtransformed value: 0.705 represents an isothermality value of 346.....	98
Figure 29. Area 3, univariate conditional inference tree. Cross-validated overall accuracy = 57 percent. Backtransformed value: 0.553 represents a temperature of -6.8 °C.....	99
Figure 30. Area 4, univariate conditional inference tree. Cross-validated overall accuracy = 61.9 percent. Backtransformed value: -0.42 represents an isothermality value of 339.....	99
Figure 31. BCfin predicted presence of mortality.	102
Figure 32. BCfin predicted probability of mortality.....	103
Figure 33. BCfin areas of misclassification.	104

LIST OF ABBREVIATIONS

Acronym	Definition
ASI	Italian Space Agency
AWC	Available water capacity
BLM	U.S. Department of the Interior Bureau of Land Management
CART	Classification and regression tree
CHELSA	Climatologies at high resolution for the earth's land surface areas
CIR	Color infrared
CO	Coarse (soil texture)
ctree	Conditional inference tree
DEM	Digital elevation model
DLR	German Aerospace Center
EAR	Endmember average root mean squared error
ELC	Empirical line calibration
ENVI	Harris Geospatial Solutions' Environment for Visualizing Images
F	Fine (soil texture)
FAO	Food and Agriculture Organization of the United Nations
FDSI	Forest Drought Stress Index
GIS	Geographic information systems
GloVis	USGS Global Visualization Viewer
GV	Green vegetation
IDS	Insect and disease survey
JHU	John Hopkins University
JPL	Jet Propulsion Laboratory
LOGIC	Land Office Geographic Information Center
LR	Logistic regression
M	Moderate (soil texture)
MAE	Mean average error
MCO	Moderately coarse (soil texture)
MESMA	Multiple Endmember Spectral Mixture Analysis

MF	Moderately fine (soil texture)
NASA	National Aeronautics and Space Administration
NDMI	Normalized Difference Moisture Index
NDVI	Normalized Difference Vegetation Index
NHD	National Hydrography Dataset
NIMA	National Imagery and Mapping Agency
NIR	Near infrared
NM	New Mexico
NPV	Non-photosynthetic vegetation
NRCS	U.S. Department of Agriculture Natural Resources Conservation Service
OOB	Out of bag
PAW	Plant available water
PPI	Pixel Purity Index
R ²	Coefficient of determination
RF	Random forest
RGB	Red-green-blue (natural color)
RMSE	Root mean squared error
SLO	State Land Office
SMACC	Sequential Maximum Angle Convex Cone
SRTM	Shuttle Radar Topography Mission
SSURGO	Soil Survey Geographic Database
SWIR	Short-wave infrared
TIGER	Topologically Integrated Geographic Encoding and Referencing
TM	Thematic Mapper
USFS	United States Forest Service
USGS	United States Geological Survey
VIF	Variance inflation factor
VIPER	Visualization and Image Processing for Environmental Research
VPD	Vapor pressure deficit

1. Introduction

Pinyon-juniper woodlands, composed of the co-dominant species pinyon pine (*Pinus edulis*, *Pinus monophylla*, *Pinus* spp.) and one or more species of juniper (*Juniperus* spp.), represent the third largest vegetation type in the United States and an important vegetation type for wildlife (Finch and Ruggiero 1993; Gottfried and Severson 1994; Paulin, Cook, and Dewey 1999; Chung-MacCoubrey 2005; Mueller et al. 2005) and humans (Gottfried and Severson 1994; Albert et al. 2004; Clifford et al. 2008; Floyd et al. 2009) in the Southwest. Circa the year 2002, the pinyon pine component of these woodlands in portions of the Southwest experienced widespread mortality (Breshears et al. 2005; Mueller et al. 2005; Shaw, Steed, and DeBlander 2005). The mortality event has been attributed to a combination of drought and an outbreak of *Ips confusus* (pinyon ips) bark beetle (Shaw, Steed, and DeBlander 2005; McDowell et al. 2013), which seem to preferentially attack stressed trees (Negrón and Wilson 2003; Raffa et al. 2008). According to Breshears et al. (2005), we can expect droughts such as the one that occurred in the early 2000s to become more frequent in the future under our changing climate.

Due to the valuable ecosystem services that forests and woodlands provide, predicting and explaining future die-off events is of great importance to land managers (Breshears et al. 2018). Much research and attention has already been directed to gaining a better understanding of the aforementioned pinyon pine mortality event (Breshears et al. 2018); however, there are aspects which are still poorly understood and warrant further study, including the role of bark beetles and the relationship of elevation and tree stem density (Meddens et al. 2015). Of particular relevance to this study, Meddens et al. (2015) noted that previous studies of drought-related pinyon mortality often included only a subset of potential

explanatory variables, and they recommend that future studies include a broader range of such variables. The current study examines the relationship between tree mortality during the drought which occurred in the early 2000s and a range of topographic, edaphic, climatic, and land use variables at the landscape-scale in four study sites in north-central New Mexico.

My objectives were to 1) map pinyon mortality across four study areas in north-central New Mexico at 30 m spatial resolution; 2) evaluate random forest, logistic regression, and conditional inference trees for their suitability to predict tree mortality, and 3) isolate the variables that have the greatest explanatory power for tree mortality. The findings of this study add to the body of knowledge regarding the spatial distribution and underlying factors of drought- and insect-related pinyon juniper woodland mortality, and may help inform forest management decisions.

2. Background

Pinyon juniper woodlands (Figure 1) are estimated to cover approximately 225,000 km² of land in the western U.S. (Huffman et al. 2008); they are both a dominant (Gottfried and Severson 1994; Huffman et al. 2008) and an important vegetation type in the Southwestern U.S. (Floyd et al. 2009). Ecologically, pinyon juniper woodlands offer important habitat, food, and/or breeding grounds to a diversity of species (Gottfried and Severson 1994; Paulin, Cook, and Dewey 1999; Chung-MacCoubrey 2005; Mueller et al. 2005), including at least 107 species of birds, 62 species of mammals, an assortment of reptiles (Finch and Ruggiero 1993), and around 600 microbial species that are associated with pinyon roots (Whitham et al. 2003). Economically,

pine nuts, produced by the pinyon pine (*Pinus spp.*), are a valuable cash crop (Gottfried and Severson 1994). From a cultural standpoint, these trees are important to several Native American tribes (Negrón and Wilson 2003; Clifford et al. 2008). Pinyon and juniper trees also offer a local supply of firewood (Albert et al. 2004), are harvested for holiday trees (Ffolliott et al. 1992), and have aesthetic value on the landscape (Floyd et al. 2009).

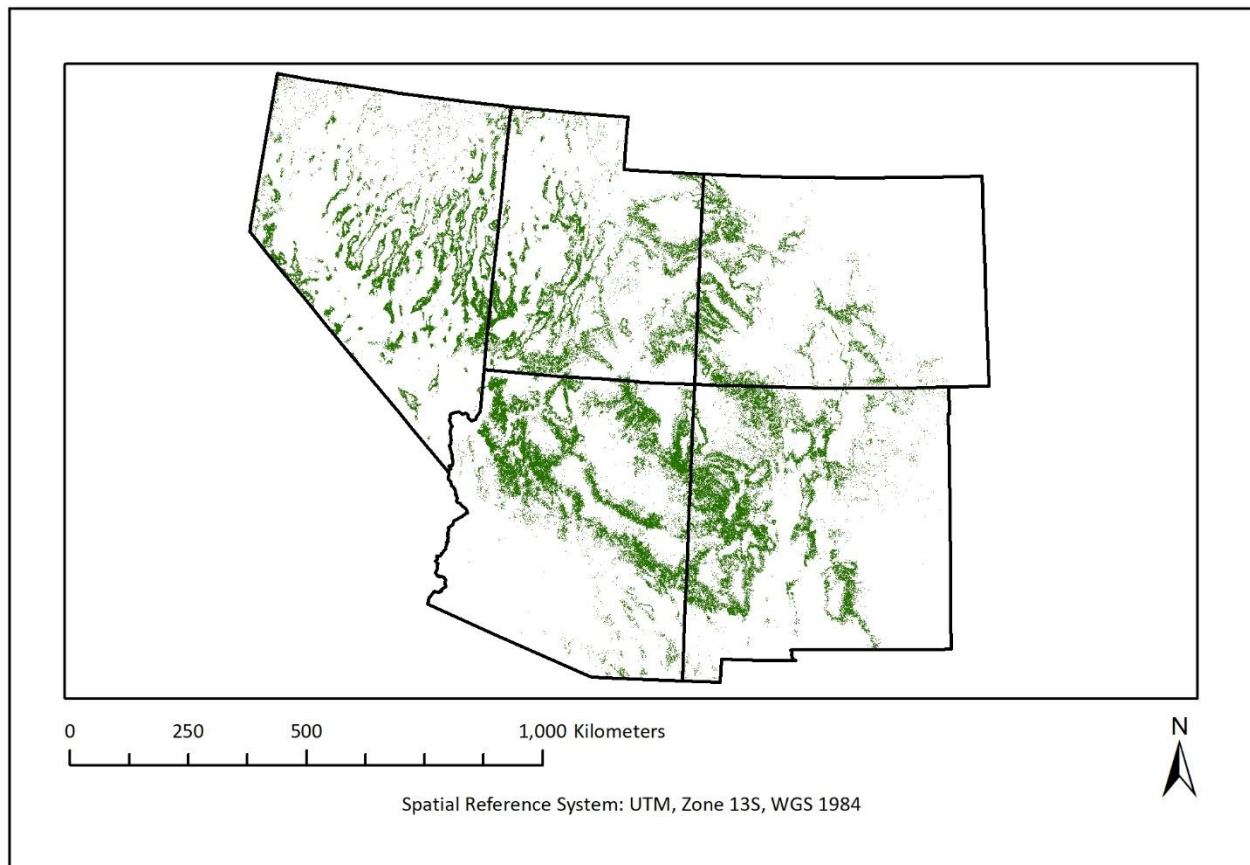


Figure 1. Distribution of pinyon-juniper woodlands in the Southwestern U.S., as mapped by the Southwest Regional Gap Analysis Project (SWReGAP) (Lowry et al. 2005)

Given all this, abrupt widespread mortality of pinyon-juniper woodlands is concerning. In the years spanning 2000-2003, a die-off event affecting an area of more than 12,000 km² occurred among the pinyon pine component of these woodlands (Breshears et al. 2005; Kleinman et al. 2012). This event had impacts on fire dynamics (Clifford et al. 2008; Progar,

Eglitis, and Lundquist 2009; Guardiola-Claramonte et al. 2011; Adams et al. 2012, 212), ecohydrology (Royer et al. 2010; Guardiola-Claramonte et al. 2011; Adams et al. 2012), and above-ground live carbon stocks (Huang et al. 2010), to name just a few.

The sudden increase in dead trees led to altered fire dynamics (Clifford et al. 2008) and elevated fuel loads in areas of high mortality (Clifford et al. 2008; Progar, Eglitis, and Lundquist 2009). In the years following the mortality event, several stand-replacing fires occurred in these areas (Progar, Eglitis, and Lundquist 2009). Heavy tree mortality has the potential to alter fire dynamics not only through increased standing fuel from dead trees, but also through processes such as the release of understory species, potential for high-density recruitment of young trees, and increased forest-floor litter (Adams et al. 2012). Wildfire can in turn increase the potential for soil erosion and affect hydrologic functioning beyond the changes already noted by Guardiola-Claramonte et al. (2011), who observed a decrease in basin wide water yield following the mortality event.

Large scale tree mortality also alters hydrology by changing the amounts of evaporation, transpiration, and precipitation interception taking place at a site (Adams et al. 2012). The results of these changes can alter streamflow in affected basins, although the exact outcome can be highly variable based on site conditions (Adams et al. 2012). Despite the substantial loss of actively transpiring trees from affected areas, a study of hydrologic impacts in four mortality-affected basins noted a decrease, rather than the expected increase, in water yield from the basin that could not be attributed to climatic variations (Guardiola-Claramonte et al. 2011). The authors suggest that the cause may be related to an increase in understory vegetation resulting in higher net transpiration and interrupting overland flow, possibly coupled with increased soil

evaporation (Guardiola-Claramonte et al. 2011) due to more incoming solar radiation reaching the ground surface (Royer et al. 2010).

Extensive forest and woodland mortality events have the potential to convert areas that were carbon sinks into carbon sources by reducing net primary production and at the same time increasing heterotrophic respiration as killed trees decay (Kurz et al. 2008; Hicke et al. 2013). In some cases, it may take years or decades for the affected area to recover (Huang et al. 2010; Hicke et al. 2013). In a study of the pinyon-juniper woodlands of southwestern Colorado, for a time period spanning 2000-2005, Huang et. al (2010) revealed that the loss of above-ground live carbon stocks due to bark beetle kills was 39 times greater than that of other disturbances such as wildfire and anthropogenic activities during the same time period. Hicke et al. (2013) similarly found in an analysis of forests (not limited to pinyon-juniper) in the western U.S. that bark beetles accounted for more killed live carbon biomass than fire, although in their study they concluded that forest harvesting accounted for slightly more than insects and fire combined. Given current climate projections, however, fires and insect outbreaks may become more severe and will likely continue to substantially affect the carbon budget associated with forest and woodland areas (Hicke et al. 2013).

The widespread pinyon mortality seen in the early 2000s drought has been attributed largely to the interacting factors of drought conditions and a co-occurring infestation by pinyon ips bark beetles (Shaw, Steed, and DeBlander 2005; McDowell et al. 2013). Severe drought stress, however, is known to predispose a tree to subsequent insect infestation (Mattson and Haack 1987; Raffa et al. 2008; Santos and Whitham 2010; Gaylord et al. 2013) and Meddens et al. (2015) note that at times it may be difficult to separate the effects of drought from the

effects of bark beetles when evaluating the impacts on mortality. It is also interesting to note that according to Mueller et al. (2005), a severe drought also occurred in parts of the Southwest in 1996 that also resulted in high pinyon mortality, although no corresponding bark beetle outbreak was reported in association with that event (Mueller et al. 2005). Due to the difficulty in separating the effects of drought vs. bark beetle infestation on mortality, the two were considered collectively in this study, although much of the pinyon mortality within my study area was officially recorded by USFS Insect and Disease Surveys as being due to pinyon ips attack. Other authors (e.g., Clifford, Cobb, and Buenemann 2011) have noted that, in the case of the 2000s drought, trees killed by pinyon ips damage were still considered to be indirectly drought-related mortality.

Some have referred to the 2000-2003 drought as a “global change-type drought” (Breshears et al. 2009) and suggested that we might expect to see such droughts with increasing frequency in the future under our changing climate (Breshears et al. 2005). By the end of the 21st century, global mean surface temperature is expected to increase, relative to 1986-2005, anywhere from 0.3°C (low end of the most optimistic emissions model RPC2.6) to 4.8°C (high end of the more pessimistic RCP8.5 model) (Pachauri, Mayer, and Intergovernmental Panel on Climate Change 2015). In the Southwestern U.S., aridity is expected to increase substantially (Seager et al. 2007). In an ensemble of 19 different climate prediction models evaluated in a study by Seager et al. (2007), only one indicated a predicted shift toward slightly wetter conditions by the end of the 21st century.

Severe droughts have occurred in this region of the southwestern U.S. in the past; however, in a study comparing pinyon pine mortality during two notable periods of drought in

the Southwest (1953-1956; 2000-2003), Breshears et al. (2005) found that, although the 1950s drought was somewhat drier, the early 2000s drought was warmer and associated with higher mortality than the 1950s drought at the studied sites in Utah, Colorado, Arizona, and New Mexico. Weiss, Castro, and Overpeck (2009) also observed that the early 2000s drought was generally (with some variation by region) wetter but warmer than the 1950s drought, which may have resulted in greater vegetation water stress.

The mortality event that occurred primarily in 2002 generated considerable activity in the published literature (discussed below), and as a result there is much that we now know about drought-related pinyon mortality, which some authors (Meddens et al. 2015; Breshears et al. 2018) have distilled neatly in short synthesis articles that summarize the studies that have been done to date on the subject. However, by way of introduction to the general classes of variables, a brief summary of relevant research is presented below.

2.1 The physiology of drought-related pinyon mortality

From a physiological standpoint, the exact mechanics of drought-related pinyon mortality are not yet perfectly understood (Breshears et al. 2013; Plaut et al. 2013) despite fairly extensive study (e.g., West et al. 2008; Plaut et al. 2012, 2013; Adams et al. 2013; Anderegg and Anderegg 2013; Limousin et al. 2013; Dickman et al. 2015). Some (McDowell et al. 2008, 2011; Breshears et al. 2009; Adams et al. 2013; Dickman et al. 2015) suggested, however, that carbon starvation as a result of stomatal closure for extended periods of time may play a role, although hydraulic failure (Anderegg and Anderegg 2013) or some combination of these mechanisms has also been hypothesized (McDowell et al. 2008, 2011). Since pinyon trees are isohydric, the tree relies on

stomatal closure to maintain a constant midday leaf-water potential by regulating gas exchange and water lost through respiration (Breshears et al. 2009). This helps the tree survive in a water-scarce environment by preventing catastrophic xylem cavitation when soil water potential is low but atmospheric demands are high (McDowell et al. 2008; Breshears et al. 2009; Plaut et al. 2012); however, it also prevents carbon assimilation as no photosynthesis is taking place (McDowell et al. 2008; Breshears et al. 2009; Limousin et al. 2013). Researchers have shown that trees can recover from relatively short periods [e.g., 2 (Plaut et al. 2012) to 4 (Breshears et al. 2009) months], of near-zero carbon assimilation (Breshears et al. 2009; Plaut et al. 2012); however, if stomatal closure continues for extended periods of time [e.g., 7 (Plaut et al. 2012) to 10 (Breshears et al. 2009) months], the tree may use up all its carbon reserves and be at risk for death from carbon starvation or inability to withstand other stressors such as insect attack (Breshears et al. 2009). My study does not address tree physiological responses directly, but instead focuses on predicting mortality from observable environmental and management-related variables.

2.2 Genetics

There has been some interest in the possible effect of genetics or phenotype on drought related mortality. Specifically, pinyon trees resistant to stem-boring moth seem to have higher mortality, suggesting that resistance to one type of pest might come at the expense of increased susceptibility to another (Santos and Whitham 2010; Breshears et al. 2018). Some researchers have also observed that pinyon trees with higher climate sensitivity, inferred from

higher interannual variability in tree ring growth, are more prone to mortality during severe drought (Ogle, Whitham, and Cobb 2000; Macalady and Bugmann 2014).

2.3 Stand density and tree size

Higher tree density has been suggested as a contributor to drought-related mortality, both because of the effects of competition (Meddens et al. 2015), and because it creates a more favorable condition for bark beetle dispersal (Negrón and Wilson 2003; Raffa et al. 2008; Santos and Whitham 2010). The results of studies which examined this dynamic, however, have been mixed (Meddens et al. 2015). In a study unrelated to the 2000-2003 mortality event, higher stand density was correlated with higher probability of ips infestation (Negrón and Wilson 2003), yet several studies that examined tree mortality patterns associated with the 2000-2003 drought in relation to stand density found either weak (Macalady and Bugmann 2014) to no correlation (Clifford et al. 2008; Clifford, Cobb, and Buenemann 2011; Ganey and Vojta 2011), or a slightly negative correlation (Floyd et al. 2009; Clifford et al. 2013). Greenwood and Weisberg (2008), by contrast, found a scale-dependent (stronger at coarser scales) positive correlation between stand density and crown mortality in their Nevada study area. It has also been noticed that larger trees are more likely to die than smaller trees and that reproductive trees have higher mortality than non-reproductive ones (Mueller et al. 2005). Mueller et al. (2005) postulate that this may be related to the higher carbon cost associated with reproduction. Yet others (Negrón and Wilson 2003; Santos and Whitham 2010) have suggested this has to do with larger diameter trees being a better and thus preferred food source for pinyon ips.

2.4 Microsites

Mueller et al (2005) note that, prior to the 2002 mortality event, a severe drought in 1996 resulted in mortality within pinyon juniper woodlands, and that locations within their study area with high mortality in 1996 also had the highest mortality in 2002, suggesting a relationship between certain conditions at these locations and vulnerability to drought-related mortality (Mueller et al. 2005). Mueller et al. (2005) also note that, while bark beetle outbreaks are largely blamed for contributing to the 2002 die-off, 1996 saw some pinyon mortality as high as 70% yet no associated bark beetle outbreak was recorded. They also observe that, although the 1996 mortality reduced competition for water and nutrients among the remaining live trees at those sites, this did not seem to ward off additional mortality in the 2000s event. Gitlin et al. (2006) caution that developing models based only on climatic variables that generalize across large areas may miss many of the site-related nuances of mortality or survival, as their results indicated that mortality was highly variable and patchy across their study area.

2.5 Historic range

In considering pinyon mortality in association with severe but historically infrequent droughts such as the one in 2000-2003, there has been some interest in the influence of long-term site suitability on the observed mortality. Some have suggested that trees most susceptible to mortality were those growing on suboptimal sites to begin with (Greenwood and Weisberg 2008). At the regional level, however, studies have indicated that mortality was actually highest within the traditional ranges of pinyon-juniper woodlands (Kleinman et al. 2012) and in the areas of the highest historic habitat suitability (Lloret and Kitzberger 2018). One suggested

explanation for this is that trees growing at the edges of the suitability envelope may be better adapted to withstand sub-optimal conditions (Lloret and Kitzberger 2018). While further study may be needed to disentangle these dynamics, there is some evidence that trees have a certain amount of plasticity to adapt to higher or lower water conditions (Hacke et al. 2000; Limousin et al. 2013).

2.6 Climatic variables

Precipitation, temperature, and evapotranspiration demands may be the most obvious place to begin looking when examining possible drivers of drought-related mortality. The literature suggests that they indeed can explain some, though not all, of the mortality associated with the early 2000s drought period. Clifford et al. (2013) found a threshold of 600 mm cumulative 2002-2003 precipitation above which very few trees died and below which results were highly variable but included high possibility of mortality. There are some limited data to suggest that increased temperature can also hasten mortality in drought-stressed trees (Adams et al. 2009, 2013); however, most studies that examined temperature in relation to drought-related pinyon mortality (Breshears et al. 2005; Weiss, Castro, and Overpeck 2009; Weiss, Betancourt, and Overpeck 2012; Clifford et al. 2013; Williams et al. 2013, but see Dickman et al. 2015) have focused on the influence of higher temperatures on higher atmospheric moisture demand, often expressed as vapor pressure deficit (VPD). Clifford et al. (2013) identified a VPD threshold of 1.7 kPa, which marked the partition between very low mortality and highly variable mortality. Williams et al. (2013) used extensive tree-ring data to devise a Forest Drought Stress Index (FDSI) which combined warm season VPD with cool season precipitation and accounted

for 82% of the variability in their tree-ring-derived FDSI, correlated strongly with satellite derived Normalized Difference Vegetation Index (NDVI), and correlated also with the mortality associated with the early 2000s drought. The authors caution, however, that more data are needed to confirm the relationship between FDSI and bark beetle outbreak as there may also be other unaccounted-for factors involved, such as stand characteristics and temperature effects on bark beetle populations. Huang et al. (2015) similarly used tree ring growth and precipitation information to calculate a tipping point of no growth after ~11 months of drought, and found that their calculated tipping point value—based on ring width index and standardized precipitation evapotranspiration index—performed well in partitioning areas of little mortality with areas of differential mortality in 2002 at the regional scale.

2.7 Topographic variables

Topography influences site conditions in a number of ways (Figure 2). South-facing slopes, for instance, are often more droughty than north-facing slopes in the same general location (Strahler and Strahler 2006). Slope steepness and slope curvature can both affect how quickly water leaves a site by runoff, which has an effect on how much or how little water infiltrates following a precipitation event (Strahler and Strahler 2006). Elevation can influence both temperature and moisture, and local relief tends to influence the likelihood of receiving rainfall run-on from other areas (Strahler and Strahler 2006).

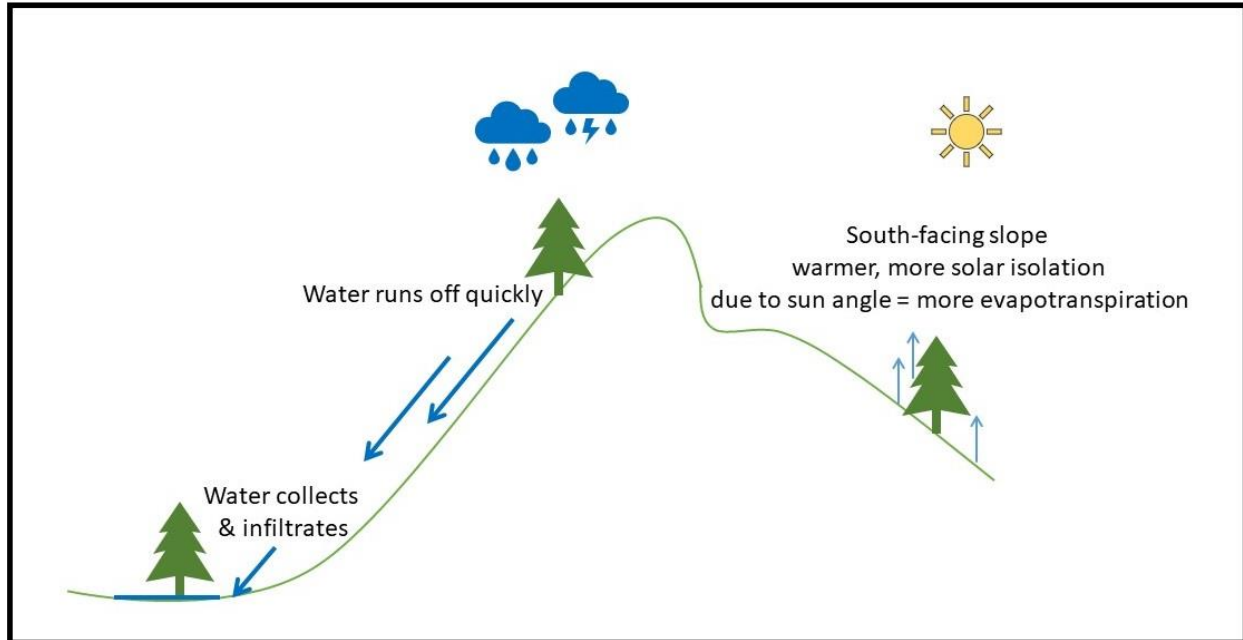


Figure 2. Influence of topography on microsite conditions.

Despite this, mortality patterns in relation to topography have generally yielded mixed results depending on the study. Breshears et al. (2005), in comparing the 2002 drought to the historic drought of the 1950s found that, although in the 1950s drought the highest mortality was at lower elevations, during the 2002 drought, the highest mortality was found in the higher (and typically wetter) elevations. In a region-wide study, Kleinman et al. (2012) similarly found that as elevation increased, so did damage intensity, although they cautioned that, due to limitations of their source data, this finding was based on absolute numbers of trees killed per acre and not a percentage of what was there to begin with. In contrast, Santos and Whitham (2010) found that probability of pinyon ips attack increases at lower elevations, likely due to increased water-stress (Santos and Whitham 2010). Others (Ganey and Vojta 2011; Clifford et al. 2013) found no relationship between elevation and tree mortality, although it should be

noted that Ganey and Vojta (2011) carried out their study on mixed conifers (which included pinyon pine) and ponderosa, not pinyon juniper woodlands. Weiss, Betancourt, and Overpeck (2012) found that most mortality occurred between 1500 m and 3500 m. Interestingly, they also note that the 1950s drought, to which the 2000s drought is often compared, was centered more over Mexico and the southeastern parts of the southwestern U.S. region, whereas the 2000s one was centered more northward and over different terrain. Studies involving comparisons of local topography have shown more agreement – drought-related pinyon mortality has been found to be higher on south-facing slopes (Ogle, Whitham, and Cobb 2000; Gitlin et al. 2006), steeper slopes (Greenwood and Weisberg 2008; Santos and Whitham 2010), and lower slope positions (Greenwood and Weisberg 2008).

2.8 Edaphic variables

Several studies have examined the effects of various soil properties on drought-related tree mortality. Collectively, these studies have explored the relationship of mortality to soil available water holding capacity (AWC) (Clifford et al. 2013; Peterman et al. 2013), soil texture and/or parent material (Ogle, Whitham, and Cobb 2000; Moore et al. 2004; Gitlin et al. 2006; Greenwood and Weisberg 2008; Koepke, Kolb, and Adams 2010; Bowker et al. 2012; Looney et al. 2012), geologic age (Floyd et al. 2009; Looney et al. 2012), soil depth (Gitlin et al. 2006; Greenwood and Weisberg 2008; Floyd et al. 2009), pH (Greenwood and Weisberg 2008), and spatial distribution of plant available water (Breshears, Myers, and Barnes 2009). I do not include in this list the studies that have made direct soil moisture/water potential

measurements to better understand hydraulic and metabolic functioning of pinyon pines under drought stress, as their focus was not on examining the soil properties involved.

Soil parent material, texture, and AWC are highly interrelated, as parent material influences texture, which in turn largely determines AWC (Petersen, Sack, and Gabler 2015). For this reason, I discuss them together here. The most broad-scale study of AWC comes from Peterman et al. (2013) who evaluated AWC and soil texture in relation to mortality across the affected region spanning four states and found that the majority of the reported mortality occurred on soils with <150 mm of AWC, with ~70% occurring on soils with an AWC <100 mm. A subsequent study (Clifford et al. 2013) done at a much finer scale, however, found that mortality was highly variable across all AWC levels, including those in the highest AWC class used by Peterman et al. (2013). Rather than directly calculating AWC, relatively more studies have looked at the influence of texture.

Soil-water relations in arid environments can be somewhat complex (Noy-Meir 1973). Despite finer textured soils having the capacity to hold a greater amount of soil moisture per unit volume than coarse textured soils, data indicate that in water-scarce environments, coarser textured soils may actually be more productive than finer-textured loamy soils; this is known as the “inverse texture effect” (Noy-Meir 1973; Sala et al. 1988; Looney et al. 2012). This may be due to better water infiltration and deeper percolation in coarser textured soils (Sala et al. 1988; Looney et al. 2012), coupled with weaker matric forces than typically encountered in clayey soils (Bowker et al. 2012; Looney et al. 2012). A coarse or rocky surface texture can also have an effect similar to a mulch by reducing water lost to evaporation from the soil surface (Noy-Meir 1973; Bowker et al. 2012).

In general agreement with the proposed advantages of coarser textured soils, several studies (Ogle, Whitham, and Cobb 2000; Bowker et al. 2012) found mortality to be higher on the comparatively finer textured soils relative to coarse textured soils with otherwise similar conditions, although Ogle, Whitham, and Cobb (2000) also describe growth to be highest on the finer textured loamy soils. Gitlin et al. (2006) similarly observed higher mortality among one-seed juniper in finer textured soils vs. coarser cinder-derived soils; however, they do also note that there was a lack of grass on the coarser soils, which may have reduced competitive stress. By contrast, Koepke, Kolb, and Adams (2010) found little difference in mortality across soils of three different parent material types and textures, although canopy dieback indicating water stress was highest at the sites with coarser texture. Greenwood and Weisberg (2008) also found at their study site in Nevada that pinyon mortality was higher on more acidic soils with low clay content and lower slope position. Incidentally, this was also the only study I have encountered that examined the role of pH. In a loosely related study regarding parent material, Moore et al. (2004) found that general mortality among several tree species differed substantially by rock type for some, but not all, of the studied species in the inland northwest; however, they hypothesize that this was in relation to nutrients available from the different rock types.

Geologic age, which influences both texture and nutrient availability (Looney et al. 2012), has also been examined for its correlation with drought stress and resultant tree mortality. In a study comparing the effects of geologic age on a chronosequence in Arizona of cinder-derived substrate and artificial water manipulations, the authors found that substrate age had a larger effect on pinyon growth than supplemental watering. They also note that tree growth dynamics and water response supported the aforementioned inverse texture effect

(Noy-Meir 1973). Unexpectedly, pinyon mortality was greatest at sites of intermediate soil age, which should have had the best combination of medium texture and adequate nutrient pool; however, since growth in those plots was also higher, the authors hypothesized that competition may have been greater there (Looney et al. 2012). Floyd et al. (2009), by contrast, note that they found no significant correlation between soil geologic age and mortality at their Colorado study site, but provided few other details enlarging on this finding.

Regarding soil depth, a few studies have examined this but their results have been somewhat less informative than those of other soil properties. Gitlin et al. (2006) found that pinyon mortality was substantially higher in red cinder shallow soils than in black cinder deep soils; however, the influence of the differing parent materials between these two soil types is unknown as they did not report if they investigated that. Greenwood and Weisberg (2008) included soil depth as an initial variable for their models of tree mortality but did not interpret their findings in relation to this variable. Finally, Floyd et al. (2009) reported no significant correlation between soil depth and mortality at a Colorado study site, but provided few other details.

Heterogeneity of plant available soil water (PAW) across space and depth has been documented at the patch level. Breshears, Myers, and Barnes (2009), quantified soil water at multiple depths for sites under tree canopies, at canopy edges, and in intercanopy spaces. Water was shown to be more frequently available near the surface beneath canopies vs. deeper in the profile at intercanopy locations; however, in severe drought years, this heterogeneity was reduced as plant available water became far less frequently available in all depths and locations. Plaut et al. (2012) reported in their study that involved making direct soil

moisture observations in regard to hydraulic function, that the measured leaf water potentials at several times indicated that trees were drawing water from a wetter layer below the depth of the deepest installed sensors (~100 cm), thus indicating the presence and utilization of deep soil water.

Finally, in a study unrelated to pinyon pine but still relevant, (Hacke et al. 2000) found that addition of fertilizer to loblolly pine (*Pinus taeda* L.) trees decreased their overall root mass percentage and water extraction potential, thus potentially putting them at higher risk for drought-related dieback than those growing in otherwise similar conditions on a poorer nutrient supply.

2.9 Grazing and management

Although I could find no studies which expressly examined the influence of grazing or management practices on mortality during the 2000s drought, there is evidence that grazing may suppress grasses and thus decrease competition for water and nutrients (Harris, Asner, and Miller 2003; Romme et al. 2009; Shinneman and Baker 2009), which could conceivably be advantageous to trees under drought stress. Other management practices, such as tree thinning, controlled burns, or fire suppression, while not considered individually in this study, may also have an influence on both stand and understory dynamics (Hartsell et al. 2020).

2.10 Scale and extent of previous studies

The scale and geographical extent of studies on the 2000s pinyon mortality event varies. I found fifteen studies that examined drought-related pinyon or pinyon-juniper mortality in the

Southwest during the early 2000s time period. Of these, five studies were conducted at the regional level, encompassing parts of all four states in which the bulk of the mortality occurred (Breshears et al. 2005; Weiss, Castro, and Overpeck 2009; Kleinman et al. 2012; Peterman et al. 2013; Lloret and Kitzberger 2018). Four studies were conducted at the landscape scale, examining a sizeable sub-section of the affected area (Gitlin et al. 2006; Huang et al. 2010; Clifford, Cobb, and Buenemann 2011; Clifford et al. 2013). Three studies were stand- or plot-level analyses (Mueller et al. 2005; Clifford et al. 2008; Floyd et al. 2009). Three studies were at the individual tree level (Breshears et al. 2009; Koepke, Kolb, and Adams 2010; Macalady and Bugmann 2014). Additionally, Clifford et al. (2008) and Breshears et al. (2005) took a hybrid approach, gathering extremely detailed site conditions data at the plot or microsite scale and using them to assist interpretations of the regional-scale observed mortality.

Of the studies listed above, four took place in Arizona (Mueller et al. 2005; Gitlin et al. 2006; Koepke, Kolb, and Adams 2010; Clifford, Cobb, and Buenemann 2011), three in New Mexico (Breshears et al. 2009; Clifford et al. 2013; Macalady and Bugmann 2014), one in Colorado (Huang et al. 2010), and seven across multiple states (Breshears et al. 2005; Clifford et al. 2008; Floyd et al. 2009; Weiss, Castro, and Overpeck 2009; Kleinman et al. 2012; Peterman et al. 2013; Lloret and Kitzberger 2018). This count does not include studies conducted on the after-effects of the mortality, such as hydrologic effects, understory response, or juvenile recruitment. Additionally, as referenced above, numerous other studies examined drought-related drivers and mechanisms of pinyon mortality in the 2000s in the southwestern U.S.

3. Methods

The study was conducted on a landscape level, in a study area carefully chosen to be representative of varying degrees of pinyon mortality (ranging light to heavy). Pinyon mortality was first mapped at a fine spatial resolution, then assessed, and finally modeled using the models and potential explanatory variables described in this section.

3.1 Study area description

The general study area is located in north-central New Mexico where substantial pinyon mortality occurred during the early 2000s drought (Breshears et al. 2005; Clifford et al. 2008; USDA Forest Service, Forest Health Protection and its partners 2014). It has a total area of 13,604 km², and the centroid is 35.73863°, -106.00309°. The area is further subdivided into four discrete Areas, hereafter referred to as Area 1, Area 2, Area 3, and Area 4 (Figure 3). The decision to maintain four discrete study Areas rather than one large one was twofold. First, it allows for comparisons between Areas with different environmental and management regimes. Second, it made the image processing feasible for an overall large area at a fine spatial resolution (30 m).

The inner boundaries of the four Areas were delineated roughly along natural breaks in the vegetation or geographic features such as mountain peaks, with attention to U.S. National Forest boundaries so that no Area contains parts of more than one National Forest. To determine the outer boundaries, I first roughly delineated a rectangular area encompassing the bulk of the 2000-2003 pinyon mortality across the region as shown by the USFS Insect and Disease Survey (IDS) shapefiles (USDA Forest Service, Forest Health Protection and its partners

2014). Then, using Southwest Regional Gap Analysis Project (SWReGAP) data (RS/GIS Laboratory, College of Natural Resources, Utah State University 2004) to isolate areas mapped as pinyon-juniper cover type, the data were resampled from 30 m to a coarser resolution of 1,500 m based on majority, and a buffer of 3,000 m was applied to create a roughly continuous study area. To preserve spatial continuity, and as a result of the large buffers used, some areas of land cover that were not pinyon-juniper were included in the initial delineation. This problem was addressed at a later step and is explained at that point. All geoprocessing and analysis for study site selection was done in ArcGIS Desktop 10.5 (Environmental Systems Research Institute, Redlands, CA).

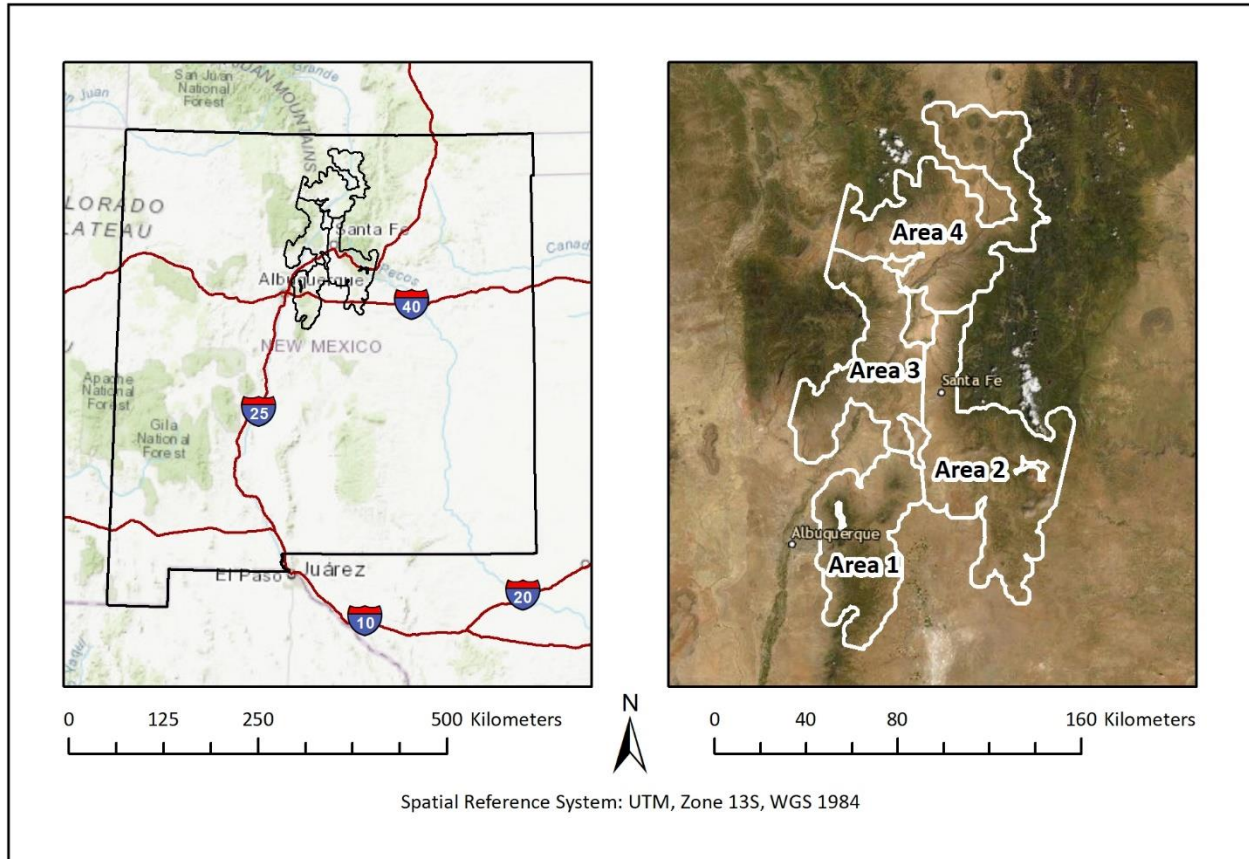


Figure 3. Left: general location of the study area within the state. Right: names and locations of the individual study areas. World Topo Basemap Sources: Esri, DeLorme, HERE, TomTom, Intermap, increment P Corp., GEBCO, USGS, FAO, NPS, NRCAN, GeoBase, IGN, Kadaster NL, Ordnance Survey, Esri Japan, METI, Esri China (Hong Kong), swisstopo, MapmyIndia, and the GIS User Community.

Area 1 encompasses an area of 2,562 km², and has its centroid at 35.09945°, -106.29915° and an elevational range of 1,576 m to 3,248 m (National Aeronautics and Space Administration (NASA), National Imagery and Mapping Agency (NIMA), German Aerospace Center (DLR), and Italian Space Agency (ASI) 2002). Mean annual temperature across the Area ranges between 4.4°C and 13.8°C and total mean annual precipitation ranges from 245 mm to 497 mm per year (Karger et al. 2017b). Both temperature and precipitation follow an elevational gradient, with lower mean annual temperatures and higher annual precipitation occurring at higher elevations. Area 1 is the southernmost study Area and includes a portion of

the Cibola National Forest. According to the IDS data, the pinyon mortality was lower here than in the other three study Areas (USDA Forest Service, Forest Health Protection and its partners 2014).

Area 2 has an area of 4,112 km², and a centroid of 35.41023°, -105.71264°. This Area includes a portion of the Santa Fe National Forest. Elevation in the Area ranges from 1,769 m to 2,892 m (National Aeronautics and Space Administration (NASA), National Imagery and Mapping Agency (NIMA), German Aerospace Center (DLR), and Italian Space Agency (ASI) 2002). Mean annual temperature across the Area ranges between 5.6°C and 12.3°C and annual precipitation ranges from 250 mm to 652 mm per year (Karger et al. 2017b). Mean annual temperature corresponds very closely to elevation in Area 2, with higher temperatures at lower elevations. Precipitation patterns generally follow elevation, with lower precipitation in lower elevation areas, however there are two small portions of Area 2 in the extreme east that appear to receive more annual precipitation than the rest of the Area.

Area 3 has an area of 2,728 km², and a centroid of 35.79419°, -106.308°. Elevation in this Area ranges from 1,570 m to 2,985 m (National Aeronautics and Space Administration (NASA), National Imagery and Mapping Agency (NIMA), German Aerospace Center (DLR), and Italian Space Agency (ASI) 2002). Mean annual temperature across the Area ranges between 5.6°C and 13.6°C and annual precipitation ranges between 220 mm and 497 mm per year (Karger et al. 2017b). Temperature and precipitation both track closely with elevation in this Area, with higher temperatures and lower precipitation occurring at the lower elevations. Area 3 includes part of the Santa Fe National Forest that is geographically separate from the portion

contained in Area 2; a lowland area that is relatively devoid of woodlands separates the two parts of this National forest.

Area 4 has an area of 4,202 km², and a centroid of 36.40371°, -105.91053°. Elevation in the Area ranges from 1,719 m to 3,388 m (National Aeronautics and Space Administration (NASA), National Imagery and Mapping Agency (NIMA), German Aerospace Center (DLR), and Italian Space Agency (ASI) 2002). Mean annual temperature across the Area ranges between 3.1°C and 11.6°C and annual precipitation ranges from 198 mm to 544 mm per year (Karger et al. 2017b). Both temperature and precipitation correspond fairly well with elevation in this Area, with the higher elevations receiving more annual precipitation and cooler temperatures, while the lower elevations are on the warm and dry end of the ranges reported here. Area 4 includes parts of the Cibola National Forest. The IDS data used in site selection indicates that the pinyon mortality in this Area was the most extensive of the four study Areas (USDA Forest Service, Forest Health Protection and its partners 2014).

As one might expect given the collective size of the study area, there exists a fair amount of variety in vegetation types, soils, geology, and topography. Major vegetation types within the four Areas include grassland, shrubland/shrub steppe, scrub, savanna, woodland, and forest, as well as some cropland. Woodland and forest types typical of the area are pinyon-juniper woodland, juniper woodland and savanna, ponderosa pine woodland, limber-bristlecone pine woodland, spruce-fir forest and woodland, aspen forest and woodland, pine-oak forest and woodland, mixed-conifer forest and woodland, and riparian woodland and shrubland (Lowry et al. 2005). Soils in the area are diverse, derived from varying parent materials that include aeolian, alluvial, and glacial deposits as well as igneous, metamorphic,

and sedimentary rock types of varying mineralogy (Stoeser et al. 2005). Topography through the area is varied, but generally gets more rugged and mountainous from south to north and from lower to higher elevations.

3.2 Overview of methods

The ultimate goal of this thesis was to predict and explain pinyon mortality across the four Areas. As described in further detail below, this required integrating data on pinyon mortality locations and data on factors that may drive or impede pinyon mortality in spatial models. Pinyon mortality locations were obtained from remotely sensed imagery; geospatial layers representing explanatory factors were obtained from various public data gateways. All data had to be processed in a series of preparatory sub-tasks, however (Figure 4). In the subsections that follow, I address first all tasks associated with remote sensing imagery acquisition, processing, and mortality mapping; I then shift to the tasks associated with the collection and preparation of potential explanatory variables and the subsequent spatial modeling of mortality.

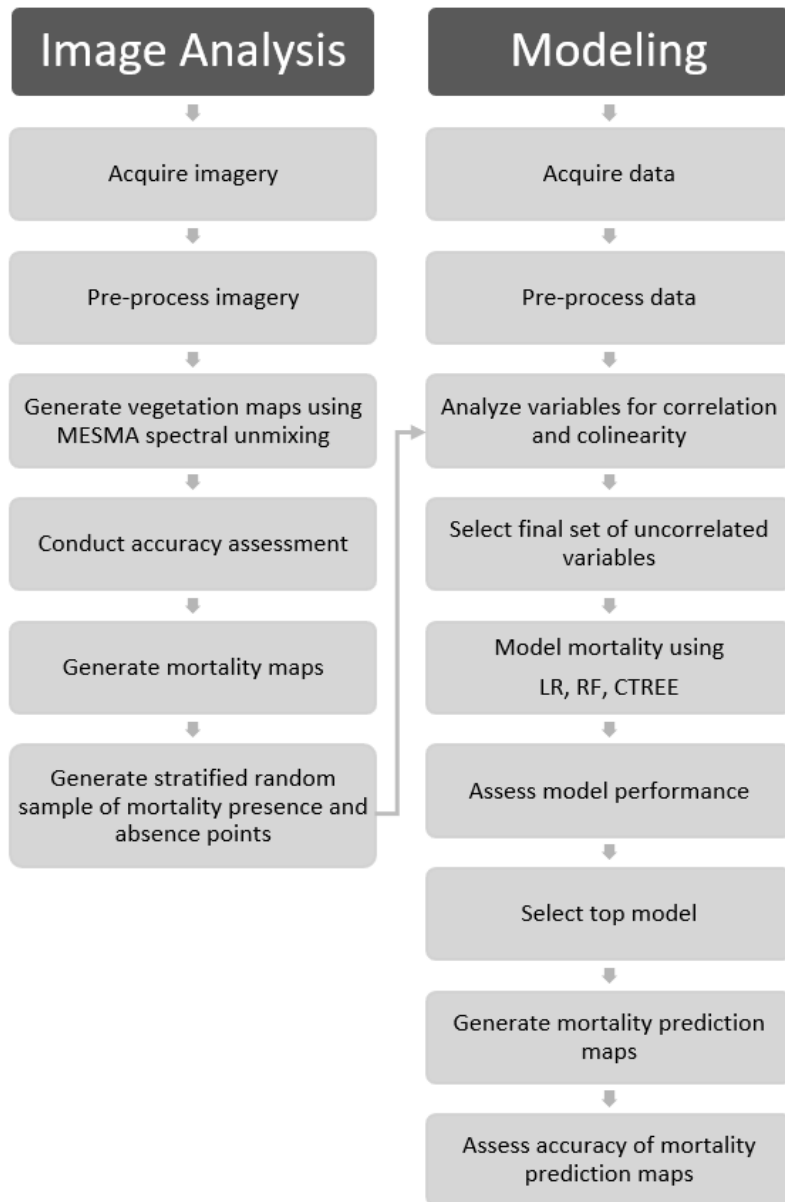


Figure 4. Flowchart of methods.

3.3 Mapping pinyon mortality

Generating a detailed map of pinyon mortality across the four Areas required four main steps: acquiring the imagery, preprocessing it in preparation for analysis, unmixing each pixel to determine the amount of tree cover present, and then comparing the pre-drought and post-

drought tree cover to determine the locations and severity of mortality. Each of these steps is detailed below.

3.3.1 Image acquisition

I used Landsat 5 Thematic Mapper (TM) imagery, acquired from the U.S. Geological Survey (USGS) Global Visualization Viewer (GloVis) (U.S. Department of the Interior 2017), for mapping tree mortality in my study area, as it covers the relatively large study area consistently at a medium spatial resolution of 30 m for the entire study period (2000-2005). In order to maximize the spectral contrast between herbaceous and woody vegetation, I acquired pre- and post-drought, leaf-off, pre-monsoon-season imagery to coincide with the time when herbaceous vegetation is senescent and pinyon pine is photosynthetically active (Huang et al. 2009). Exact anniversary dates could not be obtained due to unavailability of cloud-free imagery; however, dates as close together as possible were selected. Full coverage for all Areas required two Landsat 5 TM scenes for each time period, a north and a south scene, for a total of four images (

Table 1).

Table 1. Imagery used in the analysis.

Description	Acquisition Date	Path	Row	Sensor/source	Pixel size
Pre-drought, north	March 14, 2000	33	35	Landsat 5 TM	30 m
Pre-drought, south	March 14, 2000	33	36	Landsat 5 TM	30 m
Post-drought, north	April 13, 2005	33	35	Landsat 5 TM	30 m
Post drought, south	April 13, 2005	33	36	Landsat 5 TM	30 m
Leaf-on DOQQs	Multiple – 2005	N/A	N/A	NM Statewide Orthophotography Project	1 m

As reference data for conducting the accuracy assessment of the woody plant cover maps, I acquired 1 m spatial resolution Digital Orthophoto Quarter Quads (DOQQs) of the Areas for the year 2005. These DOQQs were derived from air photos collected as part of the NM Statewide Orthophotography Project, and were downloaded from New Mexico Resource Geographic Information System (Earth Data Analysis Center, University of New Mexico 2015). The DOQQs represent leaf-on imagery; however, due to the high spatial resolution, visual discrimination between woody and herbaceous vegetation was possible and so leaf-on imagery did not pose a problem. Where possible, I used color-infrared (CIR) imagery to help in distinguishing green vegetation from other look-alike materials; however, there were some areas where the CIR imagery was not available and in those cases I only used the natural-color (RGB) imagery. I did not obtain similar reference data for 2000 because none was available. The rationale for using only one year of reference data is discussed further in Section 3.3.3.5.

3.3.2 Preprocessing

The Landsat 5 TM Level 1 (L1TP) images were already geometrically corrected by the USGS prior to being made publicly available (Landsat collection 1 level 1 product definition. version 2.0. L5DS-1656 2019). I conducted radiometric corrections and scene-to-scene radiometric calibrations. This was necessary to convert the digital numbers in the original Landsat 5 TM imagery to percent surface reflectance, adjust for atmospheric and topographic effects, and make the multitemporal images comparable to one another (Schott, Salvaggio, and Volchok 1988).

Atmospheric and topographic corrections of all images were performed in ATCOR3 (Richter n.d.; Richter and Center 2004). For the topographic correction, I used a Shuttle Radar

Topography Mission (SRTM) 1 Arc-Second Global Topographic Digital Elevation Model (DEM) (National Aeronautics and Space Administration (NASA), National Imagery and Mapping Agency (NIMA), German Aerospace Center (DLR), and Italian Space Agency (ASI) 2002). Settings used were: rugged terrain; atmospheric file: aausrura; visibility in km from a weather station in Santa Fe, NM, which is a fairly central location in the collective study area, on the day the imagery was collected.

Following these corrections, I cross-calibrated the north and south images for each year and mosaics for the years 2000 and 2005 using the Empirical Line Calibration (ELC) tool in Harris Geospatial Solutions' Environment for Visualizing Images (ENVI). ELC is a commonly accepted method of normalizing remotely sensed imagery (Baugh and Groeneveld 2008; Ortiz et al. 2017). To calibrate the northern and southern scene to each other for each imagery year, I used three bright and three dark pseudo-invariant features (PIFs), or pixels (Schott, Salvaggio, and Volchok 1988). R-squared (r^2) values for the plotted regression lines for all bands in these calibrations were 0.990 or higher. For the imagery from 2000, the southern scene was of a slightly higher quality than the northern scene, and so I used the southern scene as the reference image in the calibration; for 2005, I used the northern scene as the reference image, as it covers a larger part of the study area. After each set of north and south scenes were calibrated to each other for that imagery year, I mosaicked them together and performed one final calibration to adjust the 2000 final image to the 2005 final image. For this I used five bright and five dark PIFs (Schott, Salvaggio, and Volchok 1988). R^2 values for the plotted regression lines for all bands were 0.983 or above for this calibration.

Following the radiometric corrections and calibrations, I masked out urban and built-up areas as well as agricultural land. Retaining these land cover types would have added no value to this analysis of woody plant cover change and would have increased the computational demand and possibility of class confusion during the image classification process. Image processing for this step was done in ArcGIS Desktop 10.5 (Environmental Systems Research Institute, Redlands, CA). Subsequent image processing and analyses were done on either ENVI or ArcGIS Desktop, depending on which was more suitable for the task at hand.

To identify major urban areas for masking, I used the New Mexico, 2010 Census Place shapefile, published by the U.S. Department of Commerce, U.S. Census Bureau, Geography Division (U.S. Department of Commerce, U.S. Census Bureau, Geography Division 2011). Due to the fact that the Census Place shapefile represents a later date than my imagery, there are some areas identified as urban that were in fact not yet built-up at the collection time of my imagery; however, these were mainly in non-forested areas and so masking them out did not negatively affect my analysis. I then used the U.S. Census Bureau, Geography Division, Topologically Integrated Geographic Encoding and Referencing (TIGER) primary and secondary roads file for New Mexico to identify main roads within my study area. While the width of most roads on the ground is generally less than 60 m (New Mexico Department of Transportation 2016), reflectance effects of roads in the Landsat imagery generally show up for about one to two pixels on either side of the centerline. To capture most of these effects and mask out roads from the imagery, I thus used a 30 m buffer around roads.

To identify agricultural areas for removal, I began by excluding areas of land immediately adjacent to sources of surface water irrigation, where a large portion of the

visually observable agricultural fields were located. To this end, I used the National Hydrography Dataset (NHD) (U.S. Department of the Interior, U.S. Geological Survey 2001) to select features identified as streams, rivers, canals, ditches, and aqueducts. To minimize the exclusion of non-agricultural areas that might be of interest to my analysis, I removed from the initial set of selected features any that were in forested areas that did not appear from visual inspection to be in close proximity to agriculture. Around the rest, I generated a 1 km buffer. The optimal size for the buffer was determined by measuring the distance from the NHD line feature to the edge of agricultural fields in several places throughout the study area. While most fields could have been captured by a 600-800 m buffer, some fields extended further than this; to be as inclusive as possible, while avoiding excessive exclusion of non-agricultural areas, I thus used a 1 km buffer. I also hand-digitized several polygons to exclude areas where center-pivot irrigated fields were visually apparent.

None of the above-described methods for identifying urban and agricultural areas are perfect and thus I acknowledge that even after these steps some scattered built-up and agricultural areas likely still exist within the masked imagery; however, they are relatively small in extent and add only a small amount of “noise” or unmodeled pixels to the results.

3.3.3 Multiple Endmember Spectral Mixture Analysis (MESMA)

Multiple Endmember Spectral Mixture Analysis (MESMA) (Roberts et al. 1998) is a remote-sensing technique for unmixing pixels in an image based on the expected materials within the scene. Pure examples of these expected materials, called endmembers, are input by the operator before running the model. I used MESMA to determine the abundance of green vegetation (GV) per pixel throughout each year’s imagery. GV can be interpreted as woody

vegetation (e.g., pinyon pine or juniper) in this case because, as noted above, the satellite images capture the dry season when herbaceous species are senescent (Huang et al. 2009). MESMA is an effective technique for mapping land cover fractions in a variety of natural and urban settings (Roth, Dennison, and Roberts 2012). Applying MESMA involves the selection of appropriate endmembers and model parameters, discussed below. All processing was done in ENVI with help of the Visualization and Image Processing for Environmental Research (VIPER) Tools 2.0 (Halligan, Crabbé, and Leuven 2014), an open-source extension for ENVI. I also conducted an accuracy assessment on the results of the MESMA modeling for GV abundance. I did not assess the accuracy of other types of materials identified in the scene through MESMA, as those outputs were incidental and not of interest in this study.

3.3.3.1 Endmember collection

The endmembers used to unmix the satellite images came from four sources: internal spectral libraries available in ENVI, endmembers collected and compiled by Brewer et al. (2017) for their own study, soil endmembers collected with a handheld field spectroradiometer from soil samples taken from within the study area during a site-visit, and endmembers extracted from the preprocessed 2005 Landsat 5 TM imagery.

Included with the standard ENVI installation are several groups of laboratory spectra from the NASA Jet Propulsion Laboratory (JPL), Johns Hopkins University (JHU), and the USGS. There are thousands of spectra in these libraries that cover a wide range of materials. I selected all those that were identified as some form of vegetation (either green or non-photosynthetic) (n=199), rocks (n=396), soil (n=49), and ice or snow (n=15), excluding those that represented mixtures of these materials such as rangeland. The endmembers supplied by Brewer et al

(2017) were collected from a location approximately 26 km south of the southernmost tip of my Area 1, and included spectra from both live and dead pinyon (live n=232, dead n=231) and juniper (live n=124, dead n= 9), herbaceous cover (n=30), and bare ground (n=12). I also collected 12 soil samples from points within the general study area, brought them back to the New Mexico State University campus, and obtained five spectral readings per sample under full sunlight with an Analytical Spectral Devices FieldSpec Pro JR field spectroradiometer, which has a spectral range of 350-2500 nm.

Endmembers extracted from the 2005 satellite imagery, after discarding “bad” pixels (explained below), consisted of GV (n=15), non-photosynthetic vegetation (NPV) (n=1), bare soil (S) (n=6), and snow (O) (n=19). I extracted spectral profiles directly from the imagery of my study area using three techniques: the Sequential Maximum Angle Convex Cone (SMACC) method (Gruninger, Ratkowski, and Hoke 2004), the Pixel Purity Index (PPI) method (Boardman, Kruse, and Green 1995), and a-priori identification of a few pure pixels based on reference imagery. Both the PPI and SMACC methods of extracting pixels from the imagery yielded a large proportion of impure or heavily shaded pixels, as determined by examining 1 m spatial resolution DOQQs at the location of each of the pixels. The potential for these methods to select pixels that are not true endmembers has been noted as a shortcoming elsewhere (e.g., Chang and Plaza 2006). The impure pixels, along with any pixels corresponding to excluded land cover types, such as water or anthropogenic features, were not used as endmembers. In the course of examining these pixels, a few pure pixels were identified through convenience – having a close proximity to a PPI or SMACC flagged pixel; these were selected a-priori and their profiles added to the spectral library.

3.3.3.2 Endmember preprocessing

After compiling the pool of endmembers from the variety of sources described, they required some preprocessing to make them usable. First, I spectrally resampled (to the six Landsat 5 TM reflectance bands) and rescaled (to at-surface reflectance x 10,000) all reference endmembers to match those of the preprocessed Landsat 5 TM bands. I then manually inspected all spectra and discarded any for which one of the following was true: appeared to be incongruent with their description (e.g., identified as dry oak leaf but having a spectral profile more characteristic of photosynthetic green vegetation); represented, according to the description, vegetation in transition from photosynthetic to senescent, such as yellowing leaves; or were highly unlikely to be found within the scene, such as spectra from ornamental flowers. I then assigned all remaining endmembers to one of the following five classes: GV (photosynthetic green vegetation), NPV (non-photosynthetic dead or senescent vegetation), R (rocks), S (bare soil), and O (“other” - snow and natural salt-flats, which have a similar spectral reflectance). The spectral library at this point consisted of 1,342 endmembers: 458 GV, 335 NPV, 122 S, 396 R, and 31 O.

3.3.3.3 Endmember selection

To increase computational processing efficiency, it is desirable to avoid using more endmembers than needed; however, this must also be balanced with the need to adequately capture endmember variability (Roth, Dennison, and Roberts 2012). In order to narrow down the initial selection of endmembers, I employed several methods. On the ENVI-derived set of endmembers, I used Iterative Endmember Selection (IES), an automated process that iteratively selects endmembers based on maximizing the overall Cohen’s kappa value (Cohen 1960)

obtained in classifying the training library (Roth, Dennison, and Roberts 2012; Tane et al. 2018). Because there was no compelling reason to think that any one of these endmembers should perform better than others on my imagery, IES was a convenient way to reduce the total number of endmembers to be used in the analysis. For the other reference endmembers, I used a different approach in order to force inclusion of endmembers that I believed would correspond well to the materials found in the scene. For these I first discarded any endmembers that appeared to be redundant based on a visual inspection of their spectral profiles. I also discarded any endmembers which appeared from visual inspection of the spectral signatures to be composed of a mixture of GV, S, and/or NPV. I then calculated a square array in VIPER for the remaining endmembers and used the Endmember Average Root Mean Squared Error (EAR) values, an indicator of how well an endmember models the other endmembers of its own spectral class (Dennison and Roberts 2003), to select the twenty most representative profiles for each target material, and discarded the rest. Regarding the endmembers derived from the imagery, they were quite few in number and thus I did not subject them to any endmember-reducing techniques beyond the initial quality control step of discarding impure and non-target materials. The set of endmembers combined from all sources resulted in a spectral library of 387 endmembers: 92 GV, 137 NPV, 93 R, 36 S, and 29 O.

As a final step, I ran 2- and 3- endmember MESMA on the 2005 imagery from each Area to identify and subsequently remove endmembers that model only negligible proportions of pixels. This was necessary to facilitate the final 4-endmember run on each image because each additional endmember exponentially increases the number of models used in the MESMA process, which adds substantially to the computational requirement. The MESMA settings were

as follows: allowable endmember fraction ranging from -0.05 to 1.05, maximum allowable shade fraction of 80%, and a maximum allowable root mean squared error (RMSE) of 0.025. Constraining the allowable endmember fraction to values between -0.05 to 1.05 ensured that overly physically impossible fraction abundances were not generated; this setting and the shade and RMSE criteria are generally in line with those used in other published studies (e.g., Brewer et al. 2017; Tane et al. 2018). Using the results of this preliminary run, I created a unique endmember library for each Area consisting of the endmembers which modeled at least between 0.08% (R, most stringent) and 0.02% (GV, most inclusive) of the pixels in the scene. Actual cutoff values varied slightly between Areas depending on which of several test runs yielded the highest accuracy results for that particular Area. The final spectral libraries consisted of 159-186 endmembers per Area (Table 2).

Table 2. Final endmembers used for the 2-, 3-, and 4-endmember run in each Area.

Endmember type	Area 1	Area 2	Area 3	Area 4
GV	50	56	54	49
NPV	62	49	50	44
R	34	30	47	29
S	23	31	26	27
O	6	1	9	10
Total	175	167	186	159

3.3.3.4 Spectral unmixing

I used the final set of endmembers selected for each Area to run 2-, 3-, and 4-endmember MESMA on both years of imagery, with the same settings as described above for the 2- and 3-endmember run. This meant that each pixel was modeled with a minimum of one endmember

plus shade, which is always included as a default, and with a maximum of three endmembers, each from a different class, plus shade. While there are options to include a higher possible number of endmembers, three seemed an adequate number of non-shade endmembers to capture the materials represented in each 30 m pixel, given the general nature of the scene and that some land cover classes had already been masked out. All MESMA raw outputs were shade-normalized before proceeding with the accuracy assessment and subsequent analyses.

3.3.3.5 Accuracy assessment

I conducted an accuracy assessment of the MESMA modeling outputs of the 2005 imagery for each of the four Areas. I used the 2005 1 m DOQQs described above to serve as reference data. In each Area, I laid out 30 plots of 90 x 90 m in a stratified random sampling plan, with 10 plots each in areas of uniformly high, uniformly medium, and uniformly low woody vegetation cover (Figure 5). These cover categories were decided subjectively by visual estimate; the relative homogeneity / consistency criterion was included to avoid having excessive in-plot variability in woody plant cover. The plot size was chosen to represent an area of 3 x 3 Landsat 5 TM pixels, to account for slight registration differences between plot edges and pixel edges (Brewer et al. 2017). To make the two data sources more comparable, I applied a 3x3 kernel low pass filter, which averages the pixels within the specified kernel, to the 30 m MESMA output.

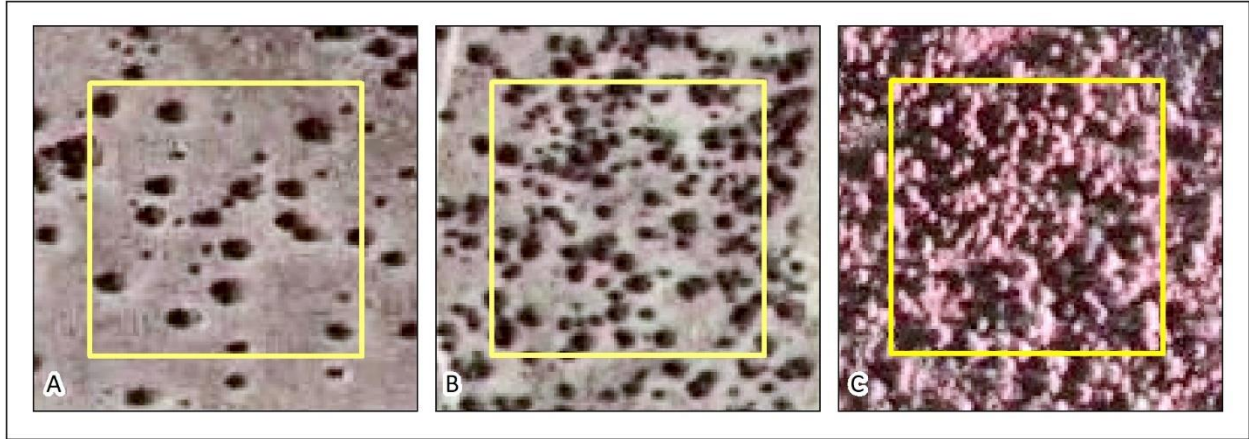


Figure 5. From left to right, examples of (A) low, (B) medium, and (C) high cover plots.

I used a photography-based grid point intercept method to quantitatively assess plot cover from the 1 m DOQQs. In each plot, I located 150 points in evenly spaced transects distributed across the plot (Figure 6). At each point, the reference imagery was inspected and cover type (GV, non-GV) was recorded. Others have relied on a similar technique for accuracy assessments of image analysis results (Karl, Duniway, and Schrader 2012; Brewer et al. 2017; Lippitt et al. 2018). Because very few natural landscapes, even across relatively small distances, are truly homogenous, I randomly selected 50 points from each plot as test points and 100 as training points. I assessed the percent cover difference between training and test data as a measure of within-plot heterogeneity and used this to inform my interpretation of the results obtained from the MESMA accuracy assessment. This was an approach similar to the method used by Duniway et al. (2012) for calibrating vegetation classification in aerial imagery.

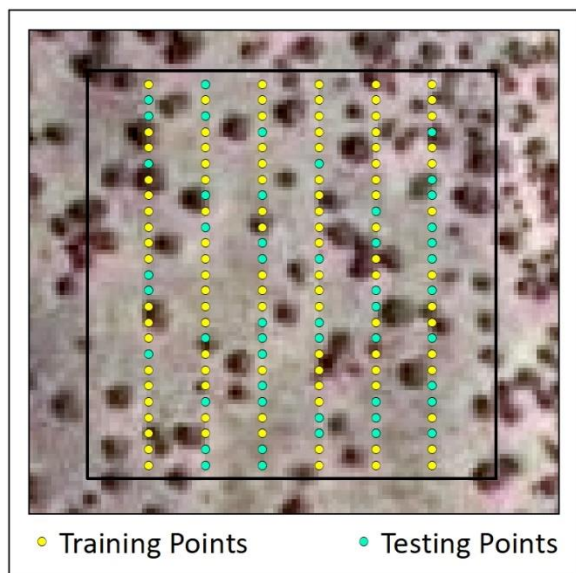


Figure 6. Accuracy assessment plot transects.

I used three measures to assess the overall error between the cover percentages obtained from the DOQQs and the GV abundance estimated by MESMA: RMSE, mean average error (MAE), and coefficient of determination (R^2). RMSE is the standard deviation of the residuals and provides a measure of how closely the data points fall along the line of best fit, MAE provides the average of the absolute errors, and R^2 indicates how well the regression line fits the data. I calculated these three measures of error for the comparison of within-plot heterogeneity also.

I did not conduct a separate accuracy assessment for the 2000 imagery. First, high spatial resolution aerial photography for the study area taken in or around 2000 was not available. Second, Schott, Salvaggio, and Volchok (1988) report that performing ELC can reduce temporally induced differences between multitemporal imagery to an error of $\sim 1\%$; therefore, after having conducted an ELC, the 2000 imagery should be highly comparable to the 2005 imagery in terms of reflectance values. Since the same spectral library and model parameters

were used for both years of imagery, and as MESMA is a physical model, I proceeded on the assumption that the accuracy assessment performed on the 2005 imagery MESMA output is generalizable to the 2000 imagery MESMA output.

3.4 Image differencing

I used image differencing to detect the change in GV cover between the two years. For each Area, I eliminated from both image layers all pixels which met the following criteria: less than 5% GV cover in 2000 and/or snow present in one or both years of imagery. This was to eliminate from the analysis pixels with few to no trees and to avoid errors introduced by snow obscuring the true GV cover in a pixel. I then aggregated the GV layers from a 30 m pixel resolution to a 210 m pixel resolution using the mean of the underlying pixels. This pixel size corresponds well with the average spatial resolution of the soils variables, which were derived from the coarsest resolution input dataset except for the bioclimatic variables. Due to the aggregation method used, selecting a more rounded number of 200 m was not an option, as the aggregated pixel size needed to be a multiple of the initial 30 m pixel resolution. While bioclimatic variables could be interpolated to partially remedy the spatial resolution mismatch, no such option was available for the nominal data type soils information. I used the land cover data layer from the SWReGAP analysis program (RS/GIS Laboratory, College of Natural Resources, Utah State University 2004; Lowry et al. 2005) to isolate only areas mapped by the project as pinyon-juniper woodland within the four Areas. The native resolution of this land cover dataset is 30 m. In using it to mask out non-target pixels in the GV cover images, I followed this rule: if at least one of the land cover pixels mapped as pinyon-juniper woodland

overlapped a cell in the GV cover image, then that GV cover pixel was retained. After masking both images to exclude areas with no pinyon-juniper woodland, I performed image differencing using two strategies. First, I subtracted the GV values in 2000 from the GV values in 2005 to detect the absolute percentage point difference in GV cover between 2000 and 2005. Second, I calculated the relative change in cover between 2000 and 2005, using the formula $(GV\ 2005 - GV\ 2000) / GV\ 2000$, where GV 2000 and GV 2005 represent the percent GV cover in the years 2000 and 2005, respectively. I used the relative change layer to determine presence of mortality, described further in Section 3.5.1.

3.5 Selection of tree mortality presence and absence locations

The modeling methods I selected require a binary outcome response variable - in this case, the presence or absence of mortality. To minimize spatial autocorrelation and create an unbiased tree mortality presence and absence point dataset for the spatial models, I drew a stratified random sample of mortality presence and absence points from various pre-drought GV cover categories for each Area, with each point spaced a minimum distance of minimum distance of 1,050 m (five pixels) away from the next nearest point. This process required three steps: determining what constituted presence or absence of mortality; determining representative pre-drought GV cover classes; and actually creating the sample. To determine what qualified as mortality having occurred, I used a combination of exploratory data assessment to evaluate natural breaks, and judgement for what seemed reasonable. I determined the GV cover classes similarly, relying mainly on the natural breaks in the data for determining these classes. This was done to make sure that the sample set I planned to draw was unbiased. I decided to

evaluate the cover densities found in each Area and design the sample stratification in such a way that the sample drawn would be reflective of the cover density in the Area, while at the same time ensuring that there were data points representative of mortality in all classes of pre-drought cover density.

3.5.1 Determination of tree mortality presence and absence

I determined class breaks for percent cover loss between 2000 and 2005 for each Area by applying a Jenks Natural Breaks classification to the MESMA-derived GV data. Based on the natural breaks in the data, which were fairly similar across the four Areas, I generalized the breaks for all Areas into the following five mortality classes:

- very low: 0.05 to 15 percent cover loss (-0.05 to -15)
- low: 15 to 30 percent cover loss (-15 to -30)
- medium: 30 to 45 percent cover loss (-30 to -45)
- high: 45 to 60 percent cover loss (-45 to -60)
- very high: 60 to 100 percent cover loss (-60 to -100)

I chose the high and very high percent cover loss categories collectively to represent mortality presence pixels for modeling. Any pixels with less than 45% cover loss between 2000 and 2005 were excluded to capture only the areas with the highest mortality and reduce the possibility of modeling noise introduced by incidental mortality or minor GV percent estimate inaccuracies. Pixels with 0% change or a positive percent change were used to represent areas of tree survival or mortality absence.

3.5.2 Determination of pre-drought woody plant cover classes

Using Jenks Natural Breaks, I divided the pre-drought year 2000 imagery GV percent into five cover classes for each individual Area and then generalized the breaks across the four Areas to come up with the following 2000 GV classes:

- very low (1): 0 to 10 percent cover
- low (2): 10 to 25 percent cover
- medium (3): 25 to 45 percent cover
- high (4): 45 to 65 percent cover
- very high (5): 65 to 100 percent cover

As with mortality, the breaks for the four Areas were quite similar even before generalizing. I excluded the very low cover category from the sampling scheme because very few mortality presence points occurred in this cover class across any of the four sites, and it was impossible to represent this cover class and still draw a reasonable number of sample points.

3.5.3 Sampling of tree mortality presence and absence sites

I selected 500 total sample points each in Areas 2, 3, and 4, and 250 points in Area 1 (Table 3). Half of these points in each Area were located at sites with mortality present, and half were located at sites that represented survival (absence of mortality); this ensured that the dataset used for creating the models was balanced with regard to mortality presence/absence. Overall mortality was lower in Area 1 than in the other Areas, and there were not enough mortality presence points to draw 500 points from this Area. In Area 3 and Area 4, the high and very high cover classes were somewhat underrepresented in the survival sample drawn, as there were not enough points to draw from in those classes. This necessitated oversampling the low and medium cover classes to make up the full number of needed survival points.

Despite great care taken to ensure that no areas with missing data from the variables layers were selected as sample locations, when processing the final analysis datasets, a very small number of data points were found to contain missing data values, and these samples were discarded before proceeding. Due to the very small number of points for which this was the case, the effect on the subsequent analyses was negligible.

Table 3. Mortality presence and absence sample points in each pre-drought GV cover category and overall for each of the four Areas.

	Number of sample points			
	Area 1	Area 2	Area 3	Area 4
Mortality presence				
Low pre-drought GV cover	46	118	101	90
Medium pre-drought GV cover	31	75	91	74
High pre-drought GV cover	27	38	34	43
Very high pre-drought GV cover	21	19	24	43
Total mortality presence points	125	250	250	250
Mortality absence				
Low pre-drought GV cover	46	118	122	124
Medium pre-drought GV cover	31	75	113	90
High pre-drought GV cover	27	38	7	14
Very high pre-drought GV cover	21	19	8	22
Total mortality absence points	125	250	250	250
Total sample points	250	500	500	500

3.6 Potential explanatory variables

The data for the potentially explanatory variables was obtained from a variety of sources, and required varying degrees of preprocessing in preparation for the modeling phase. The general steps were: acquisition of the data, preprocessing associated with the initial data preparation,

and then statistical preprocessing to standardize values and inspect for correlation and collinearity.

3.6.1 Acquisition of potential explanatory data layers

I acquired data for variables that might explain tree mortality in five general categories: bioclimatic, topographic, edaphic, vegetation, and anthropogenic. The data for these came from seven main sources. For the climatic variables, I used the Climatologies at High resolution for the Earth's Land Surface Areas (CHELSA) datasets (Karger et al. 2017b). These represent long-term averages spanning the period 1979-2013 (Karger et al. 2017a). The topographic variables as well as solar radiation variables were derived from the SRTM DEM that I also used for the topographic correction of the satellite imagery, described above (National Aeronautics and Space Administration (NASA), National Imagery and Mapping Agency (NIMA), German Aerospace Center (DLR), and Italian Space Agency (ASI) 2002). Edaphic data were sourced from the USFS and the Natural Resources Conservation Service (NRCS) Soil Survey Geographic (SSURGO) database. Vegetation indices were calculated from the preprocessed Landsat 5 TM imagery. Grazing allotment data were obtained from the USFS, the Bureau of Land Management (BLM), and the New Mexico State Land Office (SLO) to represent the anthropogenic variables.

Most of the above datasets were consumer-ready products requiring minimal additional processing; the exception to this was the USFS soils data. I hand-tabulated these data from Adobe Portable Document Format (PDF) documents of scanned field log sheets provided by the USFS Southwestern Region office, where available. In areas where detailed USFS soil data were

not available, I used SSURGO information instead. A full listing of all variables considered, including sources and native resolutions, is included in Appendix A.

3.6.2 Preprocessing of potential explanatory data layers

The preparation needed for each group of variables varied somewhat and depended largely on the source and state of the data. As one might expect, the data came in a variety of native spatial resolutions and formats. To ensure a consistent resolution across all datasets, I converted all shapefiles to raster format with a 210 m pixel size, using the Maximum Combined Area cell assignment option. All nominal type variables I dummy-coded into rasters with values of 1 for presence and 0 for absence of the feature of interest. The processing of raster-based datasets are detailed below in their respective subsections. During this initial preparation, I also excluded from further processing and analysis any features that, based on visual estimation, covered a very small area relative to the collective study area and/or had a very localized extent (e.g., one medium-sized polygon within the entire collective study area), as it appeared unlikely their inclusion would enhance the final analysis. This was the case for several of the soils variables in particular, as there were a few textural and drainage classes that were only found in a few, very small, isolated locations within the collective study area.

To avoid registration issues and pixel edge mismatches, all rasters produced in the data preprocessing tasks were snapped to the image differencing raster that represents percent change in GV between the two years. I also clipped and masked all rasters representing independent variables to have the same coverage as the image-differencing raster. Any pixels where one or more of the variables had no data were also excluded, so that no partial data areas would be included within the final layerstack of potential explanatory variables.

3.6.2.1 Bioclimatic variables

I downloaded long-term climatic averages from the CHELSA datasets, clipped them to the New Mexico state boundary, re-projected and resampled them to a 210 m pixel size using bilinear interpolation, and then clipped them that to the boundaries of the four study Areas. I also calculated solar radiation in ArcGIS using a sky size of 200 cells and the 30 m SRTM DEM as input data. Since the initial output of this operation had a 30 m pixel size, I aggregated the values to a 210 m pixel size using the average of the underlying pixels.

My reason for including long term climatic trends in these analyses was to assess the possible relationship of tree mortality to long-term environmental characteristics such as, for example, sites that typically receive low precipitation even in normal years. Some literature (Lloret and Kitzberger 2018) also suggests that historically more favorable sites may have had higher mortality during the 2000s drought. To investigate these relationships, I thus chose to include long-term climatic variables. I did not include weather variables for the drought period because a primary goal of this study is to evaluate the relationship between drought-related pinyon mortality and relatively stable site characteristics, which might be informative for management purposes. The effects of weather-related variables, such as precipitation (West et al. 2008; Plaut et al. 2012; Anderegg and Anderegg 2013; Limousin et al. 2013; Williams et al. 2013), temperature (Adams et al. 2009), and vapor-pressure deficit (Plaut et al. 2012; Weiss, Betancourt, and Overpeck 2012; Limousin et al. 2013; Williams et al. 2013; Dickman et al. 2015) on pinyon pine have already been studied and are described in the relevant literature.

3.6.2.2 Topographic variables

For elevation data, I used the 30 m SRTM DEM, aggregated to a 210 m pixel size using the mean of the underlying pixels. All other topographic variables were calculated in ArcGIS from this DEM with the help of the Geomorphometry and Gradient Metrics (version 2.0) toolbox (Evans, Oakleaf, and Cushman 2014).

3.6.2.3 Edaphic variables

Both the USFS and NRCS soils data came in polygon form, with each polygon representing a map unit composed of several distinct soils (components), each with their own unique characteristics. My first step in processing these datasets was to identify the dominant component for each soil map unit, which is the component that makes up the highest percentage of the map unit. This information is supplied within these datasets. For highly heterogenous map units in which the “dominant” component makes up only a small percentage of the unit (e.g., 35%) I selected the component which best represents the general characteristics of one or more other components described in the unit, so that the highest possible percentage of the soils within the unit was reasonably represented. After identifying the dominant component for each unit, I used the soil attributes associated with this component for the entire polygon area from that point forward. USFS data were used where available; in areas where I did not have USFS data, I used NRCS data instead.

USFS data

In areas under USFS jurisdiction, Terrestrial Ecosystem Unit shapefiles are available which, similar to NRCS soil shapefiles described below, depict polygons composed of one or more components. Some supplemental information is also provided with these, but the level of detail

needed for this study was not present in the publicly available datasets. Through a contact at the Southwestern Region office, I obtained the actual field log sheets that had been used in mapping these soils. From these, I tabulated the soil profile information into an Excel spreadsheet and processed it similarly to the NRCS sourced data as outlined below. Most of the soil profiles from this dataset were described to a depth of about 110 cm, some slightly less and some a little more. In order to round the profile depth to a standard value across all the data, I truncated all profile data at 122 cm. In practice, many soil interpretations in the U.S. are based on English units of inches and feet; 122 cm corresponds to 4 ft, which I could then evenly divide into 1 ft increments for later modeling and analysis. If the soil profile description did not go that deep, I made the assumption that the last described horizon extended to this depth with little to no change, unless a lithic contact or indurated material was noted as the last layer.

NRCS data

Part of the NRCS data download for a soil survey area is a Microsoft ACCESS® database that contains detailed soil properties in tabular form, as well as the capability to generate a variety of different written reports. Within each database, I created custom queries to extract the basic information needed for the desired variables. Some of these, such as drainage class, could be used as-is. A few properties, such as percent clay content and AWC of the entire soil profile and on a per-foot basis, had to be calculated. This is because the information in the database is on a horizon by horizon basis and horizons vary in thickness; in addition, water-holding capacity is reported on a basis of unit of water holding capacity per unit of soil, while I wanted actual summed totals. This is also sometimes referred to in agronomy as available water supply (USDA Natural Resources Conservation Service 2017), however here I refer to it as available water

capacity because supply implies the water is physically present, whereas in many arid western rangelands and woodlands that is not actually the case. Because there were so many map units to perform these calculations for, I wrote a series of python scripts to do the calculations that took, as input, data that I could query from the ACCESS® database and export into a csv file. The python scripts are included in Appendix B. Other soil property variables that needed further preparation beyond what was provided in the soil survey database included surface texture, particle size class, soil depth, calcic parent material, and presence of a restrictive layer within the described profile / presence of a clay layer within the described profile. Each of these is described next.

Surface texture. Within the databases, the recorded surface texture includes modifiers such as “gravelly”, “very cobbly”, “stony”, etc. While these modifiers are informative for many purposes, my reason for including surface texture was based on the potential for a coarse surface texture to facilitate infiltration and reduce surface evaporation (Noy-Meir 1973); thus, including the amount or type of rock content just created an unnecessarily large number of highly specific classes with small extent, from which few relationships could be drawn. To simplify the categories, I removed all texture modifiers and aggregated the areas on the base textural class, so that, for example, a sandy loam, a fine sandy loam, and a very gravelly sandy loam were all placed in the same category. Soils with an O horizon of any designation were aggregated together and categorized as having an organic surface “texture”. I also created a bedrock “surface texture” category which serves to represent map units where the dominant component was described as rock outcrops or badlands with bedrock at the surface.

To further aggregate mineral horizon surface textures, I additionally created a second surface texture variable class which even further aggregated the textures into five classes: coarse, moderately coarse, moderate, moderately fine, and fine. These categories represent functional surface texture types and have been previously used in the classification of land for agricultural use for legally determining practicably irrigable acreage. Since these textural groups are not part of the NRCS land classification system or standard descriptive attributes, I assigned these by hand based on the reported soil texture of the surface horizon.

Particle size class. This could mostly be used as provided; however, practice standards direct that no particle size class is used for psamments since it would be redundant information; this taxon designation already implies a sandy particle size (Soil Survey Staff, Soil Conservation Service, US Department of Agriculture 1999). For my analysis, however, I needed the particle size class to be specified in all units, so I entered this information manually into my tables.

Soil depth. I used the reported depth to a root restrictive layer described as cemented, indurated, or bedrock, as the source for my variable “soil depth”. In profiles where no root restrictive layer was noted within the described profile, the depth to which individual profiles were described varied somewhat. The National Soil Survey Handbook (USDA Natural Resources Conservation Service 2017) recommends describing soils to a depth of no more than 200 cm but at least 150 cm; in practice most of the soils in the databases I downloaded are described to a depth of 152 cm. A few were described to greater depths. For consistency, any soils that were described below this depth I truncated at 152 cm, recognizing as a shortcoming that many of these areas may in reality have a depth of soil that extends far beyond the described or

truncated depth. In Areas 2 and 3, I truncated soil depth at 122 cm in order for the data to be comparable to the USFS data in which soil profiles were typically described to a shallower depth than the NRCS ones.

Calcic parent material. This is not a feature of its own in the NRCS soil databases, but there is a general category for parent material to be recorded, so I simply queried out all map units where the dominant component parent material was recorded as limestone. My reasons for not including other types of parent materials are twofold. First, I wanted to capture soil material with a generally very high calcium carbonate content, which can influence soil physical properties such as water availability (Soil survey investigations for irrigation. FAO soils bulletin 42. n.d.) and nutrient availability (USDA Natural Resources Conservation Service 2017). Secondly, many of the components had more than one type of parent material specified (e.g., alluvium and eolian) and I was unable to develop a good way to represent each of them as discrete categories.

Presence of a restrictive layer within the described profile; presence of a clay layer within the described profile. Neither of these are data fields in the NRCS soils database, but were easy enough to assemble based on the information given on horizon textures and depth to root restrictive feature. In determining these two variables, I included soils with a restrictive layer or clay layer described at any depth below the soil surface.

3.6.2.4 Vegetation indices

I calculated two pre-drought vegetation indices – the Normalized Difference Vegetation Index (NDVI) and the Normalized Difference Moisture Index (NDMI) – to determine if there was a relationship between pre-drought vegetation conditions and pinyon mortality. Both indices

were calculated from the fully preprocessed 2000 Landsat 5 TM image. I then aggregated the native 30 m pixel size outputs to a 210 m pixel size using the average of the underlying pixels.

The NDVI (Rouse Jr et al. 1974) is a widely recognized vegetation index (Ji et al. 2011) which is used to quantify photosynthetic green vegetation (U.S. Department of the Interior, United States Geological Survey n.d.; Rouse Jr et al. 1974). The NDMI is an index that has been shown to be correlated to vegetation water content (Hardisky, Klemas, and Smart 1983; Hunt Jr and Rock 1989). The equations for the indices are as follows:

$$NDVI = \frac{NIR - Red}{NIR + Red}$$

where NIR is the near infrared band (band 4) and Red is the red band (band 3), and

$$NDMI = \frac{NIR - SWIR}{NIR + SWIR}$$

where NIR is the near infrared band and (band 4) and SWIR is the short-wave infrared band (band 5).

3.6.2.5 Anthropogenic variables

Although I initially considered land ownership as a potential explanatory variable, upon inspecting the spatial locations and distributions and of various ownerships (e.g., tribal, Forest Service, State), I determined that land ownership was unlikely to explain pinyon survival or mortality. Instead, I chose whether or not land was grazed as the only anthropogenic variable in the analysis to determine if there is a relationship between livestock grazing (e.g., differences such as the presence of hoof action, suppression or removal of some of the understory) and drought-induced tree mortality. To identify grazing lands, I used shapefiles depicting grazing allotments obtained from the BLM representing conditions in 2000 (Bureau of Land

Management - New Mexico State Office 2000), USFS grazing allotment shapefiles with publication dates between 2010-2013 (USDA Forest Service 2010; USDA Forest Service, Carson National Forest 2012; USDA Forest Service, Santa Fe National Forests 2013), and a shapefile of agricultural land leases representing current conditions at the time of download in 2017 from the NM SLO (Land Office Geographic Information Center (LOGIC), NM State Land Office n.d.). Although some of the data publication dates are more recent than the mortality event, I proceeded on the assumption that it is unlikely grazing allotment boundaries changed substantially in the years between 2002 and the data publication date. From the SLO agricultural land leases shapefile, I isolated those that were coded as a grazing type land use (ATYP_CDES = G or 1), and then combined the polygon shapefiles depicting grazing lands from all three sources into a single shapefile, from which I then created a dummy-coded raster indicating presence or absence of grazed land.

3.6.3 Statistical preprocessing of variables

Prior to analysis, I standardized all variables using the scale function in R, which applies the formula $(x-\bar{x})/s$, where x =value, \bar{x} =sample mean, and s =sample standard deviation, to make them comparable, as their native scales are widely variable. I also noted that many of the variables were extremely non-normally distributed; however, this did not present a problem as none of the modeling approaches I used -logistic regression, random forest, conditional inference trees- require predictor variables to be normally distributed (Peng, Lee, and Ingersoll 2002; Pohar, Blas, and Turk 2004; Hothorn, Hornik, and Zeileis 2015).

Correlation and collinearity between variables were analyzed using Pearson's r and the Variance Inflation Factor (VIF), respectively (Appendix C). Variables with Pearson's values of -0.7

$\leq r \geq 0.7$ were considered strongly correlated and hence redundant. To determine which of two correlated variables to keep or eliminate, I used judgement and single-factor logistic regression. Judgement was used when it clearly made more sense to retain one variable over another, such as mean annual temperature over the mean temperature of any given individual month. In other cases, whichever variable was the most statistically significant with the greatest r^2 value was kept and the other eliminated.

After removal of redundant variables as indicated by Pearson's r value, I evaluated the VIF to assess collinearity among all variables that were not initially dummy-coded. This is the approach recommended by Murray et al. (2012), who found that mixing dummy-coded and numeric predictor variables can produce artificially large VIF values even in the absence of variable collinearity. VIFs among the non-dummy coded variables were all at or below 5.2; thus, no additional variables were removed in this step. Adding the dummy-coded variables caused an increase in several variables' VIFs, but these were not removed, following Murray et al (2012). Overall, removal of redundant variables reduced the total number of potential explanatory variables from 136 to 42 (Table 4).

Table 4. Variables retained after statistical preprocessing.

Variable type	Initial number of variables	Final number of variables
Climatic	80	7
Topographic	20	9
Edaphic	33	24
Biotic (vegetation indices)	2	1
Anthropogenic	1	1
Total	136	42

3.7 Modeling

I used three types of models to analyze my data and model tree mortality: logistic regression (Pearl and Reed 1920), random forest (Breiman 2001), and conditional inference trees (Hothorn, Hornik, and Zeileis 2015). Logistic regression is a commonly employed statistical modeling method applied to data in which the response variable is categorical (Pohar, Blas, and Turk 2004). Random forest and conditional inference trees are somewhat similar to each other in that both are a decision-tree based approach, though each have different merits. Random forest is an ensemble approach that performs well with large sets of explanatory variables, even in cases in which a substantial number of them are unimportant, and is quite robust to overfitting (Breiman 2001; Díaz-Uriarte and De Andres 2006). A disadvantage of this modeling approach is that it is something of a black-box with regard to identifying the underlying thresholds chosen for splits in the model (Palczewska et al. 2014; Hauenstein, Wood, and Dormann 2018). Conditional inference trees by contrast fit a single decision tree to the data, and therefore do not have the advantages of an ensemble approach; however, important thresholds can be extracted from this type of model and used for interpretation. I chose conditional inference tree based modeling over more traditional classification tree modeling (CART), because conditional inference trees use a statistical significance test at each split, and so the growth of the tree automatically stops when there are no more significant relationships between the covariates and the response variable (Hothorn, Hornik, and Zeileis 2015). This can in some cases reduce the effort associated with determining optimal pruning parameters, as

the algorithm by design avoids excessive growth with diminishing returns. All modeling was done in R, and the code used is included in Appendix D. Using three different types of models allowed me to do three things: compare a substantial number of models to determine the best performing one for each Area; determine which modeling approach most consistently produced the best overall results; identify variables that seemed to be important across all model types.

3.7.1 Variables groupings for modeling

For all three types of models, I tried the full set of uncorrelated variables as well as several sub-groups based on either variable type or variable importance indicators (Table 5). Some groupings, such as long-term climate variables with solar radiation and NDMI, and the soil & topographic variables grouping, were experimental in nature, based on fairly loosely associated variable types.

Table 5. Variables groupings used in models.

Model name	Variables used
AV	All uncorrelated variables
BC1	Climate variables only (long-term bioclimatic averages)
BC2	Climate variables + solar radiation + NDMI
HU	Anthropogenic variable only (univariate – presence of grazing allotment)
SO	Soil variables only
TP	Topographic variables only
TS	Topographic + soil variables
TV1	Top 1-3 variables from each single type grouping, as determined from random forest
TV2	Top variables from the all-variables model, as determined from random forest
TV3	Top 10 variables across all Areas, as determined from random forest mean decrease in accuracy measure

Model name	Variables used
TV4	Only variables significant at the 0.05 level in the all-variables model, as determined by logistic regression.

Determination of what qualified as a top variable in random forest for models TV1 and TV2 was based on both the Gini purity and mean decrease in accuracy values, which are both indicators of variable importance. In order to be considered a top variable for use in these models, the variable had to have a considerably higher value than the other variables in the model in one or both of the variable importance indicators. What constituted a “considerably higher” value was a subjective judgement call, as the numeric values given in each of these importance measures are only relevant for within-model comparison and cannot be used in an absolute sense to compare variables across different models or to guide the selection of generalized cutoff value. If no variable had a considerably higher value than the other variables, then the variable that had the highest value as indicated by each measure was used in the “top variables” model grouping.

3.7.2 Logistic regression

I performed logistic regression on the above-mentioned groups of variables, using 5-fold cross validation to evaluate model accuracy. Although 10-fold cross validation is an often-used number, I determined that this would result in a small testing sample size (25-50 points) in each fold and thus highly variable performance; therefore, k=5 was a more appropriate number to use based on my dataset. I also manually tuned the initial models described in Table 5, by removing any variables that were not significant at least at the $p \leq 0.1$ level, and re-running the algorithm on this reduced set of variables. This resulted in approximately 20-22 models per

Area using logistic regression. Each subsequent model run was named after the original model with the addition of *-#*, so for example the model with a reduced set of variables based on AV was named AV-1, and so on.

3.7.3 Random forest

A few parameters in random forest either require or provide the option of a user-specified value. For each sample set, I performed some initial tuning analyses to determine the optimal number of trees to grow and the optimal value for the number of variables randomly selected and tried at each split (*mtry*) for the all-variables model. For the smaller groupings of variables, I allowed *mtry* to remain at the default, which is the square root of the total number of features. Liaw and Wiener (2002) have noted that the random forest modeling approach is fairly insensitive to the value of *mtry*. For all datasets and all groupings, a forest of 1,000 trees was well beyond the point at which the classification accuracy ceased to improve. Oshiro et al. (Oshiro, Perez, and Baranauskas 2012) has shown that there is no advantage to increasing the number of trees in a random forest beyond what is actually needed to classify the dataset, so, for consistency, 1000 trees were used in all models across all Areas.

Random forest is an ensemble approach that employs bagging with bootstrap replacement in the process of growing the forest. Each time the algorithm runs, approximately one third of the data set is held out of the training data. This out of bag (OOB) sample is used in calculating the generalization error and reported as the OOB error rate (Breiman 2001). Although not an identical process, this achieves the same effect as traditional cross-validation by estimating the error with data not used to train the model. Breiman (2001) has noted that using the OOB error eliminates the need for partitioning the data into training and testing sets,

and (Wolpert and Macready 1999) report that generalization error results from bagged data compare favorably to cross-validation; I therefore did not conduct an additional cross-validation for the random forest models as this would have been redundant.

Similar to my approach in logistic regression modeling, I refined the models in each Area by removing all but the most important variables (as indicated by variable importance in the initial model run on each variables group) and re-running random forest with the reduced set. This resulted in a total of 16 models per Area using random forest. I followed the same naming convention as described in the above section for models in which I reduced the set of variables from the initial base model described in Table 5.

3.7.4 Conditional inference trees

I used conditional inference trees to build a single decision tree for each grouping of variables. Conditional inference trees use a statistical significance test at each split to choose the variable to split on, and to determine when no further splits will be created. The test is based on the calculated p value of each variable, and different significance levels can be specified. In order to select the best setting for each model, I used the train function in R in combination with 5-fold cross validation to select the optimal criterion to be used in the final model for each group of variables. I specified the following possible values of *mincriterion*, which is the inverse of the α to be used in determining if a split should be made (Hothorn, Hornik, and Zeileis 2015): 0.75, 0.8, 0.85, 0.9, 0.95. I also specified in the model controls an arbitrarily chosen number of 10 as the minimum number of observations for a terminal node to contain. I used the results of the 5-fold cross validation to assess the model accuracy, sensitivity, and specificity. Since tree growth automatically stops when no more statistically significant relationships exist in the data,

regardless of how many variables have or have not been used in the tree, there was no need to manually reduce the variables in the groupings and re-run the model, as was done in the other two modeling approaches.

An advantage of conditional inference trees over random forest is the ability to extract important threshold values for the variables used in the model, above which there is more likely to be one classification outcome, and below which there is more likelihood of the opposite outcome. Once I had obtained these values from the final conditional inference trees grown, I back-transformed these to get the associated real-world values, rather than the standardized values used in the model, which are helpful for modeling but offer few insights for interpretation. The formula used to back-transform the values was: (standardized value * original sample standard deviation) + original sample mean.

3.7.5 Model comparison

I considered four metrics to compare models: overall accuracy, balanced accuracy ((sensitivity + specificity)/2), specificity, and sensitivity. Overall model accuracy was assessed as the average accuracy of the cross-validation folds for logistic regression and conditional inference tree models, and 1 minus the OOB error rate for random forest models, which in essence is once again the averaged accuracy across all iterations. Balanced accuracy differs from overall accuracy in that it can be a better estimator of true model accuracy in imbalanced data sets, and can expose overly optimistic average accuracies in biased models that take advantage of imbalanced testing data (Brodersen et al. 2010). In a perfectly balanced dataset, the balanced accuracy will be the same as the overall accuracy. Although the class imbalance in my data sets is very slight, I nonetheless considered the balanced accuracy to compensate for these slight

imbalances; in general, the difference between the balanced and overall accuracy in the models produced was negligible. Specificity and sensitivity were calculated from the confusion matrices generated for each model. In some cases, a given model produced a very high accuracy in the identification of one class while misclassifying a substantial proportion of the other. These models sometimes had a similar overall and balanced accuracy to models for which the sensitivity and specificity were more evenly balanced. In selecting the top performing model in each Area, I took this into consideration and favored models of the latter type.

3.7.6 Final model selection

After evaluating all the models tried in all Areas, I selected BC2 to refine for the final model, as it consistently had either the highest or second-highest balanced accuracy across all study Areas. To create a model that would generalize well and at the same time eliminate variables that contributed little to this model's predictive power, I took the following steps. First, for each Area, I removed variables that had low importance according to the mean decrease in accuracy produced by random forest. I did this in a backward-stepwise manner, removing in each successive run the variable with the lowest mean decrease in accuracy score. When the OOB error increased by more than 2 percentage points between runs, I stopped removing variables and re-added the one that had been last removed. If the two least important variables had a very similar mean decrease in accuracy score, I experimented by removing each in turn and then proceeded with the model version that had the lowest OOB error.

At the end of the process, I selected as the semi-finalist for each Area the model which used the smallest set of variables while still maintaining acceptable accuracy. My determination of what was acceptable accuracy was based on personal judgement, taking into account how

the initial BC2 model had performed. In Areas 1 and 2, I set the limit at an OOB error rate of no higher 19%, which was only 1-3.6 percentage points higher than the BC2 model in these Areas. In Areas 3 and 4, the OOB error was over 20% in all model versions including the original BC2, and so I chose the model refinement with the lowest OOB error. In Area 3 this model had an OOB error rate identical to BC2, and in Area 4 the semi-finalist model had an OOB error rate that was actually slightly lower than BC2. This left four, slightly different, top models based on BC2 – one per Area. I then noted which variables occurred in at least three of the four semi-finalist models and built a final model, called BCfin, to be used in all the Areas for the final mortality prediction maps. I performed a test-run of BCfin in each Area to ensure that the model was able to predict mortality in the sample data with an overall accuracy, sensitivity, and specificity comparable to the other top models before applying the BCfin model to generate prediction maps for the entire study Area.

3.7.7 Mortality prediction maps

In each of the four study Areas, I used BCfin to generate a mortality prediction map for that Area. The raster used for the final prediction map was the same raster from which the mortality presence and absence samples were drawn, as noted in Section 3.5.3, and served as the validation dataset to determine if the final model can generalize beyond the dataset of 250-500 points that it was trained and tested on. While a true validation dataset would contain only data that the model had never seen before, this raster did include the points used in the analysis dataset as well as previously unused data points. The number of total pixels in each raster, however, was quite large (19,772-30,541) in comparison to the number of points in the analysis dataset, and including those points produced a more complete mortality map.

For each Area, I generated two prediction maps: one classification map showing a binary prediction of mortality presence or absence, and one showing the predicted probability of mortality presence in each pixel. To assess the results, I created a confusion matrix from the classification map in each Area, using all pixels in the raster, and manually calculated the overall accuracy (correct predictions/total predictions), balanced accuracy ((sensitivity + specificity)/2), sensitivity (true positives/(true positives + false negatives)), and specificity (true negatives/(true negatives + false positives)).

4. Results

Results from this study are presented in three main sections: first, the results of the MESMA GV abundance estimation, upon which the rest of the analyses are based; I then turn to the assessment of tree cover changes throughout the four Areas, before finally reporting on the results of the models applied to explain tree mortality.

4.1 MESMA

MESMA image classification accuracy for GV across the four Areas ranged between 0.45 and 0.799 in terms of R-squared (R^2), between 0.179 and 0.232 in terms of RMSE, and between 0.134 and 0.189 in terms of MAE (Table 6). The lowest accuracy was associated with Area 2. However, an examination of the scatterplot of predicted (i.e., MESMA data) and observed (i.e., reference data) GV cover values for all Areas (Figure 7) reveals that predictions for Area 2 were overall fairly comparable to those for the other Areas, except Area 2 had two extreme outliers

that substantially reduced the three accuracy measures. Excluding the outliers, R^2 , RMSE, and MAE values would be 0.627, 0.214, and 0.177, respectively. It is possible that the set of endmembers used was not a good match for some of the materials found in this scene. The results for Area 2 as well as for the other Areas could likely be improved by collecting additional field reference endmembers from the study Area, both of the target vegetation and some other commonly occurring materials in the Area such as senescent background vegetation, rocks, surface litter, and perhaps some additional soil endmembers. Using imagery from a different sensor with higher spectral resolution may also produce better results (Huang et al. 2009). Vegetation mapping accuracies obtained using MESMA in other studies, however, do vary somewhat and the results I obtained were generally within the range of those that have been reported elsewhere (e.g., Thorp, French, and Rango 2013; Brewer et al. 2017; Lippitt et al. 2018).

As an additional means of evaluating my results, I also assessed the within-plot heterogeneity of vegetation cover. Accuracy assessment plots were in all cases located in areas that were as homogenous as possible in terms of cover; however, true homogeneity in natural landscapes is difficult to find. This is indicated in the R^2 , RMSE, and MAE values of testing vs. training points in the reference plots, which ranged from 0.812 to 0.96, 0.056 to 0.075, and 0.046 to 0.06, respectively (Table 7). Considering this within-plot heterogeneity, it is likely that at least some of the error in the MESMA results noted above is not due to actual modeling errors, but rather a result of the difficulty in accurately capturing 100 percent of the variability found in the reference data.

Table 6. Accuracy of MESMA GV estimates.

Study area	R ²	RMSE	MAE
Area 1	0.799	0.193	0.142
Area 2	0.450	0.232	0.189
Area 3	0.637	0.190	0.140
Area 4	0.629	0.179	0.134

Table 7. Within-plot heterogeneity: training vs. testing points.

Study area	R ²	RMSE	MAE
Area 1	0.960	0.065	0.052
Area 2	0.942	0.056	0.046
Area 3	0.812	0.075	0.060
Area 4	0.885	0.075	0.057

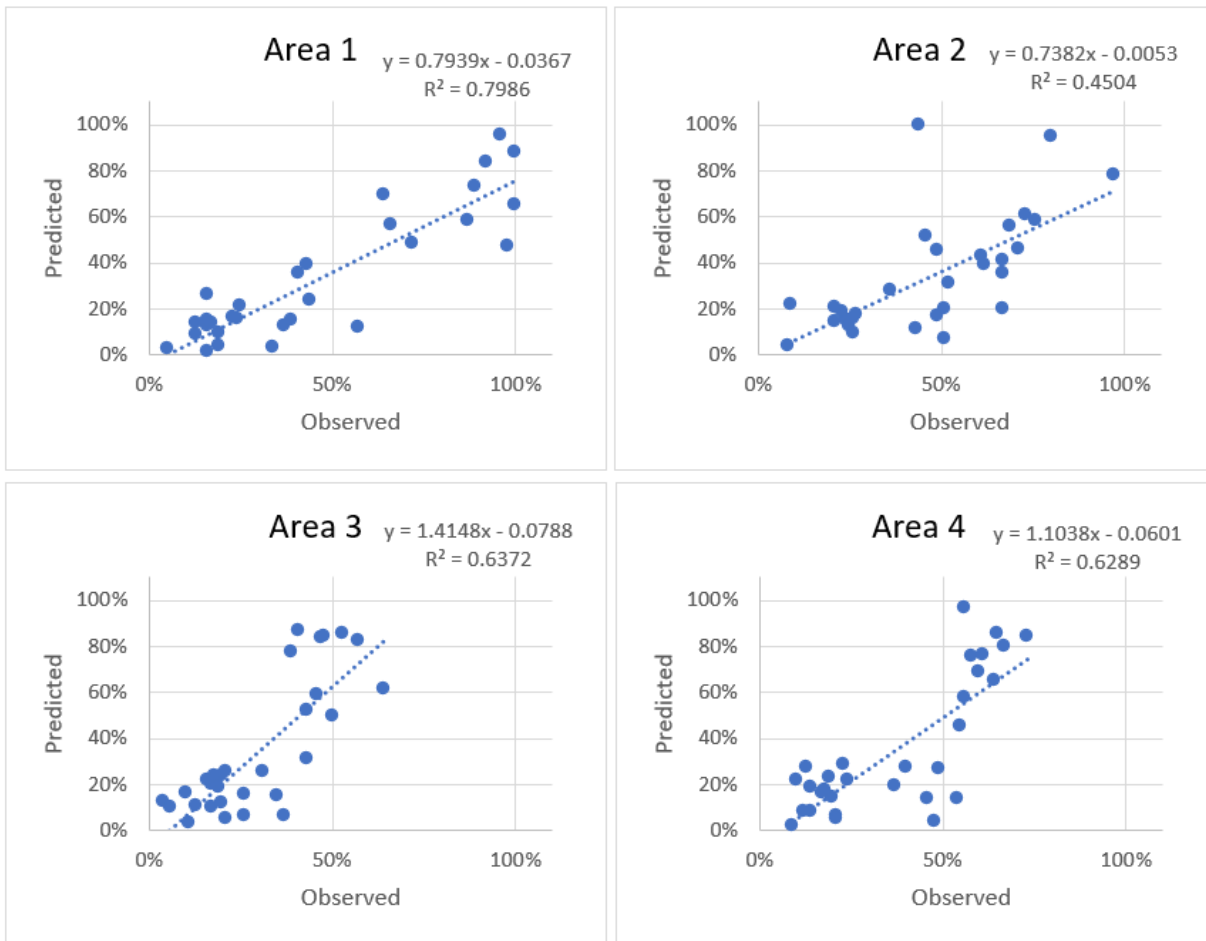


Figure 7. Observed vs. predicted green vegetation values.

4.2 Tree cover changes

All four Areas experienced some reduction in tree cover between the years 2000 (Figure 8) and 2005 (Figure 9), both in terms of absolute (Figure 10) and percent cover change (Figure 11), and all areas had some locations with increases in detected tree cover. Reduction in cover was most pronounced in Areas 3 and 4, and lightest in Area 1. Substantial portions of Areas 3 and 4 had close to 100 percent GV cover loss, and much of both Areas lost at least some cover (indicated by the red tones in Figure 11). Cover loss in Areas 1 and 2 appeared to be mainly concentrated

in the northern parts of the respective Areas, and there were relatively few areas that had a close to 100 percent cover loss on a per-pixel basis. In Area 1, most of the cover loss was localized in the far north-eastern region. Across the four Areas, high absolute cover loss was mainly concentrated in areas of high initial cover, whereas when examining relative cover loss, it becomes apparent that there was substantial mortality in areas with medium and low cover as well. This is observable in all the Areas, but most noticeable in Area 4 where the area represented in red nearly doubles in size from Figure 10 to Figure 11. The relative cover loss shown in Figure 9 also suggests that mortality was a little more widespread than indicated by the USFS IDS data, particularly in Area 3. Finally, there were also some parts of all Areas where tree cover increased between 2000 and 2005. These areas occurred almost exclusively in locations of very low or low pre-drought cover classes. In Areas 3 and 4, the locations of increase were relatively small in comparison to the areas of relative decrease, however in Area 1 and 2, the areas of increase were more comparable in total area to the areas of decrease. In all cases, areas of increase seemed to be discrete, continuous patches, and not interspersed through the areas of mortality.



Figure 8. Abundance of green vegetation in 2000, as modeled by MESMA.

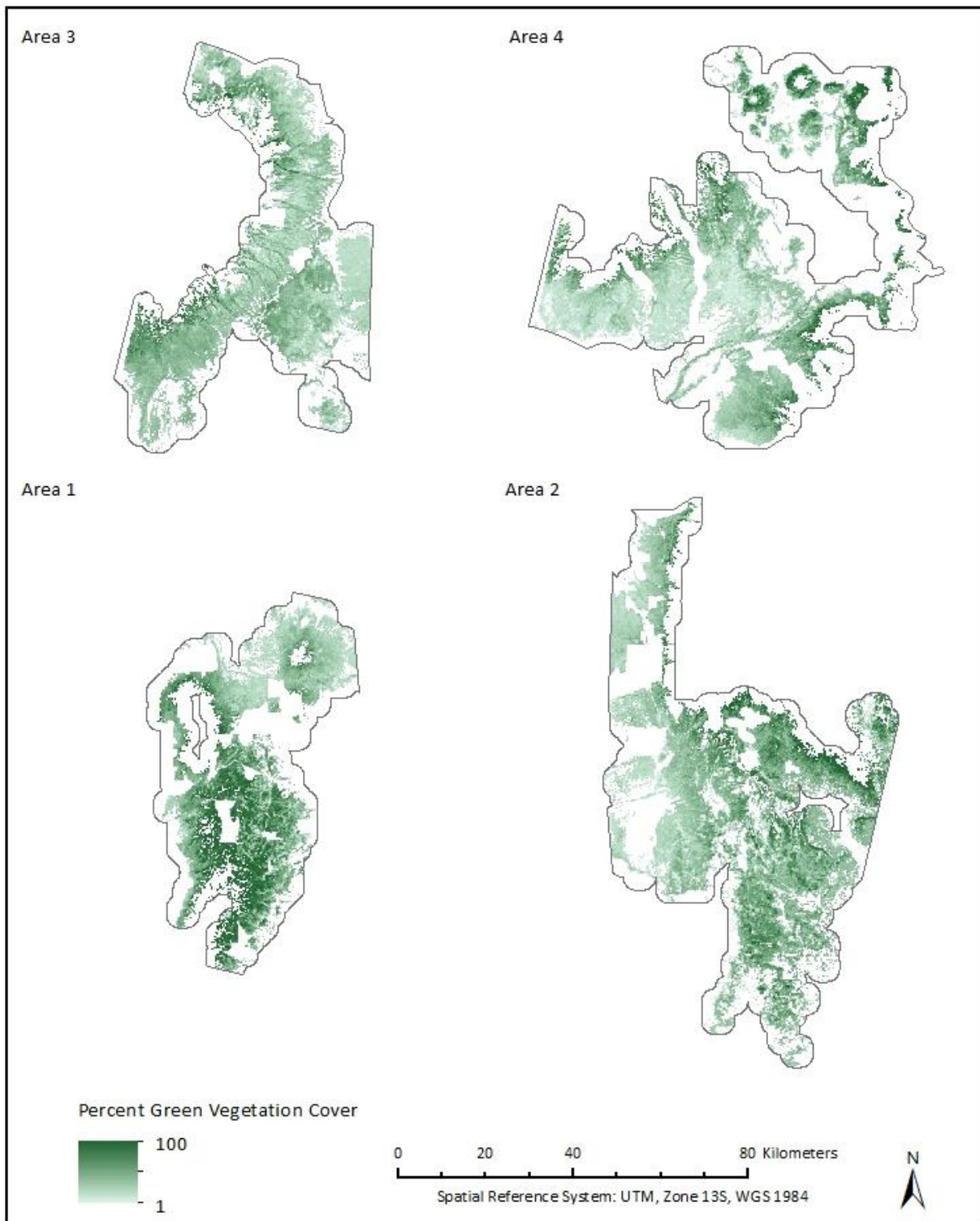


Figure 9. Abundance of green vegetation in 2005, as modeled by MESMA.

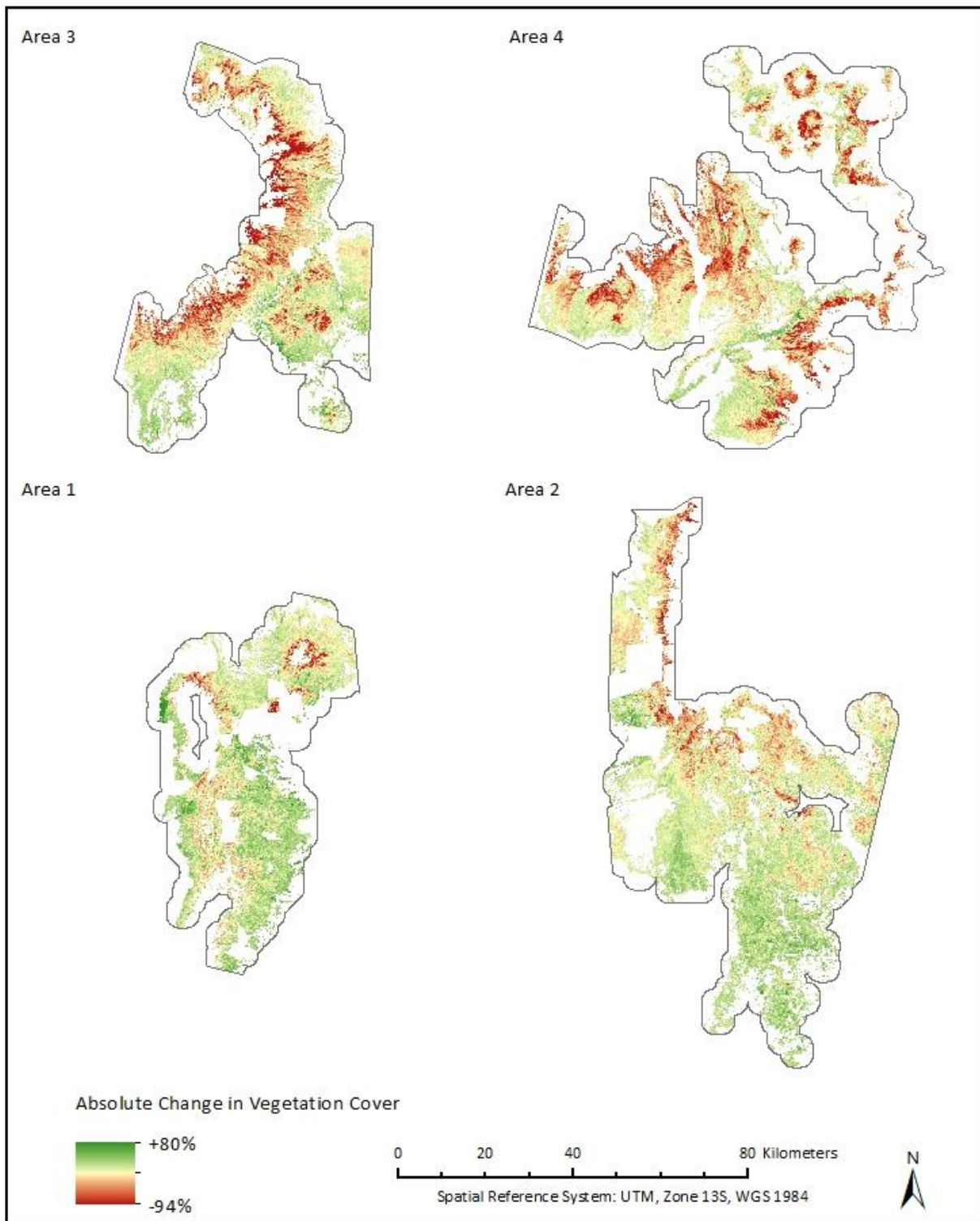


Figure 10. Absolute change in vegetation cover from 2000 to 2005, based on MESMA results.

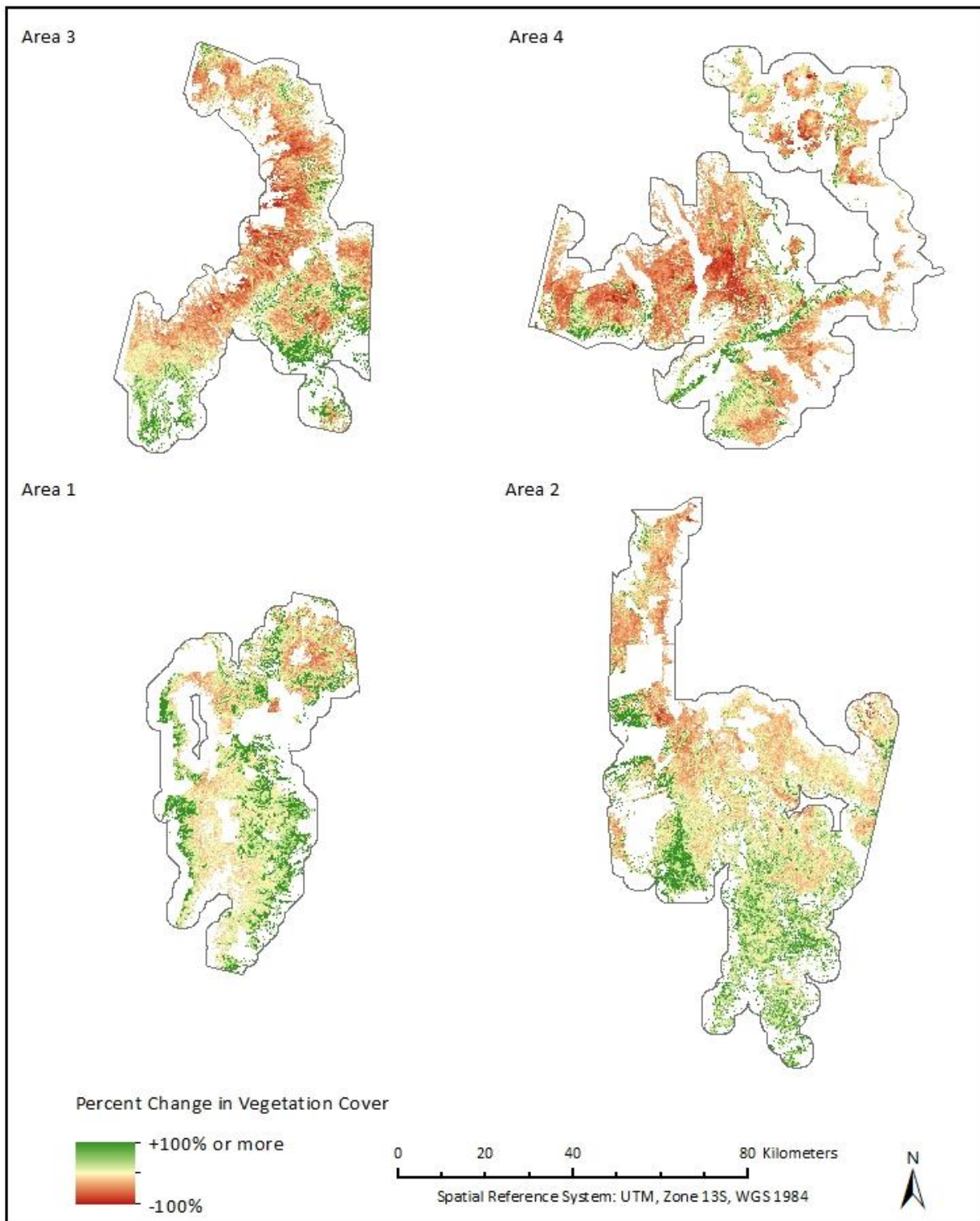


Figure 11. Percent change in vegetation cover from 2000 to 2005, based on MESMA results.

4.3 Spatial models

The second and third objectives of this study were to assess logistic regression, random forest, and conditional inference trees for their suitability to model tree mortality, and to determine which variables were most explanatory in predicting tree mortality. To achieve these objectives, I assessed the overall performance of all models tested. I also compared the three modelling techniques to each other, and assessed both the most explanatory categories of variables, and the most explanatory individual variables. Taking all of the findings into account, a final top model was built, tested, and those results are presented at the end of this section.

4.3.1 Overall model performance

Model performance exhibited some general patterns with regard to types of variables included (Figures 12-15). Models built exclusively on human or topographic variables consistently had the poorest results, with overall accuracy of the human variable models close to the no information rate of 50 percent. Models based only on topographic variables had overall accuracies across the four Areas ranging from 54 (Areas 2, 3) to 64 (Area 1) percent, with a median of 60 percent. There was a wide range of accuracy among soils-based models, from 53 percent overall accuracy (Area 3) for the worst performing model to 83 percent overall accuracy (Area 1) for the best performing model. The median overall accuracy for soils-based models was 65 percent. Models built with a combination of topographic and soils data were also somewhat variable in accuracy, ranging from 55 percent (Area 4) to 79 percent (Area 1) overall accuracy, with a median of 67 percent. Models built from bioclimatic factors ranged from 65 percent (Area 3) to 85 percent overall accuracy (Area 1), with a median of 76 percent. Models built from a combination of all variable types ranged from 64 percent (Area 4) to 83

percent (Area 1) overall accuracy, with a median of 76 percent; however, this included models built from the full set of all 42 variables, which were less optimal than models built from a smaller set of variables because of model complexity (Myung 2000).

While BC2 was the top or second top model in each Area, other competing models varied by Area. In Area 1, the model that generated the highest overall accuracy (85 percent) was the random forest run of BC2; however, a random forest model built from the most important edaphic variables (SO-3) produced only slightly lower results, with an overall accuracy of 83 percent. The random forest model TV4 produced the same overall accuracy as the aforementioned edaphic variables model, however the sensitivity and specificity of the TV4 model was more unbalanced than in the case of SO-3, with TV4 being a better predictor of mortality but a poorer predictor of survival. Both BC2 and TV4 in this Area used eight variables, while SO-3 used five, making it the more optimal model in terms of complexity. Among the three models, sensitivity ranged 82-91 percent, and specificity ranged 75-85 percent.

In Area 2, the top model was the random forest model BC2, with an overall accuracy of 82 percent. The second highest overall accuracy was achieved with the random forest model TV4, with an accuracy of 81 percent. The random forest model TV2 produced very similar results, with an overall accuracy of 81 percent, however TV4 used ten variables, while TV2 used only three. All three models had comparable sensitivity and specificity, identifying true positives (mortality) with an accuracy of around 76-78 percent, and true negatives (survival) with an accuracy of about 84-86 percent.

In Area 3, the highest accuracy was produced by the random forest model AV, with an overall accuracy of 76 percent. The BC2 random forest model, however, produced an almost

identical accuracy, also 76 percent, and used only eight variables, as compared to AV which used the full set of all variables. The next best overall accuracy of 75 percent was obtained from the random forest model TV3, which was a combination of ten bioclimatic and soil variables. Sensitivity and specificity for the three models was quite similar, with sensitivity ranging 76-77 percent and specificity ranging 73-75 percent.

In Area 4, the highest accuracy came from the random forest model TV1, with an overall accuracy of 80 percent. The random forest BC2 model produced an overall accuracy of 79 percent. The next best predictive model, with an overall accuracy of 78 percent was the random forest model AV. As noted above, however, the AV model is built from the entire set of forty two variables and so has substantially greater complexity. By comparison, TV1 in Area 4 used twelve variables, and BC2 used eight. Sensitivity and specificity range among the three models was 77-79 percent, and 76-80 percent, respectively.

While the model SO-3, built from edaphic variables only, performed very well in Area 1, this was not a pattern in the other three Areas, suggesting that edaphic variables alone are not able to consistently predict mortality well in the four Areas and at the scale studied. Apart from this one exception in Area 1, all of the other top three models in all Areas were built either from bioclimatic variables or some combination of variables of multiple types. All except SO-3 included at least three of the four variables ultimately chosen for the final model, BCfin. It appears from this evidence that, in general, models built partially or completely from bioclimatic variables are the most accurate predictors for mortality among the models considered. Model results for all Areas can be found in Appendix E.

4.3.2 Comparison of model types

Model accuracy was in general more closely tied to the set of input variables used, as discussed above, than to the model type. In general, however, random forest models tended to produce better results than conditional inference trees and logistic regression models (Figures 12-15).

This was most noticeable among the soils-only models, where random forest models had balanced accuracies which were on average 5.5-6.5 percentage points higher than the highest accuracy achieved by a logistic regression or conditional inference tree model (minimum and maximum difference averaged across all Areas). In each Area, seven to nine of the top ten highest accuracy models were random forest models, and in each Area the highest balanced accuracy was obtained from a random forest model. It may be that the ensemble approach of random forest is better able to capture the complex relationships between variables than the other two methods, and that may explain why the random forest models in general had better overall accuracies than the other two type of model. The performance of logistic regression vs. conditional inference trees showed no discernable pattern, with logistic regression producing better results in some cases and conditional inference trees performing better in others.

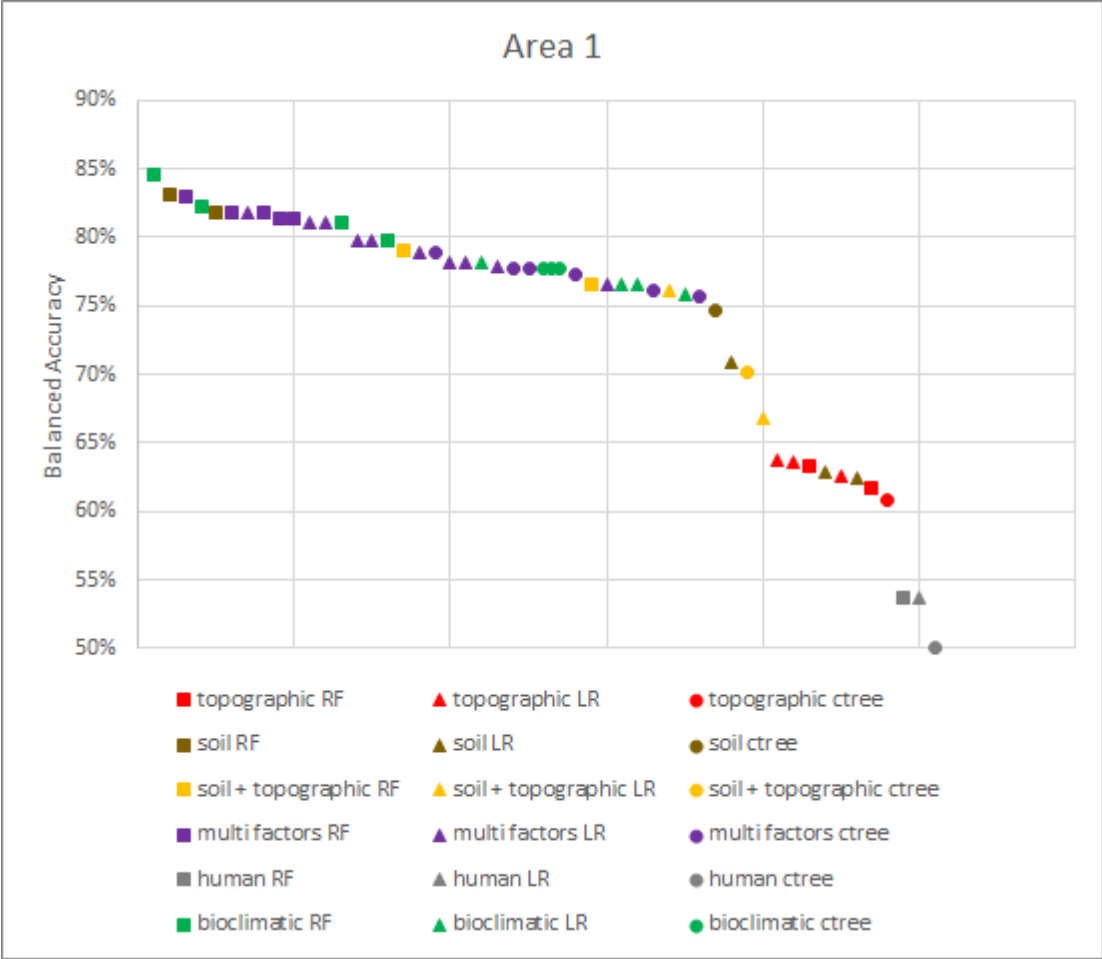


Figure 12. Area 1, all models ranked by balanced overall accuracy. RF = random forest, LR = logistic regression, ctree = conditional inference tree.

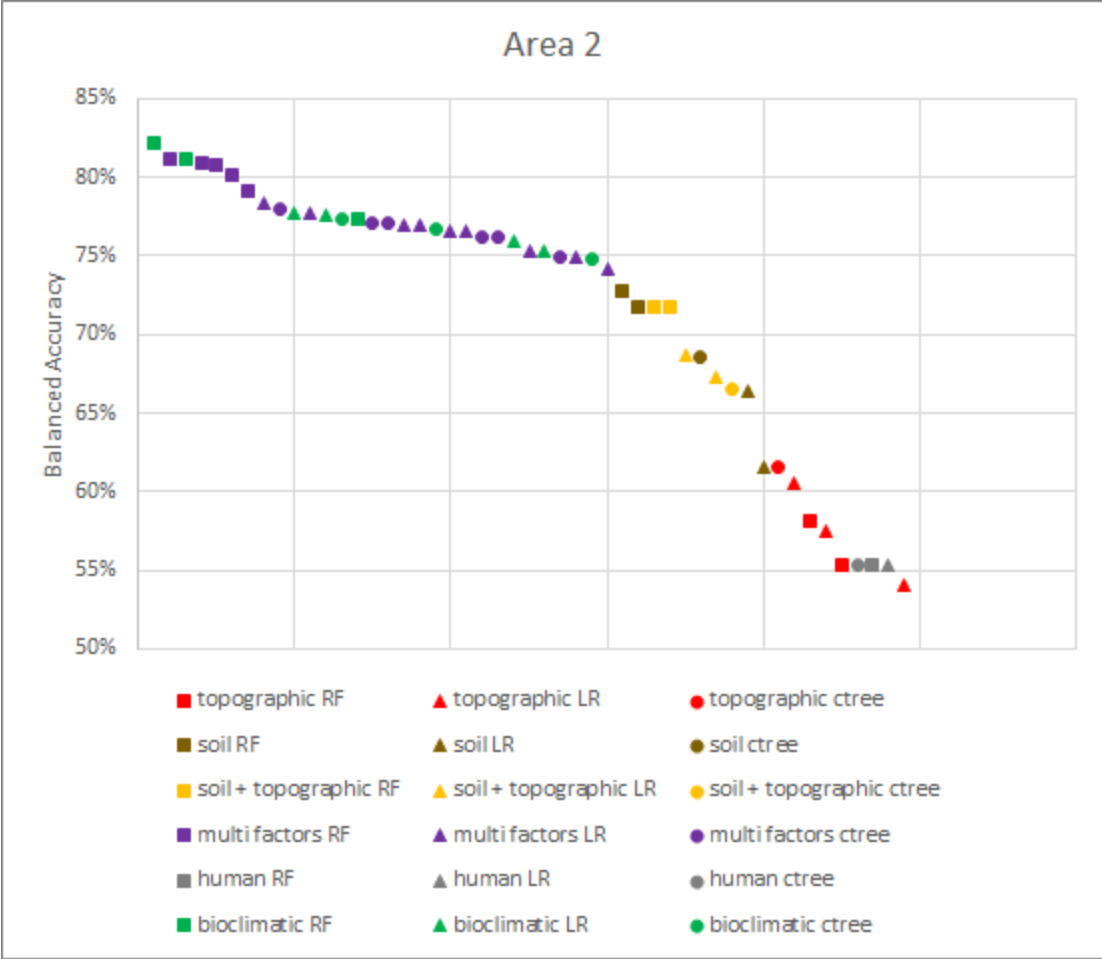


Figure 13. Area 2, all models ranked by balanced overall accuracy. RF = random forest, LR = logistic regression, ctree = conditional inference tree.

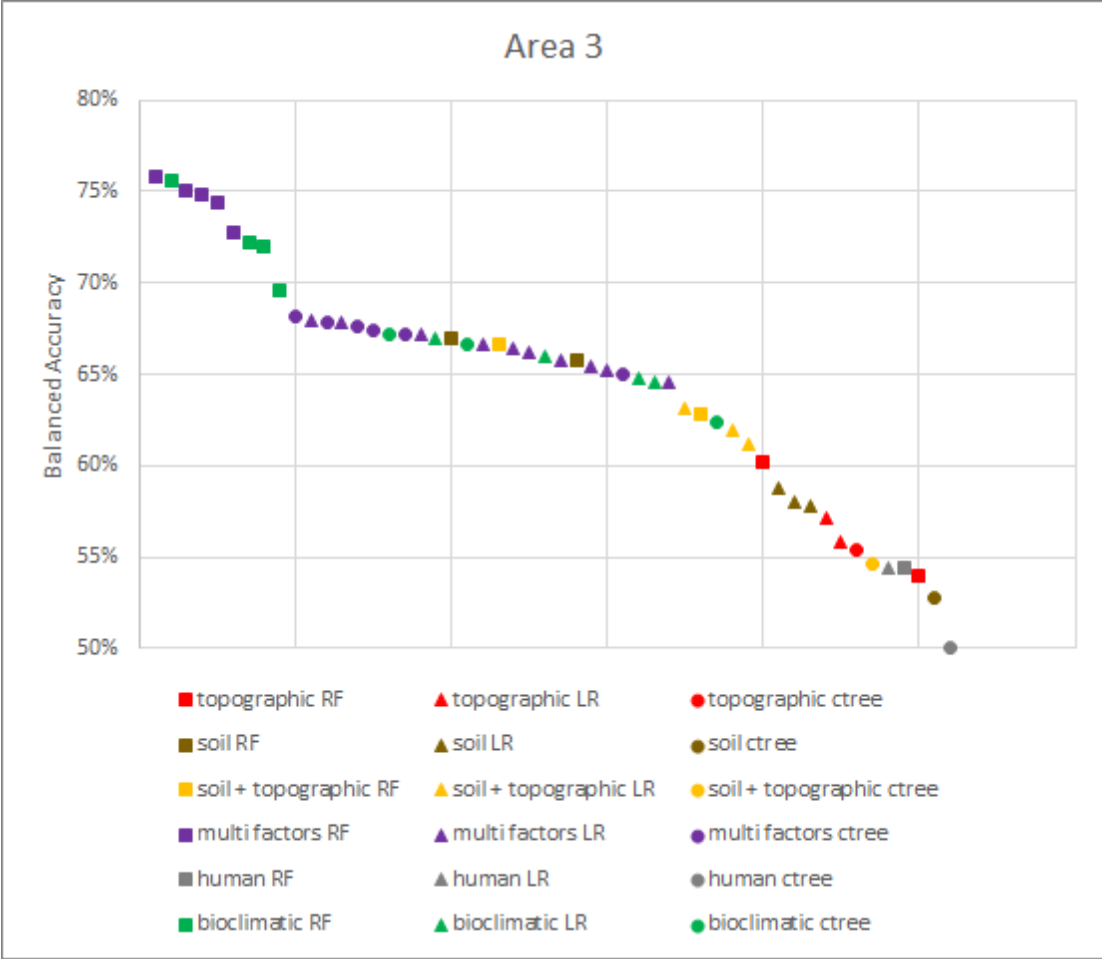


Figure 14. Area 3, all models ranked by balanced overall accuracy. RF = random forest, LR = logistic regression, ctree = conditional inference tree.

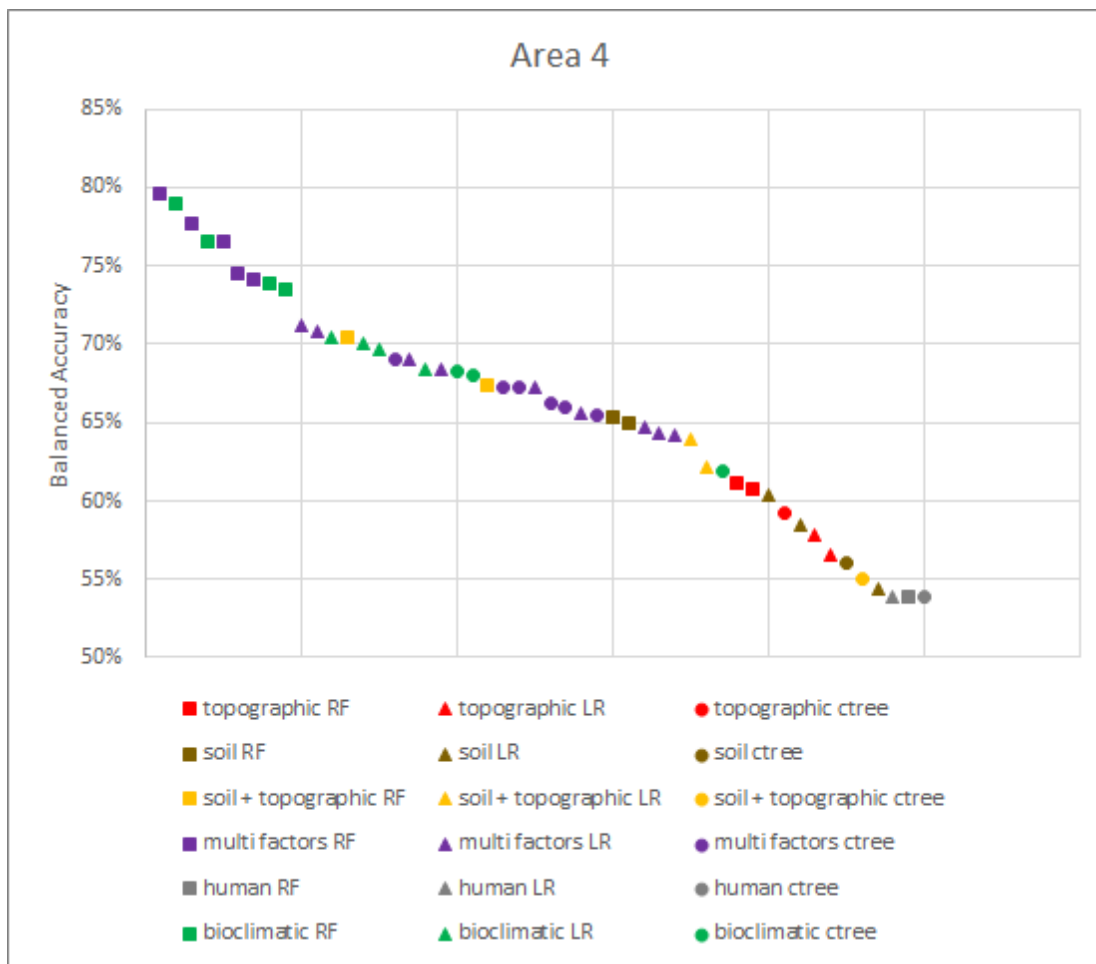


Figure 15. Area 4, all models ranked by balanced overall accuracy. RF = random forest, LR = logistic regression, ctree = conditional inference tree.

4.3.3 Factors explaining pinyon mortality

The ultimate goal of this study was to determine the variables that best explain pinyon mortality. Each of the modeling techniques used yielded information of a slightly different type, and taken together, these complementary attributes help round out the picture of the relationship of explanatory variables to tree mortality.

4.3.3.1 Variable importance from random forest

Random forest evaluates variable importance based on two criteria – mean decrease in accuracy and mean decrease in Gini Impurity, which represents how well a variable was able to split a group of observations into pure nodes. While both are meaningful measures, I present here only mean decrease in accuracy (Figures 16-20) as there were few differences in the variables indicated as important by the two measures. Mean decrease in accuracy is a measure of the change in prediction accuracy when the variable is permuted; the difference in accuracy is averaged across all trees in the forest and normalized by the standard deviation of the differences (Breiman et al. 2018). While extreme caution must be used in attempting to interpret the absolute values outside of the model for which they were generated, the numbers do give a general sense of which variables were more important than others. A large mean decrease in accuracy as a result of the permutation indicates high variable importance, while a value close to zero can be interpreted to mean that the variable is unimportant (Cassidy and Deviney 2014). Variable importance according to mean decrease in accuracy varied somewhat across the four Areas. When variable importance from all models and all Areas were evaluated together (Figure 20), seven of the top ten variables were bioclimatic, and three were edaphic (Table 8).

Table 8. Top 10 variables by mean decrease in accuracy (random forest).

Variable name	Represented feature	Areas in which this was a top 10 variable
bio3	Isothermality	A1, A2, A3, A4
bio6	Minimum temperature of coldest month	A2, A3, A4
ndmi2000	Pre-drought NDMI	A1, A2, A3, A4

Variable name	Represented feature	Areas in which this was a top 10 variable
bio9	Mean temperature of driest quarter	A1, A3, A4
bioppnov	November precipitation	A1, A2, A3, A4
bio18	Precipitation of warmest quarter	A1, A2, A3, A4
soawcft1	AWC of the top 31 cm (1 ft) of soil	A1, A2, A3, A4
soclaytot	Clay percent of top 122 cm (4 ft) of soil profile (weighted average)	A1, A2, A3
bio15	Precipitation seasonality [coefficient of variation]	A2, A3, A4
sosrfclpct	Clay percent of the surface soil	A1, A3, A4

Although there was some variation in order, half of the variables in Table 8 were among the top ten for each of the four Areas, and the other half were in the top ten for at least three of the four Areas. In Areas 1, 2, and 4, bio3 consistently ranked highest in variable importance across all the models it was used in, and in Area 3, bio6 was consistently the top variable.

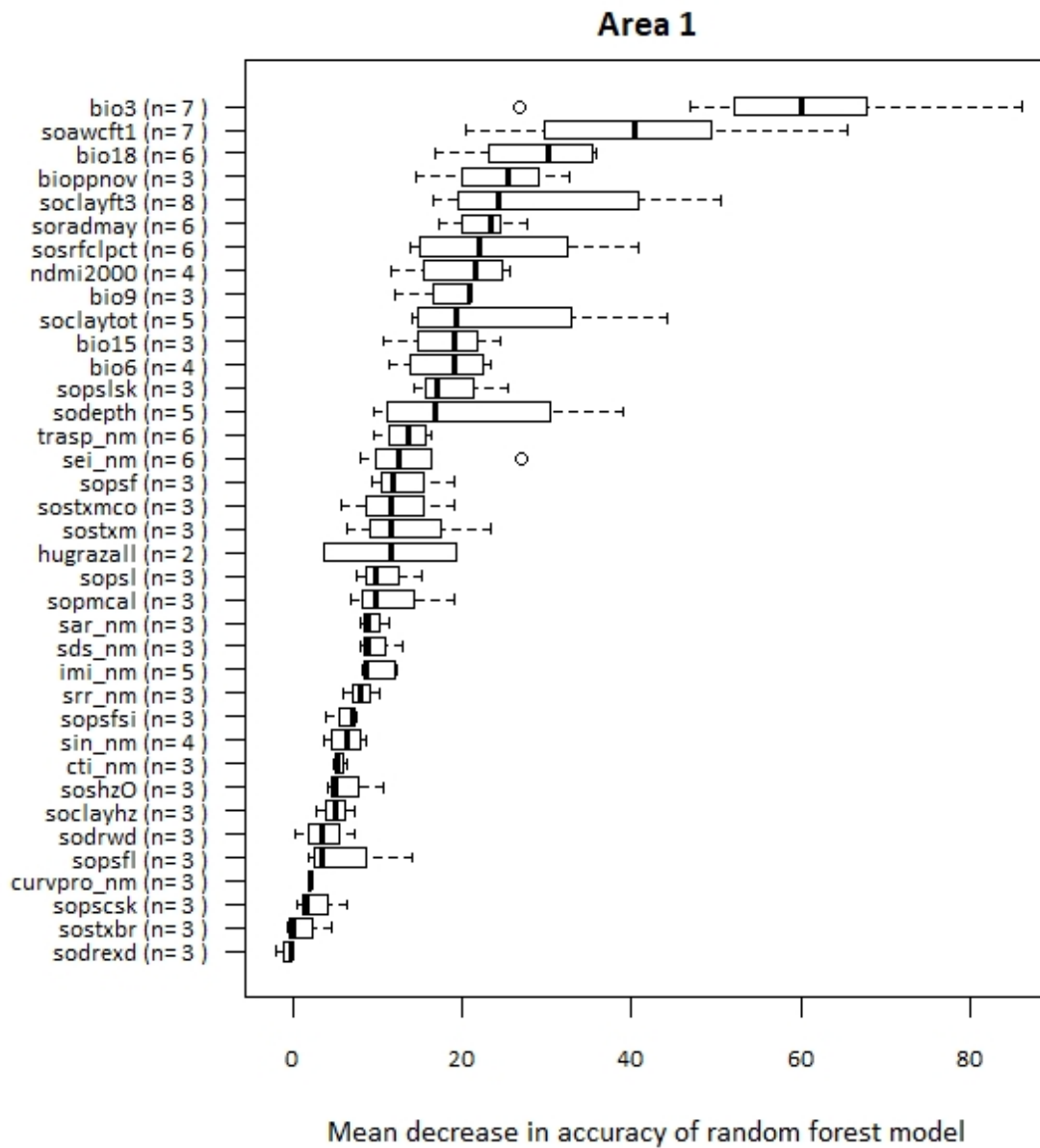


Figure 16. Area 1, variable importance in random forest models.

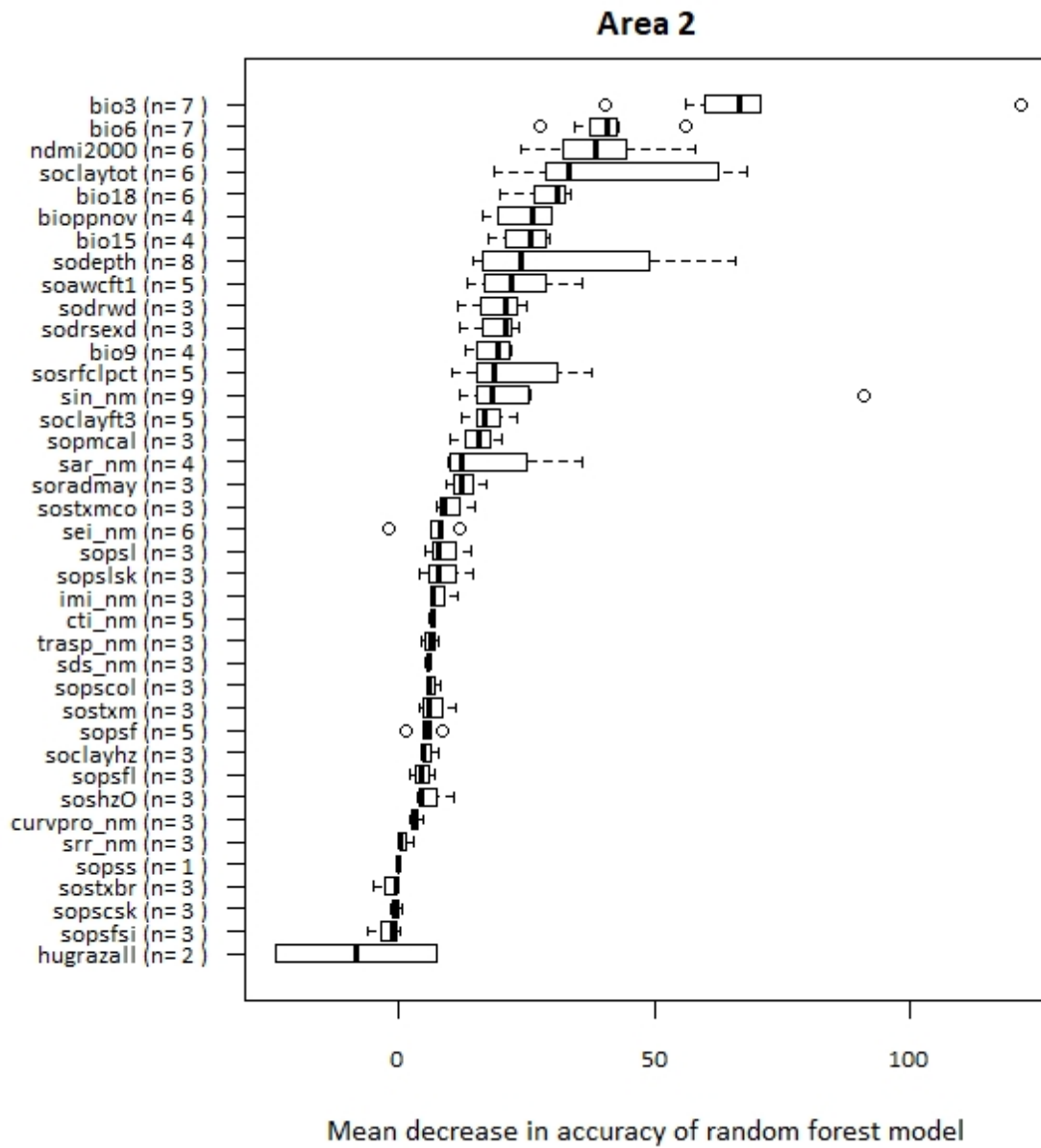


Figure 17. Area 2, variable importance in random forest models.

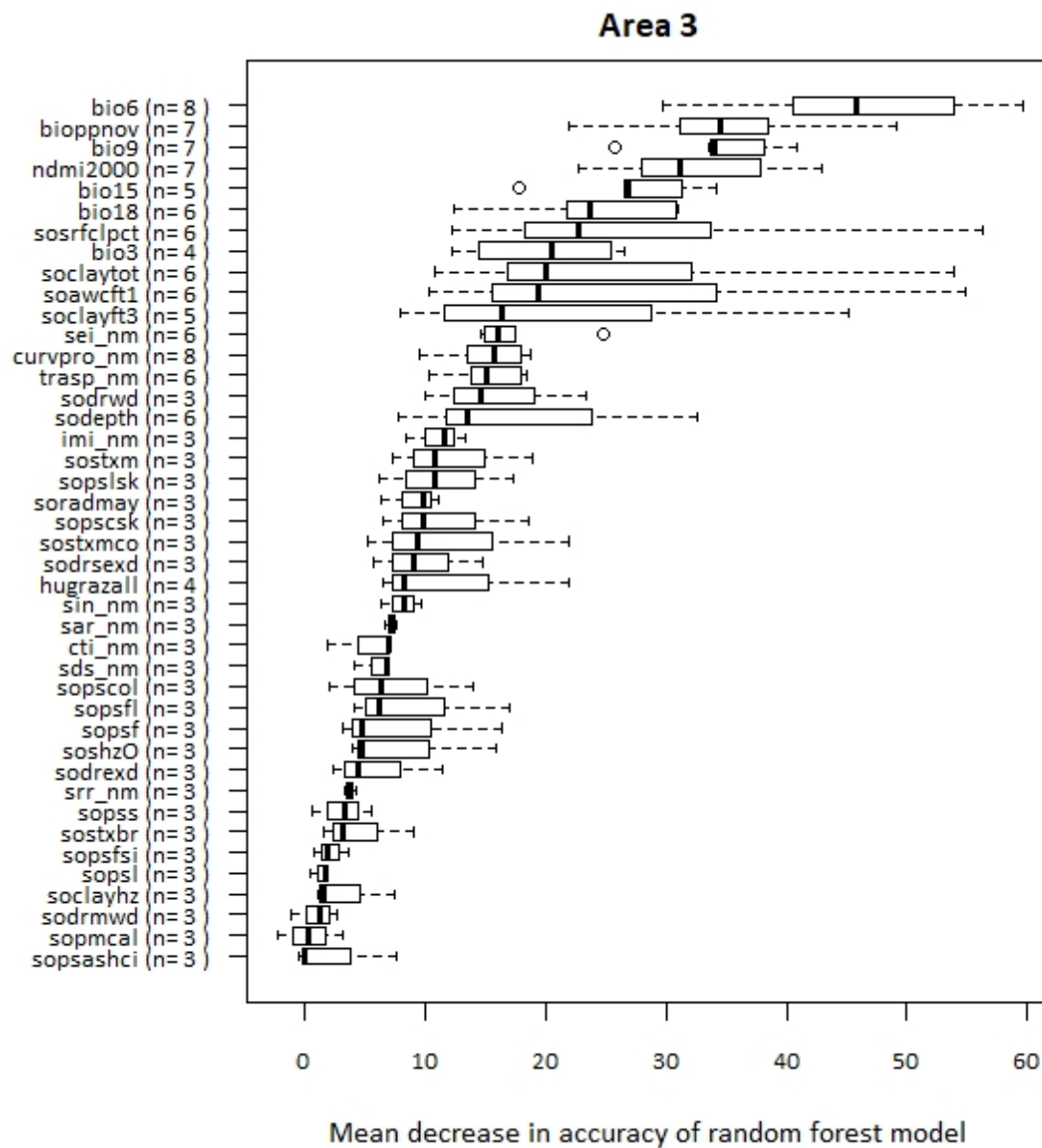


Figure 18. Area 3 variable importance in random forest models

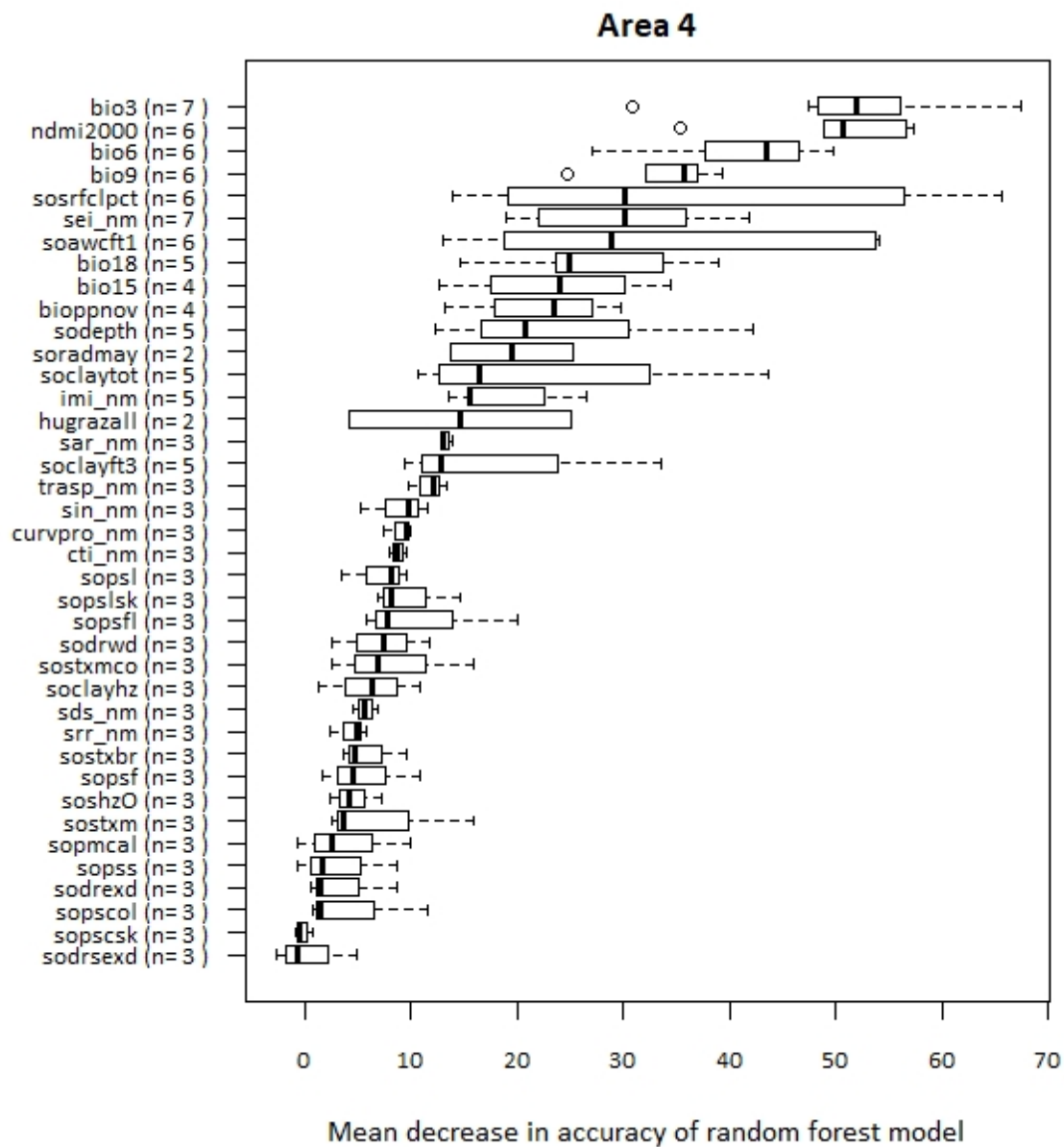


Figure 19. Area 4, variable importance in random forest models.

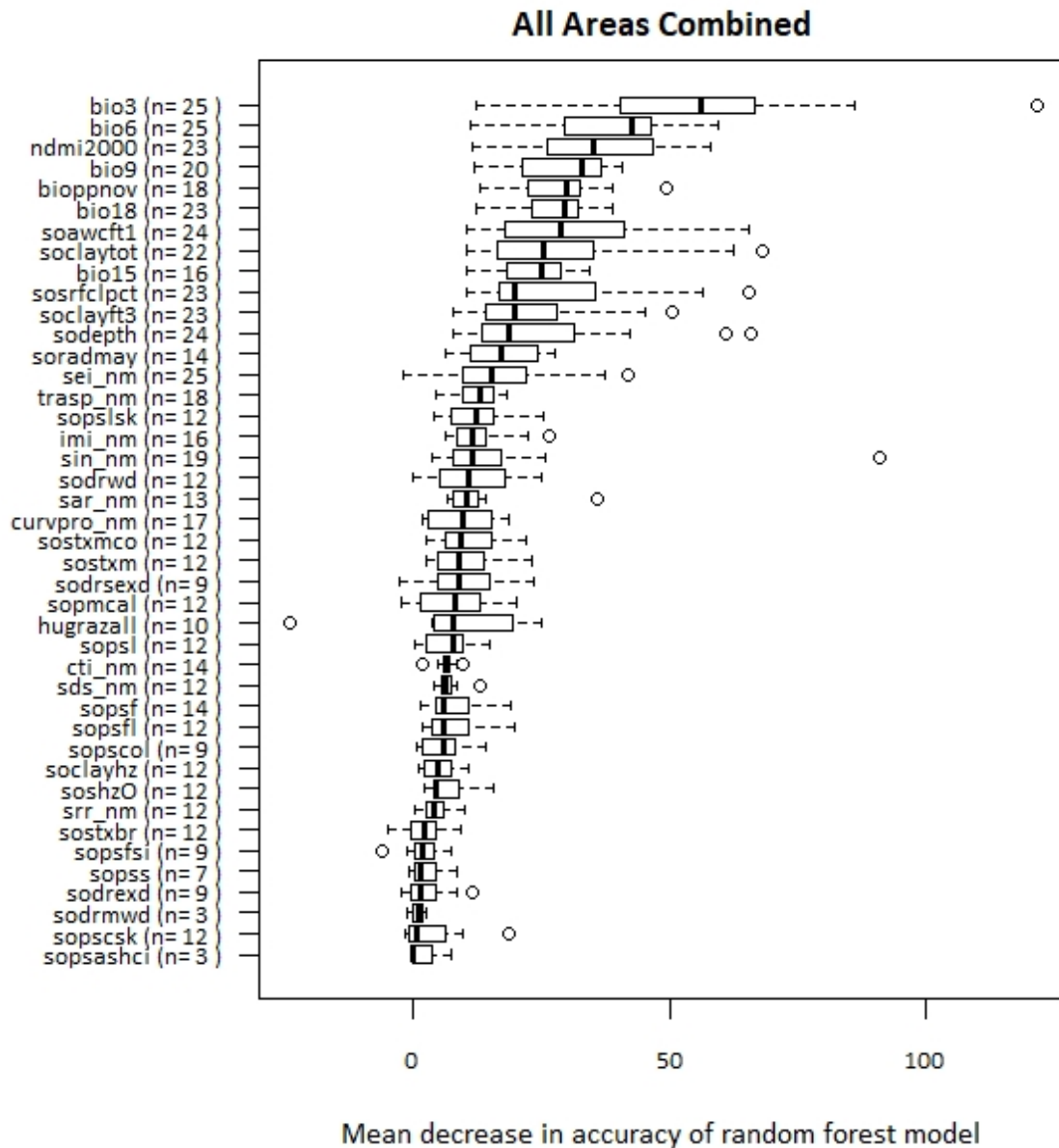


Figure 20. All areas combined, variable importance in random forest models.

4.3.3.2 Variable attributes from logistic regression models

To gain more insight about the ten variables indicated in Table 8 and their relationship to tree mortality in the study Areas, I analyzed the information I was able to gain from the logistic

regression model outputs. The two measures I inspected were the sign of the coefficient, indicating a negative or positive relationship to tree mortality, and the returned value of $Pr > |z|$, indicating the statistical significance of the relationship. Both were somewhat variable across models and Areas (Figures 22-26).

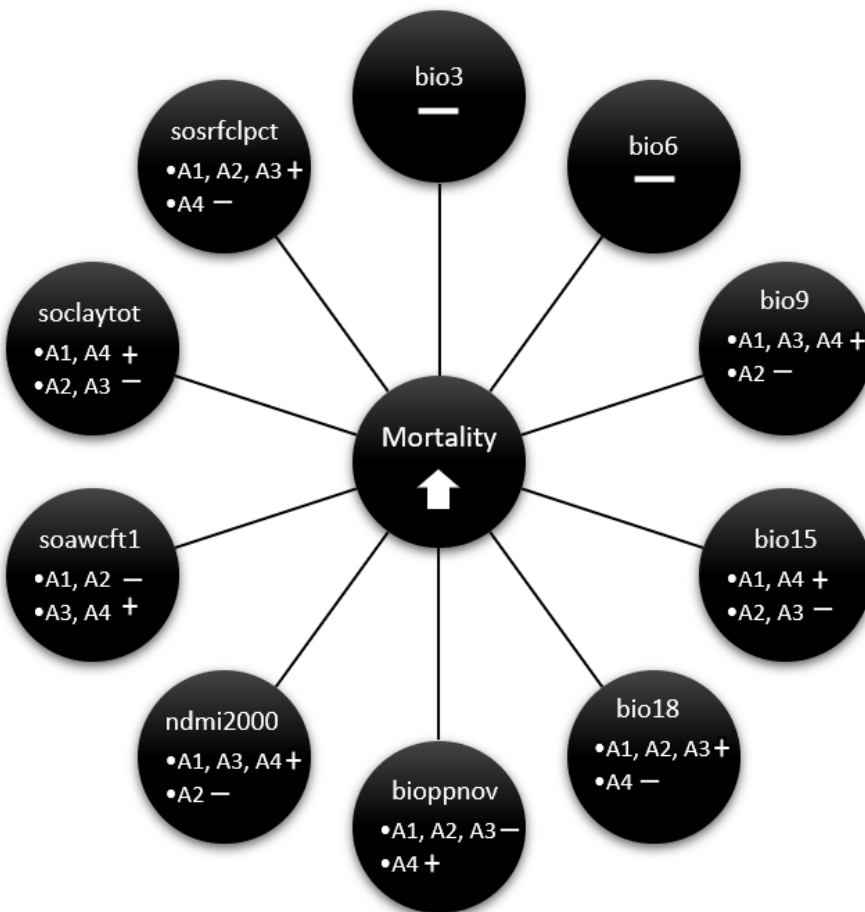


Figure 21. Direction of the relationship between the variables identified in Table 9 and tree mortality, as indicated by the sign of the coefficient across all or the majority (where results were inconsistent) of logistic regression models run in each Area.

While the value of the coefficient for each variable was understandably different in different models, I had expected the sign of the coefficient to be the same throughout, and

across all Areas, indicating a generally similar direction of relationship to tree mortality, however, this turned out not to be the case. While the coefficient sign was fairly consistent across all models in any given Area, it was not the same across all Areas for eight of the ten variables. A summary visualization is presented in Figure 21, where increasing likelihood of tree mortality is indicated by the central arrow, and the majority sign of the coefficient for each variable in each Area is presented in the diagram's branches.

With regard to variable significance, in each Area, there were certain variables that consistently had a low $Pr>|z|$ value, but the precise variables for which this was true varied by Area. Taken together, both of these findings appear to suggest that the relationships between these variables and tree mortality are complex and difficult to disentangle. There may also be other contributing factors, and a more detailed assessment of each variable is presented below.

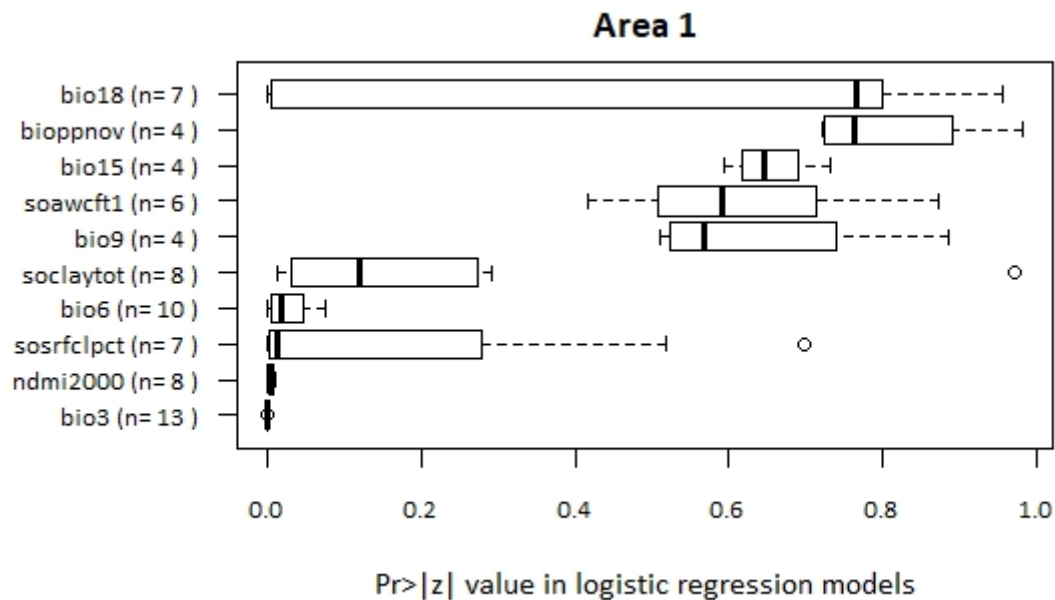


Figure 22. Significance of the relationship between variables and tree mortality in logistic regression models for Area 1. Results presented are for the ten variables identified from random forest in Table 9.

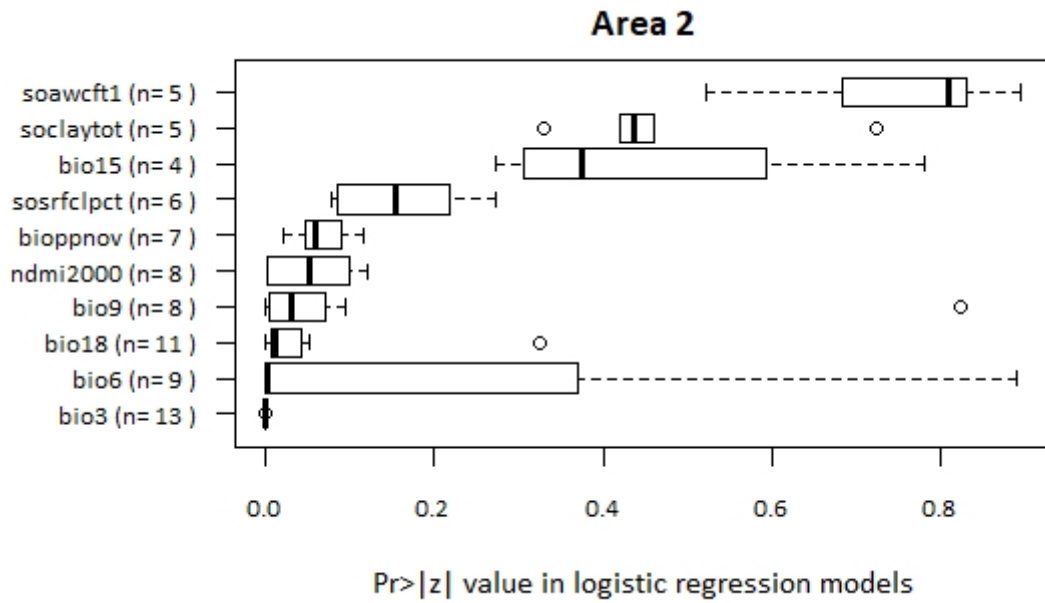


Figure 23. Significance of the relationship between variables and tree mortality in logistic regression models for Area 2. Results presented are for the ten variables identified from random forest in Table 9.

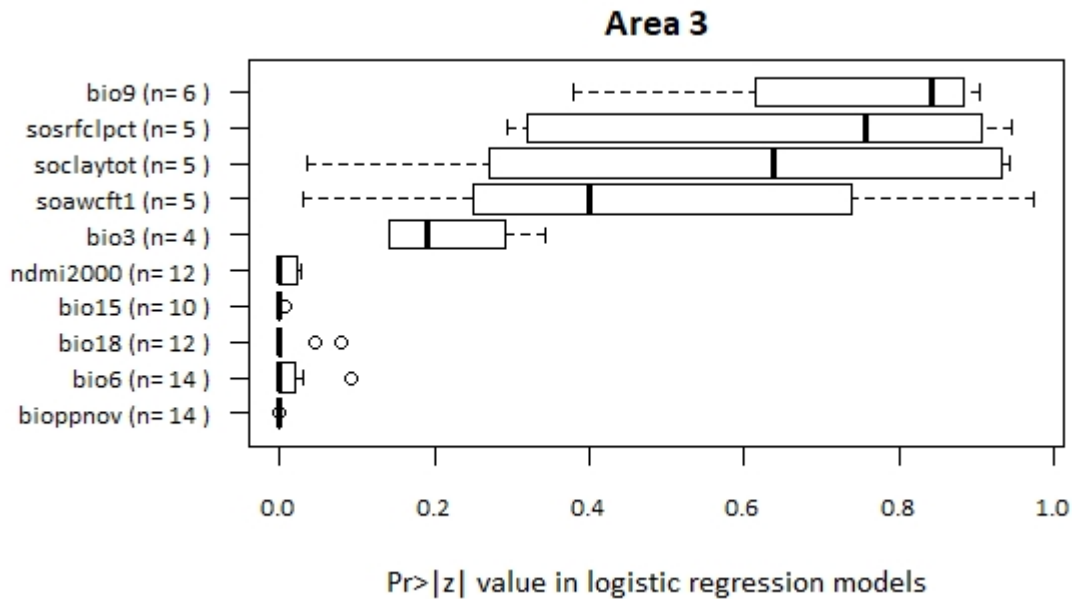


Figure 24. Significance of the relationship between variables and tree mortality in logistic regression models for Area 3. Results presented are for the ten variables identified from random forest in Table 9.

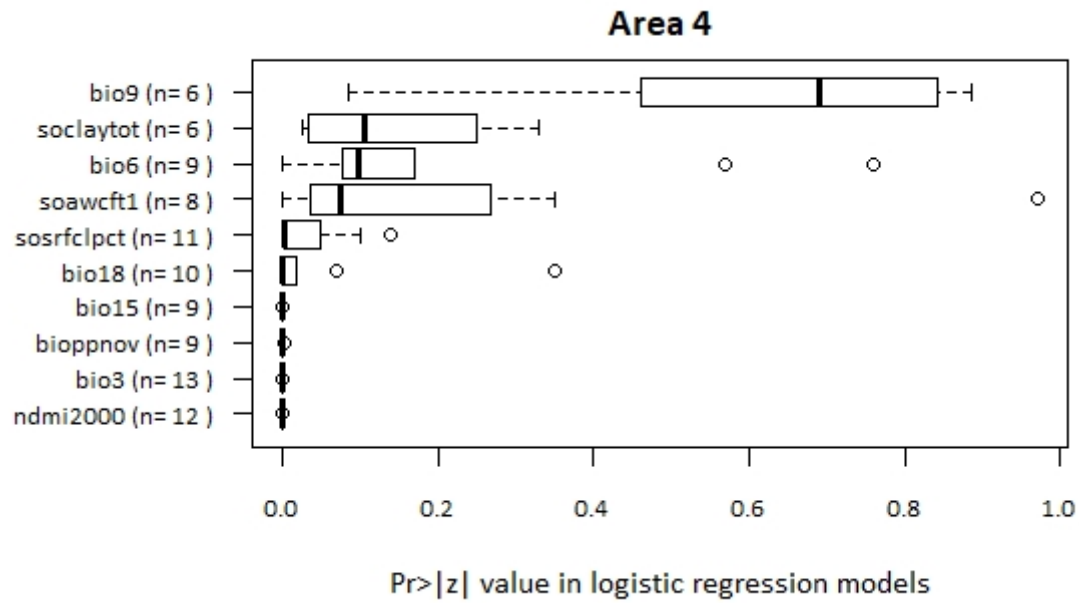


Figure 25. Significance of the relationship between variables and tree mortality in logistic regression models for Area 4. Results presented are for the ten variables identified from random forest in Table 9.

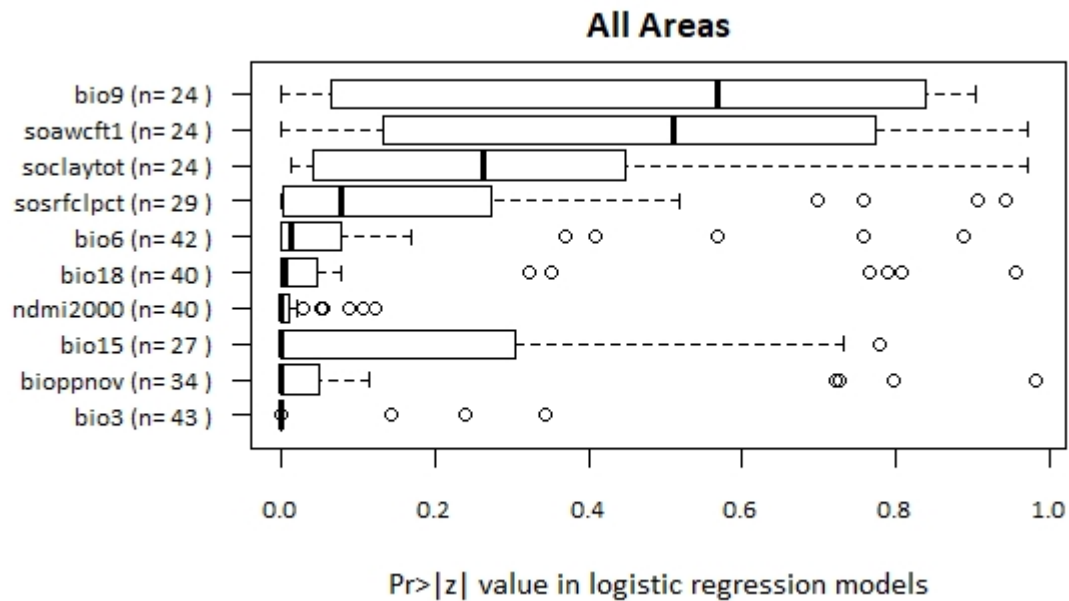


Figure 26. Significance of the relationship between variables and tree mortality in logistic regression models, aggregated across all four Areas. Results presented are for the ten variables identified from random forest in Table 9.

Bio3. Bio3, isothermality, had a consistently low $Pr>|z|$ value across all the logistic regression models it was used in. In most, it had a $Pr>|z|$ value of <0.0001 . The highest value was 0.34, in Area 3. This is consistent with the results from random forest and conditional inference trees (next subsection) that indicated bio3 is in general a highly important variable, but with a weaker relationship to tree mortality in Area 3 than in the other Areas. In all cases, the sign of the coefficient was negative, indicating a higher likelihood of mortality at sites with a lower isothermality value, and thus, a larger difference between diurnal temperature variability and annual temperature variability. Isothermality represents the ratio of the mean diurnal temperature range to the annual temperature range. Values smaller than unity indicate that temperature variability within an average month is less than the annual summer-to-winter oscillations (O'Donnell and Ignizio 2012). The smaller the value, the more difference there is between the diurnal temperature range and the annual range.

Bioppnov. Bioppnov, November precipitation, in general had a significant relationship with tree mortality, with a $Pr>|z|$ value consistently <0.0001 in Areas 3 and 4, and <0.05 in all but one model in Area 2. In Area 1, the $Pr>|z|$ value approached 1 in all models, indicating that this variable was not explanatory in logistic regression models for tree mortality in this Area. In Areas 1, 2, and 3, bioppnov was negatively related to increasing likelihood of tree mortality, and in Area 4, the relationship was positive. Williams et al. (2013) found winter precipitation to be an important variable in modeling drought-related pinyon mortality, and the importance of winter precipitation for deep soil water recharge has been noted by others (Phillips and Ehleringer 1995; West et al. 2007). It is unclear why there was a positive relationship in Area 4, however, it could be that in this Area, where the precipitation averages slightly higher than in

other Areas, sites with higher winter precipitation had higher mortality due to structural overshoot (Jump et al. 2017).

Bio15. For bio15, precipitation seasonality, the significance in logistic regression models varied by Area. In Areas 3 and 4, the $Pr>|z|$ value was consistently <0.001 . In Areas 1 and 2, it ranged from 0.27 to 0.73, depending on the model. In Areas 1 and 4, the relationship of this variable to likelihood of tree mortality was positive, and in Areas 2 and 3, the relationship was predominantly negative. Given this inconsistency, it may be that the relationships between bio15 and tree mortality are spurious, despite the apparent significance in two of the Areas.

Ndmi2000. *Ndmi2000*, the pre-drought NDMI value, had a $Pr>|z|$ value of <0.05 in all logistic regression models for in Areas 1, 3, and 4. In Area 2, the $Pr>|z|$ value ranged from 0.002 to 0.12, depending on the model. This was also the only Area in which the sign of the coefficient was negative instead of positive. NDMI was highly correlated with NDVI in the data used in this study, so from these results it appears that sites with higher green biomass and higher vegetation moisture had, in general, higher probability of mortality. As with winter precipitation in Area 4, this may be evidence of some structural overshoot (Jump et al. 2017) or perhaps some density-dependent mortality. In Areas 2, the opposite was the case, however, as noted, some of the $Pr>|z|$ values were quite high so it could be that this variable was a poor predictor in Area 2.

Bio18. For bio18, the precipitation of the warmest quarter, the $Pr>|z|$ value, while generally low (<0.05), was quite variable in all Areas, ranging overall from <0.0001 to 0.96, suggesting that the strength of the relationship for this variable is dependent upon the presence of certain other variables or certain combinations thereof. In Areas 1, 2, and 3, the

relationship between bio18 and mortality was a positive one, however in Area 4, the relationship was negative. In general, it appears that mortality was higher at sites where the precipitation of the warmest quarter is typically higher. This may indicate a heavier reliance on the summer monsoon for moisture in Areas 1, 2, and 3, and also may be evidence of some structural overshoot (Jump et al. 2017), as noted above in the case of biopnov.

Bio6. For bio 6, the minimum temperature of the coldest month, the $Pr>|z|$ value was variable across models in all Areas and ranged from <0.0001 to 0.9, suggesting that, like bio18, the usefulness of this variable in a logistic regression model depends on other variables included in the model. Unlike bio18, however, the sign of the coefficient was consistently negative across all models in all Areas, with the exception of one non-significant positive relationship in one Area 4 model. This suggests that in all four Areas, higher likelihood of mortality is associated with sites that have lower minimum temperatures. This could be a direct relationship, or it is possible that lower minimum temperature is in this case acting as a surrogate for sites with a higher elevation or higher seasonal variability.

Sosrfclpct. For sosrfclpct, the percent clay content of the surface soil, the $Pr>|z|$ value ranged from 0.0001 to 0.94, with many of the higher values occurring in models for Areas 2 and 3. In general, most of the coefficients associated with this variable were positive, indicating that the likelihood of mortality increases with increasing clay percent in the soil surface. The exception to this was Area 4, where the relationship was always negative, indicating better chances of survival with increasing clay percent in the surface soil. The soil surface clay percent minimum, maximum, and average in Area 4 did not differ appreciably from those of the other Areas, so it is unclear why there was a difference in the direction of the relationship, however it

could be that in this Area, surface clay percent covaries with some other more explanatory phenomenon not included in this study.

Soclaytot. The $Pr > |z|$ value for *soclaytot*, the weighted average clay content of the soil profile, varied by Area and model, but in no cases was it ever smaller than 0.01. In the majority of cases, the significance of this variable was quite weak, indicating that, while it may have been helpful in tree-based models, most of the logistic regression models fit were unable to make effective use of this variable. In Areas 1 and 4, the relationship was mostly positive, and in Areas 2 and 3, the relationship was mostly negative. There are two possible explanations – the first is that, as hypothesized for *bio15*, this may in fact be a spurious relationship. The second possibility is, given the difficulty that logistic regression models had in finding a significant relationship at all, there may be a threshold clay content value beyond which likelihood of mortality increases, rather than a progressively increasing/decreasing relationship. Given the water-holding properties of clay, it would not be surprising if this were the case. As compared with a sandy soil, a soil with moderate clay content typically has a higher AWC, which is usually beneficial to plants. However a soil that is very high in clay can actually be detrimental as it will hold the soil water so tightly that plants have increased difficulty accessing it.

Soawcft1. *soawcft1*, the AWC of the first foot of soil, displayed a wide range of values for $Pr > |z|$, but in general was only weakly to non-significant in most logistic regression models and was < 0.1 in only six out of twenty-four cases. In Areas 1 and 2, the direction of the relationship defined by the logistic regression model was usually negative, and in Areas 3 and 4, the coefficient was usually positive. As hypothesized with *soclaytot*, it may be that a certain

threshold value defines the relationship of this variable to mortality better than a constant rate of increase or decrease.

Bio9. bio9, mean temperature of the driest quarter, had the largest median value of $Pr>|z|$ out of the ten variables considered. In a quarter of cases, the $Pr>|z|$ value was <0.05 , however in the other three-fourths, the value ranged from 0.08 to 0.9. In Areas 1, 3, and 4, the coefficient was usually positive, however in Area 2, the coefficient was consistently negative. Given the inconsistencies observed and relatively high $Pr>|z|$ values, it could be that this variable is a poor predictor of mortality in the models tried, and the importance indicated by random forests may be the result of a spurious relationship.

4.3.3.3 Patterns in variables from conditional inference trees

In Areas 1, 2, and 4, isothermality (bio3) was the variable consistently chosen, when available, as the root node in conditional inference trees, indicating the most significant statistical relationship. In Area 3, the relationship with isothermality was comparatively weak, and instead the minimum temperature of the coldest month (bio6) was the variable consistently selected as the root node in conditional inference trees. These results follow the patterns observed in random forest models with regard to variable importance (Figures 16-20), and the patterns of statistical significance seen in the logistic regression models (Figures 22-26).

I built a single-split, univariate conditional inference “tree” -otherwise known as a stump- using bio3 for Areas 1, 2, and 4, and bio6 for Area 3. While only achieving poor to moderate overall accuracy in each Area, these stumps did reveal some interesting patterns (Figures 27-30). In Area 1, 70.3 percent of the sites that has an isothermality value of ≤ 346 experienced mortality, compared with only 5.3 percent of the sites that had an isothermality

above 346 (Figure 27). In Area 2, the isothermality threshold that provided the best split was also 346. In this Area, 86.4 percent of the sites with a value ≤ 346 had mortality, while only 30.1 percent of the sites with an isothermality value higher than this experienced mortality (Figure 28). In Area 4, 62.5 percent of the sites with an isothermality value ≤ 339 had mortality, vs. 34.6 percent of the sites with an isothermality value higher than this (Figure 30). Even though the threshold value selected by the algorithm was slightly different for Area 4 than for Areas 1 and 2, in all three Areas the prevalence of mortality increased at smaller isothermality values. As noted above, isothermality represents the ratio of diurnal to annual temperature range. In the dataset used for this analysis, the initial ratio obtained is multiplied by 1,000, so a hypothetical value of 1,000 would indicate a diurnal range that is equal to the annual temperature range.

I attempted to build a univariate stump in bio3 for Area 3 for comparability; however, the statistical relationship between this variable and mortality presence/absence was less than the minimum threshold set ($p=0.25$) and the model failed to run. A univariate tree built on bio6, however, revealed that, among observation points for which the minimum temperature of the coldest month was less than or equal to -6.8 °C, 60.1 percent of the sites had mortality, compared with 25.9 percent of the sites that had a minimum temperature higher than this, indicating that a lower minimum temperature of coldest month was correlated with higher mortality (Figure 29).

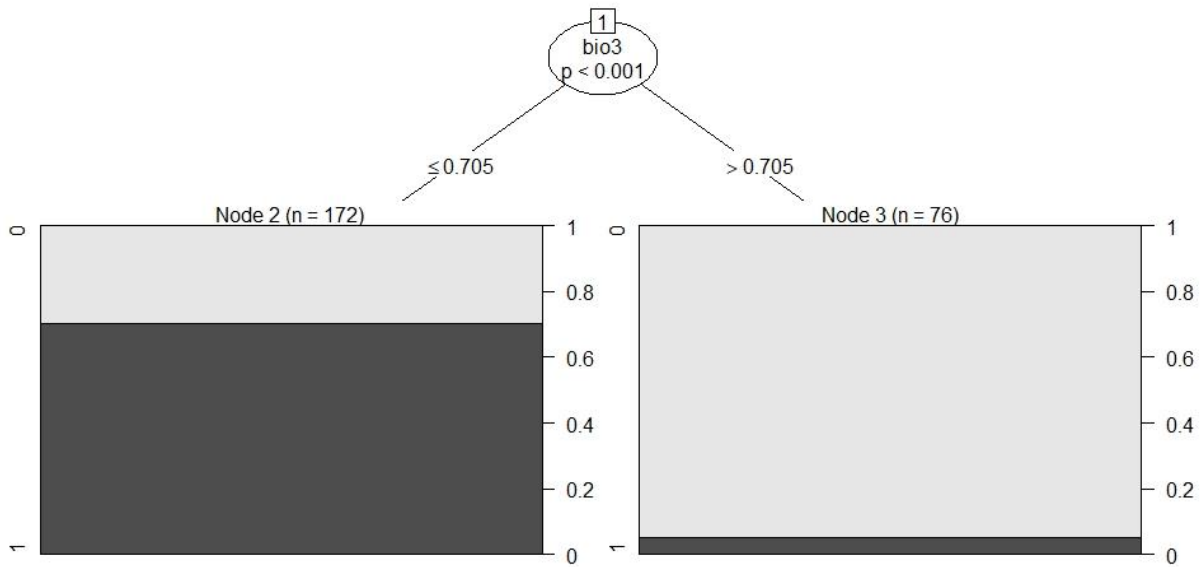


Figure 27. Area 1, univariate conditional inference tree. Cross-validated overall accuracy = 77.8 percent. Backtransformed value: 0.705 represents an isothermality value of 346.

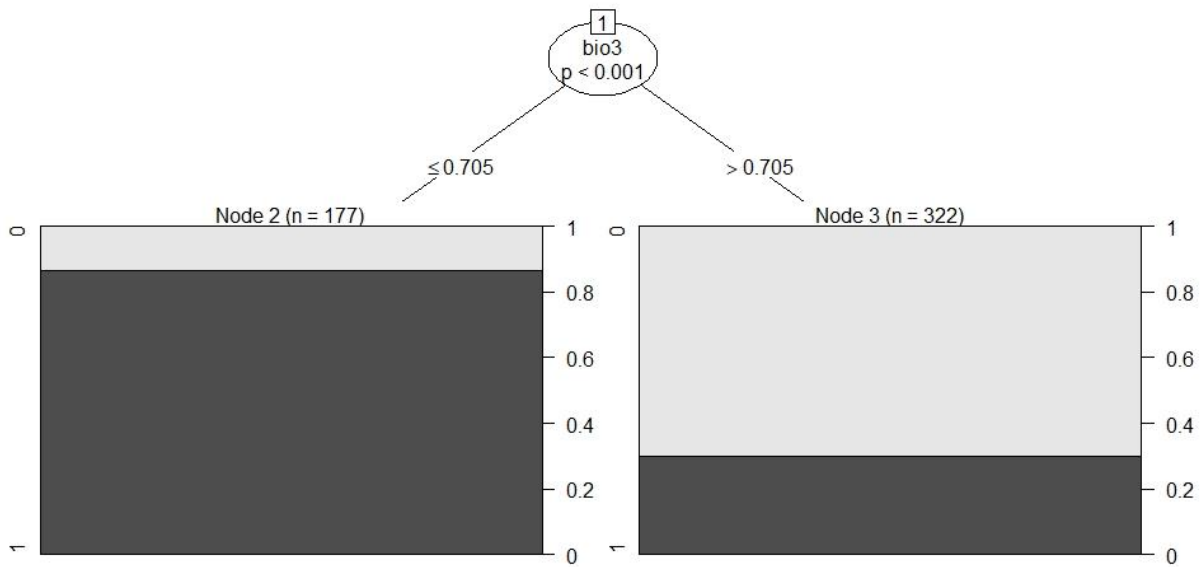


Figure 28. Area 2, univariate conditional inference tree. Cross-validated overall accuracy = 74.8 percent. Backtransformed value: 0.705 represents an isothermality value of 346.

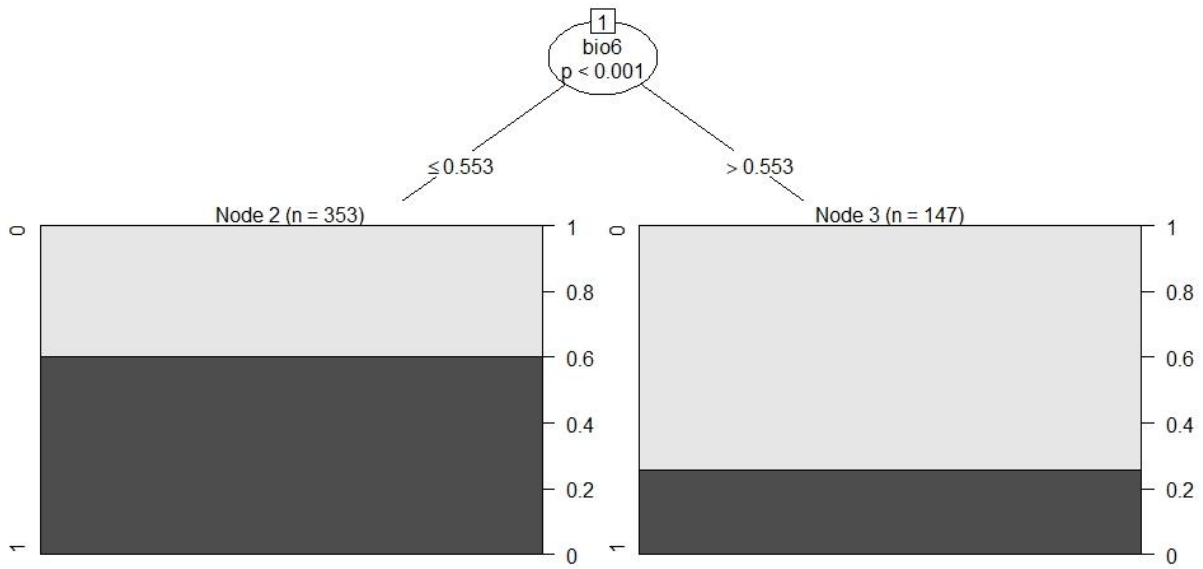


Figure 29. Area 3, univariate conditional inference tree. Cross-validated overall accuracy = 57 percent. Backtransformed value: 0.553 represents a temperature of -6.8°C .

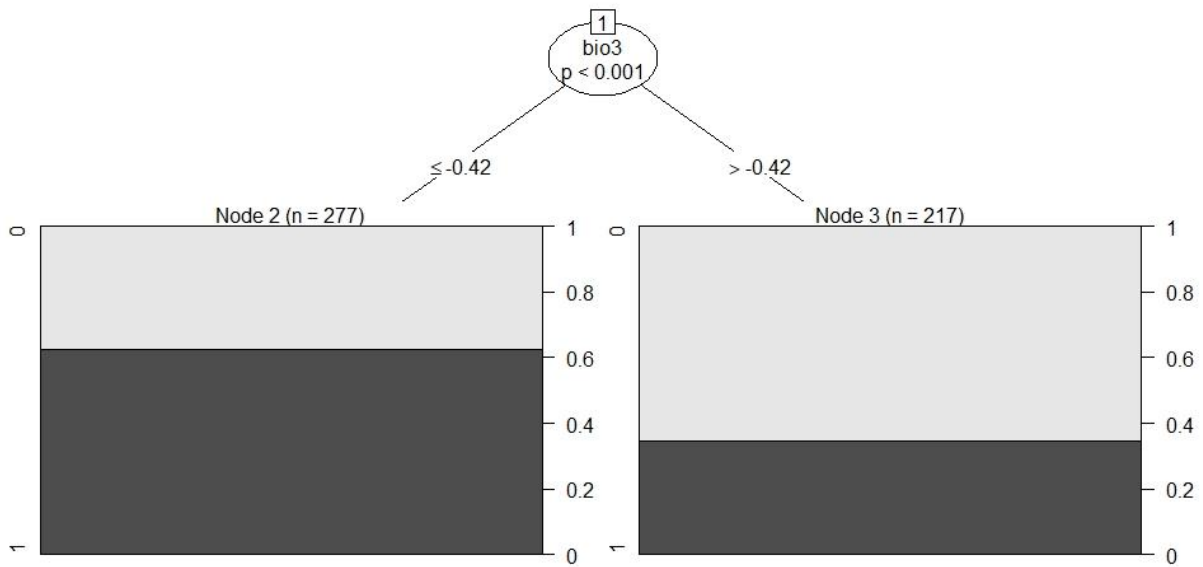


Figure 30. Area 4, univariate conditional inference tree. Cross-validated overall accuracy = 61.9 percent. Backtransformed value: -0.42 represents an isothermality value of 339.

Univariate stumps built from other top variables (Appendix F) revealed less clear patterns, with thresholds and direction of relationship being somewhat variable according to Area. These inconsistent results suggest that none of these variables is a very good ubiquitous predictor of mortality on its own, and it is only when considered together with other variables that they become predictive. This would seem to speak to the complexity of the system being modeled, and the shortcomings inherent in attempting to consider a single factor without also considering the suite of other factors present in the system.

4.3.4 Factors selected for the final model

I used the model BCfin, which included the variables isothermality (bio3), minimum temperature of coldest month (bio6), precipitation of warmest quarter (bio18), and pre-drought NDMI (ndmi2000), to create mortality prediction maps for all four Areas. I generated two sets of prediction maps: hard classification (Figure 31), and probability of mortality (Figure 32). In both cases, the mortality predictions qualitatively appear to be a good match to the areas of mapped GV cover loss. Quantitatively, the overall balanced accuracy of the prediction maps for the validation data (Table 9) was similar to -and in some cases slightly better than- the accuracy obtained on the dataset used to fit the model (Table 10), as was the sensitivity. Specificity for the predictions on the validation set vs. the analysis dataset was quite comparable as well. From these indicators it appears that the BCfin model has good generalizability and was able to predict mortality across the four study Areas with a reasonable level of accuracy.

I also assessed the spatial patterns of misclassification by the model BCfin in each Area. Most of the misclassifications (Figure 33) in Areas 3 and 4 occurred at the transition zones

between contiguous areas of mortality and contiguous areas of survival. Additionally, many of the “false-positives” in Areas 2, 3, and 4 occurred in areas that had experienced some cover loss, but not enough to be considered mortality by the cutoff of ≥ 45 percent chosen for this study. In Area 1, the BCfin model overpredicted mortality substantially, and while at the northeastern extreme of the Area, some pixels incorrectly classified as mortality did in fact experience some lesser degree of cover loss, this was not the case for the rest of the Area, in which relatively large areas of survival were misclassified as mortality. As evidenced in Table 9, the model in most Areas did a better job of accurately predicting mortality than survival.

Table 9. Accuracy of mortality prediction maps (validation dataset).

Area	Overall accuracy	Balanced accuracy	Sensitivity	Specificity
Area 1	0.744	0.834	0.934	0.734
Area 2	0.792	0.840	0.900	0.781
Area 3	0.801	0.805	0.821	0.789
Area 4	0.819	0.819	0.810	0.828

Table 10. Accuracy of BCfin (analysis dataset)

Area	Overall accuracy	Balanced accuracy	Sensitivity	Specificity
Area 1	0.811	0.810	0.872	0.748
Area 2	0.812	0.812	0.776	0.847
Area 3	0.722	0.722	0.732	0.712
Area 4	0.765	0.765	0.758	0.772

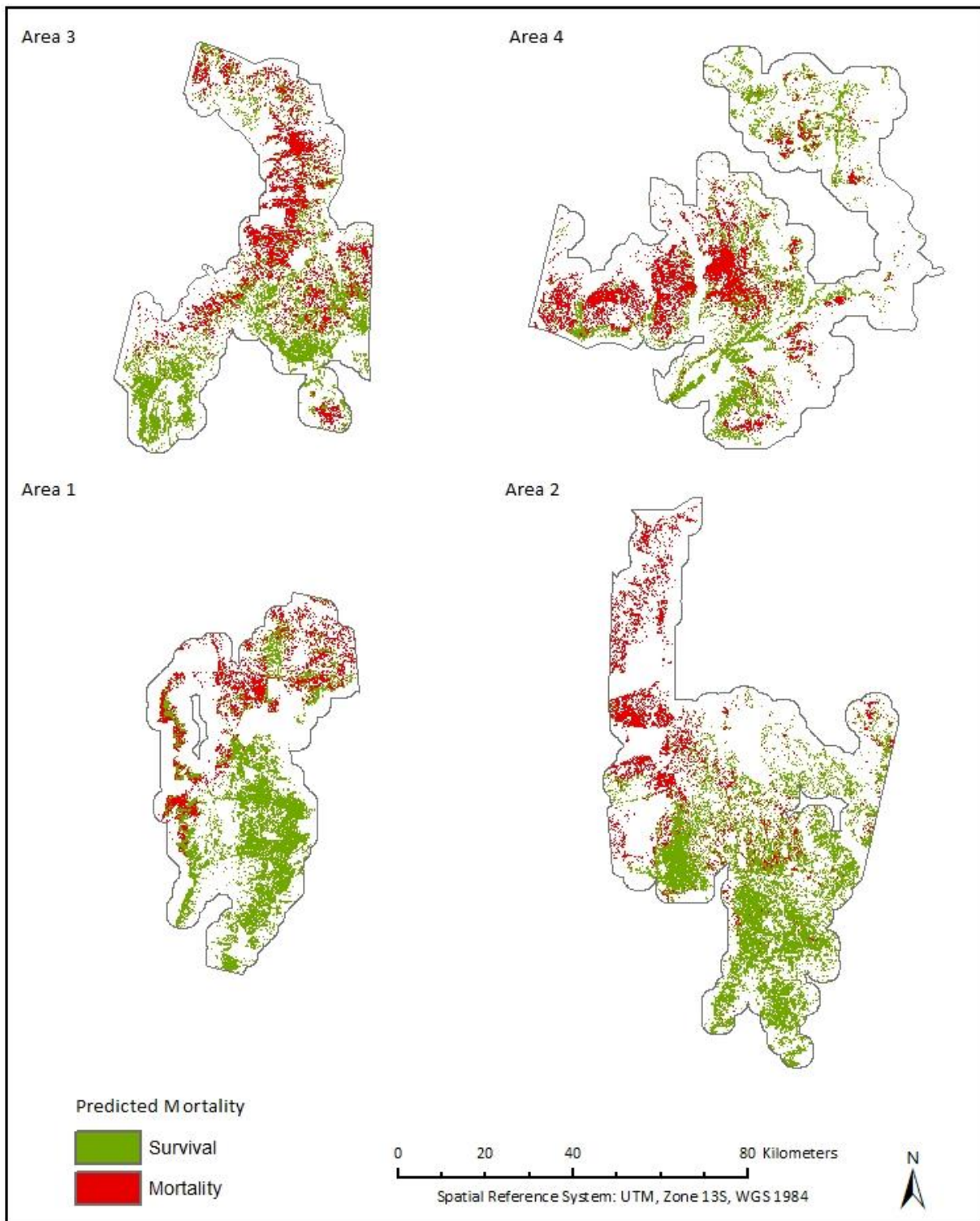


Figure 31. BCfin predicted presence of mortality.

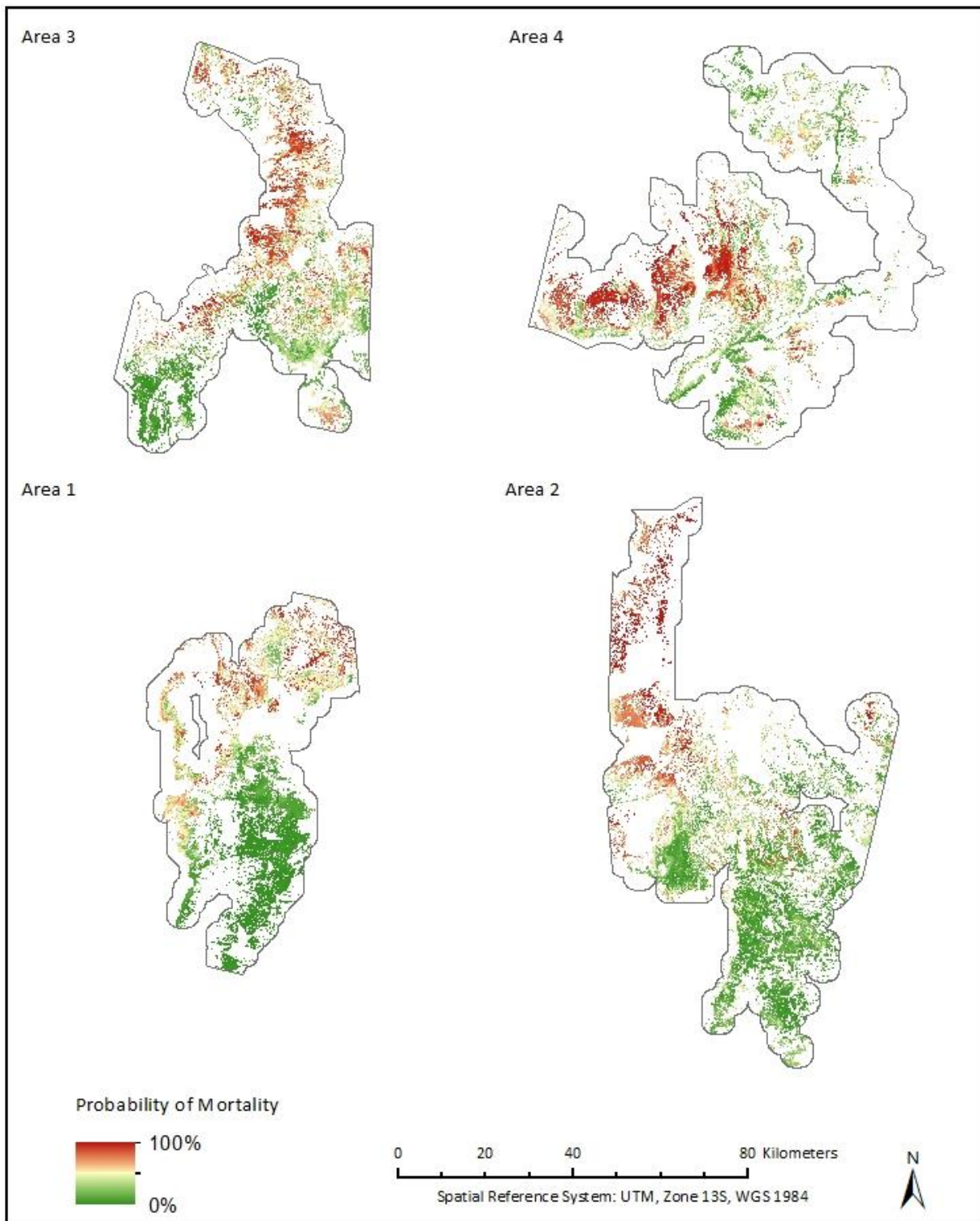


Figure 32. BCfin predicted probability of mortality.

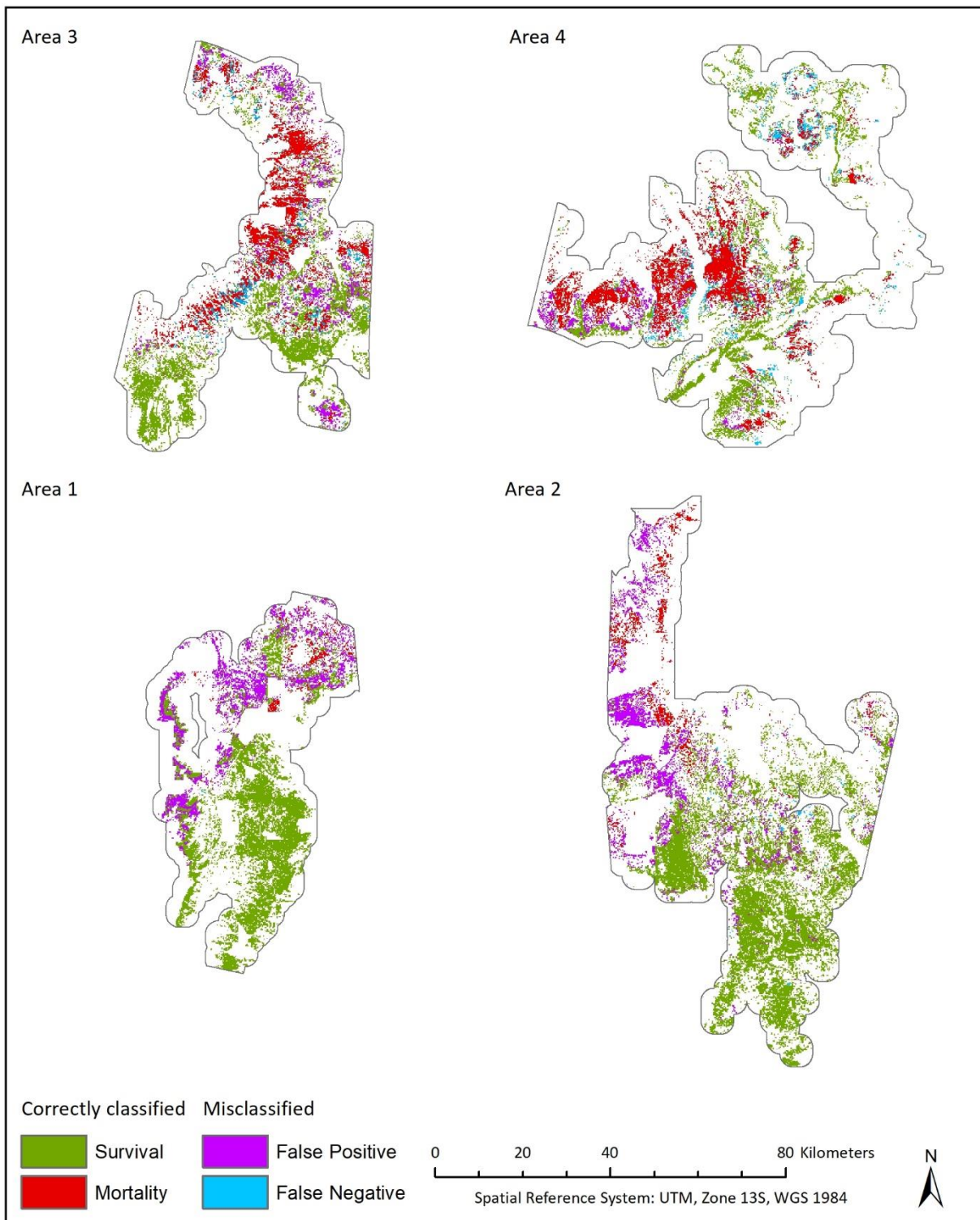


Figure 33. BCfin areas of misclassification.

5. Discussion

While the immediate combined effects of a severe drought and bark beetle outbreak during the early 2000s were the direct agents of the tree mortality observed in the region during this time period (Breshears et al. 2005; Shaw, Steed, and DeBlander 2005; McDowell et al. 2013), less transient features such as site related characteristics may put trees at a higher risk for drought stress and consequent mortality (Shaw 2006; McDowell et al. 2008). Landscape scale indicators of high mortality risk may be useful for pro-active management and conservation efforts (Gitlin et al. 2006). This study was designed to identify non-transient site characteristics that may prove helpful in predicting drought-related pinyon mortality at the landscape scale, selected from a broad range of variable types in relation to drought related pinyon mortality. Discussed below are the results of the mortality mapping, a comparison of the model types used in this study, and the variables that best explained pinyon mortality.

5.1 MESMA performance

Accuracy of the GV cover maps varied a little by Area, but overall were within acceptable ranges. The GV cover estimates produced by MESMA had MAE values of 0.13-0.19 and R^2 values between 0.45 and 0.8, with Area 2 results inferior to that of the other Areas. Collecting more endmembers in the field from within the study area would likely have improved the accuracy in all Areas. Thorp, French, and Rango (2013) report that MESMA is more sensitive to spectral resolution than spatial resolution and thus using imagery from a different sensor with more spectral bands, such as MODIS, might also have produced a higher degree of accuracy, although this would have meant conducting the analysis at a somewhat coarser spatial scale.

The accuracies I obtained, however, were not too far removed from those reported by others (Thorp, French, and Rango 2013; Brewer et al. 2017; Lippitt et al. 2018) using MESMA to map woody vegetation, and, even in Area 2, were adequate for the subsequent analyses, using the criteria of $\geq 45\%$ cover loss = mortality presence.

5.2 Tree cover changes

The mortality maps that resulted from the MESMA modeling allowed for a fine-grained look at the cover change patterns throughout the four Areas. The mortality patterns observed in the four Areas were in line with what has been reported by others (Breshears et al. 2005; Clifford et al. 2008, 2013; Kleinman et al. 2012; USDA Forest Service, Forest Health Protection and its partners 2014; Meddens et al. 2015), with light mortality in the south grading to substantially heavier mortality in the north. Hotspots of mapped mortality had good agreement with mortality locations identified by the USFS IDS polygons. However, the mortality maps generated by the image differencing also identified some additional areas of mortality, particularly in Area 3. It could be that the extent of the mortality was less noticeable during USFS aerial flights in areas where there were fewer trees to die. The MESMA pixel-by-pixel analysis also allowed for the identification of areas with varying degrees of cover loss and those with little to no mortality interspersed with the areas of higher mortality, an element important to the modeling phase.

Absolute cover loss was highest in areas of higher pre-drought cover, which agrees with the speculations of Kleinman et al. (2012). However, when relative cover loss was examined, a much more uniform pattern of mortality emerged, indicating that, in terms of percent change,

tree mortality in high-density stands was similar to that of many sites with medium or low cover, which supports the conclusions of authors who found little to no effect of stand density on mortality (Clifford et al. 2008; Clifford, Cobb, and Buenemann 2011; Ganey and Vojta 2011; Macalady and Bugmann 2014). Areas of very low pre-drought cover experienced little to no mortality, and in some cases an increase in GV, possibly due to a lack of pinyon and instead dominance by juniper and woody shrubs in these areas, although gathering the data needed to confirm this hypothesis was beyond the scope of this study. The general patterns of mortality are probably best explained by the causative agents suggested by others; for example, a south to north gradient of drought intensity (Breshears et al. 2005) and potentially higher ips populations in some areas (Clifford et al. 2008). Explaining the more fine-scale mortality patterns in relation to site-specific variables is the subject of this study and discussed further in the sections that follow.

The areas in which GV increased between 2000 and 2005 occurred almost exclusively in locations of very low or low pre-drought cover classes. While uncovering the precise reason for this was not within the scope of this study, I speculate here on several possible explanations. It could be that these areas, despite being classified as pinyon-juniper woodlands, were in fact more of a juniper savanna, or at least were areas heavily dominated by junipers. Juniper during this drought underwent far less extensive mortality than pinyon (Mueller et al. 2005; Shaw 2006), and it is possible that both the existing trees and any coinciding woody shrubs may have actually increased their biomass during the 2000-2005 time period. It may also be that, in addition to low competition for resources due to low tree density, local topography and microclimate was favorable to growth and recruitment in these areas. From a qualitative visual

assessment, at least some areas of high increase appear to be located in features likely to receive run-on during intense rainfall events, such as canyons and piedmonts. Another less likely possibility is that the trees that survived the drought -both pinyon and juniper- may have benefitted from decreased competition following the mortality of their neighbors, and subsequently increased their photosynthetic biomass in response to greater availability of resources (Mueller et al. 2019). While this explanation may be plausible in areas where the increase was patchily interspersed with decrease, it is unlikely to explain the larger continuous areas of increase; additionally, one would expect to see a response to competitive release more pronounced in areas of high pre-drought cover than in the very low cover classes. It is also possible that at least some of these areas simply represent errors in the MESMA modeling. According to the MAE obtained from the accuracy assessment, the GV abundance estimates have an average margin of error of around +/- 14-20 percent, depending on Area; it could be that in areas of lower initial cover the effects of this were more noticeable. Improving the accuracy of the underlying GV cover maps would be a priority in any future investigation. Given the size of the collective study area, it is quite likely that the true explanation for the apparent increase in GV is some combination of these hypotheses, or perhaps a mix of these and some other explanation not considered here.

5.3 Model comparisons

Due to the multi-model approach used, there were two main kinds of model comparisons to be made, first between the three general model types used, and then between the actual groupings and categories of potentially explanatory variables.

5.3.1 Comparison of model types

Each of the modeling types used proved to have its own merits and weaknesses. Random forest models generally produced higher overall accuracies than logistic regression or conditional inference tree models built on the same set of variables. Although random forest was the best among the three model types used as far as correctly modeling mortality, the “black box” nature of the algorithm (Palczewska et al. 2014; Hauenstein, Wood, and Dormann 2018) is such that it was impossible to isolate either the variable thresholds used or the nature of the relationships between the variables and mortality. While it appears that random forest is a good choice for modeling tree mortality when the interpretation of the variables used is not all that important, logistic regression and conditional inference trees may be better options when more information about the relationship is desired.

Neither logistic regression nor conditional inference trees consistently outperformed the other. This was a little unexpected, as the two methods use different approaches – conditional inference trees are based on recursive binary partitioning (Hothorn, Hornik, and Zeileis 2015), while logistic regression, through use of the logit, attempts to model a more linear relationship of probabilities to a binary outcome (Peng, Lee, and Ingersoll 2002). In logistic regression, therefore, there is only one “tipping point” in the relationship of a variable to the dichotomous outcome, whereas conditional inference trees can capture more complex relationships such as higher mortality both above and below a middle-range of values, and/or non-linear relationships that depend on the value of another variable. Logistic regression has been used successfully by others in their analyses of pinyon mortality and insect infestation (Negrón and Wilson 2003; Greenwood and Weisberg 2008; Santos and Whitham 2010), so I did

not expect poor results from this modeling approach, however, given the complexity of environmental relationships in natural systems, I had expected conditional inference trees to produce generally better results than logistic regression. This turned out to be an incorrect prediction. The most apparent explanation for this is that perhaps many of the variables can be partitioned more linearly than I had previously assumed. This supposition can be supported inferentially by the success the aforementioned authors had with logistic regression, and further bolstered by the work of Clifford et al. (2013) and Peterman et al. (2013) who were able to identify a single threshold value for one or more variables, above/below which probability of pinyon mortality was markedly lower.

5.3.2 Comparison of variable types

Of the variables considered, long-term climatic variables were the most consistently predictive of mortality across all four study Areas. Models built with bioclimatic variables or with a combination of variable types produced the highest overall accuracies, followed by models built from edaphic variables. Models built from topographic variables had consistently low overall accuracies, and models based on the presence of grazing had accuracies near the no-information rate, suggesting no relationship to mortality.

Bioclimatic variables in this study turned out to be the category of variables that most accurately predicted mortality from among the type groupings. Long term climatic habitat suitability in relationship to mortality has been the focus of several other studies (Kleinman et al. 2012; Lloret and Kitzberger 2018; Law et al. 2019). While habitat suitability was not specifically investigated in this study, climatic variables are typically a key component in Species Distribution Models, often used to model vegetation dynamics across a species' range (Lloret

and Kitzberger 2018), and are commonly used in dynamic global vegetation models modeling mortality (McDowell et al. 2011). Thus the result that climatic averages were, as a category, good predictors of mortality in this study is supported by the science of vegetation dynamics and habitat modeling, and agrees with the results of other researchers (Kleinman et al. 2012; Lloret and Kitzberger 2018) who have described a correlation between pinyon mortality during the early 2000s drought and climatic site suitability. The one biotic variable, NDMI, was also quite important in most models, and will be discussed further in the section below on factors explaining pinyon mortality.

Models built on a combination of all variable types also had generally good overall accuracy, although as noted in the results, model complexity was a concern in some cases. Natural systems are complex, however, and it is a reasonable expectation that combining variables of different types, and possibly even a relatively large number of them, would produce a decent predictive model. This result, therefore, was somewhat unremarkable, except to say that in all cases, the combinations of variables used required the inclusion bioclimatic variables, which were the most predictive category, to achieve desirable overall accuracies. Multi-type models which excluded these variables, and were built on a combination of soil and topographic variables only, did not produce similarly good results.

Edaphic variables in this study produced mixed results. A model built only from edaphic variables had high prediction accuracy in Area 1, competing with the top model in that Area, but the same was not the case in the other three Areas. One possible explanation for this is as follows: tree mortality was considerably lower in Area 1 than in the other Areas, and Clifford et al. (2008) has hypothesized that perhaps the pinyon ips outbreak wasn't as severe in this area.

Reed and Hood (2020), in a study of drought related tree mortality in California, identified the presence of insect herbivory as a confounding factor that may have masked the effects of other potentially explanatory variables such as soil texture in their study. Floyd et al. (2009) also mention the severity of the drought and the concurrent widespread beetle kill potentially masking the effects of other contributing agents. If the pinyon ips outbreak in Area 1 was in fact less severe, then it could be that the relationships between soil characteristics and drought stress were more clearly discernable because insect pressure was less. I have not encountered any studies which quantified the ips population at the time in relation to geography, so this potential explanation remains highly speculative. Another possible explanation is that soil characteristics in this study simply were not as explanatory as other variable types in Areas 2-4, or at least, were not enough to predict mortality without the addition of other variables. This would follow with the generally mixed results found in other studies. In a regional scale study, Peterman et al. (2013) found AWC was strongly related to mortality, and Ogle, Whitham, and Cobb (2000), Gitlin et al. (2006), Greenwood and Weisberg (2008) and Bowker et al. (2012) all observed that soil type or texture was correlated with mortality. However Floyd et al. (2009), Koepke, Kolb, and Adams (2010), and Clifford et al. (2013) reported no observable correlation between soil characteristics and drought-related pinyon mortality in their studies. Gitlin et al. (2006) reported that mortality at their study site was higher in shallow soils, but Flake and Weisberg (2019) reported that in their study deeper soils were linked with higher mortality.

Topographic variables as a category appeared to have very low explanatory power. Given that topographic characteristics such as slope (Greenwood and Weisberg 2008; Santos and Whitham 2010; Campbell et al. 2020), landscape position (Greenwood and Weisberg 2008)

and aspect (Ogle, Whitham, and Cobb 2000; Gitlin et al. 2006) have been identified as variables correlated with mortality in previous studies, it was somewhat surprising that topographic variables were such poor predictors of mortality in the models constructed. One possible explanation, however, is that these variables become more predictive at the microsite level, and the 210 m pixel spatial resolution of this study may have been too coarse to capture these finer scale variations. An interesting area for future study may be a multi-scale evaluation of topographic variables and their relation to drought related tree mortality.

The presence of grazing as a land use, either alone or in combination with other variables, proved to have little or no relevance to mortality occurrence. This was somewhat surprising given the anecdotal accounts of grazing pressure being conducive to pinyon-juniper expansion. One caveat to this result, however, is that I determined grazing presence or absence only, based on the locations of grazing permits, and did not consider stocking rate in my analysis, as I had no way of easily obtaining this information for land leases in the study area. Also, a minimal portion of the study area (approximately 9 percent collectively) is Native American reservation land and thus may be grazed even though no public grazing permits exist in those area, thus potentially adding a small amount of noise to the dataset.

While not helpful for building a predictive model, the lack of influence that grazing had is nonetheless a valuable finding. In a literature search I could find no studies that specifically considered the effects of grazing use on drought-related pinyon mortality, despite it being a common land use for this ecotype (Hartsell et al. 2020). It is hoped, therefore, that the results of this study contribute to rounding out the body of knowledge in that area.

5.4 Factors explaining pinyon mortality

From among the 42 variables used in the modeling process, the top ten most explanatory, as indicated by the random forest variable importance measure of mean decrease in accuracy, included six climatic variables, one vegetation index, and three edaphic variables. In the final model built, only four variables, three of which were long-term climate averages, were needed for good prediction accuracy.

5.4.1 Variables used in the final model

The final model used three climatic variables: isothermality, minimum temperature of the coldest month, precipitation of the warmest quarter, and one vegetation index: NDMI.

Isothermality and minimum temperature of the coldest month were the two most important variables across the models generated, and both were negatively correlated with mortality in all four Areas. In this study, the locations with smaller isothermality values had a diurnal temperature range similar to that of the surrounding areas, but a comparatively larger annual temperature range. It is unclear exactly why this would be such a strong predictor of mortality, however, increased temperature increases the VPD (Breshears et al. 2005; Weiss, Castro, and Overpeck 2009; Weiss, Betancourt, and Overpeck 2012; Clifford et al. 2013; Williams et al. 2013) and has been shown to hasten death in pinyon pine (Adams et al. 2009); it may be that locations with historically larger seasonal variations in temperature to begin with were more exposed during the drought to the intensified warm and dry conditions. There is also a possibility, though not explored in this study, that these climatic characteristics were related not to increased tree vulnerability, but rather to the survival, reproduction, and vigor of the

local ips population. Since pinyon ips are poor dispersers (Raffa et al. 2008), it is conceivable that the areas with the most mortality may have occurred where the ips populations were initially highest. The connection between these climatic variables, the weather conditions leading up to the drought, and pinyon ips habitat suitability might make an interesting topic for future study.

There was a positive relationship between mortality and precipitation of the warmest quarter in the three southernmost Areas, when this variable was considered in combination with other variables. This may indicate a heavier reliance on moisture from the North American monsoon, or it may simply indicate a generally wetter site, as this variable was highly correlated with annual precipitation, which was not included as a final variable. In either case, this positive correlation is in agreement with the findings of Lloret and Kitzberger (2018) who observed a high incidence of mortality during this drought in areas of historically high climatic suitability, which rapidly deteriorated during the drought period. They offer in explanation the proposal that perhaps trees growing under normally favorable conditions near the core of their suitability range are less able to cope with sudden climatic unsuitability when it occurs due to factors such as acclimation, stand density, and possibly even genetic differences, compared to those at less suitable edges of the climatic range. Work by Hacke et al. (2000) and Limousin et al. (2013) showing the ability for adaptive plasticity support this hypothesis. As an additional factor, the anomalously cool and wet conditions in much of the southwest during the early and latter parts of the 20th century (Breshears et al. 2005; Barger et al. 2009; Romme et al. 2009) may have contributed to pinyon growth and expansion beyond what is sustainable in the long term – a hypothesis proposed by several authors (Breshears et al. 2005; Jump et al. 2017; Flake

and Weisberg 2019), and a phenomenon termed by Jump et al. (2017) “structural overshoot.” Interestingly, when considered in univariate decision tree models (Appendix F), the relationship between precipitation of the warmest quarter and mortality was reversed: negative in the three southernmost Areas and positive only in the most northerly Area. This is illustrative of the complexity involved in modeling natural systems, a commonly acknowledged challenge in the research on pinyon mortality (Kerkhoff et al. 2004; Hicke and Zeppel 2013; McDowell et al. 2013; Campbell et al. 2020).

There was a generally positive correlation between mortality and NDMI, which is a representation of vegetation moisture content (Hardisky, Klemas, and Smart 1983; Hunt Jr and Rock 1989). This may suggest that trees with more favorable pre-drought moisture conditions were the hardest hit during the drought. More positive values of this index, however, are also representative of higher biomass, and may in this case be more indicative of higher pre-drought tree cover in areas of mortality. The NDMI has been shown elsewhere to be very useful for forest biomass change detection and more sensitive to light disturbances than NDVI (Jin and Sader 2005); however, this means its interpretation in this study is somewhat limited, as this index represents multiple interrelated features. Assuming, however, that NDMI values are in this study primarily indicative of cover, the positive association with mortality is in agreement with the conclusions of (Negrón and Wilson 2003; Greenwood and Weisberg 2008), though not those of (Floyd et al. 2009; Clifford, Cobb, and Buenemann 2011; Ganey and Vojta 2011; Clifford et al. 2013), and also conflicts somewhat with a qualitative assessment of patterns apparent from the mortality maps generated in the first step. One possible confounding factor, however, is that in this study all areas mapped as pinyon-juniper woodlands were considered

together, with no differentiation between species. Areas of higher pre-drought cover may have been more often dominated by pinyon, while areas of low cover may have been mostly at the warmer and drier end of the range and been primarily dominated by juniper (Koepeke, Kolb, and Adams 2010), a species which underwent far less mortality during the drought (Mueller et al. 2005; McDowell et al. 2008; Floyd et al. 2009). While some areas of low cover did appear from the maps generated to experience mortality, quantitatively these areas may have been proportionally less than mortality areas of higher initial cover.

5.4.2 Other top variables

Six of the ten variables that appeared to be most important across random forest models were climatic, one was the vegetation index NDMI, and three were edaphic. In addition to those variables included in the final model and discussed above, the other three climatic variables were temperature of the driest quarter, November precipitation, and seasonality of precipitation. The three edaphic variables that appeared to be consistently important in random forest models were clay content of the surface soil, weighted average clay percent of the soil profile, and AWC of the first 31 cm (top foot) of soil.

November precipitation had a negative relationship to mortality in three of the four Areas. As suggested above in the discussion of isothermality, it could be that trees in locations predisposed to more climatic extremes, such as higher dry-season temperatures, were already operating closer to their functional limits and were therefore more vulnerable to additional drought stress, as is often the case with trees occupying generally suboptimal sites (Greenwood and Weisberg 2008). November precipitation may be representative more broadly of winter precipitation, which has been shown to be important for tree growth and for recharging the soil

profile (Phillips and Ehleringer 1995; West et al. 2007), so the generally negative relationship modeled in this study may indicate sites where pre-drought conditions were already suboptimal. These interpretations, however, are in opposition to the results of (Lloret and Kitzberger 2018) who observed that mortality was highest in areas of high climatic suitability, as discussed above.

Seasonality of precipitation, while identified as an important variable, had an inconsistent direction of relationship in the four Areas, and this may have one of two possible interpretations: it could be that this variable represents a varying degree of dependence on monsoonal vs. winter precipitation, and that this relationship is influenced in part by other factors that differed between the Areas. A second possibility is that the relationships identified by the models were not actually meaningful and simply the result of chance.

The edaphic variables that appeared to be consistently important in random forest models, clay content of the surface soil, weighted average clay percent of the soil profile, and AWC of the first 31 cm (top foot) of soil, all have a direct influence on soil water dynamics. Given this, their importance in modeling mortality was not unexpected, and is in agreement with observations made by Clifford et al. (2013). It was, however, unexpected that none of these factors produced consistent results when evaluated as univariate models in a decision tree environment (Appendix F), indicating that the influence of these variables is dependent on interactions with other site characteristics. This is not a finding that has been reported in other studies on drought-related pinyon mortality, although it could possibly be an explanation for some of the inconsistency in results between studies that is mentioned in the discussion of variable types. Despite the variety of models and modeling styles used, I was unable to pinpoint

the precise nature of these inferred relationships within the scope of this study. This would make an interesting topic for future study, however, as alluded to by many other authors (e.g., Kerkhoff et al. 2004; Hicke and Zeppel 2013; McDowell et al. 2013; Campbell et al. 2020), in some cases the complexity of the system being modeled makes it difficult to identify clear relationships.

5.5 Final model performance and implications

The high classification accuracy of the final selected model indicates that the four variables selected for the model explained mortality well, and this explanatory power was consistent across the four Areas. While the precise interactions of the four variables included in the final model could not be ascertained due to the nature of the random forest model, the model produced detailed mortality maps that had between 80 and 83 percent balanced accuracy using only these predictors. Locations of predicted mortality were a good match for the mortality mapped by the change detection analysis. This demonstrates that a high level of prediction accuracy can be obtained using only a few variables, and that such predictions can be made using a combination of long-term climatic averages and NDMI. This finding is significant from a land management perspective, as these variables can be considered in times of non-drought to identify sites most at risk for tree mortality during drought, and thus might help inform management decisions, such as identification of areas for a specific treatment, or to help guide post-disturbance land rehabilitation efforts. Additionally, data for all of these variables are readily available or easily calculable at no cost to the user, and require minimal processing and no additional field work to obtain. This could represent substantial cost and time savings to

land managers when compared with alternative, more labor-intensive approaches or data sources. Important to note, however, is that this modeling effort was undertaken for a single mortality event, and that is a limitation of this study. An illustrative example for the need to vet a model across multiple mortality events comes from a study by McDowell et al. (2013), who observed that a model which accurately predicted mortality of trees subjected to experimental drought in a study plot in NM circa 2008 (Plaut et al. 2012; Limousin et al. 2013), it incorrectly predicted mortality in control-plot trees during a subsequent record-setting drought occurring in the area only a few years later in 2011 (McDowell et al. 2013). McDowell et al. (2013) suggest the absence of a local bark beetle population explosion in 2011 as the possible explanatory factor for the model failure in the described case. Therefore to build confidence in the final model developed in this study, it would be helpful to test it on other mortality events in the region, and this could be an area for future study.

6. Conclusion

In this study, four bioclimatic variables combined in a random forest model were able to accurately predict tree mortality in all four Areas. This finding may be helpful to natural resource managers looking for a quick and cost-effective means of estimating mortality risk over large areas. These results come with the caveat, however, that this model has not been tested across multiple drought-related mortality events, and so cannot be extrapolated beyond the temporal and geographic limits of this study. In general, long term climatic averages were more predictive than other categories of variables, soils produced mixed results, topography in

isolation was a fairly poor predictor at the scale of the study, and grazing had no effect on mortality. The results of this study add to the academic body of knowledge on the subject and highlight several areas for future study that could build upon this work. Main limitations of this study were the inability to distinguish between pinyon-dominated and juniper-dominated sites, which may have influenced mortality patterns and relationships, and the fact that only one time period spanning a single drought period was examined.

This study highlights several potential topics for future research. A multi-scale analysis of the influence of topography on mortality may shed some light on the generally poor correlations found in this study. Lloret and Kitzberger (2018) used historic and episodic climate suitability to explain drought related pinyon mortality; a potential topic for future study might be to further explore if there was an inverse effect on pinyon ips climatic suitability in areas with relatively lower isothermality values, given the correlation of these areas to mortality in this study. A deeper examination of edaphic variables and their relationships to other co-occurring variables is another area for more exploration, and finally, testing the explanatory power of the variables used in final model across multiple mortality events would help establish if the relationships identified are generalizable to other occurrences of drought related pinyon mortality.

7. Literature Cited

- Adams, H. D., M. J. Germino, D. D. Breshears, G. A. Barron-Gafford, M. Guardiola-Claramonte, C. B. Zou, and T. E. Huxman. 2013. Nonstructural leaf carbohydrate dynamics of *Pinus edulis* during drought-induced tree mortality reveal role for carbon metabolism in mortality mechanism. *New Phytologist* 197 (4): 1142–1151.
- Adams, H. D., M. Guardiola-Claramonte, G. A. Barron-Gafford, J. C. Villegas, D. D. Breshears, C. B. Zou, P. A. Troch, and T. E. Huxman. 2009. Temperature sensitivity of drought-induced tree mortality portends increased regional die-off under global-change-type drought. *Proceedings of the National Academy of Sciences* 106 (17): 7063–7066.
- Adams, H. D., C. H. Luce, D. D. Breshears, C. D. Allen, M. Weiler, V. C. Hale, A. M. S. Smith, and T. E. Huxman. 2012. Ecohydrological consequences of drought- and infestation- triggered tree die-off: Insights and hypotheses. *Ecohydrology* 5 (2): 145–159.
- Albert, S., N. Luna, R. Jensen, and L. Livingston. 2004. Restoring biodiversity to piñon-juniper woodlands. *Ecological Restoration* 22 (1): 18–23.
- Anderegg, W. R. L., and L. D. L. Anderegg. 2013. Hydraulic and carbohydrate changes in experimental drought-induced mortality of saplings in two conifer species. *Tree Physiology* 33 (3): 252–260.
- Barger, N. N., H. D. Adams, C. Woodhouse, J. C. Neff, and G. P. Asner. 2009. Influence of livestock grazing and climate on pinyon pine (*Pinus edulis*) dynamics. *Rangeland Ecology & Management* 62 (6): 531–539.
- Baugh, W. M., and D. P. Groeneveld. 2008. Empirical proof of the empirical line. *International Journal of Remote Sensing* 29 (3): 665–672.
- Boardman, J. W., F. A. Kruse, and R. O. Green. 1995. Mapping target signatures via partial unmixing of AVIRIS data.
- Bowker, M. A., A. Muñoz, T. Martinez, and M. K. Lau. 2012. Rare drought-induced mortality of juniper is enhanced by edaphic stressors and influenced by stand density. *Journal of Arid Environments* 76: 9–16.
- Breiman, L. 2001. Random forests. *Machine learning* 45 (1): 5–32.
- Breiman, L., A. Cutler, A. Liaw, and M. Wiener. 2018. Breiman and Cutler's random forests for classification and regression. <https://cran.r-project.org/web/packages/randomForest/randomForest.pdf>.

- Breshears, D. D., H. D. Adams, D. Eamus, N. McDowell, D. J. Law, R. E. Will, A. P. Williams, and C. B. Zou. 2013. The critical amplifying role of increasing atmospheric moisture demand on tree mortality and associated regional die-off. *Frontiers in Plant Science* 4: 266.
- Breshears, D. D., C. J. Carroll, M. D. Redmond, A. P. Wion, C. D. Allen, N. S. Cobb, N. Meneses, J. P. Field, L. A. Wilson, and D. J. Law. 2018. A dirty dozen ways to die: metrics and modifiers of mortality driven by drought and warming for a tree species. *Frontiers in Forests and Global Change* 1: 4.
- Breshears, D. D., N. S. Cobb, P. M. Rich, K. P. Price, C. D. Allen, R. G. Balice, W. H. Romme, J. H. Kastens, M. L. Floyd, J. Belnap, J. J. Anderson, O. B. Myers, and C. W. Meyer. 2005. Regional vegetation die-off in response to global-change-type drought. *Proceedings of the National Academy of Sciences of the United States of America* 102 (42): 15144–15148.
- Breshears, D. D., O. B. Myers, and F. J. Barnes. 2009. Horizontal heterogeneity in the frequency of plant-available water with woodland intercanopy–canopy vegetation patch type rivals that occurring vertically by soil depth. *Ecohydrology: Ecosystems, Land and Water Process Interactions, Ecohydrogeomorphology* 2 (4): 503–519.
- Breshears, D. D., O. B. Myers, C. W. Meyer, F. J. Barnes, C. B. Zou, C. D. Allen, N. G. McDowell, and W. T. Pockman. 2009. Tree die-off in response to global change-type drought: mortality insights from a decade of plant water potential measurements. *Frontiers in Ecology and the Environment* 7 (4): 185–189.
- Brewer, W. L., C. L. Lippitt, C. D. Lippitt, and M. E. Litvak. 2017. Assessing drought-induced change in a piñon-juniper woodland with Landsat: a multiple endmember spectral mixture analysis approach. *International Journal of Remote Sensing* 38 (14): 4156–4176.
- Brodersen, K. H., C. S. Ong, K. E. Stephan, and J. M. Buhmann. 2010. The balanced accuracy and its posterior distribution. In *2010 20th International Conference on Pattern Recognition*, 3121–3124. IEEE.
- Bureau of Land Management - New Mexico State Office. 2000. *Bureau of Land Management (BLM) grazing allotments in New Mexico*. Bureau of Land Management. <http://databasin.org/datasets/19c6818a555743ae9ca06996f123abea>.
- Campbell, M. J., P. E. Dennison, J. W. Tune, S. A. Kannenberg, K. L. Kerr, B. F. Coddling, and W. R. Anderegg. 2020. A multi-sensor, multi-scale approach to mapping tree mortality in woodland ecosystems. *Remote Sensing of Environment* 245: 111853.
- Cassidy, A. P., and F. A. Deviney. 2014. Calculating feature importance in data streams with concept drift using Online Random Forest. In *2014 IEEE International Conference on Big Data (Big Data)*, 23–28. IEEE.

- Chang, C.-I., and A. Plaza. 2006. A fast iterative algorithm for implementation of pixel purity index. *IEEE Geoscience and Remote Sensing Letters* 3 (1): 63–67.
- Chung-MacCoubrey, A. L. 2005. Use of pinyon-juniper woodlands by bats in New Mexico. *Forest Ecology and Management* 204 (2): 209–220.
- Clifford, M. J., N. S. Cobb, and M. Buenemann. 2011. Long-term tree cover dynamics in a pinyon-juniper woodland: Climate-change-type drought resets successional clock. *Ecosystems* 14 (6): 949–962.
- Clifford, M. J., M. E. Rocca, R. Delph, P. L. Ford, and N. S. Cobb. 2008. Drought induced tree mortality and ensuing bark beetle outbreaks in Southwestern pinyon-juniper woodlands. <http://www.treearch.fs.fed.us/pubs/31240> (last accessed 13 March 2017).
- Clifford, M. J., P. D. Royer, N. S. Cobb, D. D. Breshears, and P. L. Ford. 2013. Precipitation thresholds and drought-induced tree die-off: insights from patterns of *Pinus edulis* mortality along an environmental stress gradient. *New Phytologist* 200 (2): 413–421.
- Cohen, J. 1960. A coefficient of agreement for nominal scales. *Educational and psychological measurement* 20 (1): 37–46.
- Dennison, P. E., and D. A. Roberts. 2003. Endmember selection for multiple endmember spectral mixture analysis using endmember average RMSE. *Remote Sensing of Environment* 87 (2): 123–135.
- Díaz-Uriarte, R., and S. A. De Andres. 2006. Gene selection and classification of microarray data using random forest. *BMC bioinformatics* 7 (1): 3.
- Dickman, L. T., N. G. Mcdowell, S. Sevanto, R. E. Pangle, and W. T. Pockman. 2015. Carbohydrate dynamics and mortality in a piñon-juniper woodland under three future precipitation scenarios. *Plant, Cell & Environment* 38 (4): 729–739.
- Duniway, M. C., J. W. Karl, S. Schrader, N. Baquera, and J. E. Herrick. 2012. Rangeland and pasture monitoring: an approach to interpretation of high-resolution imagery focused on observer calibration for repeatability. *Environmental Monitoring and Assessment* 184 (6): 3789–3804.
- Earth Data Analysis Center, University of New Mexico. 2015. New Mexico Resource Geographic Information System. *New Mexico Resource Geographic Information System*. <https://rgis.unm.edu/>.
- Evans, J., J. Oakleaf, and S. Cushman. 2014. *An ArcGIS Toolbox for Surface Gradient and Geomorphometric Modeling, version 2.0-0*. <https://github.com/jeffreyevans/GradientMetrics> (last accessed 1 September 2019).

- Ffolliott, P. F., G. J. Gottfried, D. A. Bennett, V. M. Hernandez C., A. Ortega-Rubio, and R. H. Hamre. 1992. *Ecology and management of oak and associated woodlands: Perspectives in the southwestern United States and northern Mexico*. Ft. Collins, CO: U.S. Department of Agriculture, Forest Service, Rocky Mountain Forest and Range Experiment Station. <https://www.fs.usda.gov/treearch/pubs/50069> (last accessed 7 November 2018).
- Finch, D. M., and L. F. Ruggiero. 1993. Wildlife habitats and biological diversity in the Rocky Mountains and Northern Great Plains. *Natural Areas Journal*. 13(3): 191-203. : 191–203.
- Flake, S. W., and P. J. Weisberg. 2019. Fine-scale stand structure mediates drought-induced tree mortality in pinyon–juniper woodlands. *Ecological Applications* 29 (2): e01831.
- Floyd, M. L., M. Clifford, N. S. Cobb, D. Hanna, R. Delph, P. Ford, and D. Turner. 2009. Relationship of stand characteristics to drought-induced mortality in three Southwestern piñon–juniper woodlands. *Ecological Applications* 19 (5): 1223–1230.
- Ganey, J. L., and S. C. Vojta. 2011. Tree mortality in drought-stressed mixed-conifer and ponderosa pine forests, Arizona, USA. *Forest Ecology and Management* 261 (1): 162–168.
- Gaylord, M. L., T. E. Kolb, W. T. Pockman, J. A. Plaut, E. A. Yopez, A. K. Macalady, R. E. Pangle, and N. G. McDowell. 2013. Drought predisposes piñon–juniper woodlands to insect attacks and mortality. *New Phytologist* 198 (2): 567–578.
- Gitlin, A. R., C. M. Sthultz, M. A. Bowker, S. Stumpf, K. L. Paxton, K. Kennedy, A. Muñoz, J. K. Bailey, and T. G. Whitham. 2006. Mortality gradients within and among dominant plant populations as barometers of ecosystem change during extreme drought. *Conservation Biology* 20 (5): 1477–1486.
- Gottfried, G. J., and K. E. Severson. 1994. Managing pinyon-juniper woodlands. *Rangelands*. 16 (6): 234-236.
- Greenwood, D. L., and P. J. Weisberg. 2008. Density-dependent tree mortality in pinyon-juniper woodlands. *Forest Ecology and Management* 255 (7): 2129–2137.
- Gruninger, J. H., A. J. Ratkowski, and M. L. Hoke. 2004. The sequential maximum angle convex cone (SMACC) endmember model. In *Algorithms and technologies for multispectral, hyperspectral, and ultraspectral imagery X*, 1–14. International Society for Optics and Photonics.
- Guardiola-Claramonte, M., P. A. Troch, D. D. Breshears, T. E. Huxman, M. B. Switanek, M. Durcik, and N. S. Cobb. 2011. Decreased streamflow in semi-arid basins following drought-induced tree die-off: A counter-intuitive and indirect climate impact on hydrology. *Journal of Hydrology* 406 (3–4): 225–233.

- Hacke, U. G., J. S. Sperry, B. E. Ewers, D. S. Ellsworth, K. V. R. Schäfer, and R. Oren. 2000. Influence of soil porosity on water use in *Pinus taeda*. *Oecologia* 124 (4): 495–505.
- Halligan, K., A. Crabbé, and K. Leuven. 2014. *VIPER Tools Version 2.0*. University of California, Santa Barbara, Department of Geography, Visualization and Image Processing for Environmental Research (VIPER Lab). <https://sites.google.com/site/ucsbviperlab/viper-tools>.
- Hardisky, M. A., V. Klemas, and M. Smart. 1983. The influence of soil salinity, growth form, and leaf moisture on the spectral radiance of. *Spartina alterniflora* 49: 77–83.
- Harris, A. T., G. P. Asner, and M. E. Miller. 2003. Changes in vegetation structure after long-term grazing in pinyon-juniper ecosystems: Integrating imaging spectroscopy and field studies. *Ecosystems* : 368–383.
- Hartsell, J. A., S. M. Copeland, S. M. Munson, B. J. Butterfield, and J. B. Bradford. 2020. Gaps and hotspots in the state of knowledge of pinyon-juniper communities. *Forest Ecology and Management* 455: 117628.
- Hauenstein, S., S. N. Wood, and C. F. Dormann. 2018. Computing AIC for black-box models using generalized degrees of freedom: A comparison with cross-validation. *Communications in Statistics-Simulation and Computation* 47 (5): 1382–1396.
- Hicke, J. A., A. J. Meddens, C. D. Allen, and C. A. Kolden. 2013. Carbon stocks of trees killed by bark beetles and wildfire in the western United States. *Environmental Research Letters* 8 (3): 035032.
- Hicke, J. A., and M. J. B. Zeppel. 2013. Climate-driven tree mortality: Insights from the piñon pine die-off in the United States. *New Phytologist* 200 (2): 301–303.
- Hothorn, T., K. Hornik, and A. Zeileis. 2015. ctree: Conditional inference trees. *The Comprehensive R Archive Network* : 1–34.
- Huang, C., G. P. Asner, N. N. Barger, J. C. Neff, and M. L. Floyd. 2010. Regional aboveground live carbon losses due to drought-induced tree dieback in piñon–juniper ecosystems. *Remote Sensing of Environment* 114 (7): 1471–1479.
- Huang, C., G. P. Asner, R. E. Martin, N. N. Barger, and J. C. Neff. 2009. Multiscale analysis of tree cover and aboveground carbon stocks in pinyon–juniper woodlands. *Ecological Applications* 19 (3): 668–681.
- Huang, K., C. Yi, D. Wu, T. Zhou, X. Zhao, W. J. Blanford, S. Wei, H. Wu, D. Ling, and Z. Li. 2015. Tipping point of a conifer forest ecosystem under severe drought. *Environmental Research Letters* 10 (2): 024011.

- Huffman, D. W., P. Z. Fule, K. M. Pearson, and J. E. Crouse. 2008. Fire history of pinyon–juniper woodlands at upper ecotones with ponderosa pine forests in Arizona and New Mexico. *Canadian Journal of Forest Research* 38 (8): 2097–2108.
- Hunt Jr, E. R., and B. N. Rock. 1989. Detection of changes in leaf water content using near-and middle-infrared reflectances. *Remote sensing of environment* 30 (1): 43–54.
- Ji, L., L. Zhang, B. K. Wylie, and J. Rover. 2011. On the terminology of the spectral vegetation index (NIR– SWIR)/(NIR+ SWIR). *International journal of remote sensing* 32 (21): 6901–6909.
- Jin, S., and S. A. Sader. 2005. Comparison of time series tasseled cap wetness and the normalized difference moisture index in detecting forest disturbances. *Remote sensing of Environment* 94 (3): 364–372.
- Jump, A. S., P. Ruiz-Benito, S. Greenwood, C. D. Allen, T. Kitzberger, R. Fensham, J. Martínez-Vilalta, and F. Lloret. 2017. Structural overshoot of tree growth with climate variability and the global spectrum of drought-induced forest dieback. *Global Change Biology* 23 (9): 3742–3757.
- Karger, D. N., O. Conrad, J. Böhrner, T. Kawohl, H. Kreft, R. W. Soria-Auza, N. E. Zimmermann, H. P. Linder, and M. Kessler. 2017a. Climatologies at high resolution for the earth’s land surface areas. *Scientific Data* 4: 170122.
- . 2017b. Data from: Climatologies at high resolution for the earth’s land surface areas. <https://doi.org/10.5061/dryad.kd1d4>.
- Karl, J. W., M. C. Duniway, and T. S. Schrader. 2012. A technique for estimating rangeland canopy-gap size distributions from high-resolution digital imagery. *Rangeland Ecology & Management* 65 (2): 196–207.
- Kerkhoff, A. J., S. N. Martens, G. A. Shore, and B. T. Milne. 2004. Contingent effects of water balance variation on tree cover density in semiarid woodlands. *Global Ecology and Biogeography* 13 (3): 237–246.
- Kleinman, S. J., T. E. D. Gomez, G. B. Snider, and K. E. Williams. 2012. Large-scale pinyon Ips (Ips confusus) outbreak in Southwestern United States tied with elevation and land cover. *Journal of Forestry* 110 (4): 194–200.
- Koepke, D. F., T. E. Kolb, and H. D. Adams. 2010. Variation in woody plant mortality and dieback from severe drought among soils, plant groups, and species within a northern Arizona ecotone. *Oecologia* 163 (4): 1079–1090.
- Kurz, W. A., C. C. Dymond, G. Stinson, G. J. Rampley, E. T. Neilson, A. L. Carroll, T. Ebata, and L. Safranyik. 2008. Mountain pine beetle and forest carbon feedback to climate change. *Nature* 452 (7190): 987–990.

- Land Office Geographic Information Center (LOGIC), NM State Land Office. *Active agricultural leases*. Santa Fe, New Mexico: NM State Land Office.
<https://www.nmstatelands.org/maps-gis/gis-data-download/> (last accessed 12 December 2017).
- Landsat collection 1 level 1 product definition. version 2.0. LSDS-1656. 2019.
- Law, D. J., H. D. Adams, D. D. Breshears, N. S. Cobb, J. B. Bradford, C. B. Zou, J. P. Field, A. A. Gardea, A. P. Williams, and T. E. Huxman. 2019. Bioclimatic envelopes for individual demographic events driven by extremes: plant mortality from drought and warming. *International Journal of Plant Sciences* 180 (1): 53–62.
- Liaw, A., and M. Wiener. 2002. Classification and regression by randomForest. 2: 6.
- Limousin, J.-M., C. P. Bickford, L. T. Dickman, R. E. Pangle, P. J. Hudson, A. L. Boutz, N. Gehres, J. L. Osuna, W. T. Pockman, and N. G. Mcdowell. 2013. Regulation and acclimation of leaf gas exchange in a piñon–juniper woodland exposed to three different precipitation regimes. *Plant, Cell & Environment* 36 (10): 1812–1825.
- Lippitt, C. L., D. A. Stow, D. A. Roberts, and L. L. Coulter. 2018. Multidate MESMA for monitoring vegetation growth forms in southern California shrublands. *International journal of remote sensing* 39 (3): 655–683.
- Lloret, F., and T. Kitzberger. 2018. Historical and event-based bioclimatic suitability predicts regional forest vulnerability to compound effects of severe drought and bark beetle infestation. *Global change biology* 24 (5): 1952–1964.
- Looney, C. E., B. W. Sullivan, T. E. Kolb, J. M. Kane, and S. C. Hart. 2012. Pinyon pine (*Pinus edulis*) mortality and response to water addition across a three million year substrate age gradient in northern Arizona, USA. *Plant and Soil* 357 (1–2): 89–102.
- Lowry, J. H., Jr., R. D. Ramsey, K. Boykin, D. Bradford, P. Comer, S. Falzarano, W. Kepner, J. Kirby, L. Langs, J. Prior-Magee, G. Manis, L. O’Brien, T. Sajwaj, K. A. Thomas, S. Rieth, S. Schrader, D. Schrupp, K. Schulz, B. Thompson, C. Velasquez, C. Wallace, E. Waller, and B. Wolk. 2005. *Southwest Regional Gap Analysis Project: Final report on land cover mapping methods*. Logan, Utah: RS/GIS Laboratory, Utah State University.
<http://swregap.org/data/landcover/> (last accessed 10 April 2017).
- Macalady, A. K., and H. Bugmann. 2014. Growth-mortality relationships in piñon pine (*Pinus edulis*) during severe droughts of the past century: Shifting processes in space and time. *PLOS ONE* 9 (5): e92770.
- Mattson, W. J., and R. A. Haack. 1987. The role of drought in outbreaks of plant-eating insects. *BioScience* 37 (2): 110–118.

- McDowell, N. G., D. J. Beerling, D. D. Breshears, R. A. Fisher, K. F. Raffa, and M. Stitt. 2011. The interdependence of mechanisms underlying climate-driven vegetation mortality. *Trends in Ecology & Evolution* 26 (10): 523–532.
- McDowell, N. G., R. A. Fisher, C. Xu, J. C. Domec, T. Hölttä, D. S. Mackay, J. S. Sperry, A. Boutz, L. Dickman, N. Gehres, J. M. Limousin, A. Macalady, J. Martínez-Vilalta, M. Mencuccini, J. A. Plaut, J. Ogée, R. E. Pangle, D. P. Rasse, M. G. Ryan, S. Sevanto, R. H. Waring, A. P. Williams, E. A. Yezzer, and W. T. Pockman. 2013. Evaluating theories of drought-induced vegetation mortality using a multimodel–experiment framework. *New Phytologist* 200 (2): 304–321.
- McDowell, N., W. T. Pockman, C. D. Allen, D. D. Breshears, N. Cobb, T. Kolb, J. Plaut, J. Sperry, A. West, D. G. Williams, and E. A. Yezzer. 2008. Mechanisms of plant survival and mortality during drought: Why do some plants survive while others succumb to drought? *New Phytologist* 178 (4): 719–739.
- Meddens, A. J. H., J. A. Hicke, A. K. Macalady, P. C. Buotte, T. R. Cowles, and C. D. Allen. 2015. Patterns and causes of observed piñon pine mortality in the southwestern United States. *New Phytologist* 206 (1): 91–97.
- Moore, J. A., D. A. Hamilton Jr., Y. Xiao, and J. Byrne. 2004. Bedrock type significantly affects individual tree mortality for various conifers in the inland Northwest, U.S.A. *Canadian Journal of Forest Research* 34 (1): 31–42.
- Mueller, R. C., C. M. Scudder, M. E. Porter, R. Talbot Trotter, C. A. Gehring, and T. G. Whitham. 2005. Differential tree mortality in response to severe drought: Evidence for long-term vegetation shifts. *Journal of Ecology* 93 (6): 1085–1093.
- Mueller, R. C., C. M. Scudder, T. G. Whitham, and C. A. Gehring. 2019. Legacy effects of tree mortality mediated by ectomycorrhizal fungal communities. *New Phytologist* 224 (1): 155–165.
- Murray, L., H. Nguyen, Y.-F. Lee, M. D. Remmenga, and D. W. Smith. 2012. Variance inflation factors in regression models with dummy variables. *Conference on Applied Statistics in Agriculture*. <https://newprairiepress.org/agstatconference/2012/proceedings/12> (last accessed 11 November 2019).
- Myung, I. J. 2000. The importance of complexity in model selection. *Journal of mathematical psychology* 44 (1): 190–204.
- National Aeronautics and Space Administration (NASA), National Imagery and Mapping Agency (NIMA), German Aerospace Center (DLR), and Italian Space Agency (ASI). 2002. *2002, Shuttle Radar Topography Mission (SRTM) elevation dataset*. Sioux Falls, South Dakota: U.S Geological Survey. <http://seamless.usgs.gov/>.

- Negrón, J. F., and J. L. Wilson. 2003. Attributes associated with probability of infestation by the pinon ips, *ips confusus* (coleoptera: scolytidae), in pinon pine, *pinus edulis*. *Western North American Naturalist* 63 (4): 440–451.
- New Mexico Department of Transportation. 2016. *New Mexico Department of Transportation Design Manual*. New Mexico Department of Transportation.
- Noy-Meir, I. 1973. Desert ecosystems: Environment and producers. *Annual review of ecology and systematics* 4 (1): 25–51.
- O'Donnell, M. S., and D. A. Ignizio. 2012. Bioclimatic predictors for supporting ecological applications in the conterminous United States. *US Geological Survey Data Series* 691 (10).
- Ogle, K., T. G. Whitham, and N. S. Cobb. 2000. Tree-ring variation in pinyon predicts likelihood of death following severe drought. *Ecology* 81 (11): 3237–3243.
- Ortiz, J. D., D. Avouris, S. Schiller, J. C. Luvall, J. D. Lekki, R. P. Tokars, R. C. Anderson, R. Shuchman, M. Sayers, and R. Becker. 2017. Intercomparison of approaches to the empirical line method for vicarious hyperspectral reflectance calibration. *Frontiers in Marine Science* 4: 296.
- Oshiro, T. M., P. S. Perez, and J. A. Baranauskas. 2012. How many trees in a random forest? In *International workshop on machine learning and data mining in pattern recognition*, 154–168. Springer.
- Pachauri, R. K., L. Mayer, and Intergovernmental Panel on Climate Change eds. 2015. *Climate change 2014: Synthesis report*. Geneva, Switzerland: Intergovernmental Panel on Climate Change.
- Palczewska, A., J. Palczewski, R. M. Robinson, and D. Neagu. 2014. Interpreting random forest classification models using a feature contribution method. In *Integration of reusable systems*, 193–218. Springer.
- Paulin, K. M., J. J. Cook, and S. R. Dewey. 1999. Pinyon-juniper woodlands as sources of avian diversity. *Proceedings: ecology and management of pinyon-juniper communities within the Interior West. USDA Forest Service Proceedings, Ogden, UT* : 240–243.
- Pearl, R., and L. J. Reed. 1920. On the rate of growth of the population of the United States since 1790 and its mathematical representation. *Proceedings of the National Academy of Sciences of the United States of America* 6 (6): 275.
- Peng, C.-Y. J., K. L. Lee, and G. M. Ingersoll. 2002. An introduction to logistic regression analysis and reporting. *The journal of educational research* 96 (1): 3–14.

- Peterman, W., R. H. Waring, T. Seager, and W. L. Pollock. 2013. Soil properties affect pinyon pine - juniper response to drought. *Ecohydrology* 6 (3): 455–463.
- Petersen, J., D. Sack, and R. E. Gabler. 2015. *Fundamentals of physical geography* Second Edition. Cengage Learning.
- Phillips, S. L., and J. R. Ehleringer. 1995. Limited uptake of summer precipitation by bigtooth maple (*Acer grandidentatum* Nutt) and Gambel's oak (*Quereus gambelii* Nutt). *Trees* 9 (4): 214–219.
- Plaut, J. A., W. D. Wadsworth, R. Pangle, E. A. Yopez, N. G. McDowell, and W. T. Pockman. 2013. Reduced transpiration response to precipitation pulses precedes mortality in a piñon–juniper woodland subject to prolonged drought. *New Phytologist* 200 (2): 375–387.
- Plaut, J. A., E. A. Yopez, J. Hill, R. Pangle, J. S. Sperry, W. T. Pockman, and N. G. Mcdowell. 2012. Hydraulic limits preceding mortality in a piñon–juniper woodland under experimental drought. *Plant, Cell & Environment* 35 (9): 1601–1617.
- Pohar, M., M. Blas, and S. Turk. 2004. Comparison of logistic regression and linear discriminant analysis: a simulation study. *Metodoloski zvezki* 1 (1): 143.
- Progar, R. A., A. Eglitis, and J. E. Lundquist. 2009. Some ecological, economic, and social consequences of bark beetle infestations. In *In: Hayes, JL; Lundquist, JE, comps 2009. The Western Bark Beetle Research Group: a unique collaboration with Forest Health Protection-proceedings of a symposium at the 2007 Society of American Foresters conference. Gen. Tech. Rep. PNW-GTR-784. Portland, OR: US Department of Agriculture, Forest Service, Pacific Northwest Research Station: 71-83.*
- Raffa, K. F., B. H. Aukema, B. J. Bentz, A. L. Carroll, J. A. Hicke, M. G. Turner, and W. H. Romme. 2008. Cross-scale drivers of natural disturbances prone to anthropogenic amplification: the dynamics of bark beetle eruptions. *Bioscience* 58 (6): 501–517.
- Reed, C. C., and S. M. Hood. 2020. Few generalizable patterns of tree-level mortality during extreme drought and concurrent bark beetle outbreaks. *Science of the Total Environment* 750: 141306.
- Richter, R. *ATCOR 3*. ReSe Applications LLC. <http://www.rese.ch/products/atcor/atcor4/>.
- Richter, R., and R. S. D. Center. 2004. *ATCOR: Atmospheric and topographic correction. German Aerospace Center, Mars: Oberpfaffenhofen, Germany.*
- Roberts, D. A., M. Gardner, R. Church, S. Ustin, G. Scheer, and R. O. Green. 1998. Mapping chaparral in the Santa Monica Mountains using multiple endmember spectral mixture models. *Remote sensing of environment* 65 (3): 267–279.

- Romme, W. H., C. D. Allen, J. D. Bailey, W. L. Baker, B. T. Bestelmeyer, P. M. Brown, K. S. Eisenhart, M. L. Floyd, D. W. Huffman, and B. F. Jacobs. 2009. Historical and modern disturbance regimes, stand structures, and landscape dynamics in pinon–juniper vegetation of the western United States. *Rangeland Ecology & Management* 62 (3): 203–222.
- Roth, K. L., P. E. Dennison, and D. A. Roberts. 2012. Comparing endmember selection techniques for accurate mapping of plant species and land cover using imaging spectrometer data. *Remote Sensing of Environment* 127: 139–152.
- Rouse Jr, J., R. H. Haas, J. A. Schell, and D. W. Deering. 1974. Monitoring vegetation systems in the Great Plains with ERTS.
- Royer, P. D., D. D. Breshears, C. B. Zou, N. S. Cobb, and S. A. Kurc. 2010. Ecohydrological energy inputs in semiarid coniferous gradients: Responses to management-and drought-induced tree reductions. *Forest Ecology and Management* 260 (10): 1646–1655.
- RS/GIS Laboratory, College of Natural Resources, Utah State University. 2004. “PROVISIONAL” *Digital landcover dataset for the Southwestern United States*. USGS GAP Analysis Program. <http://earth.gis.usu.edu/swgap/>.
- Sala, O. E., W. J. Parton, L. A. Joyce, and W. K. Lauenroth. 1988. Primary production of the central grassland region of the United States. *Ecology* 69 (1): 40–45.
- Santos, M. J., and T. G. Whitham. 2010. Predictors of *Ips confusus* outbreaks during a record drought in Southwestern USA: Implications for monitoring and management. *Environmental Management* 45 (2): 239–249.
- Schott, J. R., C. Salvaggio, and W. J. Volchok. 1988. Radiometric scene normalization using pseudoinvariant features. *Remote sensing of Environment* 26 (1): 1–16.
- Seager, R., M. Ting, I. Held, Y. Kushnir, J. Lu, G. Vecchi, H.-P. Huang, N. Harnik, A. Leetmaa, N.-C. Lau, C. Li, J. Velez, and N. Naik. 2007. Model projections of an imminent transition to a more arid climate in southwestern North America. *Science* 316 (5828): 1181–1184.
- Shaw, J. D. 2006. Population-wide changes in pinyon-juniper woodlands caused by drought in the American Southwest: Effects on structure, composition, and distribution. <http://www.treearch.fs.fed.us/pubs/25001> (last accessed 13 March 2017).
- Shaw, J. D., B. E. Steed, and L. T. DeBlander. 2005. Forest Inventory and Analysis (FIA) annual inventory answers the question: What is happening to pinyon-Juniper woodlands? *Journal of Forestry* 103 (6): 280–285.
- Shinneman, D. J., and W. L. Baker. 2009. Historical fire and multidecadal drought as context for pinon–juniper woodland restoration in western Colorado. *Ecological Applications* 19 (5): 1231–1245.

- Soil survey investigations for irrigation. FAO soils bulletin 42. Food and Agriculture Organization of the United Nations.
- Soil Survey Staff, Soil Conservation Service, US Department of Agriculture. 1999. *Keys to Soil Taxonomy, 8th edition* 8th ed. Blacksburg, Virginia: Pocahontas Press, Inc.
- Stoeser, D. B., G. N. Green, L. C. Morath, W. D. Heran, A. B. Wilson, D. W. Moore, and B. S. Van Gosen. 2005. *Preliminary integrated geologic map databases for the United States central states: Montana, Wyoming, Colorado, New Mexico, Kansas, Oklahoma, Texas, Missouri, Arkansas, and Louisiana, - The State of New Mexico* version 1.0. Denver, CO: U.S. Geological Survey. <http://pubs.usgs.gov/of/2005/1351/> (last accessed 17 December 2017).
- Strahler, A. H., and A. N. Strahler. 2006. *Introducing physical geography* 4th ed. Wiley New York.
- Tane, Z., D. Roberts, S. Veraverbeke, Á. Casas, C. Ramirez, and S. Ustin. 2018. Evaluating endmember and band selection techniques for multiple endmember spectral mixture analysis using post-fire imaging spectroscopy. *Remote Sensing* 10 (3): 389.
- Thorp, K. R., A. N. French, and A. Rango. 2013. Effect of image spatial and spectral characteristics on mapping semi-arid rangeland vegetation using multiple endmember spectral mixture analysis (MESMA). *Remote sensing of environment* 132: 120–130.
- U.S. Department of Commerce, U.S. Census Bureau, Geography Division. 2011. *New Mexico, 2010 Census Place*. Washington D.C.: U.S. Department of Commerce, U.S. Census Bureau, Geography Division.
- U.S. Department of the Interior. 2017. USGS Global Visualization Viewer (GloVis). *USGS Global Visualization Viewer (GloVis)*. <https://glovis.usgs.gov/>.
- U.S. Department of the Interior, United States Geological Survey. Landsat Normalized Difference Vegetation Index. *Landsat surface reflectance-derived spectral indices*. https://www.usgs.gov/land-resources/nli/landsat/landsat-normalized-difference-vegetation-index?qt-science_support_page_related_con=0#qt-science_support_page_related_con (last accessed 16 October 2019).
- U.S. Department of the Interior, U.S. Geological Survey. 2001. *National Hydrography Dataset*. U.S. Geological Survey. <https://www.usgs.gov/core-science-systems/ngp/national-hydrography/access-national-hydrography-products>.
- USDA Forest Service. 2010. *AllotmentJoin*. New Mexico: USDA Forest Service.
- USDA Forest Service, Carson National Forest. 2012. *AllotmentJoin*. Taos, New Mexico: Carson National Forest.

- USDA Forest Service, Forest Health Protection and its partners. 2014. Forest Health - Insect and Disease. <http://foresthealth.fs.usda.gov/portal>.
- USDA Forest Service, Santa Fe National Forests. 2013. *sfe_allotments_join*. Santa Fe, New Mexico: Santa Fe National Forest.
- USDA Natural Resources Conservation Service. 2017. *Title 430 – National Soil Survey handbook, part 618 - Soil properties and qualities* 1st ed. https://www.nrcs.usda.gov/wps/portal/nrcs/detail/soils/ref/?cid=nrcs142p2_054240.
- Weiss, J. L., J. L. Betancourt, and J. T. Overpeck. 2012. Climatic limits on foliar growth during major droughts in the southwestern USA. *Journal of Geophysical Research: Biogeosciences* 117 (G3): G03031.
- Weiss, J. L., C. L. Castro, and J. T. Overpeck. 2009. Distinguishing pronounced droughts in the Southwestern United States: Seasonality and effects of warmer temperatures. *Journal of Climate* 22 (22): 5918–5932.
- West, A. G., K. R. Hultine, K. G. Burtch, and J. R. Ehleringer. 2007. Seasonal variations in moisture use in a piñon–juniper woodland. *Oecologia* 153 (4): 787–798.
- West, A. G., K. R. Hultine, J. S. Sperry, S. E. Bush, and J. R. Ehleringer. 2008. Transpiration and hydraulic strategies in a piñon–juniper woodland. *Ecological Applications* 18 (4): 911–927.
- Whitham, T. G., W. P. Young, G. D. Martinsen, C. A. Gehring, J. A. Schweitzer, S. M. Shuster, G. M. Wimp, D. G. Fischer, J. K. Bailey, R. L. Lindroth, and others. 2003. Community and ecosystem genetics: A consequence of the extended phenotype. *Ecology* 84 (3): 559–573.
- Williams, A. P., C. D. Allen, A. K. Macalady, D. Griffin, C. A. Woodhouse, D. M. Meko, T. W. Swetnam, S. A. Rauscher, R. Seager, and H. D. Grissino-Mayer. 2013. Temperature as a potent driver of regional forest drought stress and tree mortality. *Nature climate change* 3 (3): 292.
- Wolpert, D. H., and W. G. Macready. 1999. An efficient method to estimate bagging's generalization error. *Machine Learning* 35 (1): 41–55.

Appendix A: Potential explanatory variables

Table A1. Full set of potential explanatory variables considered n=136. For acronyms, see the [List of Abbreviations](#).

Type	Layer name	Variable description	Unit	Year	Source	Native resolution
bioclimatic	bio1.tif	Annual Mean Temperature [°C]	°C/10	1979-2013	CHELSA	1 km
bioclimatic	bio10.tif	Mean Temperature of Warmest Quarter [°C]	°C/10	1979-2013	CHELSA	1 km
bioclimatic	bio11.tif	Mean Temperature of Coldest Quarter [°C]	°C/10	1979-2013	CHELSA	1 km
bioclimatic	bio12.tif	Annual Precipitation [mm/year]	Millimeters	1979-2013	CHELSA	1 km
bioclimatic	bio13.tif	Precipitation of Wettest Month [mm/month]	Millimeters	1979-2013	CHELSA	1 km
bioclimatic	bio14.tif	Precipitation of Driest Month [mm/month]	Millimeters	1979-2013	CHELSA	1 km
bioclimatic	bio15.tif	Precipitation Seasonality [coefficient of variation]	Coefficient of variation	1979-2013	CHELSA	1 km
bioclimatic	bio16.tif	Precipitation of Wettest Quarter [mm/quarter]	Millimeters	1979-2013	CHELSA	1 km
bioclimatic	bio17.tif	Precipitation of Driest Quarter [mm/quarter]	Millimeters	1979-2013	CHELSA	1 km
bioclimatic	bio18.tif	Precipitation of Warmest Quarter [mm/quarter]	Millimeters	1979-2013	CHELSA	1 km
bioclimatic	bio19.tif	Precipitation of Coldest Quarter [mm/quarter]	Millimeters	1979-2013	CHELSA	1 km
bioclimatic	bio2.tif	Mean Diurnal Range [°C]	°C/10	1979-2013	CHELSA	1 km
bioclimatic	bio3.tif	Isothermality	Unitless	1979-2013	CHELSA	1 km
bioclimatic	bio4.tif	Temperature Seasonality [standard deviation]	Unitless	1979-2013	CHELSA	1 km
bioclimatic	bio5.tif	Max Temperature of Warmest Month [°C]	°C/10	1979-2013	CHELSA	1 km

Type	Layer name	Variable description	Unit	Year	Source	Native resolution
bioclimatic	bio6.tif	Min Temperature of Coldest Month [°C]	°C/10	1979-2013	CHELSA	1 km
bioclimatic	bio7.tif	Temperature Annual Range [°C]	°C/10	1979-2013	CHELSA	1 km
bioclimatic	bio8.tif	Mean Temperature of Wettest Quarter [°C]	°C/10	1979-2013	CHELSA	1 km
bioclimatic	bio9.tif	Mean Temperature of Driest Quarter [°C]	°C/10	1979-2013	CHELSA	1 km
bioclimatic	bioppapr.tif	Apr precipitation [mm/month]	Millimeters	1979-2013	CHELSA	1 km
bioclimatic	bioppaug.tif	Aug precipitation [mm/month]	Millimeters	1979-2013	CHELSA	1 km
bioclimatic	bioppdec.tif	Dec precipitation [mm/month]	Millimeters	1979-2013	CHELSA	1 km
bioclimatic	bioppfeb.tif	Feb precipitation [mm/month]	Millimeters	1979-2013	CHELSA	1 km
bioclimatic	bioppjan.tif	Jan precipitation [mm/month]	Millimeters	1979-2013	CHELSA	1 km
bioclimatic	bioppjul.tif	Jul precipitation [mm/month]	Millimeters	1979-2013	CHELSA	1 km
bioclimatic	bioppjun.tif	Jun precipitation [mm/month]	Millimeters	1979-2013	CHELSA	1 km
bioclimatic	bioppmar.tif	Mar precipitation [mm/month]	Millimeters	1979-2013	CHELSA	1 km
bioclimatic	bioppmay.tif	May precipitation [mm/month]	Millimeters	1979-2013	CHELSA	1 km
bioclimatic	bioppnov.tif	Nov precipitation [mm/month]	Millimeters	1979-2013	CHELSA	1 km
bioclimatic	bioppoct.tif	Oct precipitation [mm/month]	Millimeters	1979-2013	CHELSA	1 km
bioclimatic	bioppsep.tif	Sep precipitation [mm/month]	Millimeters	1979-2013	CHELSA	1 km
bioclimatic	biotempapr.tif	Apr monthly mean of daily mean temperature [°C]	°C/10	1979-2013	CHELSA	1 km
bioclimatic	biotempaug.tif	Aug monthly mean of daily mean temperature [°C]	°C/10	1979-2013	CHELSA	1 km

Type	Layer name	Variable description	Unit	Year	Source	Native resolution
bioclimatic	biotempdec.tif	Dec monthly mean of daily mean temperature [°C]	°C/10	1979-2013	CHELSA	1 km
bioclimatic	biotempfeb.tif	Feb monthly mean of daily mean temperature [°C]	°C/10	1979-2013	CHELSA	1 km
bioclimatic	biotempjan.tif	Jan monthly mean of daily mean temperature [°C]	°C/10	1979-2013	CHELSA	1 km
bioclimatic	biotempjul.tif	Jul monthly mean of daily mean temperature [°C]	°C/10	1979-2013	CHELSA	1 km
bioclimatic	biotempjun.tif	Jun monthly mean of daily mean temperature [°C]	°C/10	1979-2013	CHELSA	1 km
bioclimatic	biotempmar.tif	Mar monthly mean of daily mean temperature [°C]	°C/10	1979-2013	CHELSA	1 km
bioclimatic	biotempmay.tif	May monthly mean of daily mean temperature [°C]	°C/10	1979-2013	CHELSA	1 km
bioclimatic	biotempnov.tif	Nov monthly mean of daily mean temperature [°C]	°C/10	1979-2013	CHELSA	1 km
bioclimatic	biotempoct.tif	Oct monthly mean of daily mean temperature [°C]	°C/10	1979-2013	CHELSA	1 km
bioclimatic	biotempsep.tif	Sep monthly mean of daily mean temperature [°C]	°C/10	1979-2013	CHELSA	1 km
bioclimatic	biotmaxapr.tif	Apr monthly mean of daily maximum temperature [°C]	°C/10	1979-2013	CHELSA	1 km
bioclimatic	biotmaxaug.tif	Aug monthly mean of daily maximum temperature [°C]	°C/10	1979-2013	CHELSA	1 km
bioclimatic	biotmaxdec.tif	Dec monthly mean of daily maximum temperature [°C]	°C/10	1979-2013	CHELSA	1 km
bioclimatic	biotmaxfeb.tif	Feb monthly mean of daily maximum temperature [°C]	°C/10	1979-2013	CHELSA	1 km

Type	Layer name	Variable description	Unit	Year	Source	Native resolution
bioclimatic	biotmaxjan.tif	Jan monthly mean of daily maximum temperature [°C]	°C/10	1979-2013	CHELSA	1 km
bioclimatic	biotmaxjul.tif	Jul monthly mean of daily maximum temperature [°C]	°C/10	1979-2013	CHELSA	1 km
bioclimatic	biotmaxjun.tif	Jun monthly mean of daily maximum temperature [°C]	°C/10	1979-2013	CHELSA	1 km
bioclimatic	biotmaxmar.tif	Mar monthly mean of daily maximum temperature [°C]	°C/10	1979-2013	CHELSA	1 km
bioclimatic	biotmaxmay.tif	May monthly mean of daily maximum temperature [°C]	°C/10	1979-2013	CHELSA	1 km
bioclimatic	biotmaxnov.tif	Nov monthly mean of daily maximum temperature [°C]	°C/10	1979-2013	CHELSA	1 km
bioclimatic	biotmaxoct.tif	Oct monthly mean of daily maximum temperature [°C]	°C/10	1979-2013	CHELSA	1 km
bioclimatic	biotmaxsep.tif	Sep monthly mean of daily maximum temperature [°C]	°C/10	1979-2013	CHELSA	1 km
bioclimatic	biotminapr.tif	Apr monthly mean of daily minimum temperature [°C]	°C/10	1979-2013	CHELSA	1 km
bioclimatic	biotminaug.tif	Aug monthly mean of daily minimum temperature [°C]	°C/10	1979-2013	CHELSA	1 km
bioclimatic	biotmindec.tif	Dec monthly mean of daily minimum temperature [°C]	°C/10	1979-2013	CHELSA	1 km
bioclimatic	biotminfeb.tif	Feb monthly mean of daily minimum temperature [°C]	°C/10	1979-2013	CHELSA	1 km
bioclimatic	biotminjan.tif	Jan monthly mean of daily minimum temperature [°C]	°C/10	1979-2013	CHELSA	1 km
bioclimatic	biotminjul.tif	Jul monthly mean of daily minimum temperature [°C]	°C/10	1979-2013	CHELSA	1 km

Type	Layer name	Variable description	Unit	Year	Source	Native resolution
bioclimatic	biotminjun.tif	Jun monthly mean of daily minimum temperature [°C]	°C/10	1979-2013	CHELSA	1 km
bioclimatic	biotminmar.tif	Mar monthly mean of daily minimum temperature [°C]	°C/10	1979-2013	CHELSA	1 km
bioclimatic	biotminmay.tif	May monthly mean of daily minimum temperature [°C]	°C/10	1979-2013	CHELSA	1 km
bioclimatic	biotminnov.tif	Nov monthly mean of daily minimum temperature [°C]	°C/10	1979-2013	CHELSA	1 km
bioclimatic	biotminoct.tif	Oct monthly mean of daily minimum temperature [°C]	°C/10	1979-2013	CHELSA	1 km
bioclimatic	biotminsep.tif	Sep monthly mean of daily minimum temperature [°C]	°C/10	1979-2013	CHELSA	1 km
bioclimatic	soradapr.tif	Apr Area Solar Radiation - 2002	Watt hours per square meter	2002	SRTM	30 m
bioclimatic	soradaug.tif	Aug Area Solar Radiation - 2002	Watt hours per square meter	2002	SRTM	30 m
bioclimatic	soradec.tif	Dec Area Solar Radiation - 2002	Watt hours per square meter	2002	SRTM	30 m
bioclimatic	soradfeb.tif	Feb Area Solar Radiation - 2002	Watt hours per square meter	2002	SRTM	30 m
bioclimatic	soradjan.tif	Jan Area Solar Radiation - 2002	Watt hours per square meter	2002	SRTM	30 m
bioclimatic	soradjul.tif	Jul Area Solar Radiation - 2002	Watt hours per square meter	2002	SRTM	30 m
bioclimatic	soradjun.tif	Jun Area Solar Radiation - 2002	Watt hours per square meter	2002	SRTM	30 m
bioclimatic	soradmar.tif	Mar Area Solar Radiation - 2002	Watt hours per square meter	2002	SRTM	30 m

Type	Layer name	Variable description	Unit	Year	Source	Native resolution
bioclimatic	soradmay.tif	May Area Solar Radiation - 2002	Watt hours per square meter	2002	SRTM	30 m
bioclimatic	soradnov.tif	Nov Area Solar Radiation - 2002	Watt hours per square meter	2002	SRTM	30 m
bioclimatic	soradoct.tif	Oct Area Solar Radiation - 2002	Watt hours per square meter	2002	SRTM	30 m
bioclimatic	soradsep.tif	Sep Area Solar Radiation - 2002	Watt hours per square meter	2002	SRTM	30 m
bioclimatic	soradyr.tif	Area Solar Radiation (whole year) -2002	Watt hours per square meter	2002	SRTM	30 m
topographic	cos_nm.tif	Slope/aspect transformation based on cos method	Index -1 to 1	2000	SRTM	30 m
topographic	cti_nm.tif	Compound topographic index, also known as topographic wetness index	Index	2000	SRTM	30 m
topographic	curv_nm.tif	Slope curvature standard	(1/100) of a z-unit	2000	SRTM	30 m
topographic	curvpla_nm.tif	Slope curvature planar	(1/100) of a z-unit	2000	SRTM	30 m
topographic	curvpro_nm.tif	Slope curvature profile	(1/100) of a z-unit	2000	SRTM	30 m
topographic	diss_nm.tif	Dissection	Index	2000	SRTM	30 m
topographic	east_nm.tif	Aspect - eastness	Index -1 to 1	2000	SRTM	30 m
topographic	imi_nm.tif	Integrated moisture index	Index	2000	SRTM	30 m
topographic	ldform_nm.tif	Landform curvature	Index	2000	SRTM	30 m
topographic	north_nm.tif	Aspect - northness	Index -1 to 1	2000	SRTM	30 m
topographic	rough_nm.tif	Roughness	Index	2000	SRTM	30 m
topographic	sar_nm.tif	Surface area ratio	Index	2000	SRTM	30 m
topographic	sds_nm.tif	Second derivative slope	2nd derivate of slope	2000	SRTM	30 m
topographic	sei_nm.tif	Site exposure index	Index	2000	SRTM	30 m

Type	Layer name	Variable description	Unit	Year	Source	Native resolution
topographic	sin_nm.tif	Slope/aspect transformation based on sin method	Index -1 to 1	2000	SRTM	30 m
topographic	slopd_nm.tif	Slope degrees, planar method	Degrees	2000	SRTM	30 m
topographic	slppos_nm.tif	Slope position, based on 3 x 3 window	Index 0 to 100	2000	SRTM	30 m
topographic	srr_nm.tif	Surface relief ratio	Index	2000	SRTM	30 m
topographic	srtm_elev.tif	Elevation	Meters	2000	SRTM	30m
topographic	trasp_nm.tif	Slope/aspect transformation based on topographic radiation aspect	Index 0 to 1	2000	SRTM	30 m
edaphic	soawcft1.tif	Available water holding capacity (AWC) 0-31 cm (~0 to 1 ft)	Centimeters	Multiple years: 1999-2016	NRCS, USFS	Variable (County level soil surveys)
edaphic	soawcft2.tif	Available water holding capacity (AWC) 32-61 cm (~1 ft to 2 ft)	Centimeters	Multiple years: 1999-2016	NRCS, USFS	Variable (County level soil surveys)
edaphic	soawcft3.tif	Available water holding capacity (AWC) 62-91 cm (~2 ft to 3 ft)	Centimeters	Multiple years: 1999-2016	NRCS, USFS	Variable (County level soil surveys)
edaphic	soawcft4.tif	Available water holding capacity (AWC) 91-122 cm (~3 ft to 4 ft)	Centimeters	Multiple years: 1999-2016	NRCS, USFS	Variable (County level soil surveys)
edaphic	soawctot.tif	Available water holding capacity (AWC) of top 122 cm	Centimeters	Multiple years: 1999-2016	NRCS, USFS	Variable (County level soil surveys)
edaphic	soclayft1.tif	Estimated clay percentage (averaged) 0-31 cm (~0 to 1 ft)	Percentage	Multiple years: 1999-2016	NRCS, USFS	Variable (County level soil surveys)
edaphic	soclayft2.tif	Estimated clay percentage (averaged) 32-61 cm (~1 ft to 2 ft)	Percentage	Multiple years: 1999-2016	NRCS, USFS	Variable (County level soil surveys)

Type	Layer name	Variable description	Unit	Year	Source	Native resolution
edaphic	soclayft3.tif	Estimated clay percentage (averaged) 62-91 cm (~2 ft to 3 ft)	Percentage	Multiple years: 1999-2016	NRCS, USFS	Variable (County level soil surveys)
edaphic	soclayft4.tif	Estimated clay percentage (averaged) 92-122 cm (~3 ft to 4 ft)	Percentage	Multiple years: 1999-2016	NRCS, USFS	Variable (County level soil surveys)
edaphic	soclayhz.tif	Presence of a subsurface clay horizon at any depth within described profile	Meters	Multiple years: 1999-2016	NRCS, USFS	Variable (County level soil surveys)
edaphic	soclaytot.tif	Estimated clay percentage (averaged) of top 122 cm	Percentage	Multiple years: 1999-2016	NRCS, USFS	Variable (County level soil surveys)
edaphic	sodepth.tif	Soil depth	Centimeters	Multiple years: 1999-2016	NRCS, USFS	Variable (County level soil surveys)
edaphic	sodrexdt.tif	Drainage-class: Excessively drained	Meters	Multiple years: 1999-2016	NRCS, USFS	Variable (County level soil surveys)
edaphic	sodrmwd.tif	Drainage-class: Moderately well drained	Meters	Multiple years: 1999-2016	NRCS, USFS	Variable (County level soil surveys)
edaphic	sodrsexdt.tif	Drainage-class: Somewhat excessively drained	Meters	Multiple years: 1999-2016	NRCS, USFS	Variable (County level soil surveys)
edaphic	sodrwd.tif	Drainage-class: Well drained	Meters	Multiple years: 1999-2016	NRCS, USFS	Variable (County level soil surveys)
edaphic	sopmcal.tif	Parent material: calcareous (dummy-coded)	Meters	Multiple years: 1999-2016	NRCS, USFS	Variable (County level soil surveys)
edaphic	sopsashci.tif	soil particle-size class: miscellaneous ashy & cindery	Meters	Multiple years: 1999-2016	NRCS, USFS	Variable (County level soil surveys)

Type	Layer name	Variable description	Unit	Year	Source	Native resolution
edaphic	sopscol.tif	soil particle-size class: coarse-loamy	Meters	Multiple years: 1999-2016	NRCS, USFS	Variable (County level soil surveys)
edaphic	sopscsk.tif	soil particle-size class: clayey-skeletal	Meters	Multiple years: 1999-2016	NRCS, USFS	Variable (County level soil surveys)
edaphic	sopssf.tif	soil particle-size class: fine	Meters	Multiple years: 1999-2016	NRCS, USFS	Variable (County level soil surveys)
edaphic	sopsfl.tif	soil particle-size class: fine-loamy	Meters	Multiple years: 1999-2016	NRCS, USFS	Variable (County level soil surveys)
edaphic	sopsfsi.tif	soil particle-size class: fine-silty	Meters	Multiple years: 1999-2016	NRCS, USFS	Variable (County level soil surveys)
edaphic	sopsl.tif	soil particle-size class: loamy	Meters	Multiple years: 1999-2016	NRCS, USFS	Variable (County level soil surveys)
edaphic	sopslsk.tif	soil particle-size class: loamy-skeletal	Meters	Multiple years: 1999-2016	NRCS, USFS	Variable (County level soil surveys)
edaphic	sopss.tif	soil particle-size class: sandy	Meters	Multiple years: 1999-2016	NRCS, USFS	Variable (County level soil surveys)
edaphic	sorlpres.tif	soil unit with presence of root-restrictive layer	Meters	Multiple years: 1999-2016	NRCS, USFS	Variable (County level soil surveys)
edaphic	soshzO.tif	surface texture: organic	Meters	Multiple years: 1999-2016	NRCS, USFS	Variable (County level soil surveys)
edaphic	sosrfclpct.tif	clay percent of surface texture	Percentage	Multiple years: 1999-2016	NRCS, USFS	Variable (County level soil surveys)

Type	Layer name	Variable description	Unit	Year	Source	Native resolution
edaphic	sostxbr.tif	surface texture: bedrock	Meters	Multiple years: 1999-2016	NRCS, USFS	Variable (County level soil surveys)
edaphic	sostxco.tif	surface texture group: coarse	Meters	Multiple years: 1999-2016	NRCS, USFS	Variable (County level soil surveys)
edaphic	sostxm.tif	surface texture group: medium	Meters	Multiple years: 1999-2016	NRCS, USFS	Variable (County level soil surveys)
edaphic	sostxmco.tif	surface texture group: moderately coarse	Meters	Multiple years: 1999-2016	NRCS, USFS	Variable (County level soil surveys)
vegetation	ndmi2000.tif	Pre-drought NDMI	Numerical - 1 to 1	2000	Landsat 5 TM	30 m
vegetation	ndvi2000.tif	Pre-drought NDVI	Numerical - 1 to 1	2000	Landsat 5 TM	30 m
anthropogenic	hugrazall.tif	Grazing Allotment (dummy-coded)	Meters	Multiple: 2000-2016	USFS, BLM, SLO	Variable (polygon datasets)

Table A2. Final set of potential explanatory variables after removing correlated and collinear variables n=42. For acronyms, see the [List of Abbreviations](#).

Type	Layer name	Variable description	Unit	Year	Source	Native Resolution
bioclimatic	bio15.tif	Precipitation Seasonality [coefficient of variation]	Coefficient of variation	1979-2013	CHELSA	1 km
bioclimatic	bio18.tif	Precipitation of Warmest Quarter [mm/quarter]	Millimeters	1979-2013	CHELSA	1 km
bioclimatic	bio3.tif	Isothermality	Unitless	1979-2013	CHELSA	1 km
bioclimatic	bio6.tif	Min Temperature of Coldest Month [°C]	°C/10	1979-2013	CHELSA	1 km
bioclimatic	bio9.tif	Mean Temperature of Driest Quarter [°C]	°C/10	1979-2013	CHELSA	1 km
bioclimatic	bioppnov.tif	Nov precipitation [mm/month]	Millimeters	1979-2013	CHELSA	1 km
bioclimatic	soradmay.tif	May Area Solar Radiation - 2002	Watt hours per square meter	2002	SRTM	30 m
topographic	cti_nm.tif	Compound topographic index, also known as topographic wetness index	Index	2000	SRTM	30 m
topographic	curvpro_nm.tif	Slope curvature profile	(1/100) of a z-unit	2000	SRTM	30 m
topographic	imi_nm.tif	Integrated moisture index	Index	2000	SRTM	30 m
topographic	sar_nm.tif	Surface area ratio	Index	2000	SRTM	30 m
topographic	sds_nm.tif	Second derivative slope	2nd derivate of slope	2000	SRTM	30 m
topographic	sei_nm.tif	Site exposure index	Index	2000	SRTM	30 m
topographic	sin_nm.tif	Slope/aspect transformation based on sin method	Index -1 to 1	2000	SRTM	30 m
topographic	srr_nm.tif	Surface relief ratio	Index	2000	SRTM	30 m

Type	Layer name	Variable description	Unit	Year	Source	Native Resolution
topographic	trasp_nm.tif	Slope/aspect transformation based on topographic radiation aspect	Index 0 to 1	2000	SRTM	30 m
edaphic	soawcft1.tif	Available water holding capacity (AWC) 0-31 cm (~0 to 1 ft)	Centimeters	Multiple years: 1999-2016	NRCS, USFS	Variable (County level soil surveys)
edaphic	soclayft3.tif	Estimated clay percentage (averaged) 62-91 cm (~2 ft to 3 ft)	Percentage	Multiple years: 1999-2016	NRCS, USFS	Variable (County level soil surveys)
edaphic	soclayhz.tif	Presence of a subsurface clay horizon at any depth within described profile	Meters	Multiple years: 1999-2016	NRCS, USFS	Variable (County level soil surveys)
edaphic	soclaytot.tif	Estimated clay percentage (averaged) of top 122 cm	Percentage	Multiple years: 1999-2016	NRCS, USFS	Variable (County level soil surveys)
edaphic	sodepth.tif	Soil depth	Centimeters	Multiple years: 1999-2016	NRCS, USFS	Variable (County level soil surveys)
edaphic	sodrexd.tif	Drainage-class: Excessively drained	Meters	Multiple years: 1999-2016	NRCS, USFS	Variable (County level soil surveys)
edaphic	sodrmwd.tif	Drainage-class: Moderately well drained	Meters	Multiple years: 1999-2016	NRCS, USFS	Variable (County level soil surveys)
edaphic	sodrsexd.tif	Drainage-class: Somewhat excessively drained	Meters	Multiple years: 1999-2016	NRCS, USFS	Variable (County level soil surveys)
edaphic	sodrwd.tif	Drainage-class: Well drained	Meters	Multiple years: 1999-2016	NRCS, USFS	Variable (County level soil surveys)

Type	Layer name	Variable description	Unit	Year	Source	Native Resolution
edaphic	sopmcal.tif	Parent material: calcareous (dummy-coded)	Meters	Multiple years: 1999-2016	NRCS, USFS	Variable (County level soil surveys)
edaphic	sopsashci.tif	soil particle-size class: miscellaneous ashy & cindery	Meters	Multiple years: 1999-2016	NRCS, USFS	Variable (County level soil surveys)
edaphic	sopscol.tif	soil particle-size class: coarse-loamy	Meters	Multiple years: 1999-2016	NRCS, USFS	Variable (County level soil surveys)
edaphic	sopscsk.tif	soil particle-size class: clayey-skeletal	Meters	Multiple years: 1999-2016	NRCS, USFS	Variable (County level soil surveys)
edaphic	sopssf.tif	soil particle-size class: fine	Meters	Multiple years: 1999-2016	NRCS, USFS	Variable (County level soil surveys)
edaphic	sopsl.tif	soil particle-size class: fine-loamy	Meters	Multiple years: 1999-2016	NRCS, USFS	Variable (County level soil surveys)
edaphic	sopsfsi.tif	soil particle-size class: fine-silty	Meters	Multiple years: 1999-2016	NRCS, USFS	Variable (County level soil surveys)
edaphic	sopsl.tif	soil particle-size class: loamy	Meters	Multiple years: 1999-2016	NRCS, USFS	Variable (County level soil surveys)
edaphic	sopslsk.tif	soil particle-size class: loamy-skeletal	Meters	Multiple years: 1999-2016	NRCS, USFS	Variable (County level soil surveys)
edaphic	sopss.tif	soil particle-size class: sandy	Meters	Multiple years: 1999-2016	NRCS, USFS	Variable (County level soil surveys)
edaphic	soshzO.tif	surface texture: organic	Meters	Multiple years: 1999-2016	NRCS, USFS	Variable (County level soil surveys)

Type	Layer name	Variable description	Unit	Year	Source	Native Resolution
edaphic	sosrfclpct.tif	clay percent of surface texture	Percentage	Multiple years: 1999-2016	NRCS, USFS	Variable (County level soil surveys)
edaphic	sostxbr.tif	surface texture: bedrock	Meters	Multiple years: 1999-2016	NRCS, USFS	Variable (County level soil surveys)
edaphic	sostxm.tif	surface texture group: medium	Meters	Multiple years: 1999-2016	NRCS, USFS	Variable (County level soil surveys)
edaphic	sostxmco.tif	surface texture group: moderately coarse	Meters	Multiple years: 1999-2016	NRCS, USFS	Variable (County level soil surveys)
vegetation	ndmi2000.tif	Pre-drought NDMI	Numerical - 1 to 1	2000	Landsat 5 TM	30 m
anthropogenic	hugrazall.tif	Grazing Allotment (dummy-coded)	Meters	Multiple: 2000-2016	USFS, BLM, SLO	Variable (polygon datasets)

Appendix B: Python code for calculating soil properties

#script to convert horizon by horizon awc and clay content data into cm by cm for the entire soil profile, and at the same time truncate all data at 122 cm

```
import csv
```

```
with open('TH_awc_clay_in_nm600.csv', 'r') as e:
```

```
    soilreader = csv.reader(e, delimiter = ',')
```

```
    musym = []
```

```
    soilnames = []
```

```
    hzb = []
```

```
    awc = []
```

```
    clay = []
```

```
    for row in soilreader:
```

```
        musym.append(row[0])
```

```
        soilnames.append(row[2])
```

```
        hzb.append(int(row[3]))
```

```
        awc.append(float(row[4]))
```

```
        clay.append(float(row[5]))
```

```
soilmusym = {} #holds the map unit symbol and soil component name
```

```
soilhzdepthb = {} #holds the horizon bottom depths as a list for each component key
```

```
soilawc = {} #holds the awc associated with each horizon as a list for each component key
```

```
soilclay = {} #holds the clay content associated with each horizon as a list for each component key
```

```
#adds musym and soil names to soilmusym dictionary, initializes component key to empty list for other dictionaries.
```

```
for index, key in enumerate(musym):
```

```
    if key not in soilmusym:
```

```
        soilmusym[key] = soilnames[index]
```

```
        soilhzdepthb[key] = []
```

```
        soilawc[key] = []
```

```
        soilclay[key] = []
```

```
#adds values to dictionary lists
```

```
for index, key in enumerate(musym):
```

```
    soilhzdepthb[key].append(hzb[index])
```

```
    soilawc[key].append(awc[index])
```

```
    soilclay[key].append(clay[index])
```

```
def extract(soilhzb):
```

```
    # extracts the cm by cm values for awc & clay content for a single soil component
```

```
    i = 1
```

```
    for index, depth in enumerate(soilhzb):
```

```
        while i <= depth:
```

```
            if i > 122:
```

```
                break
```

```
            else:
```

```
                row = [soil, soilmusym[soil], i, soilawc[soil][index], soilclay[soil][index]]
```

```
                soilwriter.writerow(row)
```

```

i += 1

#do not write header to file, but header = (musym, soilname, cm, awc, claypct)

with open('NM600_awc_clay_out.csv', 'w', newline='') as out:
    soilwriter = csv.writer(out)
    # iterates through the list of soils, executing the extract function for each one
    for soil in soilhzdepthb:
        extract(soilhzdepthb[soil])

#=====
#script to convert horizon by horizon awc and clay content data into cm by cm for the first foot of the soil profile.
Essentially the same script was used for each 1-foot increment of the profile, simply changing the start and end
depths.

import csv

with open('TH_awc_clay_in_nm600.csv', 'r') as e:
    soilreader = csv.reader(e, delimiter = ',')
    musym = []
    soilnames = []
    hzb = []
    awc = []
    clay = []
    for row in soilreader:
        musym.append(row[0])
        soilnames.append(row[2])
        hzb.append(int(row[3]))
        awc.append(float(row[4]))
        clay.append(float(row[5]))

soilmusym = {} #holds the map unit symbol and soil component name
soilhzdepthb = {} #holds the horizon bottom depths as a list for each component key
soilawc = {} #holds the awc associated with each horizon as a list for each component key
soilclay = {} #holds the clay content associated with each horizon as a list for each component key

#adds musym and soil names to soilmusym dictionary, initializes component key to empty list for other
dictionaries.
for index, key in enumerate(musym):
    if key not in soilmusym:
        soilmusym[key] = soilnames[index]
        soilhzdepthb[key] = []
        soilawc[key] = []
        soilclay[key] = []

#adds values to dictionary lists
for index, key in enumerate(musym):
    soilhzdepthb[key].append(hzb[index])
    soilawc[key].append(awc[index])
    soilclay[key].append(clay[index])

```

```

def extract(soilhzb):
    # extracts the cm by cm values for awc & clay content for a single soil component
    i = 1
    for index, depth in enumerate(soilhzb):
        while i <= depth:
            if i > 31:
                break
            else:
                row = [soil, soilmusym[soil], i, soilawc[soil][index], soilclay[soil][index]]
                soilwriter.writerow(row)

            i += 1

#do not write header to file, but header = (musym, soilname, cm, awc, clay content)

with open('NM600_awc_clay_out_ft1.csv', 'w', newline='') as out:
    soilwriter = csv.writer(out)
    # iterates through the list of soils, executing the extract function for each one
    for soil in soilhzdepthb:
        extract(soilhdepthb[soil])

#=====
#script to sum the awc and compute the average clay content across a given soil depth interval (either 1 foot
increment or the whole profile, depending on the input data)

import csv

with open('NM600_awc_clay_out_ft4.csv', 'r') as e:
    soilreader = csv.reader(e, delimiter = ',')
    musym = []
    soilnames = []
    soildep = []
    awc = []
    clay = []
    for row in soilreader:
        musym.append(row[0])
        soilnames.append(row[1])
        soildep.append(int(row[2]))
        awc.append(float(row[3]))
        clay.append(float(row[4]))

soilmusym = {} #holds the component key and soil component name
soildepth = {} #holds the horizon bottom depths as a list for each component key
soilawc = {} #holds the awc associated with each horizon as a list for each component key
soilclay = {} #holds the clay content associated with each horizon as a list for each component key

#adds musym and soil names to soilmusym dictionary, initializes component musym to empty list for other
dictionaries.
for index, key in enumerate(musym):
    if key not in soilmusym:
        soilmusym[key] = soilnames[index]
        soildepth[key] = 0
        soilawc[key] = 0

```

```

    soilclay[key] = 0

#adds values to dictionary lists
for index, key in enumerate(musym):
    soildepth[key] += 1
    soilawc[key] += awc[index]
    soilclay[key] += clay[index]

def soilsum(sum):
    row = [soil, soilmusym[soil], soilawc[soil], round((soilclay[soil]/soildepth[soil]),2)]
    soilwriter.writerow(row)

def header():
    headerrow = ["musym", "component", "awcft4", "clayavgft4"]
    soilwriter.writerow(headerrow)

with open('NM600_awc_clay_out_sum_ft4.csv', 'w', newline='') as out:
    soilwriter = csv.writer(out)
    #writes header row
    header()

#iterates through the list of soils, executing the extract function for each one
for soil in soilmusym:
    soilsum(soilmusym[soil])

```

**Appendix C: Correlation matrices and variance inflation factors of
potential explanatory variables**

Table C1. Pearson's correlation coefficients for all climatic variables (n=67).

	bio1	bio10	bio11	bio12	bio13	bio14	bio15	bio16	bio17	bio18	bio19
bio1	1.000										
bio10	0.991	1.000									
bio11	0.989	0.961	1.000								
bio12	-0.295	-0.358	-0.220	1.000							
bio13	-0.104	-0.178	-0.022	0.904	1.000						
bio14	-0.500	-0.510	-0.482	0.759	0.463	1.000					
bio15	0.364	0.308	0.418	-0.014	0.395	-0.586	1.000				
bio16	-0.132	-0.212	-0.043	0.900	0.995	0.440	0.415	1.000			
bio17	-0.512	-0.520	-0.497	0.759	0.466	0.990	-0.590	0.441	1.000		
bio18	-0.342	-0.421	-0.244	0.857	0.878	0.438	0.316	0.912	0.430	1.000	
bio19	-0.492	-0.485	-0.496	0.710	0.419	0.960	-0.615	0.387	0.978	0.364	1.000
bio2	-0.781	-0.736	-0.808	-0.064	-0.277	0.259	-0.465	-0.242	0.264	0.035	0.250
bio3	0.063	-0.065	0.202	0.430	0.503	0.051	0.407	0.546	0.029	0.598	-0.081
bio4	0.208	0.334	0.063	-0.548	-0.583	-0.200	-0.326	-0.629	-0.184	-0.696	-0.064
bio5	0.958	0.986	0.910	-0.426	-0.266	-0.517	0.233	-0.303	-0.525	-0.502	-0.479
bio6	0.966	0.926	0.990	-0.140	0.068	-0.442	0.462	0.048	-0.458	-0.161	-0.461
bio7	-0.477	-0.363	-0.590	-0.332	-0.500	0.108	-0.543	-0.513	0.127	-0.400	0.196
bio8	0.986	0.999	0.952	-0.372	-0.197	-0.512	0.292	-0.231	-0.522	-0.438	-0.485
bio9	0.649	0.649	0.633	-0.165	-0.089	-0.235	0.114	-0.114	-0.225	-0.266	-0.157
bioppapr	-0.563	-0.596	-0.512	0.847	0.599	0.840	-0.382	0.609	0.854	0.684	0.809
bioppaug	-0.101	-0.176	-0.019	0.904	1.000	0.464	0.394	0.994	0.467	0.876	0.420
bioppdec	-0.258	-0.270	-0.251	0.693	0.437	0.866	-0.498	0.405	0.870	0.359	0.899
bioppfeb	-0.469	-0.499	-0.429	0.837	0.572	0.963	-0.479	0.558	0.970	0.551	0.928
bioppjan	-0.563	-0.548	-0.572	0.671	0.383	0.942	-0.626	0.354	0.962	0.343	0.979
bioppjul	-0.187	-0.274	-0.086	0.865	0.953	0.379	0.446	0.979	0.376	0.953	0.310
bioppjun	-0.046	-0.138	0.061	0.878	0.880	0.435	0.248	0.896	0.423	0.865	0.346
bioppmar	-0.464	-0.469	-0.455	0.753	0.470	0.934	-0.561	0.447	0.954	0.443	0.959
bioppmay	-0.374	-0.445	-0.279	0.897	0.771	0.643	-0.039	0.792	0.624	0.850	0.538
bioppnov	-0.500	-0.473	-0.522	0.608	0.300	0.920	-0.673	0.265	0.921	0.261	0.944
bioppoct	-0.119	-0.147	-0.090	0.890	0.749	0.782	-0.191	0.716	0.782	0.609	0.777
bioppsep	-0.014	-0.090	0.068	0.921	0.911	0.576	0.178	0.900	0.558	0.795	0.500
biotempapr	0.998	0.983	0.993	-0.269	-0.071	-0.492	0.387	-0.099	-0.504	-0.312	-0.486

Table C1, Continued. Pearson's correlation coefficients for all climatic variables (n=67).

	bio1	bio10	bio11	bio12	bio13	bio14	bio15	bio16	bio17	bio18	bio19
biotempaug	0.987	0.999	0.954	-0.369	-0.194	-0.512	0.295	-0.227	-0.522	-0.435	-0.485
biotempdec	0.994	0.973	0.998	-0.242	-0.046	-0.487	0.401	-0.070	-0.502	-0.277	-0.496
biotempfeb	0.991	0.966	0.998	-0.229	-0.029	-0.480	0.413	-0.053	-0.494	-0.259	-0.487
biotempjan	0.985	0.955	0.999	-0.209	-0.010	-0.479	0.426	-0.030	-0.495	-0.227	-0.495
biotempjul	0.985	0.999	0.949	-0.376	-0.202	-0.512	0.289	-0.236	-0.521	-0.445	-0.483
biotempjun	0.998	0.996	0.978	-0.321	-0.134	-0.502	0.342	-0.165	-0.513	-0.379	-0.484
biotempmar	0.998	0.982	0.995	-0.263	-0.066	-0.491	0.389	-0.093	-0.504	-0.305	-0.489
biotempmay	0.999	0.988	0.989	-0.286	-0.092	-0.495	0.372	-0.121	-0.506	-0.334	-0.485
biotempnov	0.999	0.987	0.992	-0.287	-0.095	-0.503	0.373	-0.121	-0.516	-0.326	-0.501
biotempoct	0.998	0.996	0.981	-0.322	-0.136	-0.508	0.343	-0.166	-0.519	-0.372	-0.494
biotempsep	0.993	0.999	0.965	-0.351	-0.172	-0.507	0.311	-0.204	-0.518	-0.413	-0.485
biotmaxapr	0.995	0.975	0.995	-0.252	-0.053	-0.487	0.400	-0.079	-0.500	-0.286	-0.486
biotmaxaug	0.967	0.990	0.924	-0.411	-0.248	-0.519	0.250	-0.283	-0.528	-0.482	-0.486
biotmaxdec	0.991	0.981	0.984	-0.319	-0.137	-0.518	0.350	-0.160	-0.532	-0.345	-0.524
biotmaxfeb	0.993	0.978	0.992	-0.295	-0.106	-0.511	0.374	-0.129	-0.524	-0.318	-0.515
biotmaxjan	0.983	0.970	0.981	-0.315	-0.136	-0.521	0.353	-0.156	-0.537	-0.329	-0.534
biotmaxjul	0.958	0.986	0.909	-0.426	-0.267	-0.517	0.233	-0.303	-0.525	-0.502	-0.479
biotmaxjun	0.995	0.998	0.971	-0.337	-0.152	-0.504	0.327	-0.185	-0.514	-0.398	-0.483
biotmaxmar	0.995	0.975	0.995	-0.270	-0.075	-0.499	0.391	-0.099	-0.512	-0.296	-0.502
biotmaxmay	0.998	0.987	0.989	-0.282	-0.088	-0.491	0.375	-0.117	-0.504	-0.329	-0.482
biotmaxnov	0.996	0.978	0.996	-0.266	-0.075	-0.497	0.388	-0.098	-0.511	-0.293	-0.501
biotmaxoct	0.998	0.994	0.982	-0.322	-0.139	-0.508	0.342	-0.167	-0.521	-0.367	-0.499
biotmaxsep	0.987	0.998	0.956	-0.370	-0.198	-0.514	0.293	-0.229	-0.525	-0.431	-0.492
biotminapr	0.999	0.989	0.989	-0.287	-0.091	-0.497	0.372	-0.121	-0.508	-0.340	-0.487
biotminaug	0.996	0.998	0.972	-0.330	-0.146	-0.502	0.329	-0.178	-0.512	-0.392	-0.481
biotmindec	0.983	0.954	0.995	-0.186	0.019	-0.460	0.433	-0.005	-0.475	-0.225	-0.470
biotminfeb	0.980	0.948	0.994	-0.178	0.028	-0.455	0.439	0.004	-0.469	-0.212	-0.463
biotminjan	0.966	0.926	0.990	-0.140	0.068	-0.442	0.462	0.048	-0.458	-0.161	-0.461
biotminjul	0.996	0.998	0.972	-0.330	-0.145	-0.501	0.330	-0.178	-0.511	-0.392	-0.478
biotminjun	0.999	0.994	0.983	-0.306	-0.115	-0.499	0.356	-0.145	-0.510	-0.359	-0.483
biotminmar	0.996	0.983	0.990	-0.256	-0.058	-0.481	0.385	-0.087	-0.493	-0.313	-0.475
biotminmay	0.999	0.990	0.989	-0.290	-0.097	-0.497	0.369	-0.126	-0.509	-0.338	-0.487
biotminnov	0.997	0.992	0.984	-0.306	-0.115	-0.506	0.356	-0.145	-0.518	-0.357	-0.497
biotminoct	0.998	0.997	0.979	-0.323	-0.134	-0.507	0.343	-0.166	-0.517	-0.378	-0.489
biotminsep	0.995	0.998	0.971	-0.333	-0.149	-0.502	0.328	-0.181	-0.512	-0.396	-0.479

Table C1, Continued. Pearson's correlation coefficients for all climatic variables (n=67).

	bio2	bio3	bio4	bio5	bio6	bio7	bio8	bio9	bioppapr	bioppaug	bioppdec
bio1											
bio10											
bio11											
bio12											
bio13											
bio14											
bio15											
bio16											
bio17											
bio18											
bio19											
bio2	1.000										
bio3	-0.259	1.000									
bio4	0.112	-0.932	1.000								
bio5	-0.649	-0.212	0.464	1.000							
bio6	-0.862	0.295	-0.035	0.855	1.000						
bio7	0.715	-0.853	0.718	-0.209	-0.686	1.000					
bio8	-0.718	-0.097	0.363	0.991	0.912	-0.329	1.000				
bio9	-0.508	0.000	0.181	0.628	0.619	-0.288	0.645	1.000			
bioppapr	0.335	0.236	-0.402	-0.615	-0.468	0.021	-0.599	-0.299	1.000		
bioppaug	-0.280	0.501	-0.581	-0.264	0.070	-0.500	-0.194	-0.087	0.597	1.000	
bioppdec	0.007	0.097	-0.127	-0.309	-0.193	-0.069	-0.281	-0.023	0.682	0.439	1.000
bioppfeb	0.190	0.196	-0.342	-0.528	-0.376	-0.032	-0.506	-0.166	0.900	0.573	0.841
bioppjan	0.343	-0.156	-0.031	-0.524	-0.550	0.302	-0.544	-0.206	0.812	0.384	0.799
bioppjul	-0.162	0.616	-0.701	-0.367	0.004	-0.520	-0.293	-0.165	0.609	0.952	0.325
bioppjun	-0.283	0.630	-0.710	-0.229	0.144	-0.590	-0.155	-0.063	0.636	0.879	0.372
bioppmar	0.246	0.033	-0.147	-0.479	-0.415	0.111	-0.472	-0.144	0.882	0.470	0.874
bioppmay	0.097	0.484	-0.650	-0.495	-0.220	-0.279	-0.454	-0.286	0.818	0.769	0.459
bioppnov	0.345	-0.215	0.075	-0.441	-0.511	0.344	-0.467	-0.226	0.725	0.302	0.831
bioppoct	-0.175	0.193	-0.231	-0.196	-0.026	-0.226	-0.158	-0.037	0.743	0.751	0.830
bioppsep	-0.347	0.520	-0.565	-0.182	0.157	-0.551	-0.109	-0.037	0.608	0.912	0.597
biotempapr	-0.804	0.110	0.162	0.941	0.978	-0.523	0.976	0.649	-0.551	-0.069	-0.242

Table C1, Continued. Pearson's correlation coefficients for all climatic variables (n=67).

	bio2	bio3	bio4	bio5	bio6	bio7	bio8	bio9	bioppapr	bioppaug	bioppdec
biotempaug	-0.719	-0.092	0.357	0.991	0.914	-0.334	1.000	0.645	-0.597	-0.191	-0.281
biotempdec	-0.805	0.151	0.110	0.928	0.984	-0.552	0.965	0.637	-0.528	-0.044	-0.259
biotempfeb	-0.815	0.188	0.083	0.914	0.990	-0.585	0.957	0.641	-0.523	-0.027	-0.235
biotempjan	-0.808	0.225	0.042	0.900	0.992	-0.607	0.945	0.630	-0.504	-0.008	-0.246
biotempjul	-0.716	-0.107	0.372	0.992	0.909	-0.321	0.999	0.645	-0.602	-0.199	-0.279
biotempjun	-0.772	0.009	0.264	0.970	0.952	-0.435	0.993	0.652	-0.581	-0.131	-0.252
biotempmar	-0.804	0.117	0.151	0.940	0.979	-0.528	0.975	0.647	-0.546	-0.064	-0.249
biotempmay	-0.795	0.079	0.196	0.951	0.971	-0.497	0.982	0.651	-0.562	-0.090	-0.241
biotempnov	-0.776	0.087	0.181	0.952	0.969	-0.492	0.982	0.645	-0.554	-0.093	-0.271
biotempoct	-0.760	0.019	0.253	0.970	0.953	-0.435	0.993	0.649	-0.576	-0.134	-0.267
biotempsep	-0.738	-0.051	0.320	0.984	0.931	-0.374	0.998	0.648	-0.590	-0.170	-0.268
biotmaxapr	-0.807	0.153	0.125	0.926	0.984	-0.556	0.966	0.646	-0.540	-0.051	-0.231
biotmaxaug	-0.664	-0.177	0.431	0.999	0.872	-0.243	0.995	0.632	-0.609	-0.246	-0.309
biotmaxdec	-0.716	0.078	0.192	0.955	0.950	-0.452	0.978	0.635	-0.555	-0.135	-0.311
biotmaxfeb	-0.746	0.130	0.149	0.940	0.968	-0.507	0.972	0.643	-0.549	-0.103	-0.281
biotmaxjan	-0.694	0.105	0.165	0.944	0.946	-0.460	0.968	0.626	-0.544	-0.134	-0.325
biotmaxjul	-0.649	-0.212	0.464	1.000	0.855	-0.209	0.991	0.628	-0.615	-0.264	-0.309
biotmaxjun	-0.759	-0.023	0.294	0.977	0.942	-0.405	0.996	0.650	-0.590	-0.150	-0.256
biotmaxmar	-0.776	0.152	0.128	0.931	0.978	-0.539	0.968	0.645	-0.541	-0.073	-0.257
biotmaxmay	-0.798	0.088	0.190	0.947	0.973	-0.505	0.980	0.651	-0.560	-0.085	-0.233
biotmaxnov	-0.778	0.143	0.135	0.935	0.978	-0.533	0.971	0.641	-0.539	-0.072	-0.256
biotmaxoct	-0.750	0.031	0.244	0.968	0.953	-0.438	0.991	0.645	-0.572	-0.137	-0.269
biotmaxsep	-0.711	-0.082	0.349	0.990	0.915	-0.336	0.999	0.642	-0.596	-0.195	-0.287
biotminapr	-0.798	0.064	0.201	0.955	0.969	-0.487	0.984	0.650	-0.563	-0.089	-0.255
biotminaug	-0.762	-0.018	0.290	0.976	0.944	-0.411	0.995	0.651	-0.583	-0.144	-0.253
biotmindec	-0.857	0.201	0.052	0.898	0.994	-0.615	0.944	0.629	-0.503	0.022	-0.219
biotminfeb	-0.859	0.230	0.033	0.886	0.997	-0.638	0.936	0.635	-0.499	0.031	-0.201
biotminjan	-0.862	0.295	-0.035	0.855	1.000	-0.686	0.912	0.619	-0.468	0.070	-0.193
biotminjul	-0.764	-0.017	0.291	0.975	0.944	-0.412	0.995	0.652	-0.584	-0.143	-0.250
biotminjun	-0.783	0.039	0.235	0.962	0.961	-0.462	0.989	0.653	-0.572	-0.112	-0.246
biotminmar	-0.826	0.083	0.172	0.944	0.975	-0.515	0.977	0.645	-0.548	-0.055	-0.241
biotminmay	-0.791	0.070	0.203	0.954	0.969	-0.488	0.984	0.651	-0.563	-0.094	-0.248
biotminnov	-0.773	0.029	0.229	0.966	0.956	-0.447	0.989	0.646	-0.568	-0.113	-0.284
biotminoct	-0.768	0.007	0.262	0.972	0.951	-0.430	0.993	0.652	-0.579	-0.132	-0.265
biotminsep	-0.763	-0.022	0.294	0.976	0.943	-0.408	0.996	0.652	-0.584	-0.146	-0.252

Table C1, Continued. Pearson's correlation coefficients for all climatic variables (n=67).

	bioppf eb	bioppj an	bioppj ul	bioppj un	biopp mar	biopp may	bioppn ov	bioppo ct	biopps ep	biotem papr	biotem paug
bio1											
bio10											
bio11											
bio12											
bio13											
bio14											
bio15											
bio16											
bio17											
bio18											
bio19											
bio2											
bio3											
bio4											
bio5											
bio6											
bio7											
bio8											
bio9											
bioppapr											
bioppaug											
bioppdec											
bioppfeb	1.000										
bioppjan	0.908	1.000									
bioppjul	0.510	0.283	1.000								
bioppjun	0.566	0.311	0.900	1.000							
bioppmar	0.940	0.934	0.387	0.413	1.000						
bioppmay	0.716	0.538	0.810	0.895	0.577	1.000					
bioppnov	0.827	0.936	0.184	0.226	0.887	0.487	1.000				
bioppoct	0.805	0.703	0.624	0.687	0.803	0.683	0.718	1.000			
bioppsep	0.654	0.424	0.849	0.905	0.528	0.814	0.416	0.855	1.000		
biotempapr	-0.453	-0.563	-0.154	-0.016	-0.455	-0.355	-0.505	-0.101	0.018	1.000	

Table C1, Continued. Pearson's correlation coefficients for all climatic variables (n=67).

	bioppf eb	bioppj an	bioppj ul	bioppj un	biopp mar	biopp may	bioppn ov	bioppo ct	biopps ep	biotem papr	biotem paug
biotempaug	-0.505	-0.545	-0.289	-0.150	-0.473	-0.449	-0.468	-0.157	-0.105	0.977	1.000
biotempdec	-0.442	-0.569	-0.117	0.032	-0.463	-0.303	-0.515	-0.100	0.045	0.996	0.967
biotempfeb	-0.430	-0.567	-0.101	0.040	-0.447	-0.306	-0.516	-0.086	0.061	0.996	0.958
biotempjan	-0.423	-0.574	-0.071	0.075	-0.451	-0.268	-0.525	-0.085	0.079	0.991	0.947
biotempjul	-0.507	-0.541	-0.299	-0.163	-0.471	-0.462	-0.464	-0.159	-0.114	0.974	0.999
biotempjun	-0.480	-0.556	-0.225	-0.090	-0.463	-0.413	-0.486	-0.125	-0.043	0.994	0.993
biotempmar	-0.451	-0.564	-0.147	-0.004	-0.458	-0.341	-0.508	-0.103	0.023	0.999	0.976
biotempmay	-0.462	-0.562	-0.178	-0.042	-0.456	-0.377	-0.497	-0.106	-0.001	0.999	0.983
biotempnov	-0.468	-0.571	-0.172	-0.027	-0.470	-0.353	-0.510	-0.124	-0.006	0.997	0.983
biotempoct	-0.484	-0.563	-0.221	-0.081	-0.471	-0.400	-0.494	-0.135	-0.045	0.994	0.993
biotempsep	-0.495	-0.550	-0.265	-0.127	-0.469	-0.434	-0.475	-0.145	-0.081	0.985	0.999
biotmaxapr	-0.443	-0.568	-0.130	0.005	-0.448	-0.339	-0.510	-0.091	0.036	0.999	0.967
biotmaxaug	-0.524	-0.533	-0.345	-0.203	-0.483	-0.477	-0.452	-0.191	-0.162	0.952	0.994
biotmaxdec	-0.485	-0.584	-0.202	-0.052	-0.490	-0.356	-0.521	-0.168	-0.050	0.986	0.979
biotmaxfeb	-0.470	-0.585	-0.172	-0.031	-0.474	-0.352	-0.525	-0.144	-0.019	0.993	0.973
biotmaxjan	-0.485	-0.592	-0.191	-0.040	-0.494	-0.337	-0.531	-0.178	-0.050	0.979	0.969
biotmaxjul	-0.528	-0.524	-0.367	-0.229	-0.479	-0.495	-0.440	-0.196	-0.182	0.941	0.991
biotmaxjun	-0.487	-0.552	-0.247	-0.111	-0.466	-0.428	-0.478	-0.133	-0.061	0.990	0.996
biotmaxmar	-0.455	-0.578	-0.145	-0.007	-0.460	-0.341	-0.521	-0.118	0.012	0.997	0.969
biotmaxmay	-0.458	-0.561	-0.173	-0.039	-0.452	-0.377	-0.496	-0.101	0.004	0.999	0.981
biotmaxnov	-0.455	-0.577	-0.143	-0.002	-0.462	-0.334	-0.516	-0.112	0.017	0.997	0.972
biotmaxoct	-0.484	-0.569	-0.219	-0.078	-0.474	-0.393	-0.497	-0.137	-0.045	0.993	0.992
biotmaxsep	-0.506	-0.551	-0.287	-0.146	-0.479	-0.442	-0.473	-0.163	-0.106	0.977	0.999
biotminapr	-0.464	-0.558	-0.180	-0.038	-0.461	-0.371	-0.499	-0.113	-0.004	0.998	0.985
biotminaug	-0.483	-0.550	-0.239	-0.104	-0.461	-0.424	-0.479	-0.127	-0.056	0.991	0.996
biotmindec	-0.407	-0.551	-0.056	0.092	-0.438	-0.262	-0.504	-0.052	0.111	0.990	0.946
biotminfeb	-0.397	-0.549	-0.047	0.093	-0.425	-0.268	-0.505	-0.043	0.118	0.989	0.938
biotminjan	-0.376	-0.550	0.004	0.144	-0.415	-0.220	-0.511	-0.026	0.157	0.978	0.914
biotminjul	-0.483	-0.549	-0.240	-0.106	-0.458	-0.427	-0.478	-0.125	-0.056	0.991	0.995
biotminjun	-0.472	-0.558	-0.204	-0.069	-0.458	-0.399	-0.491	-0.116	-0.025	0.997	0.989
biotminmar	-0.444	-0.548	-0.147	0.000	-0.453	-0.340	-0.492	-0.089	0.033	0.997	0.978
biotminmay	-0.465	-0.561	-0.183	-0.044	-0.459	-0.377	-0.498	-0.111	-0.007	0.999	0.985
biotminnov	-0.478	-0.560	-0.201	-0.051	-0.476	-0.371	-0.500	-0.136	-0.029	0.994	0.990
biotminoct	-0.483	-0.557	-0.225	-0.085	-0.467	-0.407	-0.491	-0.133	-0.047	0.994	0.994
biotminsep	-0.484	-0.549	-0.243	-0.108	-0.460	-0.427	-0.477	-0.128	-0.059	0.990	0.996

Table C1, Continued. Pearson's correlation coefficients for all climatic variables (n=67).

	biotem pdec	biotem pfeb	biotem pjan	biotem pjul	biotem pjun	biotem pmar	biotem pmay	biotem pnov	biotem poct	biotem psep	biotma xapr
biotempaug											
biotempdec	1.000										
biotempfeb	0.997	1.000									
biotempjan	0.996	0.998	1.000								
biotempjul	0.963	0.954	0.942	1.000							
biotempjun	0.986	0.983	0.973	0.992	1.000						
biotempmar	0.998	0.997	0.993	0.973	0.993	1.000					
biotempmay	0.993	0.993	0.986	0.981	0.997	0.998	1.000				
biotempnov	0.996	0.993	0.989	0.980	0.995	0.998	0.997	1.000			
biotempoct	0.988	0.984	0.977	0.991	0.999	0.994	0.997	0.997	1.000		
biotempsep	0.976	0.969	0.959	0.998	0.997	0.984	0.990	0.989	0.997	1.000	
biotmaxapr	0.996	0.998	0.994	0.964	0.989	0.998	0.997	0.995	0.989	0.977	1.000
biotmaxaug	0.941	0.927	0.915	0.995	0.977	0.951	0.960	0.963	0.978	0.989	0.938
biotmaxdec	0.989	0.982	0.981	0.976	0.985	0.988	0.986	0.994	0.991	0.984	0.983
biotmaxfeb	0.993	0.992	0.990	0.969	0.987	0.994	0.992	0.996	0.991	0.980	0.993
biotmaxjan	0.984	0.977	0.979	0.965	0.976	0.982	0.978	0.989	0.983	0.974	0.977
biotmaxjul	0.928	0.913	0.900	0.992	0.970	0.940	0.951	0.952	0.970	0.984	0.926
biotmaxjun	0.981	0.976	0.966	0.995	0.999	0.989	0.994	0.992	0.998	0.999	0.984
biotmaxmar	0.996	0.997	0.994	0.965	0.988	0.997	0.995	0.996	0.990	0.978	0.998
biotmaxmay	0.993	0.993	0.986	0.979	0.996	0.998	1.000	0.996	0.995	0.988	0.997
biotmaxnov	0.997	0.997	0.995	0.968	0.989	0.998	0.996	0.997	0.992	0.981	0.997
biotmaxoct	0.989	0.984	0.978	0.990	0.997	0.993	0.996	0.997	0.999	0.996	0.989
biotmaxsep	0.969	0.959	0.949	0.999	0.992	0.976	0.983	0.984	0.993	0.998	0.968
biotminapr	0.994	0.992	0.985	0.983	0.997	0.998	0.999	0.998	0.997	0.991	0.995
biotminaug	0.982	0.977	0.967	0.995	0.999	0.989	0.995	0.992	0.998	0.999	0.985
biotmindec	0.994	0.995	0.994	0.941	0.974	0.992	0.986	0.985	0.974	0.958	0.991
biotminfeb	0.991	0.996	0.994	0.934	0.970	0.990	0.984	0.981	0.969	0.952	0.993
biotminjan	0.984	0.990	0.992	0.909	0.952	0.979	0.971	0.969	0.953	0.931	0.984
biotminjul	0.981	0.977	0.967	0.994	0.999	0.989	0.995	0.991	0.998	0.998	0.985
biotminjun	0.989	0.988	0.979	0.988	0.999	0.996	0.999	0.996	0.998	0.994	0.993
biotminmar	0.995	0.992	0.987	0.975	0.993	0.997	0.996	0.995	0.992	0.985	0.993
biotminmay	0.994	0.992	0.986	0.983	0.998	0.998	1.000	0.998	0.998	0.991	0.996
biotminnov	0.992	0.985	0.980	0.987	0.996	0.994	0.994	0.997	0.997	0.993	0.988
biotminoct	0.987	0.983	0.974	0.992	0.999	0.993	0.996	0.996	0.999	0.997	0.988
biotminsep	0.981	0.976	0.966	0.995	0.999	0.989	0.994	0.991	0.998	0.999	0.984

Table C1, Continued. Pearson's correlation coefficients for all climatic variables (n=67).

	biotm axaug	biotm axdec	biotm axfeb	biotm axjan	biotm axjul	biotm axjun	biotm axmar	biotm axmay	biotm axnov	biotm axoct	biotm axsep
biotempaug											
biotempdec											
biotempfeb											
biotempjan											
biotempjul											
biotempjun											
biotempmar											
biotempmay											
biotempnov											
biotempoct											
biotempsep											
biotmaxapr											
biotmaxaug	1.000										
biotmaxdec	0.965	1.000									
biotmaxfeb	0.951	0.996	1.000								
biotmaxjan	0.955	0.998	0.994	1.000							
biotmaxjul	0.999	0.955	0.940	0.944	1.000						
biotmaxjun	0.983	0.983	0.983	0.973	0.977	1.000					
biotmaxmar	0.943	0.991	0.998	0.987	0.931	0.983	1.000				
biotmaxmay	0.957	0.984	0.991	0.976	0.947	0.993	0.995	1.000			
biotmaxnov	0.947	0.992	0.998	0.988	0.935	0.985	0.999	0.995	1.000		
biotmaxoct	0.976	0.993	0.992	0.986	0.968	0.997	0.991	0.995	0.993	1.000	
biotmaxsep	0.994	0.982	0.975	0.973	0.990	0.995	0.970	0.980	0.974	0.993	1.000
biotminapr	0.964	0.988	0.991	0.979	0.955	0.995	0.993	0.998	0.994	0.996	0.984
biotminaug	0.982	0.983	0.983	0.973	0.976	0.999	0.984	0.994	0.985	0.997	0.995
biotmindec	0.912	0.968	0.979	0.962	0.898	0.966	0.986	0.986	0.988	0.973	0.947
biotminfeb	0.900	0.962	0.977	0.956	0.886	0.962	0.987	0.985	0.987	0.969	0.938
biotminjan	0.872	0.950	0.968	0.946	0.855	0.942	0.978	0.973	0.978	0.953	0.915
biotminjul	0.981	0.982	0.983	0.972	0.975	0.999	0.983	0.994	0.985	0.996	0.994
biotminjun	0.970	0.986	0.990	0.977	0.962	0.998	0.991	0.998	0.992	0.997	0.989
biotminmar	0.954	0.981	0.986	0.972	0.944	0.990	0.990	0.996	0.992	0.991	0.977
biotminmay	0.964	0.988	0.992	0.980	0.954	0.995	0.995	0.999	0.996	0.997	0.985
biotminnov	0.975	0.992	0.990	0.985	0.966	0.995	0.989	0.993	0.991	0.996	0.990
biotminoct	0.979	0.988	0.988	0.979	0.972	0.999	0.988	0.995	0.990	0.998	0.993
biotminsep	0.982	0.983	0.983	0.972	0.976	0.999	0.983	0.993	0.985	0.996	0.995

Table C1, Continued. Pearson's correlation coefficients for all climatic variables (n=67).

	biotmi napr	biotmi naug	biotmi ndec	biotmi nfeb	biotmi njan	biotmi njul	biotmi njun	biotmi nmar	biotmi nmay	biotmi nnov	biotmi noct	biotmi nsep
biotempaug												
biotempdec												
biotempfeb												
biotempjan												
biotempjul												
biotempjun												
biotempmar												
biotempmay												
biotempnov												
biotempoct												
biotempsep												
biotmaxapr												
biotmaxaug												
biotmaxdec												
biotmaxfeb												
biotmaxjan												
biotmaxjul												
biotmaxjun												
biotmaxmar												
biotmaxmay												
biotmaxnov												
biotmaxoct												
biotmaxsep												
biotminapr	1.000											
biotminaug	0.995	1.000										
biotmindec	0.986	0.968	1.000									
biotminfeb	0.983	0.963	0.998	1.000								
biotminjan	0.969	0.944	0.994	0.997	1.000							
biotminjul	0.995	1.000	0.967	0.963	0.944	1.000						
biotminjun	0.998	0.998	0.979	0.977	0.961	0.998	1.000					
biotminmar	0.998	0.990	0.992	0.988	0.975	0.990	0.995	1.000				
biotminmay	0.999	0.995	0.985	0.983	0.969	0.995	0.999	0.997	1.000			
biotminnov	0.997	0.995	0.978	0.972	0.956	0.994	0.996	0.995	0.996	1.000		
biotminoct	0.997	0.999	0.973	0.969	0.951	0.999	0.999	0.993	0.997	0.997	1.000	
biotminsep	0.995	1.000	0.967	0.962	0.943	1.000	0.998	0.990	0.995	0.994	0.999	1.000

Table C2. Pearson's correlation coefficients for all solar radiation variables, n=13.

	sorada pr	sorada ug	sorad ec	soradf eb	soradj an	sorad jul	soradj un	sorad mar	sorad may	soradn ov	sorad oct	sorads ep	sorad yr
sorada pr	1.000												
sorada ug	0.994	1.000											
sorade c	0.897	0.842	1.000										
soradf eb	0.927	0.879	0.997	1.000									
soradja n	0.902	0.849	1.000	0.998	1.000								
soradju l	0.878	0.926	0.579	0.635	0.588	1.000							
soradju n	0.814	0.874	0.477	0.538	0.487	0.993	1.000						
sorad mar	0.968	0.934	0.978	0.991	0.981	0.730	0.643	1.000					
sorad may	0.924	0.961	0.662	0.714	0.671	0.994	0.974	0.799	1.000				
soradn ov	0.908	0.855	1.000	0.999	1.000	0.598	0.497	0.984	0.680	1.000			
sorado ct	0.937	0.892	0.994	1.000	0.996	0.656	0.561	0.995	0.733	0.997	1.000		
sorads ep	0.981	0.953	0.966	0.982	0.969	0.767	0.685	0.998	0.832	0.972	0.987	1.000	
sorady r	0.994	0.975	0.940	0.962	0.944	0.821	0.746	0.990	0.877	0.948	0.970	0.996	1.000

Table C3. Pearson’s correlation coefficients for all edaphic variables, n = 33.

	soawcf t1	soawcf t2	soawcf t3	soawcf t4	soawct ot	soclayf t1	soclayf t2	soclayf t3	soclayf t4	soclayh z	soclayt ot
soawcft1	1.000										
soawcft2	0.702	1.000									
soawcft3	0.532	0.859	1.000								
soawcft4	0.404	0.697	0.900	1.000							
soawctot	0.732	0.926	0.946	0.871	1.000						
soclayft1	0.579	0.399	0.263	0.182	0.392	1.000					
soclayft2	0.609	0.567	0.417	0.305	0.528	0.778	1.000				
soclayft3	0.474	0.718	0.751	0.602	0.730	0.446	0.632	1.000			
soclayft4	0.381	0.606	0.783	0.797	0.741	0.338	0.482	0.796	1.000		
soclayhz	0.139	0.008	-0.052	-0.103	-0.012	0.314	0.395	0.223	0.010	1.000	
soclaytot	0.644	0.444	0.333	0.232	0.457	0.887	0.861	0.591	0.457	0.387	1.000
sodepth	0.324	0.638	0.729	0.718	0.702	0.282	0.349	0.603	0.650	-0.030	0.214
sodrex	-0.073	-0.051	-0.023	-0.005	-0.042	-0.132	-0.119	-0.074	-0.039	-0.044	-0.133
sodrmwd	0.117	0.061	0.070	0.082	0.091	0.150	0.202	0.175	0.156	0.157	0.219
sodrsex	-0.229	-0.151	-0.108	-0.061	-0.144	-0.335	-0.320	-0.168	-0.121	-0.105	-0.329
sodrwd	0.496	0.325	0.225	0.154	0.326	0.590	0.457	0.249	0.176	0.073	0.532
sopmcal	0.091	-0.089	-0.120	-0.175	-0.092	0.039	0.017	-0.006	-0.096	0.000	0.067
sopsashci	-0.107	-0.074	-0.051	-0.033	-0.068	-0.167	-0.140	-0.082	-0.063	-0.010	-0.162
sopscol	-0.066	0.112	0.200	0.247	0.148	-0.222	-0.173	-0.053	-0.002	-0.087	-0.238
sopscsk	-0.056	-0.109	-0.143	-0.150	-0.132	0.304	0.335	0.085	-0.027	0.531	0.308
sopssf	0.306	0.333	0.283	0.179	0.310	0.297	0.373	0.422	0.260	0.276	0.379
sopssf	0.515	0.614	0.524	0.404	0.580	0.209	0.285	0.384	0.361	-0.109	0.266
sopssfi	0.149	0.176	0.187	0.174	0.195	0.040	0.049	0.076	0.095	-0.004	0.042
sopssl	0.142	-0.291	-0.357	-0.305	-0.240	-0.021	-0.074	-0.359	-0.299	-0.099	0.020
sopslsk	-0.256	-0.287	-0.227	-0.166	-0.266	0.036	-0.180	-0.080	-0.036	-0.180	-0.067
sopss	-0.134	-0.024	0.037	0.063	-0.010	-0.274	-0.195	-0.091	-0.045	-0.055	-0.247
sorlpres	-0.118	-0.425	-0.582	-0.671	-0.526	-0.051	-0.112	-0.385	-0.543	0.127	0.010
soshzO	0.169	-0.044	-0.116	-0.132	-0.046	0.026	0.150	0.076	0.012	0.163	0.081
sosrfclpct	0.317	0.274	0.255	0.219	0.301	0.614	0.362	0.238	0.207	0.072	0.495
sostxbr	-0.579	-0.358	-0.270	-0.231	-0.397	-0.580	-0.419	-0.275	-0.226	-0.075	-0.535
sostxco	-0.162	-0.043	0.020	0.048	-0.030	-0.312	-0.240	-0.114	-0.062	-0.065	-0.280
sostxm	0.257	0.242	0.203	0.148	0.239	0.524	0.430	0.276	0.258	0.067	0.466
sostxmco	-0.055	-0.048	-0.027	0.010	-0.033	-0.161	-0.258	-0.184	-0.164	-0.132	-0.177

Table C3, Continued. Pearson's correlation coefficients for all edaphic variables, n = 33.

	sodept h	sodrex d	sodrm wd	sodrse xd	sodrw d	sopmc al	sopsas hci	sopsco l	sopscs k	sopsf	sopsfl
soawcft1											
soawcft2											
soawcft3											
soawcft4											
soawctot											
soclayft1											
soclayft2											
soclayft3											
soclayft4											
soclayhz											
soclaytot											
sodepth	1.000										
sodrex	0.087	1.000									
sodrm	0.025	-0.022	1.000								
sodrse	0.104	-0.055	-0.052	1.000							
sodrw	0.155	-0.284	-0.268	-0.675	1.000						
sopmc	-0.153	0.055	-0.043	-0.008	0.047	1.000					
sopsas	-0.003	-0.016	-0.015	0.222	-0.157	-0.031	1.000				
sopsco	0.238	0.054	-0.043	0.155	-0.077	-0.089	-0.031	1.000			
sopscs	-0.027	-0.043	0.163	-0.102	0.072	-0.044	-0.030	-0.085	1.000		
sopsf	0.130	-0.042	0.277	-0.100	0.036	-0.001	-0.029	-0.083	-0.079	1.000	
sopsfl	0.240	-0.076	-0.052	-0.177	0.258	-0.091	-0.053	-0.150	-0.142	-0.140	1.000
sopfsi	0.080	-0.014	-0.013	-0.034	0.050	0.041	-0.010	-0.028	-0.026	-0.026	-0.047
sopsl	-0.353	-0.051	-0.049	0.037	0.059	0.183	-0.036	-0.102	-0.096	-0.094	-0.171
sopslsk	-0.029	-0.036	-0.091	-0.102	0.214	0.141	-0.067	-0.190	-0.180	-0.177	-0.319
sopss	0.217	0.333	-0.027	0.357	-0.354	-0.056	-0.020	-0.057	-0.053	-0.053	-0.095
sorlpres	-0.786	-0.109	-0.056	-0.180	0.059	0.143	-0.025	-0.307	0.099	-0.082	-0.087
soshzO	-0.073	-0.015	0.097	0.091	-0.047	0.156	0.006	-0.120	0.059	0.031	-0.039
sosrfclpct	0.315	-0.123	-0.045	-0.189	0.472	0.037	-0.117	-0.051	0.137	0.102	0.147
sostxbr	-0.480	-0.039	-0.037	-0.093	-0.482	-0.076	-0.004	-0.077	-0.073	-0.072	-0.129
sostxco	0.199	0.314	-0.032	0.388	-0.364	-0.066	0.290	-0.017	-0.063	-0.062	-0.105
sostxm	0.180	-0.069	0.066	-0.288	0.350	0.156	-0.086	-0.236	0.193	0.094	0.170
sostxmco	0.008	-0.035	-0.103	0.114	0.071	-0.213	-0.040	0.386	-0.171	-0.106	-0.040

Table C3, Continued. Pearson's correlation coefficients for all edaphic variables, n = 33.

	sopfsi	sopsl	sopslsk	sopss	sorlpres	soshzO	sosrfclpct	sostxbr	sostxco	sostxm	sostxmco
soawcft1											
soawcft2											
soawcft3											
soawcft4											
soawctot											
soclayft1											
soclayft2											
soclayft3											
soclayft4											
soclayhz											
soclaytot											
sodepth											
sodrex											
sodrmwd											
sodrsex											
sodrwd											
sopmcal											
sopsashci											
sopscol											
sopscsk											
sopsf											
sopsl											
sopfsi	1.000										
sopsl	-0.032	1.000									
sopslsk	-0.059	-0.216	1.000								
sopss	-0.018	-0.064	-0.120	1.000							
sorlpres	-0.088	0.295	0.015	-0.204	1.000						
soshzO	-0.037	0.039	0.099	-0.076	0.159	1.000					
sosrfclpct	0.051	0.010	0.070	-0.140	-0.156	-0.398	1.000				
sostxbr	-0.024	-0.087	-0.153	-0.049	0.238	-0.103	-0.465	1.000			
sostxco	-0.021	-0.075	-0.123	0.805	-0.197	-0.089	-0.174	-0.057	1.000		
sostxm	0.101	-0.009	0.049	-0.155	-0.073	-0.328	0.589	-0.211	-0.182	1.000	
sostxmco	-0.067	0.063	0.026	-0.116	-0.062	-0.287	-0.046	-0.185	-0.160	-0.588	1.000

Table C4. Pearson's correlation coefficients for all topographic variables, n=20.

	cos_n m	cti_nm	curv_n m	curvpl a_nm	curvpr o_nm	diss_n m	east_n m	imi_n m	ldform _nm	north_ nm
cos_nm	1.000									
cti_nm	0.033	1.000								
curv_nm	-0.065	-0.464	1.000							
curvpla_nm	-0.048	-0.491	0.840	1.000						
curvpro_nm	0.063	0.323	-0.886	-0.492	1.000					
diss_nm	-0.028	-0.452	0.765	0.567	-0.741	1.000				
east_nm	0.004	0.043	-0.020	-0.004	0.029	-0.012	1.000			
imi_nm	0.042	0.492	-0.165	-0.130	0.154	-0.214	0.005	1.000		
ldform_nm	-0.064	-0.474	0.976	0.805	-0.878	0.797	-0.016	-0.172	1.000	
north_nm	0.751	-0.034	-0.001	0.006	0.006	0.006	0.002	0.008	0.000	1.000
rough_nm	-0.015	-0.375	0.083	0.122	-0.029	-0.020	-0.039	-0.040	0.083	0.008
sar_nm	-0.010	-0.383	0.086	0.126	-0.030	-0.018	-0.040	-0.052	0.087	0.013
sds_nm	-0.027	-0.308	0.035	0.037	-0.025	0.003	-0.041	-0.017	0.043	0.001
sei_nm	-1.000	-0.033	0.064	0.047	-0.062	0.027	-0.004	-0.042	0.064	-0.759
sin_nm	0.010	0.010	-0.023	0.006	0.042	0.002	0.749	-0.023	-0.013	0.004
slopd_nm	-0.026	-0.492	0.072	0.128	-0.007	-0.052	-0.054	-0.076	0.072	0.016
slppos_nm	-0.064	-0.474	0.976	0.805	-0.878	0.797	-0.016	-0.172	1.000	0.000
srr_nm	-0.043	0.020	0.249	-0.061	-0.451	0.569	0.012	-0.028	0.295	-0.048
srtmelev	-0.124	-0.127	0.081	0.092	-0.052	0.071	-0.036	-0.026	0.083	-0.107
trasp_nm	-0.641	0.007	0.011	-0.002	-0.020	0.001	-0.527	-0.010	0.009	-0.851

Table C4, Continued. Pearson's correlation coefficients for all topographic variables, n=20.

	rough_ nm	sar_nm	sds_nm	sei_nm	sin_nm	slopd_n m	slppos_ nm	srr_nm	srtmele v	trasp_n m
cos_nm										
cti_nm										
curv_nm										
curvpla_nm										
curvpro_nm										
diss_nm										
east_nm										
imi_nm										
ldform_nm										
north_nm										
rough_nm	1.000									
sar_nm	0.990	1.000								
sds_nm	0.547	0.508	1.000							
sei_nm	0.016	0.010	0.027	1.000						
sin_nm	-0.073	-0.073	-0.042	-0.011	1.000					
slopd_nm	0.931	0.930	0.612	0.026	-0.062	1.000				
slppos_nm	0.083	0.087	0.043	0.064	-0.013	0.072	1.000			
srr_nm	-0.053	-0.054	0.009	0.043	0.013	-0.100	0.295	1.000		
srtmelev	0.106	0.104	0.058	0.123	0.005	0.125	0.083	0.016	1.000	
trasp_nm	0.014	0.010	0.020	0.648	-0.397	0.015	0.009	0.034	0.110	1.000

Table C5. Pearson's correlation coefficients for all vegetation variables, n=2.

	ndmi2000	ndvi2000
ndmi2000	1	
ndvi2000	0.742	1

Table C6. Pearson's correlation coefficients for uncorrelated variables from Tables C1-C5, n = 44.

	bio15	bio18	bio3	bio6	bio9	biopp nov	hugra zall	soawc ft1	soclay ft3	soclay hz	soclay tot
bio15	1.000										
bio18	0.316	1.000									
bio3	0.407	0.598	1.000								
bio6	0.462	-0.161	0.295	1.000							
bio9	0.114	-0.266	0.000	0.619	1.000						
bioppnov	-0.673	0.261	-0.215	-0.511	-0.226	1.000					
hugrazall	-0.200	0.057	-0.178	-0.447	-0.274	0.230	1.000				
soawcft1	0.054	0.072	0.158	0.033	0.059	0.015	0.081	1.000			
soclayft3	0.001	0.024	-0.066	-0.072	0.007	0.050	0.217	0.474	1.000		
soclayhz	0.073	0.085	-0.011	-0.086	-0.042	0.021	0.090	0.139	0.223	1.000	
soclaytot	0.036	0.125	0.106	-0.043	-0.024	0.038	0.141	0.644	0.591	0.387	1.000
sodepth	-0.179	-0.207	-0.317	-0.031	0.058	0.139	0.144	0.324	0.603	-0.030	0.214
sodrexd	-0.084	-0.120	-0.152	-0.020	0.011	0.025	0.122	-0.073	-0.074	-0.044	-0.133
sodrmwd	-0.006	-0.060	-0.085	-0.054	-0.051	0.008	0.144	0.117	0.175	0.157	0.219
sodrsexd	-0.078	0.025	-0.073	-0.011	-0.039	0.082	0.025	-0.229	-0.168	-0.105	-0.329
sodrw	0.080	0.043	0.173	0.143	0.110	-0.039	-0.095	0.496	0.249	0.073	0.532
sopmcal	0.179	0.272	0.351	0.168	0.110	-0.100	-0.019	0.091	-0.006	0.000	0.067
sopsashci	0.112	-0.027	-0.089	-0.006	-0.009	-0.072	-0.044	-0.107	-0.082	-0.010	-0.162
sopscol	-0.102	-0.156	-0.208	0.037	0.048	0.011	0.040	-0.066	-0.053	-0.087	-0.238
sopscsk	-0.013	-0.024	-0.102	-0.035	-0.042	0.069	0.142	-0.056	0.085	0.531	0.308
sopsf	0.110	0.048	0.045	0.040	0.062	-0.083	0.023	0.306	0.422	0.276	0.379
sopsfl	-0.074	0.032	-0.009	-0.191	-0.077	0.123	0.180	0.515	0.384	-0.109	0.266

Table C6, Continued. Pearson's correlation coefficients for uncorrelated variables from Tables C1-C5, n = 44.

	bio15	bio18	bio3	bio6	bio9	bioppn ov	hugraz all	soawcf t1	soclayf t3	soclay hz	soclayt ot
sopsfsi	0.074	-0.018	0.026	0.073	0.052	-0.053	-0.063	0.149	0.076	-0.004	0.042
sopsl	0.081	0.085	0.269	0.201	0.100	-0.121	-0.203	0.142	-0.359	-0.099	0.020
sopslsk	0.025	0.017	0.119	0.185	0.103	-0.028	-0.132	-0.256	-0.080	-0.180	-0.067
sopss	-0.143	-0.099	-0.145	-0.091	-0.046	0.123	0.150	-0.134	-0.091	-0.055	-0.247
soshzO	0.099	0.223	0.140	-0.071	-0.050	0.056	0.130	0.169	0.076	0.163	0.081
sosrfclpct	-0.099	-0.068	0.008	-0.002	0.038	0.020	-0.065	0.317	0.238	0.072	0.495
sostxbr	0.019	0.009	-0.049	-0.180	-0.110	-0.061	-0.038	-0.579	-0.275	-0.075	-0.535
sostxm	-0.037	0.016	-0.022	-0.045	-0.027	0.029	0.051	0.257	0.276	0.067	0.466
sostxmco	-0.014	-0.140	0.017	0.214	0.133	-0.072	-0.172	-0.055	-0.184	-0.132	-0.177
soradec	0.122	0.310	0.138	-0.217	-0.189	0.123	0.108	0.040	0.018	0.090	0.043
soradmay	0.021	0.409	0.263	-0.351	-0.277	0.219	0.172	0.240	0.042	0.080	0.156
cti_nm	0.063	0.036	0.052	0.065	0.033	-0.058	0.001	0.164	0.071	-0.045	0.026
curvpro_nm	-0.040	0.036	0.006	-0.036	-0.022	0.019	0.025	0.032	0.098	0.037	0.027
imi_nm	0.000	0.013	0.016	-0.001	-0.001	-0.041	-0.005	0.047	0.052	0.004	0.001
sar_nm	-0.104	-0.061	-0.110	-0.112	-0.059	0.087	0.017	-0.210	0.021	0.025	-0.053
sds_nm	-0.073	-0.080	-0.104	-0.067	-0.025	0.047	0.063	-0.108	0.034	0.077	-0.003
sei_nm	0.208	0.235	0.060	-0.062	-0.072	0.032	0.039	-0.031	0.012	0.059	-0.013
sin_nm	0.212	-0.092	-0.048	0.001	-0.028	-0.249	0.007	0.032	0.013	0.037	0.007
srr_nm	0.088	0.030	0.048	0.047	0.030	-0.020	-0.021	-0.010	-0.069	-0.018	-0.019
srtmelev	-0.200	0.494	0.229	-0.796	-0.579	0.447	0.308	0.086	0.083	0.151	0.148
trasp_nm	0.084	0.322	0.088	-0.060	-0.052	0.190	0.077	-0.021	0.044	0.046	-0.008
ndmi2000	-0.042	0.165	0.021	-0.223	-0.093	0.186	0.107	-0.065	0.058	0.112	0.018

Table C6, Continued. Pearson's correlation coefficients for uncorrelated variables from Tables C1-C5, n = 44.

	sodep th	sodre xd	sodrm wd	sodrs exd	sodrw d	sopm cal	sopsa shci	sopsc ol	sopsc sk	sopsf	sopsl
bio15											
bio18											
bio3											
bio6											
bio9											
bioppnov											
hugrazall											
soawcft1											
soclayft3											
soclayhz											
soclaytot											
sodepth	1.000										
sodrex	0.087	1.000									
sodrmwd	0.025	-0.022	1.000								
sodrsex	0.104	-0.055	-0.052	1.000							
sodrw	0.155	-0.284	-0.268	-0.675	1.000						
sopmcal	-0.153	0.055	-0.043	-0.008	0.047	1.000					
sopsashci	-0.003	-0.016	-0.015	0.222	-0.157	-0.031	1.000				
sopscol	0.238	0.054	-0.043	0.155	-0.077	-0.089	-0.031	1.000			
sopscsk	-0.027	-0.043	0.163	-0.102	0.072	-0.044	-0.030	-0.085	1.000		
sopsf	0.130	-0.042	0.277	-0.100	0.036	-0.001	-0.029	-0.083	-0.079	1.000	
sopsl	0.240	-0.076	-0.052	-0.177	0.258	-0.091	-0.053	-0.150	-0.142	-0.140	1.000

Table C6, Continued. Pearson's correlation coefficients for uncorrelated variables from Tables C1-C5, n = 44.

	sodep th	sodre xd	sodrm wd	sodrs exd	sodrw d	sopm cal	sopsa shci	sopsc ol	sopsc sk	sopsc sopsf	sopsc sopsl
sopsfsi	0.080	-0.014	-0.013	-0.034	0.050	0.041	-0.010	-0.028	-0.026	-0.026	-0.047
sopsl	-0.353	-0.051	-0.049	0.037	0.059	0.183	-0.036	-0.102	-0.096	-0.094	-0.171
sopslsk	-0.029	-0.036	-0.091	-0.102	0.214	0.141	-0.067	-0.190	-0.180	-0.177	-0.319
sopss	0.217	0.333	-0.027	0.357	-0.354	-0.056	-0.020	-0.057	-0.053	-0.053	-0.095
soshzO	-0.073	-0.015	0.097	0.091	-0.047	0.156	0.006	-0.120	0.059	0.031	-0.039
sosrfclpct	0.315	-0.123	-0.045	-0.189	0.472	0.037	-0.117	-0.051	0.137	0.102	0.147
sostxbr	-0.480	-0.039	-0.037	-0.093	-0.482	-0.076	-0.004	-0.077	-0.073	-0.072	-0.129
sostxm	0.180	-0.069	0.066	-0.288	0.350	0.156	-0.086	-0.236	0.193	0.094	0.170
sostxmco	0.008	-0.035	-0.103	0.114	0.071	-0.213	-0.040	0.386	-0.171	-0.106	-0.040
soradec	-0.088	-0.001	0.000	0.025	-0.017	0.094	-0.003	-0.029	-0.022	0.018	0.065
soradmay	-0.034	-0.026	0.039	0.015	0.035	0.077	-0.062	-0.038	-0.088	0.082	0.223
cti_nm	0.138	-0.005	0.045	0.056	-0.005	-0.035	0.042	0.042	-0.062	0.087	0.100
curvpro_nm	0.111	0.003	-0.023	0.054	-0.008	-0.040	0.153	0.031	0.061	0.008	0.023
imi_nm	0.034	-0.020	-0.006	-0.009	-0.002	-0.028	0.025	0.006	0.003	0.012	0.058
sar_nm	-0.052	-0.038	-0.005	-0.042	-0.026	-0.029	0.004	-0.055	0.111	-0.081	-0.139
sds_nm	-0.044	-0.017	-0.012	-0.100	0.042	-0.038	0.000	-0.081	0.092	-0.051	-0.066
sei_nm	-0.058	0.020	-0.026	0.034	-0.039	0.075	0.021	0.000	-0.005	-0.011	0.002
sin_nm	-0.038	0.014	0.066	-0.029	-0.030	0.041	0.055	-0.037	-0.017	0.051	0.009
srr_nm	-0.069	-0.036	-0.002	0.011	0.005	0.013	-0.063	-0.036	-0.013	0.008	-0.039
srtmelev	-0.153	-0.104	0.067	-0.038	-0.034	0.050	-0.026	-0.187	0.028	0.042	0.161
trasp_nm	-0.022	-0.005	-0.089	0.078	-0.024	0.095	0.001	0.051	0.013	-0.039	0.007
ndmi2000	-0.069	-0.046	-0.018	-0.046	0.010	0.128	0.015	-0.100	0.121	-0.033	-0.043

Table C6, Continued. Pearson's correlation coefficients for uncorrelated variables from Tables C1-C5, n = 44.

	sopsfs i	sopsl	sopsls k	sopss	soshz O	sosrfc lpct	sostxb r	sostx m	sostx mco	sorad ec	sorad may
sopsfsi	1.000										
sopsl	-0.032	1.000									
sopslsk	-0.059	-0.216	1.000								
sopss	-0.018	-0.064	-0.120	1.000							
soshzO	-0.037	0.039	0.099	-0.076	1.000						
sosrfclpct	0.051	0.010	0.070	-0.140	-0.398	1.000					
sostxbr	-0.024	-0.087	-0.153	-0.049	-0.103	-0.465	1.000				
sostxm	0.101	-0.009	0.049	-0.155	-0.328	0.589	-0.211	1.000			
sostxmco	-0.067	0.063	0.026	-0.116	-0.287	-0.046	-0.185	-0.588	1.000		
soradec	-0.006	-0.020	-0.028	0.002	0.121	-0.044	-0.003	-0.035	-0.047	1.000	
soradmay	0.016	0.048	-0.168	0.043	0.032	0.118	-0.088	0.045	-0.042	0.662	1.000
cti_nm	0.009	0.009	-0.104	0.097	-0.081	0.092	-0.103	0.085	-0.035	-0.078	0.153
curvpro_nm	-0.004	-0.037	-0.030	-0.008	0.038	0.026	-0.056	0.020	-0.046	-0.186	-0.096
imi_nm	-0.012	-0.039	-0.034	-0.012	-0.011	0.021	0.008	0.047	-0.058	-0.062	-0.024
sar_nm	-0.039	-0.111	0.171	-0.074	0.143	-0.154	0.128	-0.047	-0.077	-0.079	-0.584
sds_nm	-0.033	-0.112	0.161	-0.078	0.137	-0.087	0.074	-0.048	-0.054	-0.019	-0.300
sei_nm	-0.004	-0.024	0.005	0.000	0.104	-0.101	0.024	-0.058	-0.028	0.868	0.417
sin_nm	0.001	-0.016	-0.024	-0.003	0.045	-0.034	0.033	-0.001	-0.045	-0.006	0.011
srr_nm	-0.001	0.037	0.028	0.026	-0.050	0.031	0.008	0.030	0.011	0.062	0.069
srtmelev	-0.045	-0.082	-0.086	-0.061	0.265	-0.046	0.130	0.013	-0.232	0.340	0.511
trasp_nm	0.009	-0.030	0.002	0.031	0.098	-0.076	-0.004	-0.061	-0.027	0.575	0.301
ndmi2000	-0.060	-0.105	0.119	-0.120	0.290	-0.115	0.076	-0.029	-0.170	-0.046	-0.034

Table C6, Continued. Pearson's correlation coefficients for uncorrelated variables from Tables C1-C5, n = 44.

	cti_n m	curvp ro_n m	imi_n m	sar_n m	sds_n m	sei_n m	sin_n m	srr_n m	srtmel ev	trasp_ nm	ndmi2 000
sopsfsi											
sopsl											
sopslsk											
sops											
soshzO											
sosrfclpct											
sostxbr											
sostxm											
sostxmco											
soradec											
soradmay											
cti_nm	1.000										
curvpro_nm	0.323	1.000									
imi_nm	0.492	0.154	1.000								
sar_nm	-0.383	-0.030	-0.052	1.000							
sds_nm	-0.308	-0.025	-0.017	0.508	1.000						
sei_nm	-0.033	-0.062	-0.042	0.010	0.027	1.000					
sin_nm	0.010	0.042	-0.023	-0.073	-0.042	-0.011	1.000				
srr_nm	0.020	-0.451	-0.028	-0.054	0.009	0.043	0.013	1.000			
srtmelev	-0.127	-0.052	-0.026	0.104	0.058	0.123	0.005	0.016	1.000		
trasp_nm	0.007	-0.020	-0.010	0.010	0.020	0.648	-0.397	0.034	0.110	1.000	
ndmi2000	-0.206	0.024	-0.054	0.180	0.190	-0.070	-0.039	-0.031	0.352	-0.007	1.000

Table C7. Variance inflation factors (VIFs) of uncorrelated variables from Table 6, without dummy-coded variables.

Variable	VIF
soradmay	5.142356
bio18	5.046763
bio15	4.971012
bioppnov	4.800428
bio6	4.738056
bio3	3.699583
soclaytot	3.440616
sar_nm	3.300309
soclayft3	2.817262
sei_nm	2.712856
trasp_nm	2.574332
sodepth	2.485953
bio9	2.215679
soawcft1	2.160101
cti_nm	2.068413
sosrfclpct	1.680005
curvpro_nm	1.581844
sin_nm	1.523809
imi_nm	1.486698
sds_nm	1.435715
srr_nm	1.345768
soclayhz	1.279007
ndmi2000	1.24436

Table C8. Variance inflation factors (VIFs) of uncorrelated variables from Table 6, with dummy-coded variables.

Variable	VIF	Variable	VIF
sodrwd	68.61024	sopsf	3.724356
sodrsexd	36.75412	sar_nm	3.353964
sostxbr	34.95635	sopscsk	3.219583
sostxm	14.19956	sosrfclpct	3.147548
sostxmco	12.82718	sopsl	2.976283
sodrmwd	10.28204	sopscol	2.781234
sodrexid	9.636681	sei_nm	2.775516
soshzO	8.010649	trasp_nm	2.688383
bio6	6.317222	bio9	2.67792
sopsl	6.206236	cti_nm	2.083072
bio18	5.808298	soclayhz	1.862899
soclaytot	5.769712	curvpro_nm	1.672925
bio15	5.678827	sopsashci	1.632676
bioppnov	5.383735	sin_nm	1.578826
sopslsk	5.349394	hugrazall	1.568201
soawcft1	5.32554	imi_nm	1.483004
soradmay	5.281852	sds_nm	1.477994
soclayft3	4.674032	ndmi2000	1.397465
sodepth	4.195942	srr_nm	1.389977
bio3	4.081133	sopmcal	1.38947
sopss	3.94883	sopfsi	1.27356

Appendix D: R scripts for spatial models

Random forest

```
#Random Forest
#Load spatial data packages
require(randomForest)
require(raster)
require(sp)
require(rgdal)
require(maptools)
require(RStoolbox)
require(plyr)
require(caret)
require(snow)

#set working directory
setwd("C:\\Thesis_R_data\\210mpix_2019-12-05")

#read in dataset from csv file
samples <- read.csv("Treemort_std_210mpix_A1.csv")
samples <- as.data.frame(samples)
class_data <- cbind(samples$presence, samples[4:45])

#apply column names to data frame
names(class_data)[1:43] <- c("class", "bio15", "bio18", "bio3", "bio6", "bio9", "bioppnov", "hugrazall", "soawcft1",
  "soclafyft3", "soclafyhz", "soclafytot", "sodepth", "sodrexnd", "sodrmwd", "sodrsexnd", "sodrwd", "sopmcal",
  "sopsashci", "sopscol", "sopscsk", "sopsf", "sopsfl", "sopsfsi", "sopsl", "sopslsk", "sopss", "soshz0",
  "sosrfclpct", "sostxbr", "sostxm", "sostxmco", "soradmay", "cti_nm", "curvpro_nm", "imi_nm", "sar_nm",
  "sds_nm", "sei_nm", "sin_nm", "srr_nm", "trasp_nm", "ndmi2000")

#convert the response variable to a factor data type
class_data$class <- as.factor(class_data$class)

#take a look at the data structure
str(class_data)

#=====
#Preliminary tuning
#tune the model: determine the optimal number of variables to sample at each split (mtry)
t <- tuneRF(class_data[,-1], class_data[,1],
  stepFactor = 0.5,
  plot = TRUE,
  ntreeTry = 1000,
  trace = TRUE,
  improve = 0.05)

#show plot of the model: gives an indication of how many trees are actually needed or useful
plot(rf.mod)

#=====
#fit the RF model

#all variables model
```

```

set.seed(42)
rf.mod <- randomForest(class~., data = class_data, ntree=1000, importance=TRUE, do.trace=100, mtry=6,
  keep.forest=TRUE)

#show model results
rf.mod

#repeat with the other variables groupings
set.seed(42)
rf.genericmodel <- randomForest(class~ var1+var2+var3+etc, data=class_data, ntree=1000, importance=TRUE,
  do.trace=100, keep.forest=TRUE)

# show RF results
rf.genericmodel

# show variable importance in table
importance (rf.genericmodel)

# show variable importance in plot
varImpPlot (rf.genericmodel)

```

Logistic regression

```

#Logistic Regression

#load data packages
library(party)
library(rpart)
library(rpart.plot)
library(rattle)
library(caret)

setwd("C:\\Thesis_R_data\\210mpix_2019-12-05")

#read in data
samples <- read.csv("Treemort_std_210mpix_A1.csv")
samples <- as.data.frame(samples)
class_data <- cbind(samples$presence, samples[4:45])

#assign column names
names(class_data)[1:43] <- c("class", "bio15", "bio18", "bio3", "bio6", "bio9", "bioppnov",
  "hugrazall", "soawcft1", "soclafyft3", "soclafyhz", "soclafytot",
  "sodepth", "sodrex", "sodrmwd", "sodrsex", "sodrw", "sopmcal",
  "sopsashci", "sopscol", "sopscsk", "sopsf", "sopsf", "sopfsi",
  "sopsl", "sopslsk", "sopss", "soshzO", "sosrfclpct", "sostxbr",
  "sostxm", "sostxmco", "soradmay", "cti_nm", "curvpro_nm", "imi_nm",
  "sar_nm", "sds_nm", "sei_nm", "sin_nm", "srr_nm", "trasp_nm", "ndmi2000")

#convert the class data to factor
class_data$class <- as.factor(class_data$class)

#take a look at the data structure

```

```

str(class_data)

#fit a logistic regression model using k-fold cross validation
#define the k-fold validation controls
fitControl <- trainControl(method='cv', number=5, savePredictions = T)

#all variables model
#fit the model
set.seed(42)
LR1cv <- train(class ~., data=class_data, method='glm', family = binomial(link = "logit"), trControl=fitControl)

# repeat with the other variables groupings
#fit the model
set.seed(42)
LR1cv <- train(class ~ var1+var2+var3+etc, data=class_data, method='glm', family = binomial(link = "logit"),
               trControl=fitControl)

#print cv results
LR1cv
summary(LR1cv)

#final selected model
finLRmod1 <- LR1cv$finalModel

#generate confusion matrix
confusionMatrix(table((LR1cv$pred)$pred,(LR1cv$pred)$obs),positive='1')

```

Conditional inference trees

```
#Conditional Inference Trees

#load data packages
library(party)
library(rpart)
library(rpart.plot)
library(rattle)
library(caret)

setwd("C:\\Thesis_R_data\\210mpix_2019-12-05")

#read in data
samples <- read.csv("Treemort_std_210mpix_A1.csv")
samples <- as.data.frame(samples)
class_data <- cbind(samples$presence, samples[4:45])

#assign column names
names(class_data)[1:43] <- c("class", "bio15", "bio18", "bio3", "bio6", "bio9", "bioppnov",
  "hugrazall", "soawcft1", "soclayft3", "soclayhz", "soclaytot",
  "sodepth", "sodrex", "sodrmwd", "sodrsex", "sodrw", "sopmcal",
  "sopsashci", "sopscol", "sopscsk", "sopsf", "sopsfl", "sopsfsi",
  "sopsl", "sopslsk", "sopss", "soshzO", "sosrfclpct", "sostxbr",
  "sostxm", "sostxmco", "soradmay", "cti_nm", "curvpro_nm", "imi_nm",
  "sar_nm", "sds_nm", "sei_nm", "sin_nm", "srr_nm", "trasp_nm", "ndmi2000")

#convert the class data to factor
class_data$class <- as.factor(class_data$class)

#take a look at the data structure
str(class_data)

#fit a ctree model using k-fold cross validation
#define the k-fold validation controls
fitControl <- trainControl(method='cv', number=5, savePredictions = T)

#all variables model
#select the optimal mincriterion parameter and fit the model
set.seed(42)
ctree1cv <- train(class~ ., data=class_data, method='ctree', tuneGrid = expand.grid(mincriterion = c(0.75, 0.8, 0.85,
  0.9, 0.95)), trControl=fitControl, minbucket=10)

# repeat with the other variables groupings
#select the optimal mincriterion parameter and fit the model
set.seed(42)
ctree1cv <- train(class~ var1+var2+var3+etc, data=class_data, method='ctree', tuneGrid =
  expand.grid(mincriterion= c(0.75, 0.8, 0.85, 0.9, 0.95)), trControl=fitControl, minbucket=10)

#print cv results
ctree1cv
```

```

#generate an aggregated confusion matrix using the cv results
cfmtab <- confusionMatrix.train(ctree1cv, norm = "none")
cfmtab

#calculate the sensitivity
#note: the call says specificity, however, by default caret assumes the first value encountered
#is the positive. In our case, the first value encountered (0) is the negative.
specificity(cfmtab$table)

#calculate the sensitivity
#note: the call says sensitivity, however, by default caret assumes the second value #encountered is the negative.
In our case, the second value encountered (1) is the positive.
sensitivity(cfmtab$table)

#plot the final selected model
#according to the documentation, this model is fitted on the whole data set using the
#optimal parameters as determined by the train function
finmod1 <- ctree1cv$finalModel
plot(finmod1)

#text output version of the final tree
finmod1

#=====
#Code used to generate univariate stumps

#fit a ctree model using k-fold cross validation
#define the k-fold validation controls
fitControl <- trainControl(method='cv', number=5, savePredictions = T)

#select and fit the model
set.seed(42)
ctree1cv <- train(class~ var1, method='ctree', tuneGrid = expand.grid(mincriterion = c(0.75, 0.8, 0.85, 0.9, 0.95)),
  trControl=fitControl, controls = ctree_control(stump = TRUE, minbucket = 25))

#print cv results
ctree1cv

#plot the final model
finmod1 <- ctree1cv$finalModel
plot(finmod1)
plot(finmod1, type='simple')

#text output version of the final tree
finmod1

```

Mortality prediction maps

```
#Predict Raster
#Load spatial data packages
require(randomForest)
require(raster)
require(sp)
require(rgdal)
require(maptools)
require(RStoolbox)
require(plyr)
require(caret)
require(snow)

setwd("C:\\Thesis_R_data\\210mpix_2019-12-05")

#####image and shapefile processing#####
img <- brick("A1_finvars_lyrstk.tif")
shp <- shapefile("A1_final_sample_points_all_clean.shp")

names(img)[1:42] <- c("trasp_nm", "srr_nm", "sostxmco", "sostxm", "sostxbr", "sosrfclpct", "soshzO", "soradmay",
  "sopss", "sopslsk", "sopsl", "sopsfsi", "sopsfl", "sopsf", "sopscsk", "sopscol", "sopsashci", "sopmcal",
  "sodrwd", "sodrsexd", "sodrmwd", "sodrex", "sodepth", "soclaytot", "soclayhz", "soclayft3", "soawcft1",
  "sin_nm", "sei_nm", "sds_nm", "sar_nm", "ndmi2000", "imi_nm", "hugrazall", "curvpro_nm", "cti_nm",
  "bioppnov", "bio9", "bio6", "bio3", "bio18", "bio15")

#check naming results
names(img)
names(shp)
shp$presence

#extract values from shp
samples <- extract(img, shp)
samples <- as.data.frame(samples)
class_data <- cbind(shp$presence, samples)

#eliminate values with no-data, skip this if already taken care of in previous data preparation
class_data[2:43][class_data[2:43]==0] <- NA
class_data <- na.omit(class_data)

names(class_data)[1:43] <- c("class", "trasp_nm", "srr_nm", "sostxmco", "sostxm", "sostxbr", "sosrfclpct",
  "soshzO", "soradmay", "sopss", "sopslsk", "sopsl", "sopsfsi", "sopsfl", "sopsf", "sopscsk", "sopscol",
  "sopsashci", "sopmcal", "sodrwd", "sodrsexd", "sodrmwd", "sodrex", "sodepth", "soclaytot", "soclayhz",
  "soclayft3", "soawcft1", "sin_nm", "sei_nm", "sds_nm", "sar_nm", "ndmi2000", "imi_nm", "hugrazall",
  "curvpro_nm", "cti_nm", "bioppnov", "bio9", "bio6", "bio3", "bio18", "bio15")

#convert the class data to factor
class_data$class <- as.factor(class_data$class)

##### run and save the rf model#####
set.seed(42)
```

```

rf.BCfin <- randomForest(class~ bio18+bio3+bio6+ndmi2000, data=class_data, ntree=1000, importance=TRUE,
do.trace=100, keep.forest=TRUE)
rf.BCfin

#Save the model
save(rf.BCfin, file= "rf_BCfin.rda")
load('rf_BCfin.rda')

#=====
#Generate the predictive maps

#predict and write a classification raster to file

#Order the classes
classNames=data.frame("name"=unique(class_data$class),"code"=as.numeric(unique(class_data$class)))
attach(classNames) sort.classnames <- classNames[order(+code),] print(sort.classnames)

#Predict and write the raster to a file
beginCluster(7)

system.time(preds_rf <- clusterR(img, raster::predict, args = list(model = rf.BCfin), progress="text"))

writeRaster(preds_rf, filename="BCfin_preds",format="GTiff", datatype="INT1U", overwrite=TRUE) endCluster()

#=====
#predict and write a probabilities raster to file

#Order the classes
classNames=data.frame("name"=unique(class_data$class),"code"=as.numeric(unique(class_data$class)))
attach(classNames)
sort.classnames <- classNames[order(+code),]
print(sort.classnames)

#create an object with predictions from the layerstack
preds <- predict(img, rf.BCfin, type='prob', index=1:2)
preds

#multiply probabilities by 100 so that they're integers
#otherwise ArcMap will round them all to zeros or ones and it won't display right
preds2 <- preds*100
preds2

#write the raster using the object preds2
#band 1 will be probability of survival
#band 2 will be probability of mortality
writeRaster(preds2, filename="BCfin_probs",format="GTiff",
datatype="INT1U", overwrite=TRUE)

```

Appendix E: Model performance

Table E1. Model performance data for Area 1.

Model name	Model type	Overall accuracy	Balanced accuracy	Sensitivity	Specificity	P-Value [Acc > NIR]	AIC
BC2	RF	0.847	0.846	0.904	0.789	--	--
SO-3	RF	0.831	0.831	0.816	0.846	--	--
TV4	RF	0.831	0.830	0.912	0.748	--	--
BC1	RF	0.823	0.822	0.896	0.748	--	--
SO	RF	0.819	0.818	0.848	0.789	--	--
TV1	RF	0.819	0.818	0.856	0.781	--	--
TV3	RF	0.819	0.818	0.872	0.764	--	--
AV	RF	0.815	0.814	0.856	0.772	--	--
TV2	RF	0.815	0.814	0.856	0.772	--	--
BCfin	RF	0.811	0.810	0.872	0.748	--	--
BC2-2	RF	0.798	0.798	0.856	0.740	--	--
TS	RF	0.790	0.790	0.792	0.789	--	--
TS-2	RF	0.766	0.766	0.784	0.748	--	--
TP	RF	0.633	0.633	0.640	0.626	--	--
TP-3	RF	0.617	0.617	0.626	0.608	--	--
HU	RF	0.540	0.537	0.920	0.155	--	--
TV4	LR	0.819	0.818	0.864	0.772	<2e-16	223
AV-2	LR	0.811	0.810	0.848	0.772	<2e-16	219
TV4-1	LR	0.811	0.810	0.848	0.772	<2e-16	222
TV3	LR	0.798	0.798	0.832	0.764	<2e-16	235
AV-1	LR	0.798	0.798	0.840	0.756	<2e-16	220
TV2-1	LR	0.790	0.790	0.888	0.691	<2.2e-16	255
TV1-1	LR	0.782	0.782	0.816	0.748	<2e-16	237
TV2	LR	0.782	0.782	0.864	0.699	<2.2e-16	256
BC1-1	LR	0.782	0.782	0.872	0.691	<2.2e-16	247
AV	LR	0.778	0.778	0.792	0.764	<2e-16	225
TV1	LR	0.766	0.766	0.800	0.732	<2e-16	247
BC2-1	LR	0.766	0.766	0.808	0.724	<2e-16	240
BC1	LR	0.766	0.765	0.856	0.675	<2.2e-16	249
TS	LR	0.762	0.762	0.800	0.724	<2e-16	269
BC2	LR	0.758	0.758	0.808	0.707	<2e-16	238
SO	LR	0.710	0.709	0.776	0.642	3.67E-11	277
TS-1	LR	0.669	0.669	0.744	0.594	1.03E-07	302
TP-2	LR	0.637	0.637	0.672	0.602	1.64E-05	327
TP-1	LR	0.637	0.636	0.736	0.537	1.64E-05	326
SO-1	LR	0.629	0.629	0.640	0.618	4.92E-05	321
TP	LR	0.625	0.625	0.608	0.642	8.31E-05	327

Model name	Model type	Overall accuracy	Balanced accuracy	Sensitivity	Specificity	P-Value [Acc > NIR]	AIC
SO-2	LR	0.625	0.625	0.624	0.626	8.31E-05	320
HU	LR	0.540	0.537	0.920	0.155	0.1402	344
TV1	CTREE	0.790	0.789	0.944	0.634	--	--
AV-1	CTREE	0.778	0.777	0.968	0.585	--	--
BC1	CTREE	0.778	0.777	0.968	0.585	--	--
BC2	CTREE	0.778	0.777	0.968	0.585	--	--
TV2	CTREE	0.778	0.777	0.968	0.585	--	--
AV	CTREE	0.774	0.773	0.920	0.626	--	--
TV3	CTREE	0.762	0.762	0.792	0.732	--	--
TV4	CTREE	0.758	0.757	0.832	0.683	--	--
SO	CTREE	0.746	0.746	0.728	0.764	--	--
TS	CTREE	0.702	0.701	0.744	0.659	--	--
TP	CTREE	0.609	0.609	0.600	0.618	--	--
HU	CTREE	0.504	0.500	0.944	0.057	--	--

Table E2. Model performance data for Area 2.

Model name	Model type	Overall accuracy	Balanced accuracy	Sensitivity	Specificity	P-Value [Acc > NIR]	AIC
BC2	RF	0.822	0.822	0.784	0.859	--	--
TV4	RF	0.812	0.812	0.784	0.839	--	--
BCfin	RF	0.812	0.812	0.776	0.847	--	--
TV2	RF	0.810	0.810	0.764	0.855	--	--
TV1	RF	0.808	0.808	0.788	0.827	--	--
TV3	RF	0.802	0.802	0.768	0.835	--	--
AV	RF	0.792	0.792	0.756	0.827	--	--
BC1	RF	0.774	0.774	0.748	0.799	--	--
SO-5	RF	0.728	0.728	0.620	0.835	--	--
SO	RF	0.717	0.718	0.624	0.811	--	--
TS-4	RF	0.717	0.718	0.676	0.759	--	--
TS	RF	0.717	0.717	0.700	0.735	--	--
TP	RF	0.581	0.581	0.564	0.598	--	--
TP-5	RF	0.553	0.553	0.560	0.546	--	--
HU	RF	0.553	0.553	0.720	0.386	--	--
TP-6	RF	0.541	0.541	0.548	0.534	--	--
AV-4	LR	0.784	0.784	0.752	0.815	<2e-16	476
BC1-2	LR	0.778	0.778	0.728	0.827	<2e-16	501
TV4-2	LR	0.778	0.778	0.792	0.763	<2e-16	483
BC1	LR	0.776	0.776	0.732	0.819	<2e-16	504
AV-3	LR	0.770	0.770	0.732	0.807	<2e-16	484
TV4	LR	0.770	0.770	0.788	0.751	<2e-16	487
TV1-2	LR	0.766	0.766	0.752	0.779	<2e-16	503
TV2	LR	0.766	0.766	0.756	0.775	<2e-16	502
BC2-3	LR	0.760	0.760	0.736	0.783	<2e-16	501
TV3	LR	0.754	0.754	0.704	0.803	<2e-16	507
BC2	LR	0.754	0.754	0.724	0.783	<2e-16	503
TV1	LR	0.750	0.750	0.704	0.795	<2e-16	507
AV	LR	0.742	0.742	0.720	0.763	<2e-16	497
TS	LR	0.687	0.688	0.608	0.767	<2.2e-16	568
TS-3	LR	0.673	0.674	0.592	0.755	5.22E-15	586
SO	LR	0.663	0.664	0.544	0.783	1.76E-13	583
SO-4	LR	0.615	0.616	0.340	0.892	1.88E-07	615
TP-4	LR	0.605	0.605	0.616	0.594	1.85E-06	655
TP	LR	0.575	0.575	0.584	0.566	5.31E-04	663
HU	LR	0.553	0.553	0.720	0.386	0.01116	689
AV-3	CTREE	0.780	0.780	0.724	0.835	--	--

Model name	Model type	Overall accuracy	Balanced accuracy	Sensitivity	Specificity	P-Value [Acc > NIR]	AIC
BC2	CTREE	0.774	0.774	0.744	0.803	--	--
TV1	CTREE	0.772	0.772	0.752	0.791	--	--
TV3	CTREE	0.772	0.772	0.760	0.783	--	--
BC1	CTREE	0.768	0.768	0.716	0.819	--	--
TV4	CTREE	0.762	0.762	0.708	0.815	--	--
TV2	CTREE	0.762	0.762	0.712	0.811	--	--
AV	CTREE	0.750	0.750	0.664	0.835	--	--
SO	CTREE	0.685	0.685	0.628	0.743	--	--
TS	CTREE	0.665	0.666	0.560	0.771	--	--
TP	CTREE	0.615	0.615	0.528	0.703	--	--
HU	CTREE	0.553	0.553	0.720	0.386	--	--

Table E3. Model performance data for Area 3.

Model name	Model type	Overall accuracy	Balanced accuracy	Sensitivity	Specificity	P-Value [Acc > NIR]	AIC
AV	RF	0.758	0.758	0.768	0.748	--	--
BC2	RF	0.756	0.756	0.760	0.752	--	--
TV3	RF	0.750	0.750	0.768	0.732	--	--
TV1	RF	0.748	0.748	0.768	0.728	--	--
TV4	RF	0.744	0.744	0.736	0.752	--	--
TV2	RF	0.728	0.728	0.740	0.716	--	--
BCfin	RF	0.722	0.722	0.732	0.712	--	--
BC1	RF	0.720	0.720	0.728	0.712	--	--
BC2-5	RF	0.696	0.696	0.724	0.668	--	--
SO	RF	0.670	0.670	0.688	0.652	--	--
TS	RF	0.666	0.666	0.680	0.652	--	--
SO-8	RF	0.658	0.658	0.660	0.656	--	--
TS-7	RF	0.628	0.628	0.664	0.592	--	--
TP	RF	0.602	0.602	0.616	0.588	--	--
HU	RF	0.544	0.544	0.520	0.568	--	--
TP-8	RF	0.540	0.540	0.560	0.520	--	--
TV3	LR	0.680	0.680	0.732	0.628	2.90E-16	630
AV	LR	0.678	0.678	0.692	0.664	6.17E-16	605
TV4-3	LR	0.672	0.672	0.712	0.632	5.64E-15	608
BC2-4	LR	0.670	0.670	0.728	0.612	1.16E-14	628
TV1	LR	0.666	0.666	0.672	0.660	4.76E-14	639
TV4	LR	0.664	0.664	0.700	0.628	9.51E-14	608
AV-6	LR	0.662	0.662	0.684	0.640	1.89E-13	610
BC2	LR	0.660	0.660	0.720	0.600	3.70E-13	632
AV-5	LR	0.658	0.658	0.680	0.636	7.21E-13	609
TV1-3	LR	0.654	0.654	0.672	0.636	2.67E-12	634
TV2-2	LR	0.652	0.652	0.712	0.592	5.06E-12	650
BC1	LR	0.648	0.648	0.724	0.572	1.77E-11	642
BC1-3	LR	0.646	0.646	0.716	0.576	3.28E-11	640
TV2	LR	0.646	0.646	0.700	0.592	3.28E-11	652
TS-6	LR	0.632	0.632	0.624	0.640	1.91E-09	659
TS-5	LR	0.620	0.620	0.612	0.628	4.48E-08	660
TS	LR	0.612	0.612	0.600	0.624	3.11E-07	660
SO-6	LR	0.588	0.588	0.636	0.540	4.81E-05	672
SO-7	LR	0.580	0.580	0.568	0.592	2.00E-04	672
SO	LR	0.578	0.578	0.572	0.584	2.81E-04	678
TP-7	LR	0.572	0.572	0.608	0.536	7.36E-04	681

Model name	Model type	Overall accuracy	Balanced accuracy	Sensitivity	Specificity	P-Value [Acc > NIR]	AIC
TP	LR	0.558	0.558	0.584	0.532	5.36E-03	679
HU	LR	0.544	0.544	0.520	0.568	2.72E-02	693
AV	CTREE	0.682	0.682	0.696	0.668	--	--
TV4	CTREE	0.678	0.678	0.692	0.664	--	--
TV1	CTREE	0.676	0.676	0.644	0.708	--	--
TV3	CTREE	0.674	0.674	0.704	0.644	--	--
BC2	CTREE	0.672	0.672	0.700	0.644	--	--
TV2	CTREE	0.672	0.672	0.696	0.648	--	--
BC1	CTREE	0.666	0.666	0.668	0.664	--	--
AV-5	CTREE	0.650	0.650	0.688	0.612	--	--
TP	CTREE	0.554	0.554	0.552	0.556	--	--
TS	CTREE	0.546	0.546	0.560	0.532	--	--
SO	CTREE	0.528	0.528	0.488	0.568	--	--
HU	CTREE	0.500	0.500	0.380	0.620	--	--

Table E4. Model performance data for Area 4.

Model name	Model type	Overall accuracy	Balanced accuracy	Sensitivity	Specificity	P-Value [Acc > NIR]	AIC
TV1	RF	0.796	0.796	0.794	0.797	--	--
BC2	RF	0.790	0.790	0.774	0.805	--	--
AV	RF	0.777	0.777	0.790	0.764	--	--
BCfin	RF	0.765	0.765	0.758	0.772	--	--
TV3	RF	0.765	0.765	0.758	0.772	--	--
TV4	RF	0.745	0.745	0.718	0.772	--	--
TV2	RF	0.741	0.741	0.726	0.756	--	--
BC1	RF	0.739	0.739	0.754	0.724	--	--
BC2-8	RF	0.735	0.735	0.718	0.752	--	--
TS-9	RF	0.705	0.704	0.726	0.683	--	--
TS	RF	0.674	0.674	0.685	0.663	--	--
SO	RF	0.654	0.654	0.669	0.638	--	--
SO-11	RF	0.650	0.650	0.633	0.667	--	--
TP-10	RF	0.611	0.611	0.621	0.602	--	--
TP	RF	0.607	0.607	0.601	0.614	--	--
HU	RF	0.541	0.539	0.823	0.256	--	--
AV-7	LR	0.713	0.713	0.726	0.699	<2e-16	571
AV-8	LR	0.709	0.708	0.718	0.699	<2e-16	567
BC2	LR	0.705	0.704	0.710	0.699	<2e-16	578
BC2-6	LR	0.700	0.700	0.710	0.691	<2e-16	576
BC2-7	LR	0.696	0.696	0.714	0.679	<2e-16	576
TV4	LR	0.690	0.690	0.718	0.663	<2e-16	604
BC1	LR	0.684	0.684	0.686	0.683	<2e-16	615
AV	LR	0.684	0.684	0.722	0.646	<2e-16	587
TV3	LR	0.672	0.672	0.669	0.675	1.59E-14	589
TV2-3	LR	0.656	0.656	0.657	0.655	3.68E-12	617
TV1-4	LR	0.648	0.648	0.673	0.622	4.53E-11	601
TV2	LR	0.644	0.644	0.621	0.667	1.51E-10	619
TV1	LR	0.642	0.642	0.665	0.618	2.72E-10	604
TS	LR	0.640	0.640	0.682	0.598	4.86E-10	643
TS-8	LR	0.622	0.621	0.653	0.589	6.12E-08	651
SO	LR	0.603	0.603	0.589	0.618	3.92E-06	653
SO-10	LR	0.585	0.585	0.593	0.577	1.30E-04	668
TP	LR	0.579	0.579	0.682	0.476	3.61E-04	664
TP-9	LR	0.567	0.566	0.746	0.386	2.27E-03	667
SO-9	LR	0.545	0.544	0.581	0.508	3.25E-02	668
HU	LR	0.541	0.539	0.823	0.256	0.04792	684

Model name	Model type	Overall accuracy	Balanced accuracy	Sensitivity	Specificity	P-Value [Acc > NIR]	AIC
TV2	CTREE	0.690	0.691	0.573	0.809	--	--
BC1	CTREE	0.682	0.682	0.649	0.715	--	--
BC2	CTREE	0.680	0.681	0.597	0.764	--	--
TV3	CTREE	0.672	0.673	0.512	0.833	--	--
AV	CTREE	0.672	0.672	0.577	0.768	--	--
AV-7	CTREE	0.662	0.662	0.577	0.748	--	--
TV4	CTREE	0.660	0.660	0.560	0.760	--	--
TV1	CTREE	0.654	0.654	0.556	0.752	--	--
TP	CTREE	0.593	0.593	0.722	0.463	--	--
SO	CTREE	0.561	0.560	0.690	0.431	--	--
TS	CTREE	0.551	0.550	0.718	0.382	--	--
HU	CTREE	0.541	0.539	0.823	0.256	--	--

Appendix F: Univariate conditional inference stumps

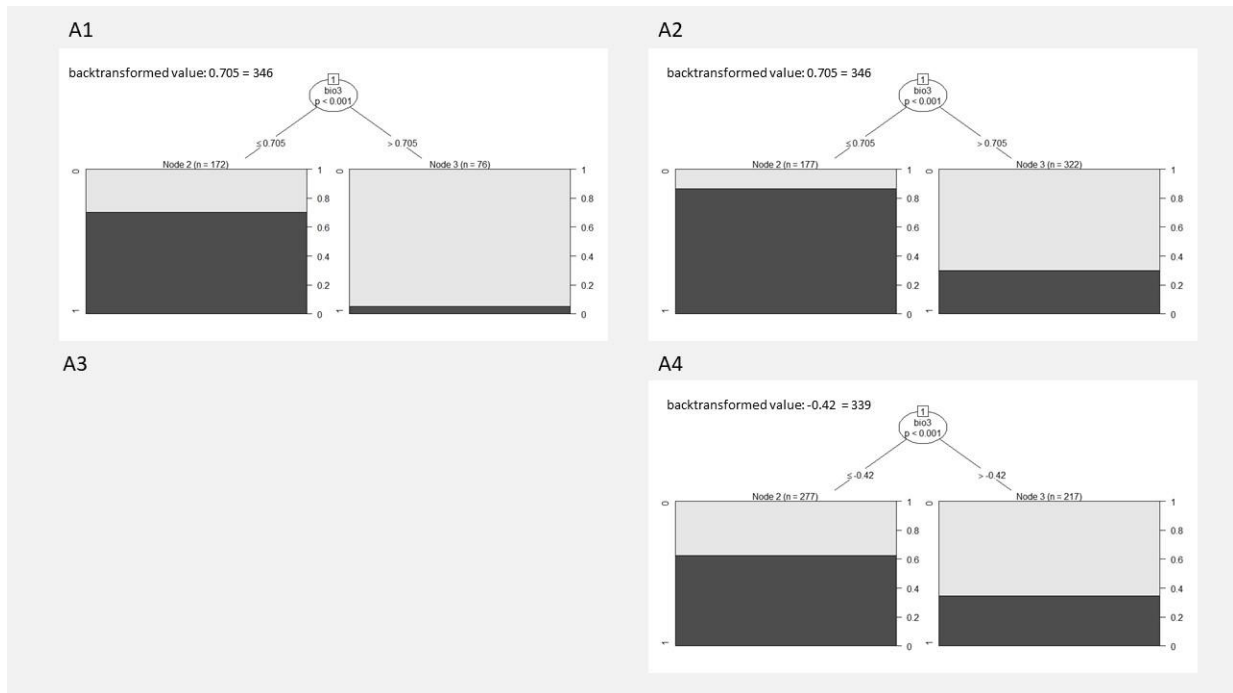


Figure F1. Conditional inference tree univariate stumps for the variable *bio3*, isothermality. Dark gray represents mortality presence and light gray indicates mortality absence. The relationship in Area 3 was too weak for the model to run, hence no image.

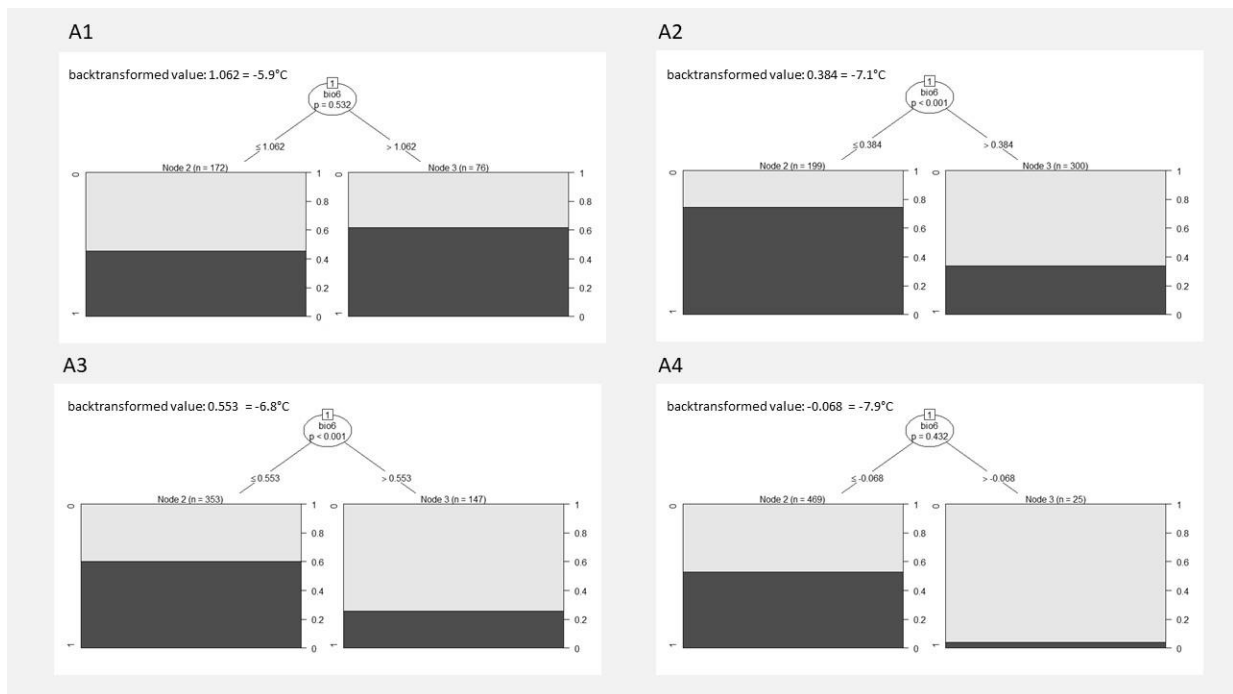


Figure F2. Conditional inference tree univariate stumps for the variable *bio6*, minimum temperature of the coldest month. Dark gray represents mortality presence and light gray indicates mortality absence.

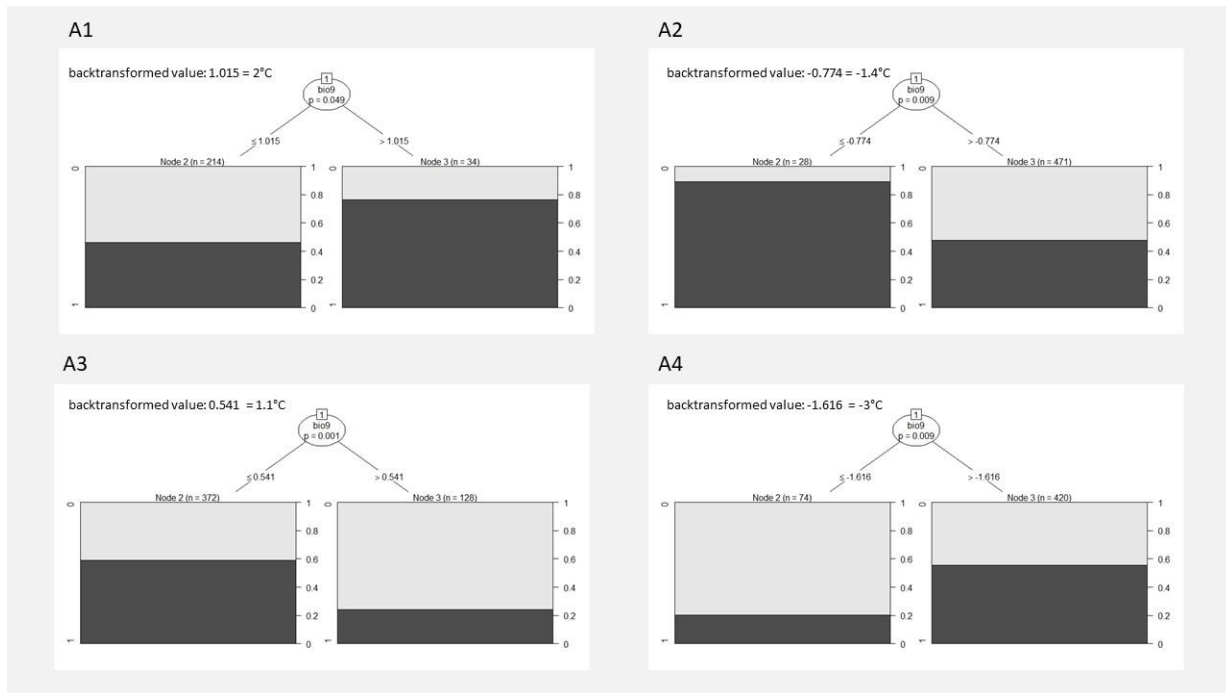


Figure F3. Conditional inference tree univariate stumps for the variable bio9, mean temperature of the driest quarter. Dark gray represents mortality presence and light gray indicates mortality absence.

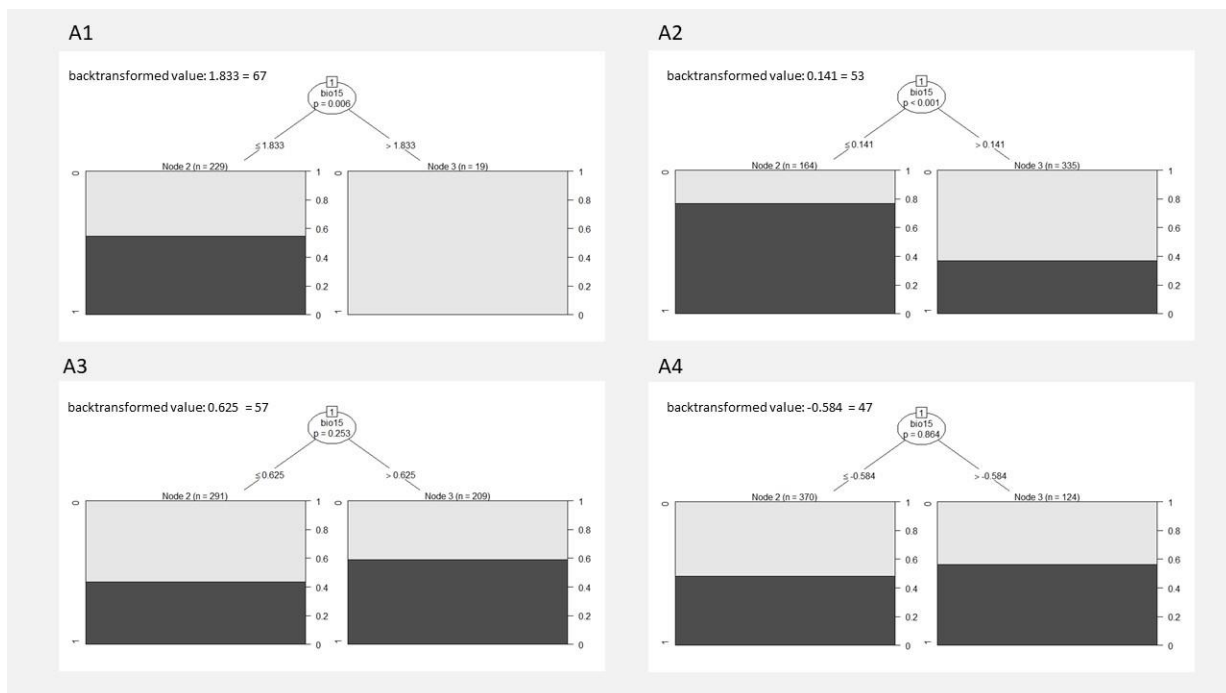


Figure F4. Conditional inference tree univariate stumps for the variable bio15, precipitation seasonality (coefficient of variation). Dark gray represents mortality presence and light gray indicates mortality absence.

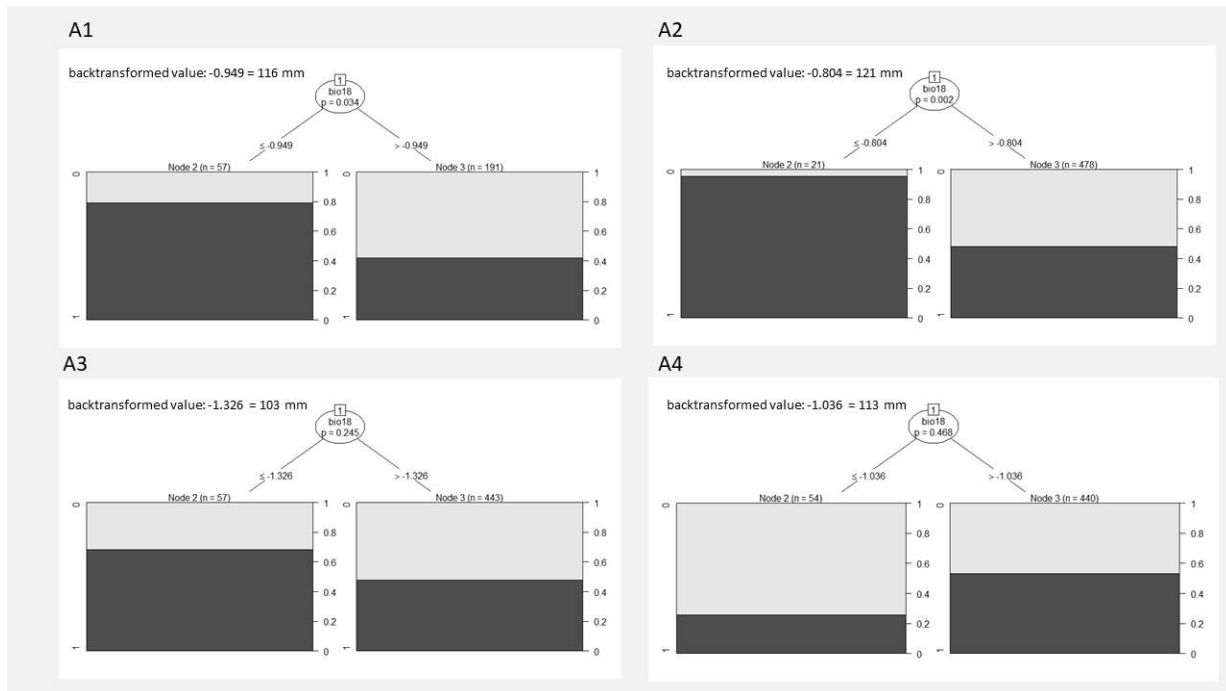


Figure F5. Conditional inference tree univariate stumps for the variable bio18, precipitation of warmest quarter. Dark gray represents mortality presence and light gray indicates mortality absence.

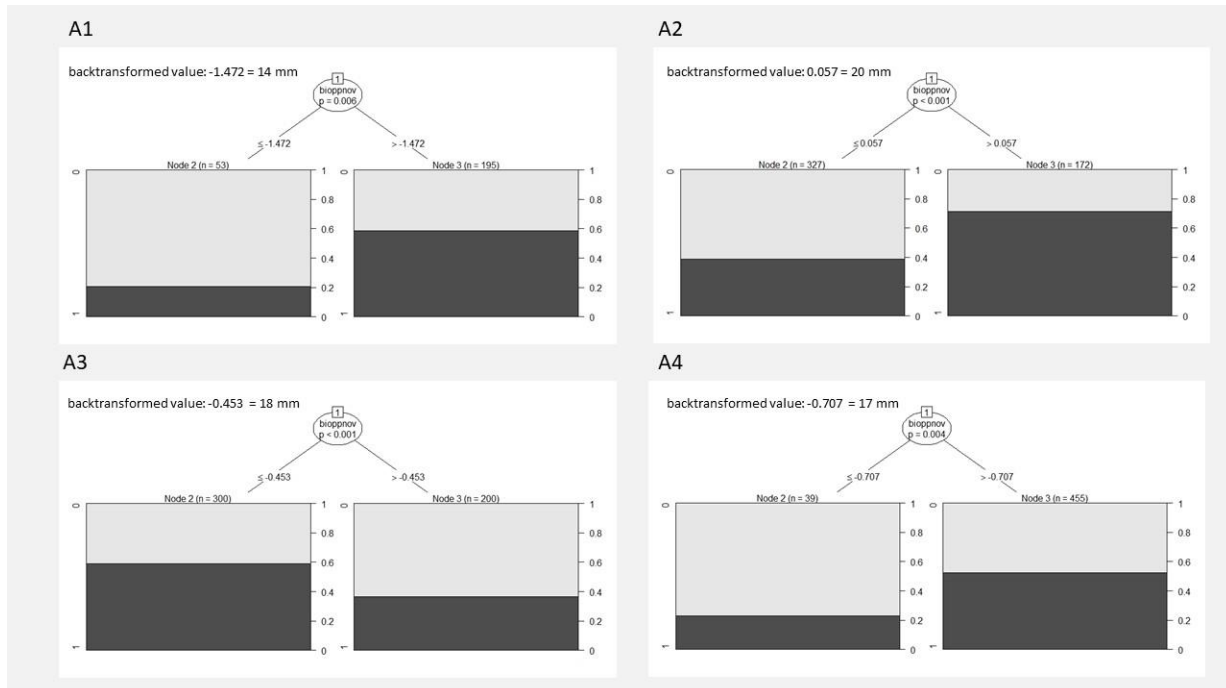


Figure F6. Conditional inference tree univariate stumps for the variable biopppov, November precipitation. Dark gray represents mortality presence and light gray indicates mortality absence.

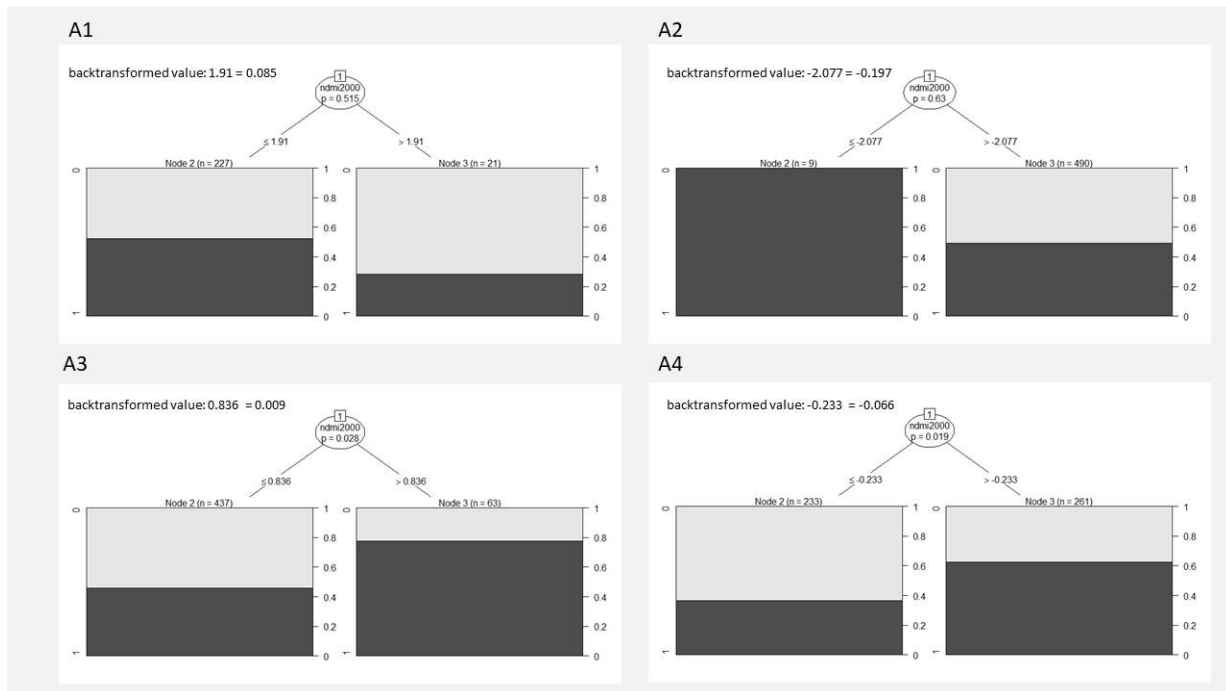


Figure F7. Conditional inference tree univariate stumps for the variable ndmi2000, pre-drought NDMI. Dark gray represents mortality presence and light gray indicates mortality absence.

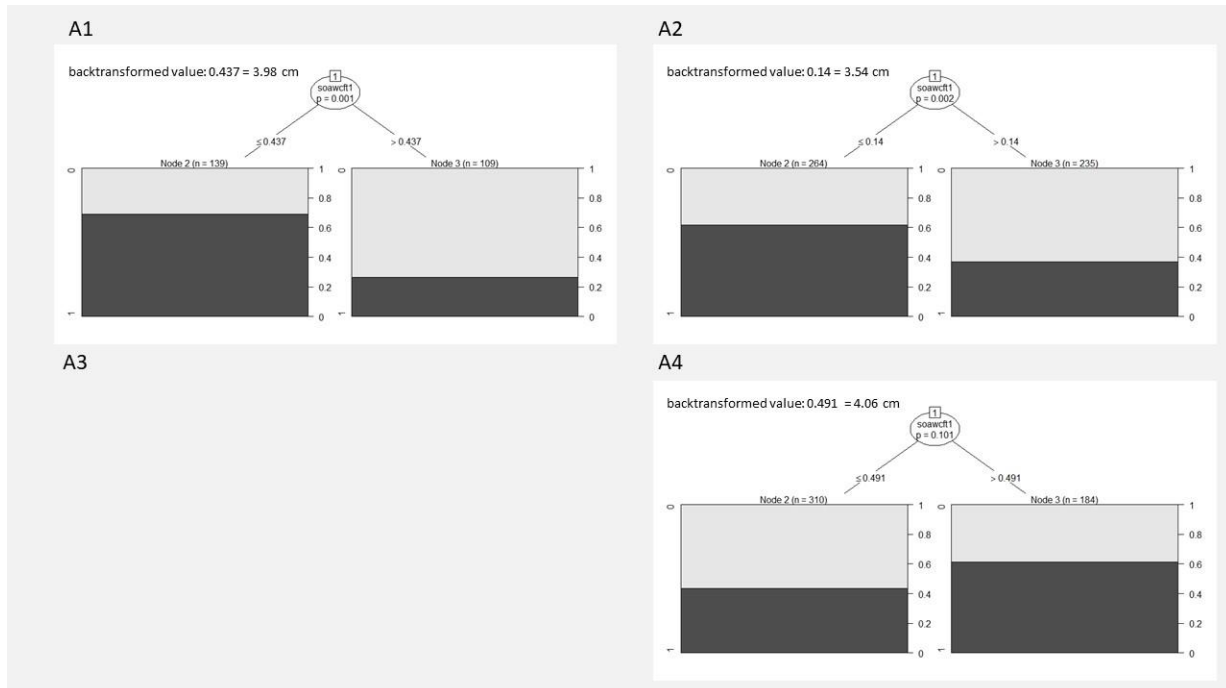


Figure F8. Conditional inference tree univariate stumps for the variable soawcft1, AWC of the top 31 cm (1 ft) of soil. Dark gray represents mortality presence and light gray indicates mortality absence. The relationship in Area 3 was too weak for the model to run, hence no image.

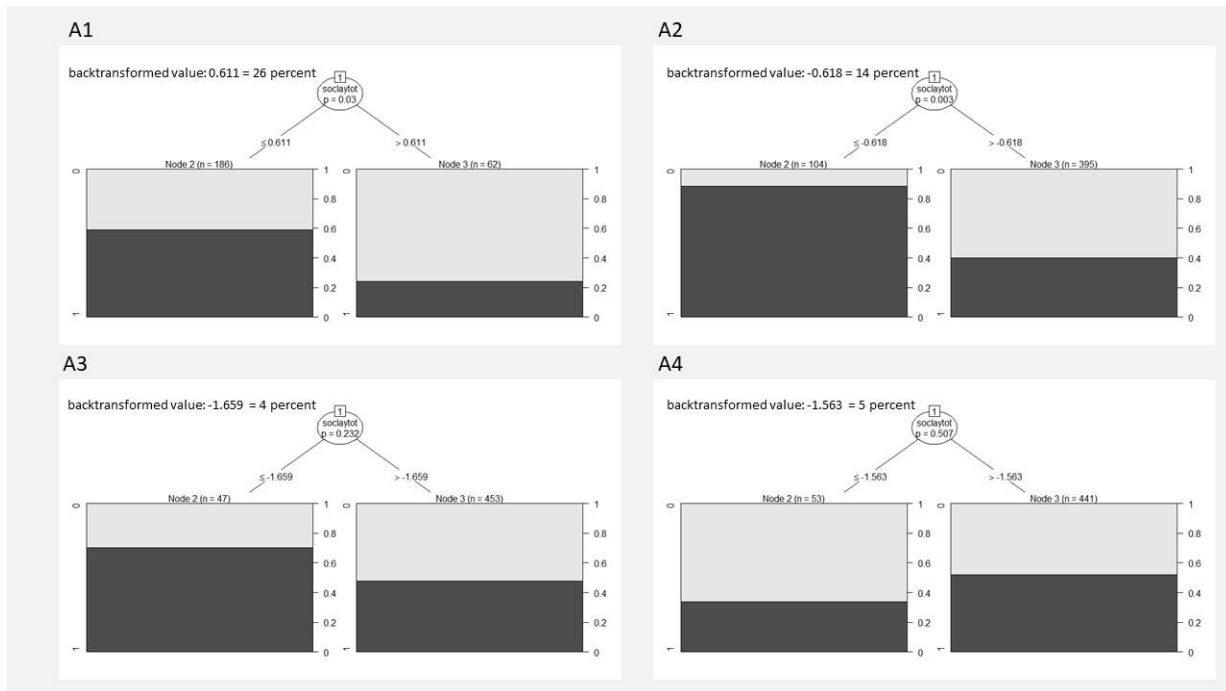


Figure F9. Conditional inference tree univariate stumps for the variable soclaytot, clay percent of top 122 cm (4 ft) of soil profile (weighted average). Dark gray represents mortality presence and light gray indicates mortality absence.

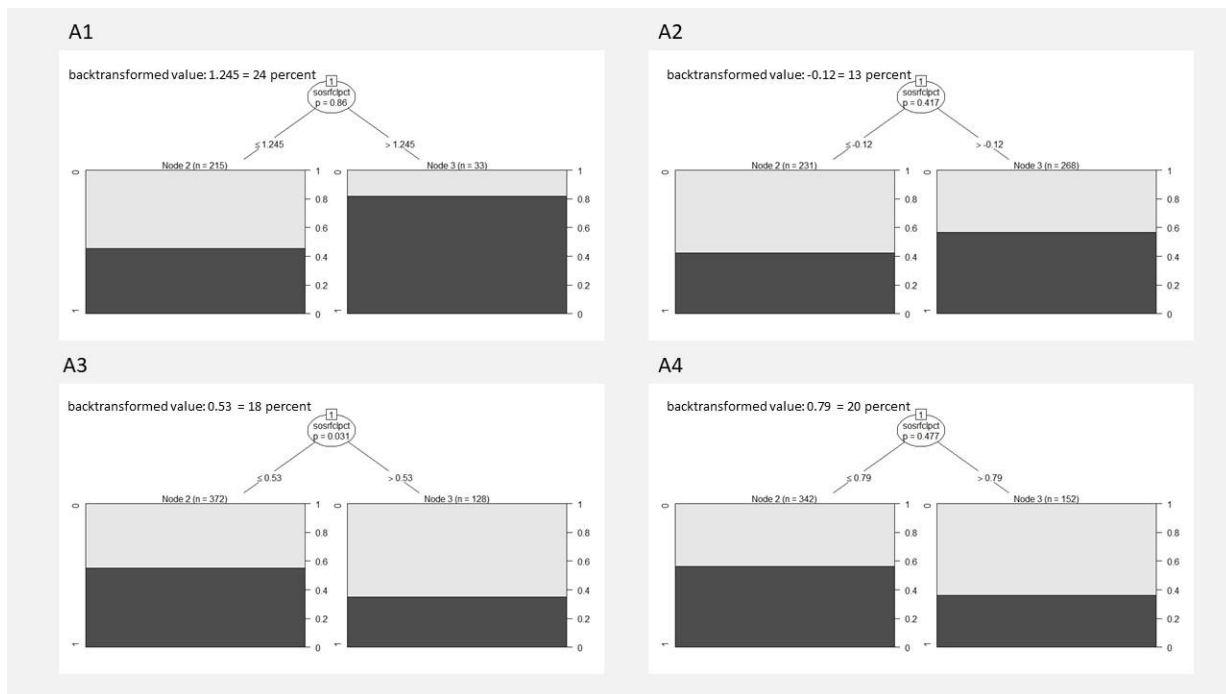


Figure F10. Conditional inference tree univariate stumps for variable sosrfclpct, clay percent of the surface soil. Dark gray represents mortality presence and light gray indicates mortality absence.